Multimodality functional imaging in rectal cancer treated with radiotherapy



Tessa Greenhalgh

St Hilda's College

University of Oxford

A thesis submitted for the degree of Doctor of Philosophy

Hilary 2022

Acknowledgements

I am grateful to my supervisors Professor Ricky Sharma and Professor Fergus Gleeson who gave me this opportunity and provided much support and guidance, Dr Brian Burns who supported me particularly with MR imaging and Professor Tim Maughan for his ongoing guidance and encouragement.

I thank my colleagues and friends within the Department of Oncology and the NHS who have supported me and contributed to this research project.

I am thankful to my friends and family whose support and help has been invaluable.

Special thanks must go to the patients who generously provided their time when undergoing treatment for cancer.

Contents

Abstract 1
Glossary 1
List of tables 6
List of figures 9
Chapter 1: Introduction 13
1. Rectal cancer epidemiology 13
2. Management of rectal adenocarcinoma 13
2.1 Diagnosis & staging 13
2.2 Locally advanced rectal cancer 14
3. Standard imaging in rectal cancer 19
3.1 Rectal MRI 19
4. Functional imaging in rectal cancer 21
4.1 Personalised management in rectal cancer 22
4.2 Functional imaging in rectal cancer management 23
5. Hypoxia 24
5.1 Measuring hypoxia in human tumours 25
6. Perfusion 33
6.1 Perfusion CT 33
6.2 Dynamic Contrast-Enhanced MRI 34
7. Glucose metabolism 37
7.1 ^{18}F-Fluorodeoxyglucose PET-CT (FDG PET) 37
7.2 Glucose Chemical Exchange Saturation Transfer (glucoCEST) MRI 39
8. Immunohistochemistry 41
9. Thesis outline 44
Chapter 2: Rectal cancer imaging studies 46
1. RHYTHM study 46
1.1 Study aims 46

1.2 Patient selection 46
1.3 Study timeline 47
1.4 Trial interventions 49
1.5 Major protocol amendments 50
1.6 Recruitment 50
1.7 Patient characteristics 50
1.8 Response assessment 53
2. RIT study 57
3. Discussion of response outcome 67
Chapter 3: Hypoxia imaging using FMISO-PET and Oxygen-enhanced MRI 68
1. Introduction 68
2. 18F-Misonidazole PET-CT 68
2.1 Methods 68
2.2 Results 70
2.3 FMISO challenges 85
2.4 Discussion of FMISO PET in rectal cancer 88
3. Oxygen-enhanced MRI 89
3.1 Methods 90
3.2 Results 92
3.3 Discussion of ShMOLLI T1 mapping with oxygen 106
4. Comparing imaging with histopathological markers of hypoxia 108
4.1 Methods 109
4.2 Results 110
4.3 Discussion 119
4.4 Conclusion of IHC and imaging 120
5. Conclusion 121

Chapter 4: Perfusion and dynamic imaging with perfusion CT, dynamic contrast enhanced MRI and dynamic FMISO PET-CT 122
1. Introduction 122
2. Dynamic FMISO PET-CT 122
2.1 Methods 122
2.2 Results 126
2.3 Discussion of dynamic FMISO PET 136
3. Perfusion CT 138
3.1 Methods 138
3.2 Results 139
3.3 Discussion of pCT 151
4. DCE-MRI 152
4.1 Methods 152
4.2 Results 154
4.3 Discussion of DCE-MRI 168
5. Comparison of dynamic imaging findings 168
5.1 Change in perfusion parameters with radiotherapy 168
5.2 Discussion of dynamic imaging methods 170
6. Conclusion 170
Chapter 5: Glucose metabolism imaging 171
1. Introduction 171
2. ^{18}F-Fluorodeoxyglucose (FDG) PET-CT 171
2.1 Methods 171
2.2 FDG PET-CT results 172
2.3 Discussion of FDG PET-CT in rectal cancer 178
3. GlucoCEST MRI 181
3.1 Methods 181
3.2 Phantom studies 182

3.3 Volunteer studies 186
3.4 Patient studies 187
3.5 Discussion of glucoCEST 207
4. Conclusion 208
Chapter 6: Conclusions & future directions 210
Appendix 214
Appendix 1: Imaging acquisition parameters and sequences 214
Appendix 2: IHC 220
References 235

Abstract

The successful treatment of locally advanced rectal cancer often relies upon the response to neoadjuvant radiotherapy to improve the chances of surgical resection. Diagnostic imaging is vital to determine appropriate patient management but there is a range of responses to radiation in those who undergo treatment. Multimodality functional imaging provides non-invasive assessment of several aspects of tumour pathophysiology such as hypoxia, perfusion and glucose metabolism, and can characterise heterogeneity within. This may be useful to determine suitable treatment strategy and to target tumour appropriately. Furthermore, it may guide to appropriate systemic radiosensitisers. Following neoadjuvant therapy, a complete response is possible in a minority of patients who could avoid major surgery if they could be confidently identified. Functional imaging may have a further role to play in this setting.

In this thesis, the role of multimodality functional imaging is investigated in patients undergoing neoadjuvant chemoradiotherapy for locally advanced rectal cancer within two imaging studies, RIT and RHYTHM. Hypoxia, known to be an important cause of radioresistance, is assessed through static ^{18}F-Fluoromisonidazole PET-CT and oxygen-enhanced MRI, which is compared with immunohistochemical markers of hypoxia. This process relies significantly on tumour perfusion, which is investigated through dynamic ^{18}F-Fluoromisonidazole PET-CT. Dynamic enhanced MRI and perfusion CT provide a further indication of the effects of radiation on tumour perfusion. Within the heterogeneous environment created, tumour metabolism is altered and this can be measured in order to evaluate appropriate treatment and response. ^{18}F-Fluorodeoxyglucose PET-CT scanning is one method to assess glucose metabolism. A novel technique, glucoCEST MRI, may also provide this information with the anatomical superiority of this modality. It is explored further in BIOPIC, an imaging study of oropharyngeal squamous cell carcinoma patients undergoing radical radiotherapy.

The results demonstrate that rectal tumours are heterogeneous and a multitude of interacting pathophysiological factors likely affect the response to radiation. Defining complete response may require a multimodality solution in order to confidently avoid resection. Significant challenges in undertaking functional imaging are discussed and potential solutions considered.

Glossary

AIC	Akaike information criteria
AIF	Arterial Input Function
AJCC	American Joint Committee on Cancer
AUC	Area under curve
BF	Blood flow
BSA	Bovine serum albumin
BV	Blood volume
CAIX	Carbonic Anhydrase IX
CD31	Cluster of differentiation 31
CEST	Chemical Exchange Saturation Transfer
cm	Centimetre
CRC	Colorectal cancer
CRM	Circumferential resection margin
CRT	Chemoradiotherapy
CTV	Clinical target volume
CT	Computerised tomography

DCE	Dynamic contrast enhanced
d.f.	Degrees of freedom
DFS	Disease free survival
EMVI	Extramural vascular invasion
FDG	^{18}F-fluorodeoxyglucose
FMISO	^{18}F-Fluoromisonidazole
fMRI	Functional MRI
GLUT	Glucose transporter
GTV	Gross tumour volume
Gy	Gray
H&E	Haematoxylin and eosin
HIF	Hypoxia-inducible factor
HNSCC	Head and neck squamous cell carcinoma
HU	Hounsfield unit
IHC	Immunohistochemistry
IMRT	Intensity modulated radiotherapy
Kg	Kilogram

LARC	Locally advanced rectal cancer
MBq	Megabecquarels
MDT	Multidisciplinary team
Min	Minute
mL	Millilitre
MRI	Magnetic resonance imaging
MTC	Magnetisation transfer contrast
MTR	Magnetisation Transfer Ratio
MTV	Metabolic Tumour Volume
MVD	Microvessel density
NHS	National Health Service
NICE	The National Institute for Health and Care Excellence
NSCLC	Non small cell lung cancer
O_2	Oxygen
OAR	Organ(s) at risk
OS	Overall survival
PBS	Phosphate buffer solution

pCR	Pathological complete response
pCT	Perfusion CT
PET	Positron emission tomography
ppm	Parts per million
PTV	Planning target volume
RF	Radiofrequency
ROI	Region of interest
RFS	Recurrence free survival
RT	Radiotherapy
s	Second
SABR	Stereotactic ablative body radiotherapy
SD	Standard deviation
sFOV	Small field of view
ShMOLLI	Shortened modified look-locker inversion recovery
SNR	Signal-to-noise ratio
SSV	Single slice volume
SUV	Standardised uptake value

TAC	Time activity curve
T:B	Tumour to blood ratio
TLG	Total lesion glycolysis
T:M	Tumour to muscle ratio
TME	Total mesorectal excision
TRG	Tumour regression grade
TTV	Total tumour volume
T2W	T2 weighted
Vol	Volume

List of tables

Table 1.1: Pathological tumour regression grade scoring systems

Table 1.2: MRI tumour regression grade

Table 1.3: Studies of hypoxia imaging using PET-CT in rectal cancer

Table 2.1: RHYTHM Study Patient Characteristics

Table 2.2: Overall response assessment of RHYTHM B patients undergoing CRT

Table 2.3: RIT Patient Characteristics

Table 2.4: Mercury group MRI and AJCC pathological tumour regression grade with overall response assessment of RIT 1 & RIT2 patients undergoing CRT

Table 3.1: RHYTHM A tumour volumes

Table 3.2: RHYTHM B Tumour volume and SUVmax changes on neoadjuvant CRT for rectal cancer

Table 3.3: RHYTHM A 4h static FMISO PET Tumour (T) SUVmax and T:Muscle (M) & T:Blood (B) ratios

Table 3.4: RHYTHM B 4h static FMISO PET Tumour (T) SUVmax and T:Muscle (M) & T:Blood (B) ratios

Table 3.5 RHYTHM B Tumour volume and SUVmax changes with 8-10 fractions neoadjuvant radiotherapy for rectal cancer

Table 3.6: ShMOLLI MRI tumour slice volume (SSV) as a proportion of T2 axial MRI total tumour volume (TTV) in RHYTHM A/B and RIT studies

Table 3.7: ShMOLLI MRI tumour T1 & ΔR1* with and without supplemental inspired oxygen in RHYTHM A

Table 3.8: ShMOLLI MRI tumour T1 & ΔR1* with and without supplemental inspired oxygen in RIT and RHYTHM B studies before, during and after chemoradiotherapy

Table 3.9: Mean ShMOLLI T1 in muscle on air and oxygen at 3 imaging time points

Table 3.10: Pimonidazole staining characteristics in RHYTHM A

Table 3.11: CAIX staining characteristics in RHYTHM A

Table 3.12: Tumour area and microvessel density defined by CD31 in RHYTHM A

Table 3.13: Summary of hypoxia IHC and imaging results

Table 4.1: Tumour AIC values for 0 – 45 minute dynamic FMISO PET data fitting to pharmacokinetic models - 1, 2 and 3 tissue compartmental (TCM) and Casciari

Table 4.2: Tumour AIC values for 0 – 45 minute dynamic FMISO PET data fitting to pharmacokinetic models - 1, 2 and 3 tissue compartmental (TCM) and Casciari

Table 4.3: Casciari model tumour parameters perfusion (*F,* mL/g/min) and hypoxia (K_A min^{-1}) for 0 – 45 minute dynamic FMISO PET data at baseline and after 8 – 10 fractions radiotherapy

Table 4.4: Casciari model muscle parameters perfusion (*F,* mL/g/min) and hypoxia (K_A min^{-1}) for 0 – 45 minute dynamic FMISO PET data at baseline and after 8 – 10 fractions radiotherapy

Table 4.5: Table 4.5: RHYTHM A pCT and MRI tumour volume

Table 4.6: RHYTHM A mean blood volume (BV) and mean blood flow (BF)

Table 4.7: RHYTHM B pCT* and MRI** tumour volume

Table 4.8: RHYTHM B pCT mean blood volume and mean blood flow

Table 4.9: RIT1 and RIT2 tumour volumes pre and 6 weeks post chemoradiotherapy on T2 axial sFOV MRI

Table 4.10: RHYTHM and RIT mean Ktrans (min^{-1}) at baseline, on radiotherapy and 6 weeks post treatment

Table 4.11: Comparison of dynamic imaging parameter changes on radiotherapy

Table 5.1: FDG PET-CT parameters in rectal adenocarcinomas within RIT study at baseline

Table 5.2: Percentage MTR asymmetry at different applied RF pulse B1 (µT) and glucose concentration (mM) levels

Table 5.3: BIOPIC study demographics and tumour staging

Table 5.4: Baseline tumour MTR with and without I.V. dextrose and on air versus 100% inspired oxygen in oropharyngeal SCC

Table 5.5: Baseline nodal MTR with and without i.v. dextrose and on air versus 100% inspired oxygen in oropharyngeal SCC

Table 5.6: Changes in capillary blood glucose levels (mM) during baseline and on CRT scans

Table 5.7: Baseline MOLLI mean (S.D.) T1 (ms) for tumour and nodes of oropharyngeal SCC on air and oxygen

Table 5.8: On CRT MTR with and without I.V. dextrose and on air versus 100% inspired oxygen in oropharyngeal SCC

Table 5.9: On CRT MOLLI mean (S.D.) T1 (ms) for tumour and nodes of oropharyngeal SCC on air and oxygen

List of figures

Figure 1.1: Tofts-Kety 2-compartmental model

Figure 1.2: The mechanism of glucoCEST MRI showing z-spectra

Figure 2.1: RHYTHM study group A and B timelines

Figure 2.2: RIT study timeline

Figure 3.1: ROIs for tumour (red outline), muscle (yellow outline) and artery (white arrow) on FMISO PET CT at 4 hours in a RHYTHM-B patient (poor responder)

Figure 3.2: MRI assessed tumour volume in cm^3 a) at baseline and b) on CRT

Figure 3.3: Box plot of a) baseline tumour SUVmax, b) week 2 chemoradiotherapy tumour SUVmax, c) percentage change in tumour SUV max by outcome

Figure 3.4: RHYTHM B outcomes by hypoxic volumes (cm^3) defined as: T:M > 1.3 at a) baseline; b) week 2 CRT; c) % change; and T:B >1.3 at d) baseline; e) week 2; CRT f) % change

Figure 3.5: Changes in a) T:B >1.3 and b) T:M >1.3 defined hypoxic volumes by response - Good responders (dashed) and Poor (solid) lines

Figure 3.6: Spill-over affecting interpretation of FMISO PET-CT images. a) Faecal excretion of tracer (area of interest indicated by black arrow); b) Bladder excretion of tracer (tumour outlined in red, bladder maximum uptake in blue)

Figure 3.7: Mechanisms of bladder spill-in affecting FMISO PET 4-hour results: Scatter of photon leads to false detection of event in tumour; Two annihilation events occur with one of each photon pair lost/undetected

Figure 3.8: Baseline oxygen-enhanced ShMOLLI MRI T1 maps in a good responder

Figure 3.9: ShMOLLI MRI ΔR1 changes with chemoradiotherapy (baseline, after 8-10 fractions and 6 weeks post treatment)

Figure 3.10: Changes in ShMOLLI MRI mean T1 (ms) with inspired oxygen at a) baseline, b) during radiotherapy and c) 6 weeks post treatment

Figure 3.11: ShMOLLI results by response at baseline, after 8-10 fractions CRT, 6 weeks post CRT for mean T1 on air (s), mean T1 on 100% oxygen (ms) and ΔR1 (s^{-1})

Figure 3.12: Example of Rhythm A tumour imaging (MRI, FMISO PET) & staining for pimonidazole

Figure 3.13: Example slice of consecutive stained histopathology slices for RHYTHM A patient a) H&E, b) pimonidazole, c) CAIX, d) CD31

Figure 3.14: RHYTHM A example of slice cell level analysis and heatmapping for tumour stain intensity for pimonidazole and CAIX

Figure 3.15: RHYTHM A CD31 vessel density quantifation a) stained slide, b) vessel density visualisation, c) detailed higher magnification vessel density visualisation

Figure 4.1: Example FMISO time activity curve in tumour, blood and muscle

Figure 4.2: Examples of change in activity (KBq/mL) between baseline FMISO PET scans over time in a) tumour and b) bladder in RHYTHM B study

Figure 4.3: RHYTHM B study RHB02 FMISO imaging at a) 45 mins b) 2 hours (post bladder void) and c) 4 hours (bladder refilled)

Figure 4.4: Casciari model tumour parameters perfusion (*F*) and hypoxia (K_A) for 0 – 45 minute dynamic FMISO PET data at baseline and 8 – 10 fractions radiotherapy by response

Figure 4.5: Example of Blood Volume (BV) maps in a RHYTHM B patient (good responder) at a) baseline and b) after 2 weeks of radiotherapy (Tumour ROI outlined in red)

Figure 4.6: RHYTHM B pCT mean blood volume (mL/100g tissue) a) at baseline and b) during week 2 CRT and mean blood flow (mL/min/100g tissue) c) at baseline and d) during week 2 CRT

Figure 4.7: Change with RT from baseline in blood volume (mL/100g tissue) by response as a) absolute and b) percent, and blood flow (mL/min/100g tissue) as c) absolute and d) percent

Figure 4.8: DCE MRI Ktrans (min^{-1}) in tumour slice of a good responder in RIT at a) baseline, b) after 2 weeks RT and c) 6 weeks post RT

Figure 4.9: Mean Ktrans (min^{-1}) in RHYTHM-B and RIT2 at baseline, on treatment and 6-8 weeks post radiotherapy (Red = poor responders, Green = good responders)

Figure 4.10: Mean Ktrans by response in RIT1, RIT2 and RHYTHM-B studies for all patients at a) baseline and for those with 3 imaging timepoints at b) baseline c) on RT and d) 6 weeks post RT

Figure 5.1: FDG PET-CT parameters by response a) volume (cm^3), b) SUVmax (g/mL), c) SUVpeak (g/mL), d) TLG (g cm^3/mL)

Figure 5.2: FDG PET parameters versus volume (cm^3) - a) Tumour SUVmax (g/mL); b) Tumour SUVpeak (g/mL)

Figure 5.3: GlucoCEST phantom imaging: a) Phantom with solutions of glucose and PBS with BSA at different concentrations; b) GlucoCEST image of phantom

Figure 5.4: MTR asymmetry % at different B1 (μT) and glucose concentration (mM) levels

Figure 5.5: Examples of phantom study MTR asymmetry Z-spectra at various B1 inputs in glucose concentration a) 12.5 mM, b) 200 mM, c) 0 mM

Figure 5.6: CEST imaging in healthy volunteer brain without contrast showing a) Healthy volunteer brain MTR asymmetry image; b) *In vivo* spectrum obtained at 1uT RF saturation B1; c) B0 map; d) B1 map

Figure 5.7: Rectal cancer Magnetisation Transfer Ratio at baseline and on radiotherapy +/- 100% inspired oxygen +/- i.v. dextrose

Figure 5.8: BIOPIC study timeline

Figure 5.9: BIO4 imaging a) GlucoCEST imaging at baseline and on CRT +/- i.v. dextrose and inspired oxygen; b) standard imaging (MRI, FDG PET-CT)

Chapter 1: Introduction

1. Rectal cancer epidemiology

Cancer will affect over half of the population in Great Britain in their lifetime[1] and the diagnosis has multifaceted effects on the lives of patients and those that care for them. Colorectal cancer (CRC) is the fourth commonest and leads to 10% of cancer mortality[2]. The UK lifetime risk for developing CRC is 1 in 14 for men and 1 in 19 for women[3]. Incidence has risen by around 4% since the 1990s in men, although in women rates have remained stable[3]. Rectal primaries account for 32% of CRC in males and 23% in females[3]. Around a quarter of patients present with metastatic disease[4] and of those who present with earlier stage disease, around 30% develop metastases, the majority within five years of resection[5, 6]. Five year relative survival ranges from 93.2% in early stage disease (Dukes A) to 6.6% in those with metastases (Dukes D)[7]. Advances in cancer management therefore have great potential to improve patient outcomes and survivorship.

2. Management of rectal adenocarcinoma

2.1 Diagnosis & staging

The management of rectal cancer is based primarily on stage, established through endoscopic assessment and imaging with Magnetic Resonance Imaging (MRI) and Computed Tomography (CT) scans[8-10]. Staging is based on tumour size (T), nodal involvement (N) and distant metastasis (M), most recently defined in The Eighth Edition American Joint Committee on Cancer (AJCC) Cancer Staging Manual[11]. The NHS Cancer Plan 2000 introduced the widespread use of the multidisciplinary team (MDT) meeting in the management of cancer in the NHS[12].

2.2 Locally advanced rectal cancer

'Locally advanced' rectal cancer (LARC) refers to T3 or T4 tumours (extending through the bowel wall) and/or N1 or N2 regional lymph node involvement without evidence of distant metastases for the purposes of this thesis.

Neoadjuvant radiotherapy

Neoadjuvant therapy is offered to some patients based upon anatomical features of the tumour such as stage and circumferential resection margin (CRM) being threatened or involved[8]. Broadly, two regimens are currently recommended as standard; short and long course radiotherapy.

Short course radiotherapy of 25Gy in 5 fractions is given shortly prior to surgery (usually within a few weeks) and is recommended for patients with resectable tumours with at least T3b or N1 rectal cancer or in the presence of extramural vascular invasion (EMVI)[13]. An improvement in local recurrence and marginally improved overall survival compared to surgery alone has been demonstrated with this regimen[14, 15].

Neoadjuvant long course radiotherapy 45 to 50.4 Gray in 25 to 28 fractions with the addition of chemotherapy in the form of a fluoropyrimidine (capecitabine orally or 5-fluorouracil intravenously) is considered for patients with high risk operable disease and those with borderline or unresectable tumours[13]. Tumours may be threatening or breaching the resection margin or low and encroaching onto the intersphincteric plane or involving the levator muscles. Radiotherapy for sphincter sparing is not recommended. The German Rectal Cancer Study Group[16] established the use of neoadjuvant rather than adjuvant chemoradiotherapy, with significantly improved local recurrence rates (6 vs 13% respectively) although difference in overall survival was not seen. Improvement in local recurrence rates and disease free survival was confirmed by Roh et al[17].

Comparing neoadjuvant chemoradiotherapy with radiotherapy alone demonstrated improved local control with higher grade 3 or 4 toxicity[18-20]. The latter may still be given where chemotherapy is contraindicated or declined. For the purposes of this thesis, only neoadjuvant long course chemoradiotherapy (CRT) or radiotherapy (RT) will be considered.

Total neoadjuvant therapy for LARC, with the sequential addition of oxaliplatin/5FU doublet or triplet with irinotecan chemotherapy to CRT, has shown evidence of increased pCR[21, 22] and sphincter preservation rates[23]. In addition, it may improve DFS and OS[21].

Surgery

Surgical standard of care has been established as total mesorectal excision (TME), through anterior or abdominoperineal resection[24, 25]. Laparoscopic surgery is increasingly being used due to better short term post-surgical outcomes and improved recovery time with comparable survival outcomes to date[26]. Depending on the disease status and proximity of the tumour to the anal sphincter, a temporary or permanent stoma may be required. Surgical approaches continue to evolve, for example, use of the transanal approach for TME, which may have advantages over laparoscopic and open TME such as improved pelvic views and sphincter preservation whilst maintaining oncological quality of resection[27]. Robotic surgery is associated with lower morbidity and equivalent outcomes to open TME and may be at least equivalent to the laparoscopic approach whilst less technically challenging[28].

Pathology

Tumour regression grade (TRG) is established as a reporting tool for radiotherapy response following surgical resection. It is based upon the degree of fibrosis versus tumour cells remaining. Various grading techniques have been published and are summarised in Table 1.1. There are limitations of these grading systems, including the potential for subjectivity in reporting, difficulty in interpreting for certain tumour types such as mucinous, lack of information regarding nodal

information and how best to report heterogeneous tumours[29]. Whilst all have been shown to correlate with outcomes, AJCC version 7.0 has been found to most accurately predict recurrence free survival at 5 years, ranging from 98% for TRG 0 to 68% for TRG 3[30]. Around 10 to 25% of patients have a pathological complete response (pCR) following CRT[31-33]. This is associated with better long term outcomes with respect to local recurrence, 5 year disease free survival (DFS) and overall survival (OS)[31, 34, 35].

Table 1.1: Pathological tumour regression grade scoring systems

TRG	Mandard[36]	AJCC 7.0[11]	Dworak/Rodel 5 tier[37]	Ryan[38]
0		No residual tumour cells	No regression	
1	No residual cancer cells	Single cell or small group of cells	Fibrosis <25% of tumour mass	No viable or single cells or small groups cancer cells
2	Rare residual cancer cells	Residual cancer with desmoplastic response	Fibrosis 25-50% of tumour mass	Residual cancer outgrown by fibrosis
3	Fibrosis outgrowing residual cancer	Minimal evidence of tumour response	Fibrosis >50% of tumour mass	Significant fibrosis outgrown by cancer or no fibrosis with extensive residual cancer
4	Residual cancer outgrowing fibrosis		Complete regression	

5	No regressive change			

3. Standard imaging in rectal cancer

Anatomical imaging has significantly improved over the last few decades with the availability of high resolution CT scanning, magnetic resonance imaging (MRI) and positron emission topography (PET) with nuclear tracers. Baseline CT Chest, Abdomen and Pelvis (CAP) and rectal MRI are advised for all patients without contraindication[13]. ^{18}F-fluorodeoxyglucose (FDG) PET may be utilised for suspected distant metastases[39]. The presence of lymphovascular invasion suggests a higher probability of metastatic disease and is another potential indicator to consider FDG PET scanning[40, 41].

For patients who have neoadjuvant CRT, restaging with CT CAP and MRI rectum is undertaken routinely around 6-8 weeks post-CRT[13] to assess tumour regression and resectability and to confirm M0 disease. Assessment of local disease will be focused on here.

3.1 Rectal MRI

MRI technology has advanced considerably over recent years with improvements in speed and quality of data acquisition, image reconstruction and post processing. MRI sensitivity and specificity are dependent not only on technique and verification standards but also patient selection and field strength. Standard clinical MRI strength is 1.5 T or 3 T - the latter has a higher signal-to-noise ratio (SNR) permitting higher resolution imaging and can generally detect lesions as small as 3mm[42].

Rectal MRI morphology has been correlated with pathological features known to be prognostic of high risk, including extramural vascular invasion (EMVI) and CRM involement[43]. These features identified preoperatively on MRI have been correlated with local recurrence and overall survival at 5 years[44]. The MR Tumour Regression Grade (TRG)[45] utilised histopathological features associated with survival outcomes to develop an imaging based score found in Table 1.2. Imaging was undertaken on a 1.5T scanner to obtain axial, coronal and sagittal T2-weighted sequences.

Intravenous contrast enhancement was not used as it was not found to be helpful[46].

Table 1.2: MRI tumour regression grade[45]

TRG	Description
1	Absence of any tumour signal
2	Small amounts of residual tumour visible. Predominant fibrotic low signal intensity
3	Mixed areas of low signal fibrosis and intermediate signal intensity present, without predominance of tumour
4	Predominantly tumour signal intensity remains with minimal fibrotic low signal intensity
5	No fibrosis evident, only tumour signal visible

Contrast agents such as gadolinium are however used routinely in rectal MRI protocols. Gadolinium-chelate contrast shortens both T1 and T2, with a greater effect on the former, increasing the T1 signal. Pathology such as tumours often accumulate contrast mainly due to vasculature abnormalities, enhancing the signal[47-49].

Prediction and assessment of response with standard imaging does remain challenging[50-52]. Whilst the MERCURY group MRI TRG assessment predicts DFS and OS as well as providing information about the CRM[45], the agreement with pathological TRG has been shown to be limited[53]. The ability to determine who will benefit from treatment is important as radiation, particularly given with concurrent chemotherapy, may be associated with significant toxicity and effects on quality of life[54, 55]. Neoadjuvant CRT necessarily delays definitive surgical resection and can make it more challenging in case of excess tissue oedema leading to loss of surgical planes[56], yet for some there is little to no benefit of treatment[14-16, 57]. Furthermore, other

pathophysiological factors such as hypoxia may significantly impact the effectiveness of treatment[58, 59].

4. Functional imaging in rectal cancer

Functional imaging allows for tumour characterisation with assessment of physiology, molecular processes and metabolites[60]. It encompasses a range of imaging techniques from nuclear medicine and PET to multiparametric MRI. The ability to image cancer physiology and particularly changes with therapy may guide future treatments as laid out in Box 1.1.

BOX 1.1: Potential uses of functional imaging in malignancy

- Diagnosis based on physiological characteristics
- Improved detection of metastases
- More accurate identification of responders
- Predictive/prognostic markers
- Targeted agent choice and monitoring
- Assessing resistance to therapy
- Response assessment by physiological parameters (versus size)
- Improved identification of target or regions for radiotherapy dose boost

For patients undergoing radiotherapy, there are several potential applications of functional imaging. Firstly, as a predictive biomarker to identify those less likely to respond[61] or at higher

risk of developing distant metastatic disease[62] who may benefit from an alternative management strategy; secondly to define a target volume[63] using advanced radiotherapy techniques and dose escalation[41]; thirdly to assess response, for example to targeted radiosensitisers[64], or identify patients who have a complete response and could avoid major surgery[65].

4.1 Personalised management in rectal cancer

The use of targeted modifying agents with radiotherapy will require identification of those who may benefit[66, 67]. The addition of chemotherapeutic agents to fluorouracil for radiosensitisation has been explored including irinotecan[68, 69] and oxaliplatin[70, 71]. Biological agents such as vascular endothelial growth factor (VEGF) inhibitor bevacizumab[72], anti-epidermal growth factor receptor (EGFR) cetuximab[73] and PI3K/Akt pathway inhibitor nelfinivir[74] have also been assessed but none have shown significant improvement in overall survival beyond standard CRT, although toxicity was often increased[75]. Understanding the underlying biological mechanisms of radiosensitisers will be fundamental to progess in this area.

Within the field of radiotherapy, advances over recent years include the introduction of intensity modified radiotherapy (IMRT). IMRT uses multiple radiotherapy fields (usually 5 or 7) to target the treatment volume with superior conformality to conventional three-field radiotherapy for rectal cancer. IMRT allows for dose escalation and simultaneous integrated boost whilst reducing the dose to organs at risk (OAR) in retrospective studies[76-78]. IMRT may therefore be used to modify radiotherapy treatment planning and delivery to improve patient outcome. The ability to boost specific areas within a heterogeneous tumour is known as ‘dose painting’. Identification of these areas relies upon reliable and accurate imaging. Early studies using FDG PET-CT imaging to guide subvolume dose escalation suggest the technique provides a high rate of response with acceptable toxicity rates in rectal cancer[79] and head and neck squamous cell carcinoma (HNSCC)[80].

A significant minority of patients have a seemingly complete response of their tumour to

radiotherapy clinically[81]. Previously, they would have routinely proceeded to surgery, which may involve significant morbidity, potential need for stoma formation and a mortality risk[82]. However, evidence from Habr-Gama et al[83, 84] suggests over 50% of patients with a complete clinical response following chemoradiotherapy have a sustained response at 12 months. A subsequent meta-analysis supports conservative management in those with complete clinical response although numbers included were relatively small[85]. An international watch and wait database opened in 2015 and retrospective data from over 600 patients, of whom 56% had a definite tumour response and 27.8% probable, demonstrated local regrowth in 26% of all cases[86]. In the UK, a cohort study has suggested selected patients may avoid permanent colostomy without compromising safety at three years[87]. Results are awaited for prospective randomised studies investigating the use of radiotherapy without surgery for rectal cancer including STAR-TREC[88] and the TRIGGER trial[89].

It appears the paradigm of treating rectal cancer is changing. Biomarkers that allow confident assessment of tumour pathophysiology and phenotype will be vital in order to assess response to therapy, tailor management and improve outcomes. The expanded use of functional imaging may improve the ability to personalise patient management at all stages of the cancer journey.

4.2 Functional imaging in rectal cancer management

Optimal utilisation of radiotherapy in rectal cancer and improved methods to identify those most likely to benefit from treatment are required. Imaging has the advantage of being non- or minimally invasive with the potential to capture the whole tumour. Assessment of tumour physiology using imaging is a potential method to determine characteristics that impact on response to therapy. The next sections discuss hypoxia, perfusion and glucose metabolism imaging.

5. Hypoxia

Hypoxia is a reduction in the normal level of tissue oxygen tension. It is a common feature of solid tumours linked to chemo- and radio-resistance and a more aggressive phenotype[67]. Whilst hypoxaemia is defined as an arterial oxygen tension below the normal level of 80 mmHg, hypoxia is a failure of oxygenation at the tissue level, with no absolute cut-off defined[90] although levels of less than 5 - 10 mmHg are often considered to be pathological[91]. A pathological hypoxia may be said to exist when compensatory mechanisms to maintain optimal oxygenation of tissue are inadequate, overwhelmed or maladapted. This may be demonstrated at a cellular or tissue level through a reduced oxygen consumption rate[92].

Limited oxygenation in the malignant setting is largely due to decreased diffusion, inadequate and structurally abnormal vasculature and disturbed microcirculation[93]. Hypoxia, as a result, may be acute or chronic. Acute hypoxia occurs as a result of abnormal microvasculature leading to fluctuating blood flow and hence oxygen supply. It may also be known as cyclic hypoxia as it is characterised by recurring episodes of hypoxia over a range of minutes to days. Chronic hypoxia is caused by an increase in diffusion distance from vessel to cellular tissue[94]. Relevant also to radiotherapy is anaemic hypoxia, related to reduced oxygen carrying capacity in the blood. Evidence from some cancers has shown that a reduced haemoglobin leads to worse outcomes for example in head and neck cancer[95].

As there exists a gradient of oxygenation between supply from blood vasculature to consumption by mitochondria, within hypoxic conditions in tumours, degrees of hypoxia may have potential differing consequences and these may vary between tumour types[96]. In terms of radiobiology, the hypoxic fraction i.e. the fraction of viable radiation-resistant hypoxic cells at a given partial pressure of oxygen (pO_2) or other relevant defined threshold is often used. An oxygen concentration of around 0.02% has been associated with maximum radiation resistance. However,

in malignancy, oxygen deprivation at more moderate levels of around 1 - 2% oxygen leads to activation of several biological pathways that can also affect resistance[97]. Hypoxia-inducible factor 1 (HIF-1) is a key modulator in hypoxia. It is normally constitutively expressed and in cancer may be overexpressed[98]. In normoxia the hydroxylated α subunit interacts with von Hippel-Lindau, part of a ligase complex that targets HIF-1α for ubiquitin-proteasomal degredation. In hypoxia, HIF-1α is stabilised and dimerises with HIF-1β to bind to the hypoxia response element (HRE)[99]. Further interactions lead to transcription of target genes involved with glucose metabolism (including glucose transporters such as GLUT-1)[100], intracelluar pH regulation (including carbonic anhydrases [CA] such as CAIX)[101], angiogenesis[102], survival, proliferation[99] and metastasis[103]. Changes with low oxygenation have been demonstrated in the proteome, both of the neoplasm and surrounding stroma, as well as the genome, ultimately altering cell phenotype[92]. Given that hypoxia is linked to resistance to standard therapy, both identification and targeting to reduce these effects is of significant interest.

5.1 Measuring hypoxia in human tumours

There are several potential methods to detect hypoxia within tumours *in vivo* and *ex vivo*. The ideal technique would be simple, rapid and non-invasive, with no toxicity. Results would be consistent across time and location, without the need for substantial calibration. Current techniques range from the invasive histopathology and gene expression profiling to needle electrode oximetry and non-invasive imaging. Each technique has benefits and challenges and these are now discussed with respect to functional imaging.

5.1.1 ^{18}F-Misonidazole PET-CT imaging

Imaging techniques for hypoxia include PET-CT with two main tracer classes: ^{18}Fluorine-labelled nitroimidazoles and copper-labelled diacetyl-bis(N-methylthiosemicarbazone) or Cu-ATSM. The most widely studied compound is ^{18}F-Misonidazole (FMISO). Nitroimidazoles are lipophilic

compounds that enter cells through diffusion and are reduced by various enzymes such as cytochrome P450 reductase and xanthine oxidase. In the presence of adequate intracellular oxygen, the resulting radical anion is converted back to the intact compound and leaves the cell via diffusion. *In vitro* data have suggested that FMISO uptake occurs in hypoxic cells with a pO_2 of ≤ 2 - 3 mmHg[104]. However, *in vivo* accumulation of FMISO has been shown to occur at oxygen levels ≤ 10 mmHg[105, 106]. An irreversible reduction takes place leading to fragmentation and binding to macromolecules. The tracer is then retained within the cell[107]. The half-life of ^{18}F is 110 minutes[108] and optimal imaging time is between 2 – 4 hours[109].

In vivo studies of FMISO PET in a variety of malignant tumours have demonstrated a good correlation between hypoxic volumes identified by imaging when compared to those derived from tumour sections stained with pimonidazole[110-112] and CAIX[110]. However there are potential issues with scale when comparing imaging to pathological specimens. For example, Troost et al[112] examined the correlation using a variety of methods in head and neck cancer xenografts and found that correlation between mean signal intensity of FMISO and hypoxic fraction defined by pimonidazole labelling was strongly dependent on tumour microarchitecture. Tumours with more homogenous, patchy microregional pattern of hypoxia showed less correlation between imaging and immunohistochemistry (IHC). The diffuse FMISO signal seen in these tumours may at least in part result from inherent scatter seen in autoradiography. However there remained a significant correlation, albeit weaker, across tumours. They concluded that in larger, clinical tumours, FMISO may be useful in providing global information regarding hypoxia but urged caution when evaluating smaller subvolumes.

FMISO PET-CT parameters

Key parameters for interpreting FMISO PET results have been examined in both animal and human studies. The Standardised Uptake Value (SUV) is a semiquantitative measure of normalised radioactivity concentration in PET images. The SUVmax is the highest SUV value within a single

voxel in the volume of interest. In HNSCC, FMISO SUVmax has been significantly correlated with HIF-1 α, a key mediator of cellular response to hypoxia[113]. It was found to be a useful prognostic metric prior to stereotactic body radiotherapy (SBRT) for NSCLC where combined with FDG PET-CT SUVmax, a significant difference in PFS was found between different patterns of uptake[114].

There are evident limitations in using a single voxel value to define tumour hypoxia – it may be affected by noise and does not reflect tumour heterogeneity nor represent a target for therapy[115, 116]. The ability to define a hypoxic subvolume can provide serial quantification of tissue hypoxia over time[109] and a target for radiotherapy dose boost. Tissue to blood ratios have been investigated to define hypoxic subvolumes. In animal studies, mean FMISO uptake in normal tissue to blood ratio was <1.3 in over 90% of tissues[117]. Following from this, in humans, a ratio of tumour:blood (T:B) FMISO activity of ≥1.4 at two hours or more post injection to define hypoxia was derived through arterial blood sampling at regular intervals during imaging in a variety of tumours[118, 119]. Less conservative values have been established for example ≥1.2 in sarcoma although this was based on venous blood sampling[120]. Others have suggested higher ratios such as >1.5 in HNSCC[121].

Blood and particularly arterial sampling is invasive and methods of establishing hypoxic volumes using imaging alone were sought. T:B ratio using imaged blood volumes were compared with blood sample derived values and showed good correlation, suggesting this could be used as a surrogate measure[122]. Tumour to Muscle (T:M) ratio was established as an alternative parameter which could be obtained through imaging alone. A threshold of 1.24 (2 standard deviations above normal tissue to muscle to retention ratio) meant all primary nasopharyngeal carcinomas being investigated demonstrated some level of hypoxia[123]. Eschmann[124] retrospectively defined a T:M ratio of >1.6 at 4 hours post injection as significant on the basis that all HNSCC patients with those levels had tumour recurrence. However, numbers in the study were small and a minority of patients with T:M <1.6 also experienced recurrence. The results were not replicated in a

subsequent study of HNSCC by another group[125]. In comparison with pO_2 polography in HNSCC, Zinny et al established a T:M of <1.4 in normoxic tumours versus 1.8 in hypoxia[126].

FMISO PET-CT in malignancy

Multiple small-scale clinical studies have assessed FMISO for identification of hypoxia in the malignant setting. In HNSCC, FMISO has been well established in identifying hypoxic regions[127]. Zinny et al compared FMISO to FDG PET and pO_2 polography in patients with metastatic HNSCC and found FMISO retention was significantly higher in hypoxic tumours than normoxic, whereas FDG showed no correlation[126], confirmed by Gagel[128]. In NSCLC, FMISO has identified changes in regional hypoxia on RT[129] and the same was demonstrated in colorectal cancer patients receiving bevacizumab and chemotherapy[130]. FMISO was found to be a prognostic indicator for patients with NSCLC[124, 131] and HNSCC undergoing radiotherapy[121]. Various dose modelling studies have suggested FMISO PET could be used to indicate hypoxic subvolumes for dose boosting in radiotherapy in HNSCC[125, 132, 133] and NSCLC[134]. In rectal cancer, there have been a limited number of studies investigating hypoxia PET-CT imaging (Table 1.3).

FMISO PET is likely to reflect both areas of chronic and acute hypoxia[108]. Nehmeh et al[135] performed two baseline FMISO-PET scans three days apart in patients with head and neck cancer and found 6 of 13 had a strong voxel by voxel correlation, concluding that acute hypoxia is likely to have played a part in the difference seen in the remaining patients. However, cyclic variations in tumour hypoxia can occur over timescales of a few minutes compared to the few hours required for FMISO PET imaging. Warren et al suggest based on modelling data that the signal observed represents a 'time-averaged oxygenation'[136]. There is a slow washout in non-hypoxic tissue necessitating a long interval between tracer injection and scanning of 2 to 4 hours[118, 137]. There remains a small risk of incomplete clearance of unbound tracer. As the tracer is excreted via the urinary and faecal routes, there is a risk of background activity particularly in pelvic imaging[138].

Table 1.3: Studies of hypoxia imaging using PET-CT in rectal cancer

Article	Participants	Interventions	Parameters	Findings
Havelund et al 2013[139]	n = 14; LARC T3/4, <5mm to CRM RT 60 Gy/30# + 5 Gy brachy boost + UFT	^{18}F-FAZA PET BL Static @ 2h	SUV T, M, normal intestinal (I) wall; T:M & T:I	SUVmax & mean higher in T vs M or I T:I mean > T:M.
Roels et al 2008[140]	n = 15 (10 FMISO) LARC	FMISO-PET BL, on RT, static @ 3h FDG PET	PET activity defined vol	Mean PET-defined T vol ↓ during CRT FDG vol > FMISO vol (65% mismatch)
Dietz et al 2008[141]	n = 19; T2-T4 or N+ rectal cancer CRT 45Gy/25# + 5FU	^{60}Cu-ATSM, 60 min dynamic	T:M ratio Response Survival	OS and PFS worse with T:M >2.6 Mean T:M good response < poor
Loi et al 2005[142]	n = 6, inoperable/M1 Oxali + 5FU with 45Gy/25# + 5.4Gy boost	BL FMISO	Qualitiative FMISO measures	Hpoxia in 4 of 6 FMISO scans

UFT = Tegafur/uracil; BL = baseline; T = tumour; M = muscle; FAZA = ^{18}F-fluoroazomycinarabinofuranoside, Gy = Gray, # = fraction, oxali = oxaliplatin; 5FU = 5-fluorouracil; vol = volume

Dynamic FMISO PET-CT

FMISO uptake is variable with slow clearance so the contribution of hypoxia and perfusion may be difficult to differentiate using static PET imaging alone. Kinetic modelling of dynamic FMISO PET data provide a method for quantification of tumour hypoxia and perfusion. The acquisition of serial PET images and derivation of time activity curves (TAC) provides information about tracer metabolism and allows characterisation of these physiological processes. Standard 2- and 3-compartmental models have been evaluated in NSCLC[124, 143, 144], HNSCC[124, 145] and brain tumours[146].

Eschmann et al[124] in their study of NSCLC and HNSS found that early phase data acquisition could be classified as 'rapid washout', 'intermediate' or 'accumulation'. The first category was likely related to tracer perfusion and patients demonstrating this pattern did not have tumour recurrence during the follow-up period. The interplay between hypoxia and perfusion was considered by Thorwarth et al[145] in HNSCC who observed patterns of high perfusion and no hypoxia, perfusion and hypoxia, and reduced perfusion with hypoxia. This could provide an indication as to appropriate intervention with radiosensitisers. Casciari et al developed a four compartmental model with a number of free parameters specifically for FMISO, in an attempt to relate tissue oxygenation status to the metabolic rate of FMISO in tissues, in order to better reflect the chemical processes that occur during FMISO uptake[147].

5.1.2 Oxygen-enhanced MRI

Oxygen (O_2) is a weakly paramagnetic agent which may be used as a contrast agent for MRI.

Supplemental inspired oxygen provided during imaging alters both T1 and T2*. As oxygen levels rise, dissolved arterial pO_2 increases as haemoglobin is already highly saturated. When this reaches tissues, bound oxygen is released from haemoglobin and the dissolved oxygen may then bind to this deoxyhaemoglobin or diffuse into local tissue. Hyperoxia initially directly reduces the T1 relaxation of arterial blood due to the dissolved oxygen, increasing signal intensity. Over longer periods it can affect the T1 in tissues as local pO_2 increases[148]. Hyperoxia increases T2* MRI signal due to reduced deoxyhaemoglobin in venous plasma[149]. T1 mapping techniques will be the focus of this thesis.

Changes in T1 with supplemental oxygen vary in normal tissue. For example, a reduction in T1 has been demonstrated in the spleen, renal cortex[148, 150] and lung[151] in healthy volunteers breathing 100% oxygen imaged on a 1.5T MRI scanner. However, T1 in liver, fat and skeletal muscle did not consistently demonstrate a reduction[148, 150]. In malignancy, supplemental oxygen breathing has been shown to provide additional information about tumour oxygenation whilst avoiding the use of exogenous gadolinium contrast agents[152, 153]. O'Connor et al.[153] imaged 10 patients with advanced pelvic and abdominal malignancies (majority ovarian carcinoma) on air and 100% inspired oxygen using a T1 mapping technique with variable flip angles. In 8 patients, there was a significant increase in the longitudinal relaxation rate (R1), calculated from the change in T1 between room air and oxygen inspiration for each timepoint. This effect was independent of baseline tumour size and R1. In these patients, there was also an increase in R1 seen in skeletal muscle with oxygen breathing. They postulated that the remaining 2 patients had a failure of oxygen delivery either due to external e.g. delivery circuit or internal e.g. respiratory factors. They also found generally good agreement between the spatial distribution of oxygen-enhanced and dynamic contrast enhanced (DCE) MRI[153], with generally high levels at tumour peripheries and lower levels at the core seen, consistent with central necrosis. There were some areas of mismatch where moderate Initial Area Under the Curve at 60 seconds (IAUC60) was associated with low

median O_2 AUC, which may indicate regional tumour hypoxia, where the delivered oxygen is consumed quickly and change in T1 is low despite reasonable perfusion. These are areas that may benefit from modulation to improve the effect of radiation.

T1 mapping

T1 mapping MRI has been established in the cardiac setting where it has been correlated with pathological findings of fibrosis[154-156]. This relationship has also been demonstrated in liver disease[157]. In pre-clinical cancer research, native MRI T1 values have been shown to provide a quantitative tool for assessing the interstitial environment and response to treatment[158, 159]. In a study of rectal cancer patients undergoing radiotherapy, T1 mapping has been suggested to demonstrate changes in tumours which may reflect tumour microcirculation[160]. Quantitative T1 changes were also seen in patients with glioblastoma being treated with bevacizumab, in some cases earlier than conventional contrast-enhanced T1-weighted images[161], with similar findings by Müller et al[162] in the same tumour type.

ShMOLLI T1 mapping

Using a protocol developed for myocardial tissue characterisation[163], Shortened Modified Look-Locker Inversion recovery (ShMOLLI) T1 mapping has been developed at the University of Oxford to detect changes in the extracellular space, including oedema[164] and fibrosis[165]. Three trials have demonstrated correlation between histological measures of fibrosis and ShMOLLI T1 values in the setting of cardiovascular[166, 167] and liver disease[165]. ShMOLLI builds upon T1 mapping sequences with a shorter breath-hold and immediate map reconstruction directly on the scanner. It is postulated that the addition of supplemental oxygen breathing to ShMOLLI T1 mapping will provide a practical, relatively rapid method of assessing changes in rectal tumours with therapy.

6. Perfusion

Tumour vasculature often differs significantly to that of normal tissue. Release of factors promoting angiogenesis can cause formation of tortuous, hyper-permeable and disorganised vasculature[168]. Tumour perfusion may be altered as a result, which can lead to restricted delivery of systemic therapy[169] and varying degrees of hypoxia, limiting response to RT[170]. Dynamic imaging with contrast-enhanced CT and MRI provides a non-invasive means of evaluating tumour vasculature and angiogenesis[171]. Evaluation over time may highlight changes in perfusion with tumour growth, evolution and response to treatment.

Whilst the relationship between morphological pathological features and clinical imaging has been established[43, 63], correlation with functional imaging parameters has proved more challenging. In rectal cancer, both perfusion CT (pCT)[172-176] and DCE-MRI[177-179] parameters have not correlated consistently with histopathological markers of vascularity. Reasons may include differences in spatial resolution and difficulties in matching tumour regions. However, it may represent real differences in postoperative anatomical specimen data and *in vivo* measures of tumour pathophysiology[180].

6.1 Perfusion CT

Perfusion CT has been evaluated as both a predictive and prognostic biomarker and for monitoring treatment effects in various tumours[176]. Dual compartmental modelling provides various parameters outlined in Box 1.2. The Johnson Wilson distributed parameter model[181] is based upon the use of arterial and tissue-time concentration curves to calculate impulse residue function (IRF). The IRF is the fraction of contrast medium remaining in tissue over time, following a bolus injection into arterial input[182].

In rectal cancer, chemoradiation has been shown to alter blood volume (BV), blood flow (BF),

permeability surface area product (PS) and mean transit time (MTT), useful to discriminate patients by response[183-185]. Blood flow was also found to be a marker for predicting survival in rectal cancer patients undergoing surgery[186]. However pCT parameters have not correlated consistently with histopathological markers of vascularity[172-176]. Reasons may include differences in spatial resolution and difficulties in matching tumour regions. However, it may represent real differences in postoperative anatomical specimen data and *in vivo* measures of tumour pathophysiology[180].

BOX 1.2: Definitions of pCT Quantitative parameters[187]	
Blood volume (BV)	The proportion of tissue that comprises flowing blood (mL/100g tissue)
Blood flow (BF)	Blood flow per unit mass of tissue (mL/min/100g tissue)
Permeability surface area produce (PS)	The product of permeability and total surface area of capillary endothelium in unit mass of tissue (mL/100g/min)
Mean Transit Time (MTT)	Meant time for blood to perfuse a region of tissue (s)

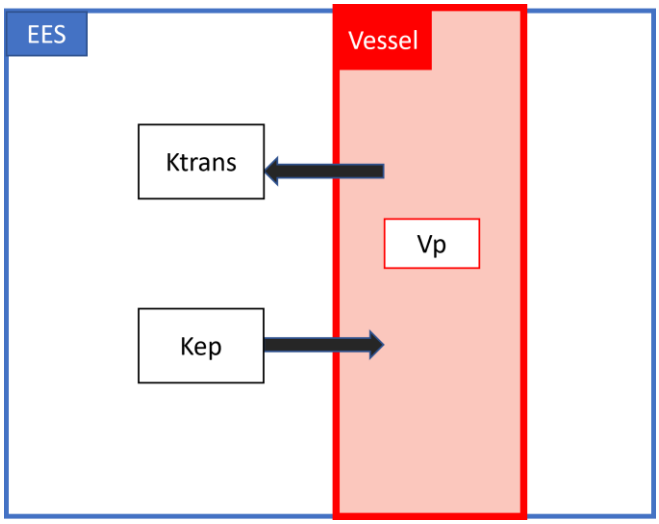
6.2 Dynamic Contrast-Enhanced MRI

DCE-MRI involves the baseline acquisition of a T1 map prior to injection of an intravenous bolus of gadolinium with rapid acquisition of T1-weighted images[188]. The enhancement pattern obtained from DCE-MRI depends on a variety of factors including vascularity, capillary permeability, and volume and composition of extracellular fluid[189]. The Arterial Input Function (AIF) is the concentration of contrast in the blood as a function of time. It is required for quantitative DCE-MRI analysis and may be obtained through three approaches. The first is with arterial blood sampling[190] which provides for accurate, individualised readings but is invasive and may be

ambiguous as to the exact time of sampling. The second method assumes a population AIF[191], which is less invasive and simplifies data analysis. However, it can introduce errors due to ignoring potential differences in AIF between subjects. The third method involves obtaining AIF from the DCE-MRI data, using a large blood vessel within the field of view[192]. Advantages are that it is non invasive and individualised. However it necessitates adequate imaging of a suitable blood vessel within the field of view and unaffected by factors such as flow effects or partial volume. This requires a high spatial resolution and SNR[188].

The Tofts-Kety 2-compartmental model[193] is most frequently employed in DCE-MRI analysis[188] and is shown in Figure 1.1. The relevant quantitative parameters are defined in Box 1.3.

Figure 1.1: Tofts-Kety 2-compartmental model[193] (adapted from[194]



EES: Extravascular, extracellular space; Ktrans: volume transfer constant; Kep: transfer function from EES to plasma (vessel) space; Vp: blood plasma volume

BOX 1.3: Definitions of DCE-MRI Quantitative parameters[193, 195]	
Ktrans	Volume transfer constant between blood plasma and EES (min^{-1})
Kep	Rate constant between EES and blood plasma (Ktrans/Ve) (min^{-1})
Ve	Volume of extravascular extracellular space per unit volume of tissue
Vp	Blood plasma volume per unit tissue volume

These DCE-MRI quantitative parameters have been evaluated for response prediction and assessment following CRT. In rectal cancer, few have been consistently linked with outcome, save for Ktrans, which reflects blood flow and permeability. It was demonstrated to predict response at baseline[61, 196] and determine good response[197-199] or pCR[200] at post-treatment imaging. It has also been associated with the development of distant metastases[201, 202].

7. Glucose metabolism

7.1 ^{18}F-Fluorodeoxyglucose PET-CT (FDG PET)

2-[^{18}F]-Fluoro-2-deoxy-d-glucose is a radiopharmaceutical tracer widely used in the oncological setting. The half life is 109.8 minutes and it is rapidly distributed throughout the body once injected. Once transported into cells via glucose transporters such as GLUT (often overexpressed in malignancy), it is phosphorylated to ^{18}F-FDG-6-phosphate at a rate proportional to the rate of glucose utilisation within a given tissue. This entity cannot then diffuse out of the cell although can be dephosphorylated slowly by glucose-6-phosphate[203]. Most cancer cells have elevated glucose metabolism via various mechanisms, a significant one being the phenomenon known as the Warburg effect[204]. Broadly speaking, in normal cells, glucose utilisation occurs through mitochondrial oxidative phosphorylation, generating adenosine triphosphate (ATP). In a low oxygen environment, a less efficient glycolysis pathway leading to lactate via fermentation of pyruvate occurs[205]. Warburg found that in malignancy, this pathway was frequently enhanced even in the presence of abundant oxygen.

The mechanisms of FDG accumulation in cancer cells relies on a variety of factors in addition to tumour glucose metabolism. These include vascularity, tumour size and hypoxia[206]. Imaging may also be affected by serum glucose level and local inflammation, such as may occur with infections, leading to false-positives and lower specificity[203]. A variety of parameters has been proposed to describe FDG PET-CT and are shown in Box 1.4.

Box 1.4: FDG PET parameters[207-210]

SUV (g/mL): Activity in the volume of interest *r* (kBq/mL) normalised by the decay-corrected injected dose *a'* (kBq) by weight of patient *w* (g)

$$SUV = r/(\frac{a'}{w})$$

SUVmax: The highest SUV value within a single voxel in the volume of interest

SUVpeak: The activity in a small volume (in this study a sphere of 1 cm^3) centred over the highest uptake region in the volume of interest

Metabolic tumour volume (MTV in cm^3): metabolically active tumour region of interest (ROI) defined by user or algorithm

Total lesion glycolysis (TLG in g cm^3/mL): product of mean SUV and MTV

The use of FDG PET-CT for outlining of gross tumour volume in rectal cancer has been shown to produce smaller volumes than CT alone and reduce interobserver variation[211]. Roels et al[41] found that FDG PET-CT at baseline could define a target volume for dose escalation with reimaging during radiotherapy allowing for treatment adaptation according to response. In addition, a meta-analysis has indicated that SUV parameters measured early during RT may be predictive of response[212]. Further studies have demonstrated that FDG-PET provides information about metabolic response based on SUV changes, which has been correlated with TRG[213, 214]. However, identification of patients with pCR has not been shown consistently[215-218]. One meta-analysis has suggested that responders have a significantly lower post-CRT SUVmax[219]. However a major limitation of SUV is that it provides information about one voxel within a tumour, which may not accurately reflect heterogeneous tumours.

Total lesion glycolysis (TLG)[210] provides an indication of both metabolic activity and volume, potentially better reflecting the disease burden in various solid tumours[220]. In resectable colorectal adenocarcinomas, unlike SUV, pre-operative TLG was found to be predictive for DFS[221] and OS[222] in multivariate analysis. In terms of response to neoadjuvant long course radiotherapy, Guillem et al[223] found changes in TLG four to five weeks post treatment compared with baseline did not consistently correlate with pathological response. Bang et al[224] found similarly analysing pre-treatment scans but did show an association between TLG and 3 year disease survival, albeit weak. Alongi et al[225] demonstrated higher TLG values at baseline where pathological TRG was greater than 2. In a retrospective analysis, Sert et al[226] found TLG was an unfavourable prognostic factor for OS with a median follow-up of 39 months. Okuno et al[227] in a further retrospective study found that SUVmax was associated with pCR and TLG with poor prognosis both in terms of recurrence risk and 5 year mortality.

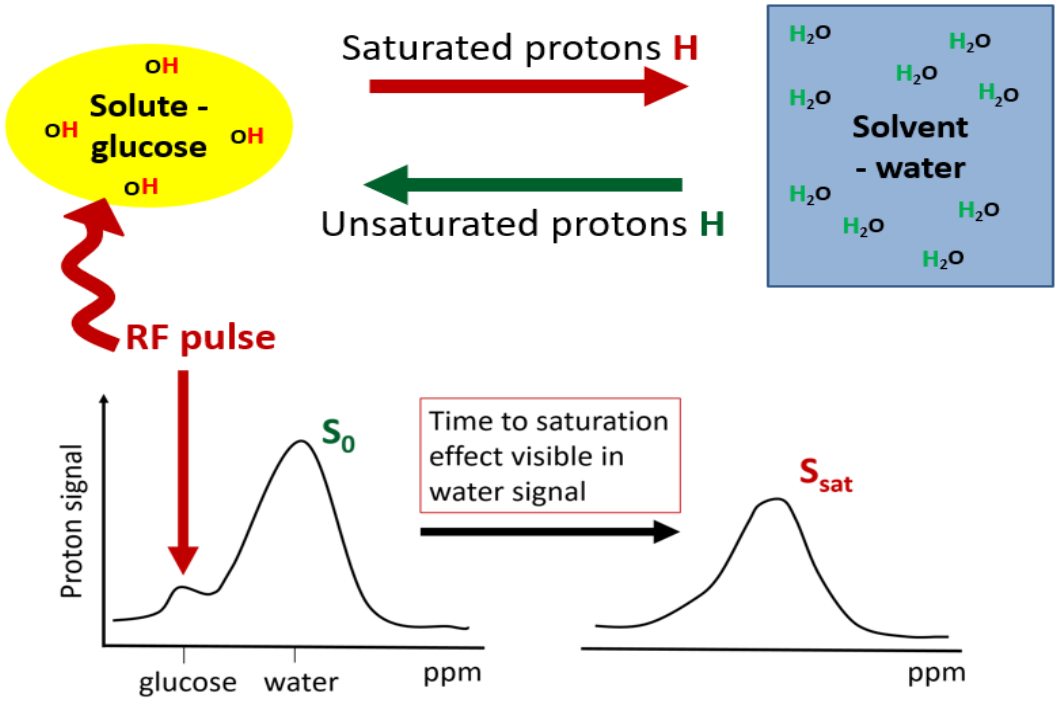
7.2 Glucose Chemical Exchange Saturation Transfer (glucoCEST) MRI

Chemical exchange saturation transfer (CEST) MRI allows for the indirect detection of specific compounds. A signal is obtained when a radiofrequency (RF) pulse is applied at the natural frequency of a compound with exchangeable protons or molecules (Figure 1.2). In glucoCEST MRI, this is the hydroxyl groups of dextrose (D-glucose), which may be endogenous and exogenous. The saturated protons within the solute (glucose) are exchanged with unsaturated protons in the solvent (water) until a steady state is reached. Z-spectra are plotted at S_0 and S_{sat}.

Comparison is made between the signal at baseline (S_0) and saturation (S_{sat}). This provides a relative measure of the target compound, provided by the decrease in water signal reduced by the saturation transfer process. Other effects as a result of the RF pulse must also be considered, including the magnetisation transfer contrast (MTC) and direct water saturation. MTC, like the CEST effect, involves the transfer of saturated protons with non-saturated protons in water. Unlike CEST

this process is within semi-solid macromolecules across a broad spectrum and is more affected by the bandwidth of the RF pulse than spectral position. The direct water saturation effect is due to the RF pulse affecting the local water-proton magnetisation[228]. To account for this, the CEST effect at position +τ is compared with the water signal reduction at the opposite spectral location -τ, with the spectrum centred on water at 0 ppm. A key assumption is that MTC and direct water saturation effects are symmetrical about the water frequency[229]. Magnetisation Transfer Ratio (MTR) asymmetry is calculated as per Box 1.5.

Figure 1.2: The mechanism of glucoCEST MRI showing z-spectra



ppm = parts per million

Box 1.5: Magnetisation Transfer Ratio asymmetry (MTRasym)[228]

$MTRasym\ (+\tau) = S_{sat}(-\tau) - S_{sat}(+\tau) / S_0$

S_0: Signal at baseline

S_{sat}: Signal at time of saturation following radiofrequency pulse

τ: Spectral position with respect to water

GlucoCEST was found to be comparable to FDG-PET autoradiography in human colorectal tumour xenograft mouse models[230] and Capozza et al[231] found that the MRI findings appeared more sensitive than FDG-PET in murine triple negative breast cancer. Wang et al[232] demonstrated the feasibility of glucoCEST imaging in HNSCC patients on 3T MRI. FDG-PET is used routinely in the assessment of cancer patients but it is time-consuming and involves ionising radiation; MRI may represent a potential alternative modality with enhanced anatomical detail.

8. Immunohistochemistry

Immunohistochemical confirmation of imaging findings has been important for validation, as an established method for qualitatively and quantitatively assessing multiple tumour pathological features. As discussed above, the correlation between functional imaging findings and pathology is not always clear as living physiological processes are compared with fixed tissue staining.

8.1 Carbonic Anhydrase IX (CAIX)

At the molecular level, hypoxia-inducible factors (HIF) are key transcription factors induced by hypoxia. CAIX, an inducible downstream gene expressing a transmembrane protein, is widespread and stable, providing a reliable endogenous histological marker of hypoxia[233]. It is known to be

expressed in colorectal adenocarcinomas, often in a diffuse pattern associated with areas of high proliferation[234]. An *in vivo* study using a colorectal cancer line in a murine model has suggested that poorly perfused areas are associated with increased CAIX expression, often in perinecrotic regions[235].

A meta-analysis of the prognostic significance of CAIX in common solid tumours found strong significant associations with endpoints including OS, DFS, PFS and locoregional control[236]. In the colorectal subgroup, this remained significant for DFS and PFS. Bekku et al[237] noted that in colorectal cancer, the expression of CAIX correlated with biological aggressiveness and synchronous distant metastases. In rectal cancer, Korkeila et al[238] found CAIX expression was associated with worse DFS in a mixed cohort of patients, over half of whom had some form of neoadjuvant radiotherapy. CAIX has a long half life and remains in cells after the inducing hypoxia has eased[239], therefore it could be present in oxygenated tissue that has previously been hypoxic.

8.2 Pimonidazole

Pimonidazole is an exogenous agent which may be taken orally prior to tumour resection in order to indicate areas of hypoxia. It has a short half life and diffuses into tumour and normal tissue irrespective of blood supply. Like FMISO, pimonidazole contains a 2- nitroimidazole molecule that is reduced intracellularly at pO_2 < 10 mmHG to intermediates that form stable complexes with cellular macromolecules via covalent bonding. This can then be detected by specific antibody staining[240].

In a control group of murine human colorectal xenografts, Shin et al[241] found that pimonidazole exhibited similar though not identical spatial distribution. The fraction of positive staining was also comparable. In the experimental groups, they provided carbogen to increase tumour oxygenation and hydralazine to reduce oxygenation respectively, shortly prior to sacrifice. In both groups, the

CAIX positive fraction was unaltered compared with controls whereas the pimonidazole increased in the hydralazine group and reduced with carbogen. This suggests pimonidazole is better able to demonstrate acute hypoxia and comparing this with CAIX may allow for detection of reoxygenation.

This mismatch between CAIX and pimonidazole was found in colorectal cancer liver metastectomy specimens. Co-localisation was observed between the two markers but micoregional areas of mismatch were also seen. There was no correlation in staining intensity[242]. However, in human colorectal cancer primary tumour resections, Verstraete et al[243] compared the distribution of CAIX, pimonidazole and microvessel density (MVD) and found no correlation between the intrinsic markers and pimonidazole. Within patients undergoing RT, Kaanders et al[244] found that a higher pimonidazole-defined pre-treatment hypoxic fraction on HNSCC biopsies correlated with a reduced locoregional tumour control. CAIX expression showed a similar distribution pattern to pimonidazole but was generally observed at shorter distances from the blood vessels. There was no relationship found between CAIX expression and treatment outcome. In xenograft HNSCC models, the residual pimonidazole hypoxic volume at two weeks into a course of fractionated RT was associated with radioresistance[245]. Pre-treatment hypoxic volumes did not demonstrate this finding, which suggests hypoxia imaging during radiotherapy could provide useful prognostic information and potential for intervention in terms of radiotherapy boost.

8.3 Cluster of differentiation 31 (CD31)

CD31 is a transmembrane glycoprotein constitutively expressed on endothelial and some haematopoetic cells. It is widely used as a relatively specific and sensitive vascular IHC marker[246]. It has been used in the clinical setting to determine MVD, for example in colorectal cancer[247, 248] where a high MVD has been related to poor recurrence free survival (RFS) and OS[249, 250]. Pimonidazole expression has been inversely correlated with MVD as might be expected but the

relationship was less clear with CAIX and MVD[251].

8.4 IHC and functional imaging

Comparing IHC and functional imaging has significant challenges, as demonstrated by the inconsistent results discussed above. The differences in scale are considerable as even with clinical 3T MRI, the resolution of a few millimetres is significantly greater than the micrometer scale used in pathology. Formalin fixation of tissue for histopathological analysis can result in shrinkage and distortion, leading to further difficulties in direct spatial comparison[252]. Functional imaging aims to capture a living physiological process which ceases at the point of resection and therefore cannot be fully captured by pathological methods. Nevertheless, it remains important to interpret imaging findings, particular novel modalities, in the context of likely underlying pathophysiology indicated by IHC.

9. Thesis outline

The work presented in this thesis explores multimodality functional imaging in rectal cancer patients treated with radiotherapy.

Chapter 2 introduces the RHYTHM and RIT studies upon which much of the work presented is based. These studies recruited patients undergoing radical treatment for rectal cancer.

Chapter 3 explores the use of FMISO PET and oxygen-enhanced MRI in rectal cancer and compares this to IHC. The aims are:

- Identification of an FMISO-PET derived hypoxic volume based upon uptake thresholds and changes with radiotherapy
- Investigation of changes in MRI T1 with oxygen breathing and with radiotherapy

- To compare IHC markers of hypoxia (CAIX, pimonidazole) with functional imaging findings

Chapter 4 investigates the use of dynamic and perfusion imaging in rectal cancer in the form of pCT, DCE MRI and dynamic FMISO PET-CT. The aims are:

- Identification of changes in blood volume and flow with radiotherapy using perfusion CT
- Investigation of DCE MRI parameter Ktrans in patients being treated with radiotherapy
- Assessment of dynamic FMISO PET imaging parameters in tumour response to radiotherapy

Chapter 5 assesses the role of glucose metabolism in LARC assessment with FDG PET-CT and novel imaging technique glucoCEST MRI. The latter is investigated further in HNSCC patients undergoing RT. The aims are:

- Assess the utility of FDG-PET for CRT response prediction in LARC
- Establish the use of glucoCEST using phantoms and volunteers
- Evaluate glucoCEST MRI use in LARC and HNSCC patients undergoing radiotherapy

The thesis concludes in Chapter 6 with a summary of the results and discussion of areas for future study that have arisen.

Chapter 2: Rectal cancer imaging studies

1. RHYTHM study

The RHYTHM (modulation of Radiotherapy according to HYpoxia: exploiting changes in the Tumour Microenvironment to improve outcome in rectal cancer) study was originally conceived by Dr J. Wilson (Clinical Research Fellow, Department of Oncology, University of Oxford) and Professor T. Maughan (Chief Investigator, Department of Oncology, University of Oxford). Patients with adenocarcinoma of the rectum were recruited into two groups, going either straight to surgery or for neoadjuvant chemoradiotherapy depending on the clinical management plan.

1.1 Study aims

The primary objective of the RHYTHM A study was to assess the utility of FMISO-PET imaging in quantifying and defining the spatial distribution of hypoxic regions within rectal cancer. Within RHYTHM B the aim was to assess the changes in hypoxia after 8 – 10 fractions of neoadjuvant chemoradiotherapy.

Secondary objectives included comparison of FMISO-PET findings with perfusion CT parameters, oxygen-enhanced and DCE MRI and immunohistochemical markers of hypoxia and vascularity.

1.2 Patient selection

All patients must be at least 18 years old and able to consent to participate in the study.

RHYTHM A

Patients were eligible if they had a T2 or T3 N0 M0 adenocarcinoma of the rectum which did not involve or threaten the circumferential resection margin (CRM). The tumour had to measure at

least 2 cm x 2 cm on clinical CT or MRI and be confirmed by the MDT as resectable without neoadjuvant therapy.

RHYTHM B

Patients were eligible if they had non-metastatic histologically confirmed adenocarcinoma of the rectum threatening or involving the mesorectal fascia, or low tumours involving or close to levators or sphincters. They were to be considered suitable for surgery post CRT.

Exclusion criteria

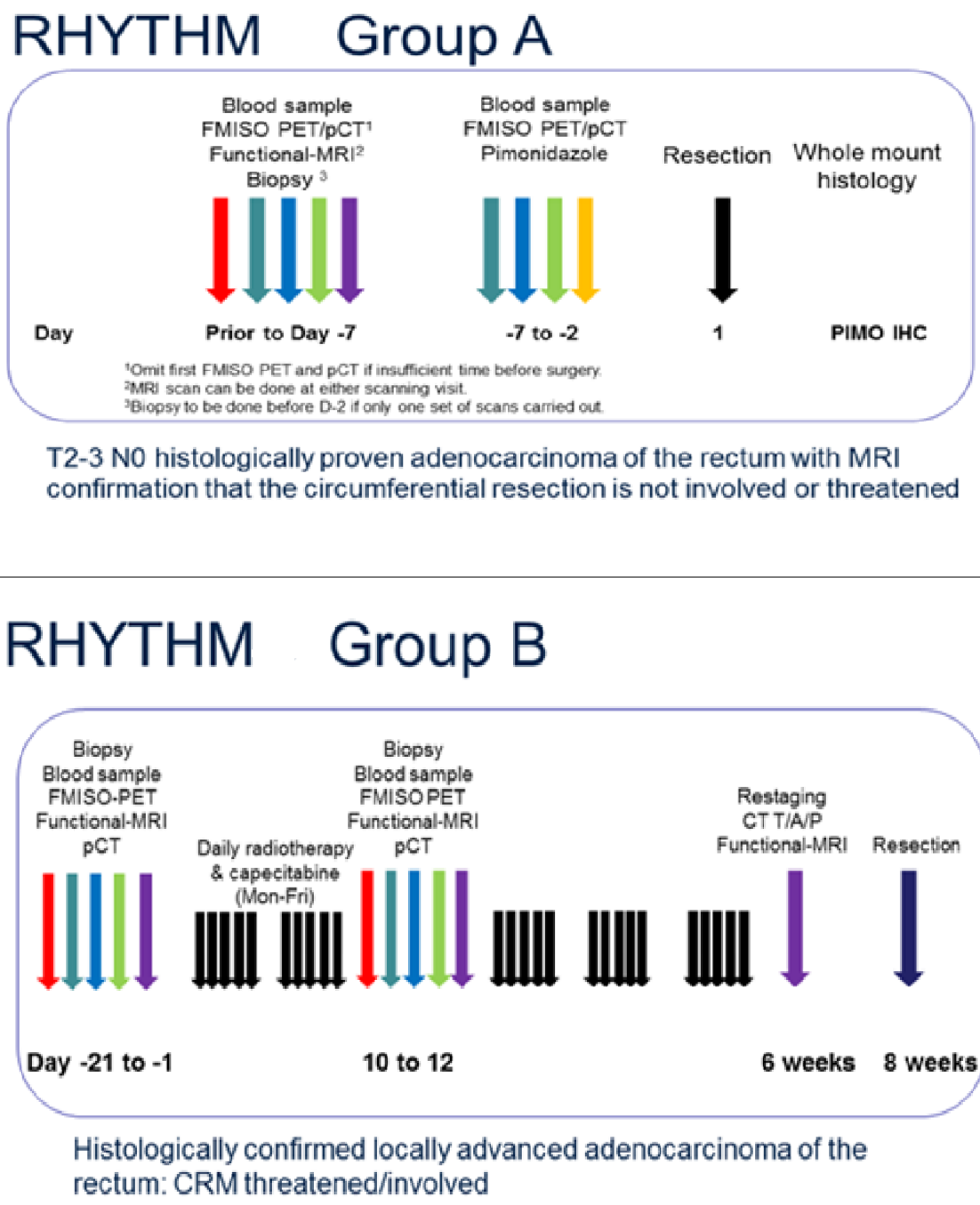
Patients were excluded if they had any contraindications to study intervention or had previous pelvic radiotherapy. Patients could still participate in the study if they were unable to undergo oxygen-enhanced MRI for example if they had lung disease with risk of hypercapnia.

1.3 Study timeline

Figure 2.1 shows the timeline of events for RHYTHM A and B.

RHYTHM A provided for test-retest validation of FMISO PET in the initial iteration. A protocol amendment allowed for one scan only prior to surgery if necessary due to time constraints.

Figure 2.1: RHYTHM study group A and B timelines



FMISO = ^{18}F-Misonidazole; PET = positron emission tomography; pCT = perfusion CT; MRI = magnetic resonance imaging; PIMO = pimonidazole; CT T/A/P = Computerised tomography thorax/abdomen/pelvis

1.4 Trial interventions

RHYTHM A

Straight-to-surgery patients underwent an additional tumour biopsy under proctoscopy guidance prior to Day -7. Between Day -7 and -2, patients underwent FMISO-PET, pCT and fMRI. The PET and pCT were to be repeated (if time allowed, following protocol amendment). Between 16 to 24 hours prior to surgical excision, oral pimonidazole 500mg/m^2 was taken. Patients underwent surgical resection on Day 1 (either low anterior resection of abdominoperineal resection depending on the MDT decision). The resected specimen was then mounted such that it could be directly correlated with imaging studies.

RHYTHM B

Baseline FMISO PET, pCT and fMRI were undertaken within the 21 days prior to initiation of CRT but preferably within the week prior to starting therapy. Functional MRI included DCE with the later addition of oxygen-enhanced T1 mapping. Additional tumour biopsies were taken under proctoscopy guidance at least 24 hours apart from the imaging. Biopsies and all imaging modalities were repeated following 8 to 10 fractions of radiotherapy. A further fMRI was undertaken with routine staging CT and MRI rectum 6 to 8 weeks following completion of CRT. Patients were then considered again for surgical resection by the MDT.

Chemoradiotherapy was delivered as per standard of care[253] with patients receiving 45 Gray in 25 fractions over five weeks, attending five days a week. Oral capecitabine chemotherapy 900mg/m^2 BD was given concurrently. Intensity modulated radiotherapy (IMRT) was delivered using a 5 or 7 field technique as per departmental protocol. The primary tumour, pelvic lymph nodes and mesorectum comprised the planned target volume.

A full list of scan acquisition parameters and MRI sequences can be found in Appendix 1.

1.5 Major protocol amendments

Following recruitment and analysis of the first 6 patients, the addition of an enema prior to the 4 hour FMISO PET-CT at each time point was made. Oxygen-enhanced MRI was added to the fMRI scan and the requirement for two sets of imaging prior to surgery in RHYTHM A was removed if time constraints would not allow for this.

1.6 Recruitment

The RHYTHM study opened to recruitment in December 2013. Recruitment was undertaken at the Oxford University Hospitals NHS Foundation Trust. The initial protocol planned for recruitment of 5 patients in group and 10 in group B. These numbers were chosen to give reasonable assessment of the endpoints in this observational study within a reasonable time frame At the time of trial closure, three patients were recruited in the straight to surgery arm (RHYTHM A). Eleven patients who were receiving standard neoadjuvant chemoradiotherapy prior to resection were recruited into RHYTHM B. As per the protocol, a further patient was recruited as RHB10 did not have FMISO PET scans due to cyclotron breakdown pre-treatment. Dr J. Wilson recruited the first RHYTHM A patient and the first 5 RHYTHM B patients with the remaining 2 and 6 patients respectively recruited by the author. Due to continued difficulties recruiting to group A because of time constraints in the patient pathway, recruitment was stopped on 30/04/2016 before reaching the intended number of participants. The trial closed on 22/11/2016.

1.7 Patient characteristics

The RHYTHM study patient characteristics are shown in Table 2.1.

Demographics and tumour features

The median age of patients recruited in RHYTHM A was 49 (IQR 10) compared with 67 (IQR 19) in

RHYTHM B. All patients in RHYTHM A were male as were 9 (82%) in RHYTHM B. All patients had T2 or T3 disease with the majority being T3 (67% in RHYTHM A and 82% in RHYTHM B). All RHYTHM A patients had node negative disease on preoperative imaging. In RHYTHM B, 4 (36%) patients had N0 disease, 6 (55%) had N1 and 1 (9%) had N2. All had no evidence of metastatic disease on a routine baseline staging CT scan.

Treatment

All RHYTHM A patients underwent TME as planned. All patients in RHYTHM B received neoadjuvant CRT 45Gy in 25 fractions with capecitabine. RHB06 did not have capecitabine for 11 days due to thrombocytopenia but otherwise all patients completed the treatment course as planned. Of 7 (64%) patients who underwent TME in RHYTHM B, 1 had complete response in the primary but a residual involved node. Of 3 patients who did not have surgery, 2 had a good clinical response initially, 1 then going on to have surgery after 6 months. The other declined surgery despite residual disease. Response to CRT was defined as good in 7 (64%) of patients and poor in 4 (36%) of patients.

Table 2.1: RHYTHM Study Patient Characteristics

(Median (IQR) or Number of patients (%))

Group	**RHYTHM A**	**RHYTHM B**
Number	3	11
Age	49 (IQR 10)	67 (IQR 19)
Male	3 (100%)	9 (82%)
Tumour stage (MRI)		
T2	1 (33%)	2 (18%)
T3	2 (67%)	9 (82%)
Nodal stage (MRI)		
N0	3 (100%)	4 (36%)
N1	-	6 (55%)
N2	-	1 (9%)
Metastasis stage (CT)		
M0	3 (100%)	11 (100%)
Differentiation		
Well	-	1 (9%)
Moderate	3 (100%)	6 (55%)

Poor	-	1 (9%)
Not specified*	-	3 (27%)
Underwent TME	3 (100%)	7 (64%)
Response to CRT		
Good	-	7 (64%)
Poor	-	4 (36%)

*no single value specified –mix of well to moderate or moderate to poor

1.8 Response assessment

Response to chemoradiotherapy was defined by AJCC 7th edition TRG scoring[254]. This was undertaken by two consultant pathologists blinded to the other's results (Professor R. Goldin [RG], University College London and Dr Lai-Mun Wang [LMW], Oxford University Hospitals). The score ranges from 0 (complete tumour response) to 3 (poor response with minimal or no tumour cells killed). Response was defined as good where patients had AJCC TRG score 0/1, or good clinical response where surgery was not undertaken. Poor responders had AJCC TRG score 2/3 or poor clinical response.

Clinical response was based upon imaging, endoscopy and biopsy post CRT. MRI rectum scans 6 – 8 weeks post radiotherapy were assessed by a consultant radiologist (MA) using the TRG graded ratings 1 (complete response) – 5 (no response) proposed by the Mercury group[44, 45, 255]. Where surgery was delayed post radiotherapy due to a good clinical response and subsequently

undertaken due to progression, initial imaging/endoscopic findings were used rather than pathological TRG. In view of this, a composite definition for 'good' and 'poor' outcome was used (see Box 2.1).

Box 2.1: Response to chemoradiotherapy criteria

Good response:

Pathological TRG 0/1 if available & no delay to surgery OR

MRI TRG 1-2 AND

Flexible sigmoidoscopy shows no active disease with decision for active surveillance

Poor response:

Pathological TRG 2/3 if available & no delay to surgery OR

MRI TRG 3-5 AND/OR

Flexible sigmoidoscopy confirms disease persists

Response outcomes for RHYTHM study

These results are shown in Table 2.2. There was discrepancy seen between MRI and histological TRG in 2 of 8 patients with data available. These cases were reviewed. Two patients (RHB01, RHB08) did not have surgery for 2 months after the MRI scan for operational/personal reasons, which may explain the discrepancy seen between imaging and pathological TRG. In these patients the pathological outcome was taken as the true outcome for subsequent analyses. One patient (RHB11) underwent active surveillance due to a good response on the 6-week post-treatment MRI and confirmed at flexible sigmoidoscopy. Surgery was undertaken at sign of disease progression

approximately 6 months later. Three patients did not undergo surgery, one as the patient declined due to risks and two with good clinical response who opted against TME. Histological TRG is available in 8 patients and MRI TRG in all patients.

Table 2.2: Overall response assessment of RHYTHM B patients undergoing CRT

	MRI		Pathological		Outcome
Study #	**BL stage**	**TRG post CRT**	**AJCC TRG**	**Stage (yp)**	
RHB01	T3N1	5	1	T3N2	Good*
RHB02	T3N1	2	1	T3N1	Good
RHB03	T3N0	4	3	T3N0	Poor
RHB04	T2N0	2	2	T3N0	Poor
RHB05	T3N0	1	N/A	N/A	Good
RHB06	T2N1	5	N/A	N/A	Poor
RHB07	T2N0	2	N/A	N/A	Good
RHB08	T3N2	5	1	T3N2	Good*
RHB09	T3N0	4	2	T3N1	Poor
RHB10	T3/4N2	5	0	T0N1	Good
RHB11	T3N1	2	2	T3N0	Good**

BL = baseline; TRG = tumour regression grade; CRT = chemoradiotherapy; AJCC = American Joint Committee on Cancer; *MRI and tumour TRG show discrepancy in response outcome (see text for discussion); **Delayed surgery due to good response on imaging & active surveillance, clinical outcome used

Further methodology is discussed in the relevant results chapters.

2. RIT study

The Rectal Imaging Trial (RIT) was initially conceived by Professor F. Gleeson (Chief Investigator, Department of Radiology, University of Oxford). Patients with rectal adenocarcinoma for neoadjuvant chemoradiotherapy had FDG PET-CT and fMRI at baseline with a repeat fMRI after 6 to 10 fractions of radiotherapy and again at 6 to 8 weeks post CRT with standard staging CT and MRI rectum. RIT was divided into three phases or cohorts, discussed below in 'Major protocol amendments'.

2.1 Study aims

The primary objective was to assess an association between FDG PET parameters and histological regression grade. The secondary objective was to assess the ability of fMRI to predict or confirm response to CRT.

2.2 Patient selection

Inclusion criteria

Any patient of at least 18 years of age, able to consent and for whom neoadjuvant CRT for rectal adenocarcinoma was advised by the MDT was eligible to participate.

Exclusion criteria

Patients were excluded if they had any contraindications to study interventions. Patients could still participate in the study if they were unable to undergo oxygen-enhanced MRI or glucoCEST MRI, for example if they had type 1 or poorly controlled type 2 diabetes mellitus.

2.3 Trial interventions

Within the three weeks prior to commencing CRT but as close as possible to D1, patients underwent

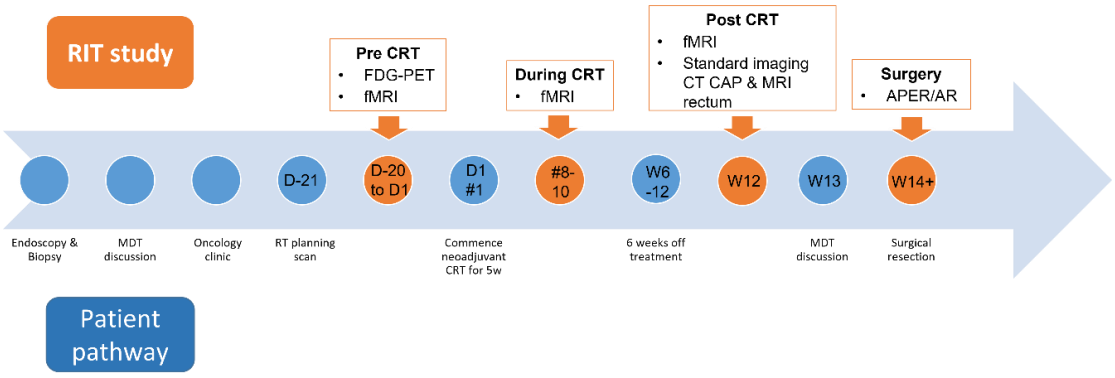
an FDG PET-CT and functional MRI. This included DCE MRI for all patients and oxygen-enhanced and glucoCEST MRI following protocol amendments.

Chemoradiotherapy was delivered as per standard of care in RHYTHM section 1.4, except that a radiotherapy boost was permitted to 50.4 Gy in 28 fractions in RIT 1.

2.4 Study timeline

Figure 2.2 shows the timeline of events for RIT.

Figure 2.2: RIT study timeline



2.5 Major protocol amendments

RIT 1 patients underwent functional MRI including DCE. During RIT 2, oxygen-enhanced MRI was added and for RIT3, glucoCEST MRI was included and imaging was transferred from the 1.5T to 3T scanner.

2.6 Recruitment and patient characteristics

RIT was conceived as a pilot study without a formal power calculation. Protocol update had allowed

for up to 88 patients to be recruited. Recruitment was undertaken at the Oxford University Hospitals NHS Foundation Trust. The RIT study has been divided into three groups to reflect the two major protocol amendments discussed above. The first 46 patients (RIT1) were recruited by Dr M. Anderson (MA, Consultant Radiologist, Department of Radiology, Oxford University Hospitals NHS Foundation Trust) and Dr J. Franklin (JF, Clinical Research Fellow, Department of Oncology, University of Oxford) from 2007 to 2014. However, 16 participants' scans were unsuitable for the analysis below as they were scanned on an alternative MRI due to breakdown. All information regarding these participants has been excluded.

The remaining patients (15 in RIT 2, 2 in RIT 3) were recruited by the author from 2015 to 2017 before the study was closed in 2018 as it was not feasible to recruit the amended total number within a reasonable time period. Table 2.3 shows the characteristics of the RIT patients.

Within RIT 1, one patient died during treatment. Five patients had a pCR, including one who had TEM rather than TME. Two patients did not proceed to surgery, both of whom were poor responders.

In RIT2, two patients were found to have hepatic metastases on FDG-PET; one was withdrawn as they did not go on to have neoadjuvant radiotherapy. All other patients received 45 Gy in 25 fractions with concurrent capecitabine chemotherapy 900 mg/m^2 BD. Eight had TME with 1 pCR. Three patients who did not undergo surgery all had a good clinical response to treatment and were followed up as per a 'watch and wait' policy with regular endoscopy and imaging.

Table 2.3: RIT patient characteristics (Median (Inter Quartile Range) or Number of patients (%*))

Group	**RIT overall**	**RIT1**	**RIT2**	**RIT3**
Number of patients	47	30	15	2
Median age	67 (IQR 15)	66 (IQR 14)	67 (IQR 12)	46
Tumour stage (MRI)				
T2	4 (9%)	3 (10%)	1 (7%)	0
T3	30 (64%)	18 (60%)	10 (67%)	2 (100%)
T4	13 (28%)	9 (30%)	4 (27%)	0
Nodal stage (MRI)				
N0	13 (28%)	7 (23%)	4 (27%)	2 (100%)
N1	20 (43%)	12 (40%)	8 (53%)	0
N2	14 (30%)	11 (37%)	3 (20%)	0
Metastasis stage (CT)				
M0*	47 (100%)	30 (100%)	12 (100%)	2 (100%)
Surgery				
TME	37 (79%)	27 (90%)	9 (60%)	2 (100%)
TEM	2 (4%)**	1 (3 %)	1 (7%)**	0

None	8 (17%)	3 (10%)	5 (33%)	0
Response to CRT***				
Good	20 (43%)	12 (40%)	6 (40%)	2 (100%)
Poor	25 (53%)	17 (57%)	8 (53%)	0
Not applicable	2 (4%)	1 (3%)	1 (7%)	0

* Includes 1 RIT1, 2 RIT2 and 1 RIT3 patients identified as having metastases on PET but not visible on CT; ** Good responder had TEM for recurrence; *** Response defined as per RHYTHM study

RIT 3 comprised of 2 patients both of whom were good responders and went on to have TME.

For RIT 1 and RIT 2 cohorts the median age was similar at 69 (IQR 16) and 67 (IQR 12) respectively, whereas for RIT 3 the median was 46 (2 patients). The majority of patients had T3 disease and N1 status was most common. No patients had definitive metastatic disease on baseline CT CAP.

There were some differences seen between patients in RIT1 and RIT2. Firstly the chemoradiotherapy regimens varied in that in RIT1, radiotherapy boosts to tumour up to 50.4 Gy in 28# whereas in RIT2 with the national Aristotle trial setting the benchmark, a move to 45Gy in 25 fractions was made[256]. Similarly, infusional 5-fluorouracil for 5 days during weeks 1 and 5[20] was being replaced by oral capecitabine twice daily 5 days a week for weeks 1 to 5[257].

This did not appear to have led to any change in response outcome between the two groups as a result, being 'good' in 40% of patients in each. However, there was a difference in terms of surgical resection rates. TME in RIT1 was done in 90% of patients compared with 60% in RIT2 – this is statistically significant (χ^2=7.78, d.f.=1, p=0.01). This may also reflect changes in practice over time as RIT1 patients were recruited from 2007 – 2011 whereas RIT2 were recruited from 2015 – 2017.

Increasing acceptance of active surveillance may be one reason as pCR rates are found in 10 – 20% of patients post CRT and major surgery may be avoided[258]. The pCR rates between the two groups were similar, being 15% (4 of 27 TMEs) in RIT1 versus 13% (1 of 8 TMEs) in RIT2. This was not statistically significant for resected patients or intention to treat (for TME patients χ^2=0.53, d.f.=1 p=0.47. For all patients χ^2=1.35, d.f.=1, p=0.25) using SPSS (IBM Corp. Released 2017. IBM SPSS Statistics for Windows, Version 25.0. Armonk, NY).

2.7 RIT response outcomes

Response to chemoradiotherapy was defined as good or poor as described in RHYTHM Box 2.1 i.e. based on pathological tumour regression grade where available and provided surgery was undertaken in a timely manner with no active surveillance. Table 2.4 shows the outcomes for the RIT study.

Table 2.4: Mercury group MRI and AJCC pathological tumour regression grade with overall response assessment of RIT 1 & RIT2 patients undergoing CRT

Study #	MRI TRG	AJCC TRG	Response
RIT01	3	3	Poor
RIT02	5	3	Poor
RIT03	3	3	Poor
RIT04	1	3	Poor*
RIT05	3	2	Poor
RIT06	3	2	Poor
RIT07	2	3	Poor*
RIT08	3	N/A	Poor
RIT09	1	0	Good
RIT10	3	2	Poor
RIT11	3	2	Poor
RIT12	2	0	Good
RIT13	4	3	Poor
RIT14	N/A	N/A	Withdrawn
RIT15	3	3	Poor

Patient	MRI TRG	AJCC TRG	Response
RIT16	3	1	Good*
RIT17	2	1	Good
RIT18	2	1	Good
RIT19	4	3	Poor
RIT20	2	1	Good
RIT21	2	1	Good
RIT22	2	0	Good
RIT23	3	2	Poor
RIT24	2	1	Good
RIT25	5	1	Good**
RIT26	4	N/A	Poor
RIT27	3	3	Poor
RIT28	2	0	Good
RIT29	1	3	Good**
RIT30	3	2	Poor
RIT31	2	N/A	Good

Patient	MRI TRG	AJCC TRG	Response
RIT32	-	-	Withdrawn
RIT33	4	4	Poor
RIT34	2	1	Good
RIT35	3	4	Poor
RIT36	3	4	Poor
RIT37	2	N/A	Good
RIT38	2	2	Good
RIT39	2	N/A	Good
RIT40	4	3	Poor
RIT41	3	4	Poor
RIT42	3	3	Poor
RIT43	5	N/A	Poor
RIT44	4	2	Good*
RIT45	2	2	Good
RIT46	1	1	Good
RIT47	2	1	Good

N/A = not applicable (see text); AJCC = American Joint Committee on Cancer; TRG = tumour regression grade; *discrepancy between MRI and pathological TRG (see text); **delayed surgery due to good response initially, radiological TRG used

In RIT 1, TRG was assessed using the Dworak system and was transposed to AJCC 7 as per Table 1.1 in Chapter 1. If there was no resection, the post treatment MRI TRG was used as assessed by MA (radiologist with 13 years' experience). Outcome data are not available for the 2 patients who were withdrawn from the study - one died during therapy and the other had neoadjuvant chemotherapy first as they were found to have metastases on study PET-CT.

There was a discrepancy between MRI and pathological TRG in 6 of 39 patients who had both sets of data available. There was a delay between radiotherapy and surgery for RIT25. This patient had surgery 6 months post radiotherapy having also had neoadjuvant chemotherapy when found to have metastases on post RT scans. Interestingly, the 6 weeks post radiotherapy MRI for this patient showed little response in the primary but an excellent pathological response to neoadjuvant treatment was seen. RIT029 had surveillance following good response on MRI, only having surgery at sign of progression. RIT16 showed improvement from MR TRG to surgery, which could be due to ongoing radiotherapy effects. Likewise, RIT44 appeared to have progressed to stage T4 on imaging but at surgery done 8 weeks post imaging, there was a good TRG response. For RIT 04 and 07 there was no significant delay between radiotherapy and surgery or other reason found for the discrepancy between MRI and pathological TRG.

Further methodology is discussed in the relevant results chapters.

3. Discussion of response outcome

The use of pathological tumour regression grade was planned as an outcome measure as it is well established and has been associated with recurrence free survival[30]. The system also identifies those who have had a complete pathological response and does not require longer term follow-up over time as would survival. However, in the cohorts studied, several patients did not proceed to surgery for clinical and personal reasons. In order to include their data given the overall small numbers of participants, a composite score involving imaging, endoscopic and clinical follow-up was used in these cases. This definition for response is used throughout this thesis and should be considered a potential source of error as it is used to define good and poor response.

Chapter 3: Hypoxia imaging using FMISO-PET and Oxygen-enhanced MRI

1. Introduction

In this chapter, the assessment of hypoxia using FMISO-PET and oxygen-enhanced MRI in rectal cancer is discussed. These imaging modalities are compared with histopathological findings at resection.

The aims are to assess the use of hypoxia imaging in rectal cancer by:

- Identification of an FMISO-PET derived hypoxic volume based upon uptake thresholds and changes with radiotherapy
- Investigation of changes in MRI T1 with oxygen breathing and with radiotherapy
- To compare IHC markers of hypoxia (CAIX, pimonidazole) with functional imaging findings

2. 18F-Misonidazole PET-CT

2.1 Methods

FMISO PET scanning was undertaken in RHYTHM Arm A patients going straight to surgery who had a minimum of one scan preoperatively and, time allowing, a second scan for test-retest purposes. In Arm B, patients receiving neoadjuvant radiotherapy were planned for imaging at baseline and at the time of fraction 8 – 10 of treatment.

2.1.1 FMISO manufacture and source

^{18}F-fluoromisonidazole (FMISO) was obtained from the Radiochemistry GMP laboratory, Wolfson

Brain Imaging Centre, Department of Clinical Sciences, University of Cambridge. A GE PETtrace 800 cyclotron is used to produce the radionuclide and Synthra RNPlus automated system prepares ^{18}F-labelled radiopharmaceuticals. The half-life of ^{18}F is 109.8 minutes and it decays by largely positron emission[259].

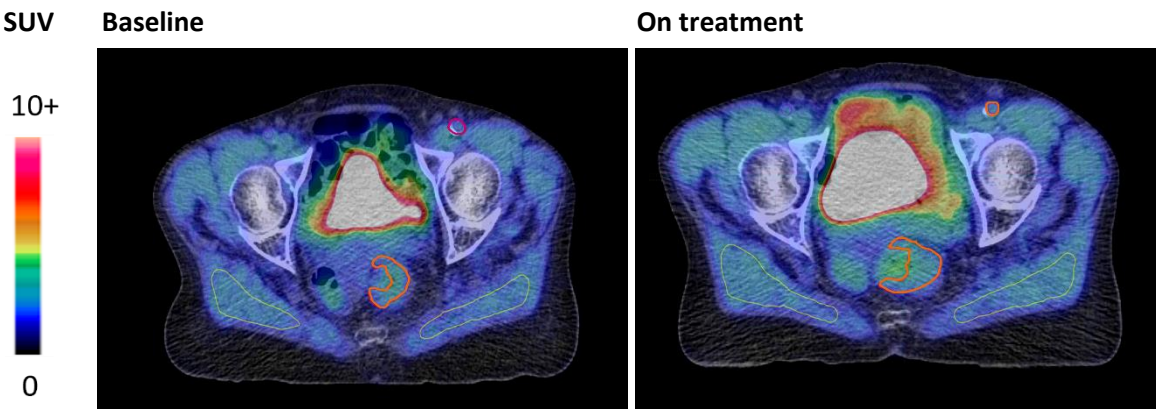
2.1.2 FMISO PET-CT scan acquisition

Imaging was performed on a Discovery 690 PET-CT scanner (see Appendix 1 for acquisition parameters). Patients were positioned supine on the flat-top couch, head to scanner, by a radiotherapy radiographer. The radiotherapy Combifix was used to support knees and feet in an identical position to the RT planning scan. Pelvic tattoos were aligned with room-mounted lasers. ^{18}F-misonidazole was injected with the patient on the scanner bed at a prescribed administered activity of 370 MBq. Dynamic imaging was acquired over 45 minutes in variable time frames (12 x 5 s, 6 x 10 s, 5 x 30 s, 10 x 60 s and 6 x 5 minutes) This was followed by a CT scan and a 10 minute static acquisition. Further static scanning at 2 and 4 hours post-injection took 10 minutes each. Venous blood sampling was performed at 4 minutes, 60 minutes, 2 hours and 4 hours. Following a protocol amendment after recruitment of 1 patient in RHYTHM A and 5 in RHYTHM B, patients were given an enema prior to the 4-hour static scan.

2.1.3 Processing of static FMISO scans

Static images were obtained at 4 hours. Rectal tumour ROI was outlined by one radiologist (JF, 7 years' experience) on T2-weighted axial small field of view (T2w sFOV) MRI. Tumour ROIs were rigidly registered to the CT component of the FMISO-PET taken at the same time point and transposed using Eclipse radiotherapy planning software (Varian Medical Systems Inc., Palo Alto, CA, USA). They were modified for air and to ensure contiguity of tumour. ROIs in the gluteus muscle and pelvic arteries (5 mm diameter in femoral or iliac) in the same frame as the tumour were outlined by the researcher (Figure 3.1).

Figure 3.1: ROIs for tumour (orange outline), muscle (yellow outline) and artery (red outline) on FMISO PET-CT at 4 hours in a RHYTHM-B patient (poor responder)



The ROIs were transferred to PMOD imaging software (PMOD technologies LLC, Zurich, Switzerland) to extract PET parameters including standardised uptake values (SUV) for tumour, muscle and blood. Tumour SUVmax, T:Mmax and T:Bmax were calculated and a mean ratio obtained. To define a hypoxic subvolume, tumour with an uptake value greater than T:M >1.3 or T:B >1.3 was considered hypoxic.

2.1.4 Statistical analysis

The PET parameter results are not normally distributed as identified by the difference between mean and median for each outcome in this small sample size. Therefore, non-parametric statistical methodology has been adopted with median and inter quartile ranges (IQR) reported. Spearman's rank and binary logistic regression were undertaken using SPSS (IBM Corp. Released 2017. IBM SPSS Statistics for Windows, Version 25.0. Armonk, NY).

2.2 Results

2.2.1 Scan scheduling

In arm A, the intent was that two sets of imaging would be collected before resection to assess

intra-patient variation on repeat imaging. However, of the 3 recruited, only 1 patient in RHYTHM A had 2 sets of imaging prior to resection. Patient preference and limited time prior to surgery meant this was not possible for the other 2 participants.

In arm B, 11 patients were recruited, of whom 10 had baseline FMISO imaging and 9 had on-treatment scans. Baseline scans were undertaken at median 1 day (IQR 4) prior to CRT starting. On-treatment scans were done at median 10 days (IQR 2).

Baseline FMISO scans were not undertaken for 1 patient due to tracer not being available and the on-treatment scan was therefore not done for lack of comparator. Tracer was not available for the on-treatment scan for 1 patient due to cyclotron breakdown. Two patients did not have their on-treatment scan at the specified time - RHB08 was scanned at fraction 7 due to staffing issues and RHB11 had the scan at fraction 15 due to earlier cyclotron failure.

The results below refer to the 4-hour post injection static FMISO PET-CT. Dynamic FMISO-PET was also undertaken in the RHYTHM study and the results are discussed in Chapter 4.

2.2.2 Tumour volume

RHYTHM A tumour volume

Table 3.1 summarises the tumour volume characteristics based on the MRI ROI for RHYTHM A patients. RHA03 was a small T2 tumour, the others being T3.

Table 3.1: RHYTHM A MRI tumour volumes

Study #	Volume (cm^3)	
	Scan 1	**Scan 2**
RHA01	15.4	15.4
RHA02	28.8	N/A
RHA03	7.1	N/A

RHYTHM B tumour volume

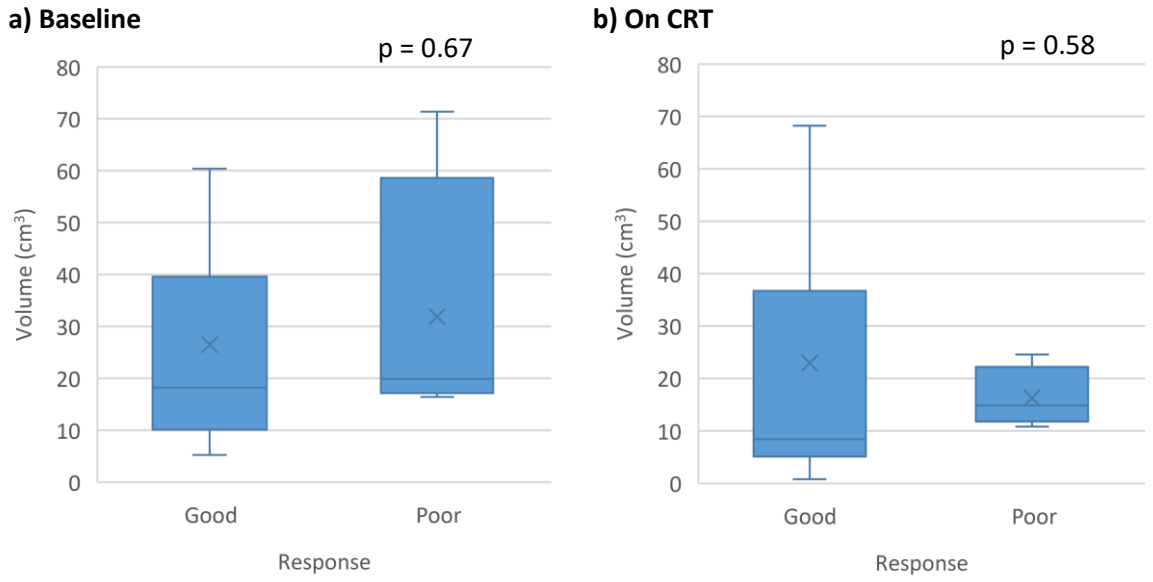
Table 3.2 demonstrates the change in total tumour volume on sFOV MRI with treatment for patients in arm B receiving neoadjuvant chemoradiotherapy. Median tumour volume at baseline was 19.4 cm^3 (IQR 22.4). By week 2 chemoradiotherapy it fell to 14.7 cm^3 (IQR 23.1). Baseline tumour size did not significantly correlate with tumour size change (Spearman's rank order correlation 2-tail ($r(9) = 0.45$; $p = 0.17$). Median size change was -44.3% (IQR 48.2)and tumour volume reduced on treatment in all but one of the patients, RHB01.This tumour response outcome was good and the size increase may be due to radiation-induced changes in the tumour such as inflammatory response, oedema or intralesional haemorrhage rather than true disease progression. Tumour size became more homogenous on treatment in the poor responder group. This may reflect a differing biology in this group, for example existence of a hypoxic core region that remains despite RT. Logistic regression analysis did not demonstrate a statistically significant relationship between tumour volume and response outcome at either timepoint (Figure 3.2). At baseline $\chi2(1) = 0.18$, $p = 0.67$ and on treatment $\chi2(1) = 0.34$, $p = 0.58$.

Table 3.2: RHYTHM B response outcomes and MRI tumour volume changes on neoadjuvant CRT for rectal cancer

Study #	Response	Tumour volume (cm^3)		
		BL	**On RT**	**% Δ**
RHB01	Good	60.4	68.2	13.0
RHB02	Good	18.2	5.1	-72.0
RHB03	Poor	71.4	24.6	-65.6
RHB04	Poor	20.3	10.8	-46.8
RHB05	Good	15.1	8.4	-44.3
RHB06	Poor	19.4	14.7	-24.2
RHB07	Good	5.2	0.8	-85.4
RHB08	Good	36.7	35.6	-3.0
RHB09	Poor	16.4	15.0	-8.7
RHB10	Good	39.6	36.7	-7.3
RHB11	Good	10.1	5.6	-44.9
Median (IQR)	-	19.4 (22.4)	14.7 (23.1)	-44.3 (48.2)

BL = baseline, CRT = chemoradiotherapy; Δ = change

Figure 3.2: MRI assessed tumour volume in cm^3 a) at baseline and b) on CRT



2.2.3 RHYTHM A tumour SUVmax, T:B and T:M ratios and hypoxic volumes

Two patients within RHYTHM A (straight to surgery) had analysable baseline scans. The tumour SUVmax for RHA02 of 3.4 was just above the median seen in RHYTHM B of 3.2 (IQR 1.1), whereas that for RHA03 was well below at 2.2 (Table 3.3). There were no analysable scans for validation at baseline as both for RHA01 were affected by faecal excretion of tracer adjacent to the tumour ROI. T:M and T:B was ≤1.8 for both patients with analysable scans.

Table 3.3: RHYTHM A 4h static FMISO PET Tumour (T) SUVmax and T:Muscle (M) & T:Blood (B)

Study #	SUVmax	Ratio		Hypoxic volume (cm^3)	
	Tumour	T:M	T:B	T:M (% total)	T:B (% total)
RHA01a	*	*	*	*	*
RHA01b	*	*	*	*	*
RHA02	3.4	1.8	1.8	0.12 (0.4)	0.15 (0.5)
RHA03	2.2	1.4	1.6	0.10 (1.6)	0.19 (2.7)

*Scan could not be analysed/artefact present

2.2.4 RHYTHM B tumour SUVmax; T:B and T:M ratios

SUVmax

Table 3.4 shows the change in tumour SUVmax, T:M and T:B ratios with radiotherapy for patients with response outcome in RHYTHM B. Median and IQR tumour SUVmax were calculated at baseline and week 2 radiotherapy. There was a non-significant negative relationship between baseline tumour SUVmax and tumour size change (Spearman's rank $r_s(8)$ =-0.24; p = 0.95). It would be expected that a higher SUVmax and therefore more hypoxic tumour was associated with less change in tumour size or a reduced response to chemoradiotherapy.

Table 3.4: RHYTHM B 4h static FMISO PET Tumour, SUVmax and T:M & T:B changes with CRT

	Arm B BL			**Arm B week 2 RT**		
Study #	**T SUVmax**	**T:M**	**T:B**	**T SUVmax (% Δ)**	**T:M**	**T:B**
RHB01	2.1	1.4	1.8	1.8 (-14.4)	2.2	2.6
RHB02	*	*	*	*	*	*
RHB03	3.4	2.4	2.8	2.2 (-33.9)	1.6	2.0
RHB04	4.2	2.8	3.3	2.7 (-35.1)	2.1	2.4
RHB05	*	*	*	1.8 (N/A)	1.4	1.7
RHB06	3.4	1.7	2.4	N/A	N/A	N/A
RHB07	3.5	2.3	2.7	2.4 (-30.7)	1.6	1.9
RHB08	5.3	2.2	3.1	2.5 (-53.1)	1.3	1.5
RHB09	3.0	2.1	2.3	1.8 (-40.1)	1.3	1.5
RHB10	N/A	N/A	N/A	N/A	N/A	N/A
RHB11	1.9	1.1	1.5	2.4 (+23.7)	1.3	1.6
Median [IQR]	3.4 [0.9]	2.2 [0.7]	2.6 [0.7]	2.3 [0.6] (-33.9% [15.1])	1.5 [0.4]	1.8 [0.5]

T = tumour; M = muscle; B = blood; SUV = standardised uptake value; Δ = change; N/A = not applicable; *Scan could not be analysed/artefact present.

The median tumour SUVmax at baseline was 3.4 (S.D. 0.9), which fell to 2.3 (S.D. 0.6) in week 2 chemoradiotherapy. There was no clear association using logistic regression analysis between baseline tumour SUV max, on-treatment SUV max or change in tumour SUVmax and response to treatment; $\chi2(1) = 0.17$, $p = 0.68$, $\chi2(1) = 0.48$, $p = 0.83$ and $\chi2(1) = 1.21$, $p = 0.27$ respectively (Figure 3.3). This suggests that FMISO tumour SUVmax at 4 hours either at baseline or during treatment is not a useful predictive marker for chemoradiotherapy response in patients undergoing neoadjuvant therapy for rectal cancer. SUVmax is the most avid voxel within the ROI, normalised for body weight and may therefore not provide a reflection of tumour hypoxic volume, or distribution within the tumour, both of which would potentially be relevant to radiotherapy targeting and response.

The baseline median SUVmax results for RHYTHM B were above those for RHYTHM A. The hypoxic volumes and percentage of total tumour for RHYTHM A patients were comparable with the lower end of values for RHYTHM B. This may reflect a less hypoxic and therefore less aggressive nature of a tumour not requiring neoadjuvant therapy, although would need to be confirmed with a larger sample.

T:M and T:B ratios

Both T:M and T:B ratios fell with chemoradiotherapy in the majority of patients to median of 1.5 (IQR 0.4) and 1.8 (IQR 0.5) respectively. However, in patients RHB01 and RHB11, the ratios rose following 2 weeks of treatment, though both were good responders. This may suggest SUVmax ratios are not a useful predictor of outcome. Tumour hypoxic volume was calculated for each time point as a potential marker of response.

2.2.5 RHYTHM B tumour hypoxic volumes

Table 3.5 summarises the changes in tumour hypoxic volume with chemoradiotherapy as calculated using T:M > 1.3 and T:B of >1.3.

Figure 3.3: Box plot of tumour SUVmax by outcome a) at baseline (BL); b) week 2 chemoradiotherapy (CRT); c) percentage change

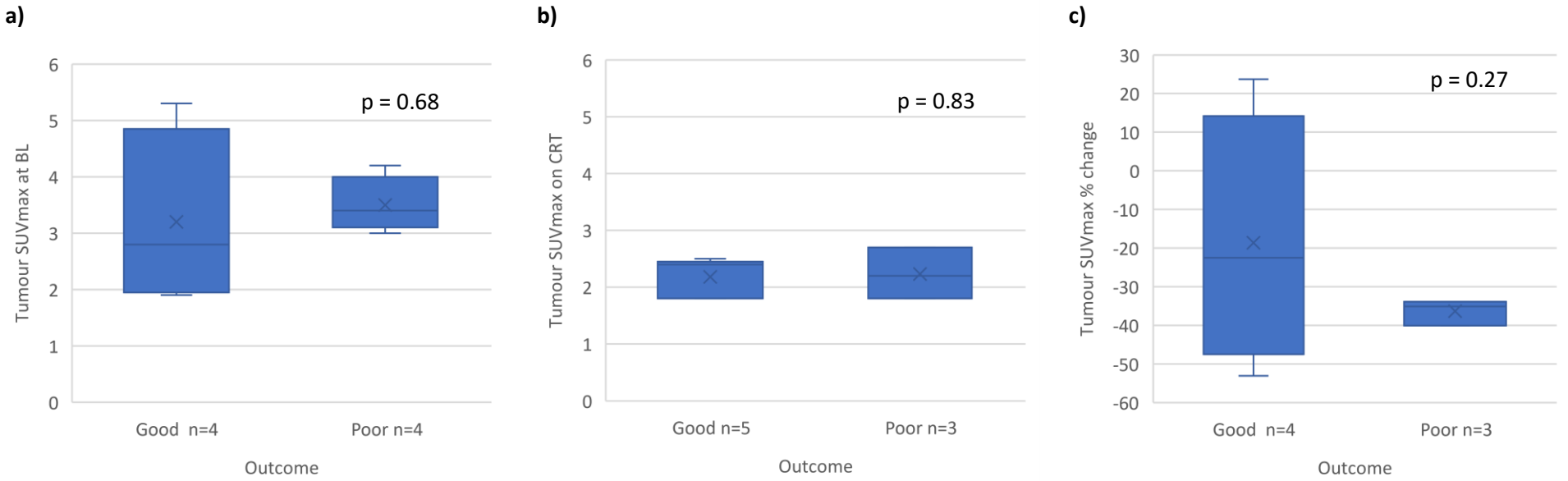


Table 3.5 RHYTHM B Tumour hypoxic volume (hVOL) change (Δ) with 8-10 fractions neoadjuvant radiotherapy for rectal cancer

Study #	Response	T:M hVOL (IQR) [cm^3]			T:B hVOL (IQR) [cm^3]		
		Baseline	**Week 2**	**% Δ**	**Baseline**	**Week 2**	**% Δ**
RHB01	Good	0.1 (0.1)	0.2 (0.2)	200.0*	0.4 (0.5)	1.3 (1.4)	225.6
RHB02	Good	**	**	**	**	**	**
RHB03	Poor	1.0 (0.5)	0.0 (0.0)	-100.0	5.3 (3.0)	0.6 (0.7)	-88.9
RHB04	Poor	4.0 (13.2)	0.2 (1.5)	-95.0	6.6 (21.5)	0.8 (5.7)	-88.4
RHB05	Good	**	0.0 (0.0)	**	**	0.0 (0.0)	**
RHB06	Poor	0.8 (4.3)	N/A	N/A	6.1 (32.4)	N/A	N/A
RHB07	Good	0.4 (9.4)	0.1 (12.9)	-69.2	1.2 (28.1)	0.5 (54.8)	-56.4
RHB08	Good	1.2 (4.1)	0.0 (0.0)	-100.0	10.7 (37.5)	1.9 (6.7)	-82.1
RHB09	Poor	1.4 (9.6)	0.0(0.0)	-100.0	2.1 (13.8)	1.3 (9.6)	-37.5
RHB10	Good	N/A	N/A	N/A	N/A	N/A	N/A
RHB11	Good	0.0 (0.0)	0.0 (0.0)	0.0	2.2 (19.9)	0.2 (2.8)	-93.0
Median	-	0.9 (4.2)	0.0 (0.0)	-95.0	3.7 (20.7)	0.7 (4.3)	-82.1
IQR	-	0.9 (9.0)	0.1 (0.5)	65.4	4.3 (18.1)	0.9 (6.2)	41.7

*Due to rounding percentage change does not reflect values in table; **Scan could not be analysed/artefact present. N/A – not applicable

Absolute hypoxic volume

The baseline median T:M hypoxic volume of 0.9 cm^3 (IQR 0.9) was smaller than that defined by the T:B ratio at 3.7 cm^3 (IQR 4.3). The same was true during week two chemoradiotherapy, with median volumes of 0.0 cm^3 (IQR 0.1) and 0.7 cm^3 (IQR 0.9) respectively. Both T:M and T:B measures demonstrated an overall median reduction in hypoxic volume on CRT, by 95% (IQR 65.4) for that defined by T:M ratio >1.3 and 82.1% (IQR 41.7) for T:B ratio >1.3.

Figure 3.4 does seem to suggest a trend of lower hypoxic volumes at baseline in good versus poor responders particularly for T:M-defined hypoxic volume ($\chi2(1) = 4.74$, $p = 0.17$, Nagelkerke $R^2 = 60\%$ using binary logistic regression analysis). This difference is lost after 8-10 fractions of radiotherapy, perhaps suggesting that poor responders with higher baseline hypoxic volumes have more therapeutic value with chemoradiation in terms of reduction of hypoxia ($\chi2(1) = 0.02$, $p = 0.90$, Nagelkerke $R^2 = 0.3\%$). The relationship was less clear for T: B hypoxic volume at these time points (baseline $\chi2(1) = 0.38$, $p = 0.55$, Nagelkerke $R^2 = 6.1\%$ and on treatment $\chi2(1) = 0.03$, $p = 0.86$, Nagelkerke $R^2 = 0.6\%$). This may be due to the small sample size or cut off for hypoxic volume used. Other factors may have a greater impact on outcome than hypoxic volume, such as tumour stage, grade or nodal status[260].

RHB08, a good responder, had the highest baseline hypoxic volume defined by T:B at 10.7 cm^3 (37.5% of total tumour volume), which fell to 1.9 cm^3 (6.7% of total volume) in week 2 chemoradiotherapy. Reductions in hypoxic volume with CRT were also seen in all 3 poor responders with paired scans. The only patients of 7 with interpretable paired FMISO scans to show an increase in total hypoxic volume, defined both by T:M and T:B ratio, was RHB01 (Figure 3.5). The hypoxic volume in this case was small at <1.5 cm^3 in a total tumour size of >80 cm^3 and the patient went on

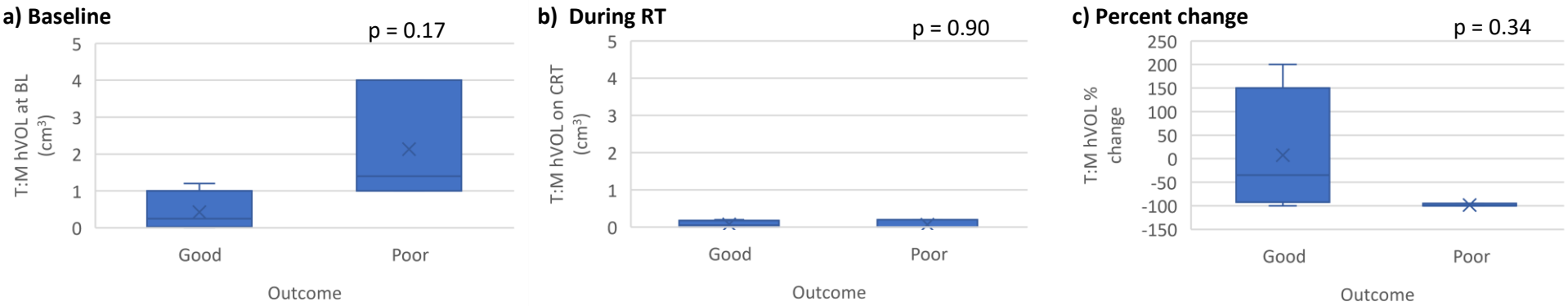
to have a good outcome, suggesting proportion of volume that is hypoxic may be relevant.

Proportion of hypoxic volume

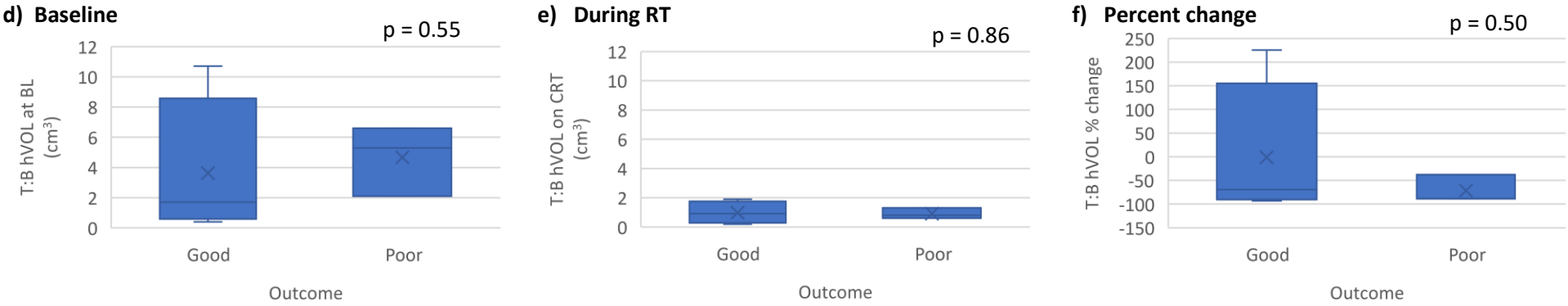
The proportion of tumour represented by FMISO-defined hypoxic volume as defined by T:B was between 0.5 – 32.4% (median 20.7%, IQR 18.1). On CRT this was 0.0 – 54.8% (median 4.3%, IQR 6.2). Neither was significantly related to outcome using binary logistic regression; at baseline $\chi2(1) = 0.19$, $p = 0.66$ and on treatment $\chi2(1) = 0.46$, $p = 0.57$). For T:M hypoxic volume as a percent of total ranged from 0.0 - 13.2% at baseline, median 4.2% (IQR 9.0) to 0 - 12.9%, median 0% (IQR 0.5) on CRT, neither showing a clear relationship with outcome (baseline $\chi2(1) = 1.17$, $p = 0.28$; on CRT $\chi2(1) = 0.58$, $p = 0.56$). There was a rise in the proportion of hypoxic volume in two patients, one of whom had a significant shrinkage in overall tumour volume as a result of CRT (RHB07). RHB07 had the largest percentage hypoxic volume as defined by T:B >1.3, increasing from 28.1% to 54.8%. on CRT. This tumour also showed the largest reduction in overall volume, falling to under a quarter of pre-treatment size, with overall good response.

Figure 3.4: RHYTHM B outcomes by hypoxic volumes (hVOL) (cm^3) defined as: T:M > 1.3 and T:B >1.3 at baseline and during RT

T:M hypoxic volume



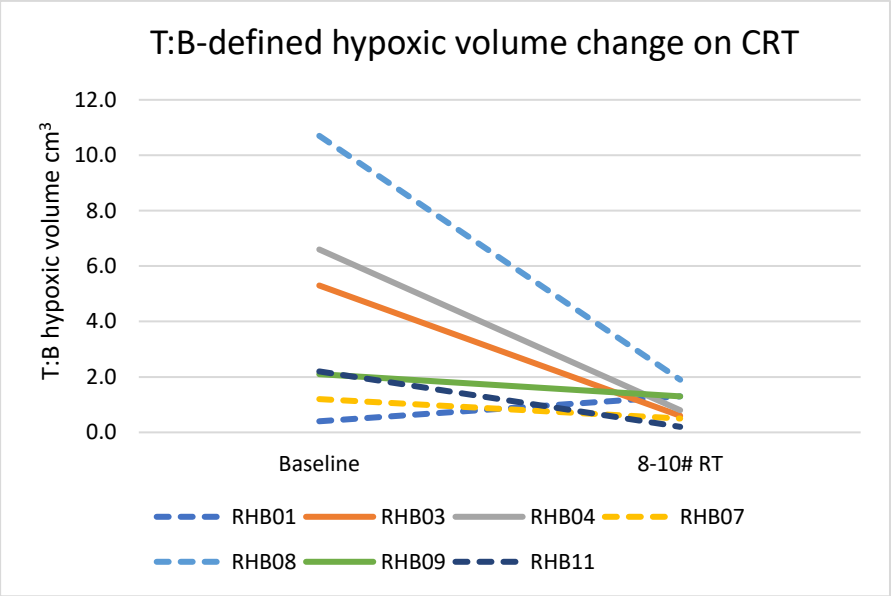
T:B hypoxic volume



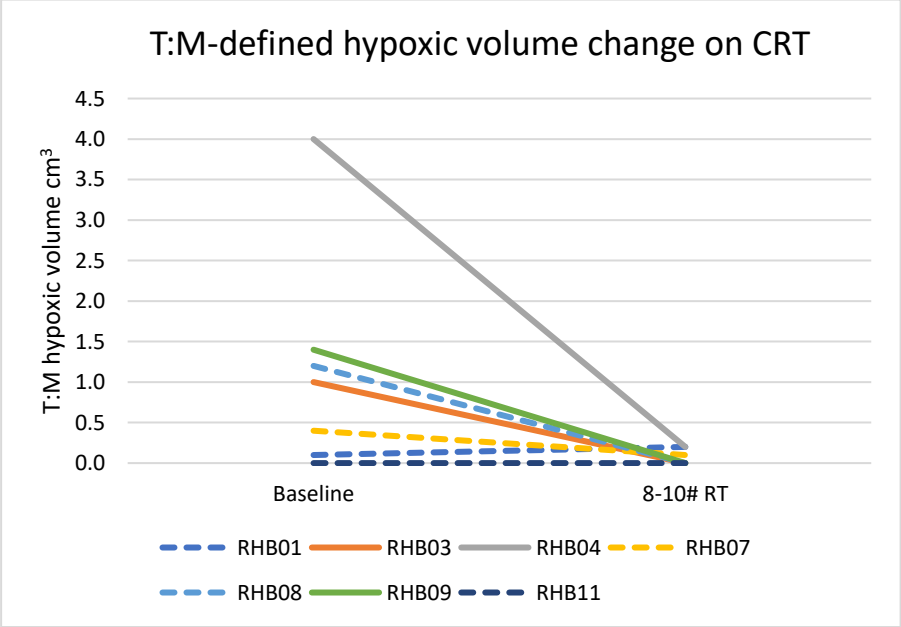
Note: Data unavailable for two good responders. On CRT data & percentage change data missing for 1 poor responder

Figure 3.5: Changes in a) T:B >1.3 and b) T:M >1.3 defined hypoxic volumes at 4 hour FMISO PET-CT by response (Good responders (dashed) and Poor (solid) lines)

a)



b)



2.3 FMISO challenges

3.1.1 FMISO scan failures

Two scans could not be undertaken due to tracer production failure at the cyclotron. As one was a baseline scan, RHB10 did not have the planned week 2 CRT scan done either. One patient in arm A (2 scans, at day 0 and 3) and two in arm B (2 scans at baseline and 1 during week 2 CRT) had uninterpretable scans.

3.1.2 Faecal excretion of tracer

There were multiple issues encountered with the use of FMISO in the RHYTHM study. Early in the study, four 4-hour FMISO scans could not be interpreted due to faecal excretion via the biliary pathway of tracer affecting measure of tumour uptake in the rectum as seen in Figure 3.6a.

Unfortunately, one of the patients affected was RHA01 who was the only patient to have two FMISO PET-CT scans. Time did not allow for any other RHYTHM A patients to have two scans prior to surgery. Therefore, the planned analysis of intrapatient variability was not possible.

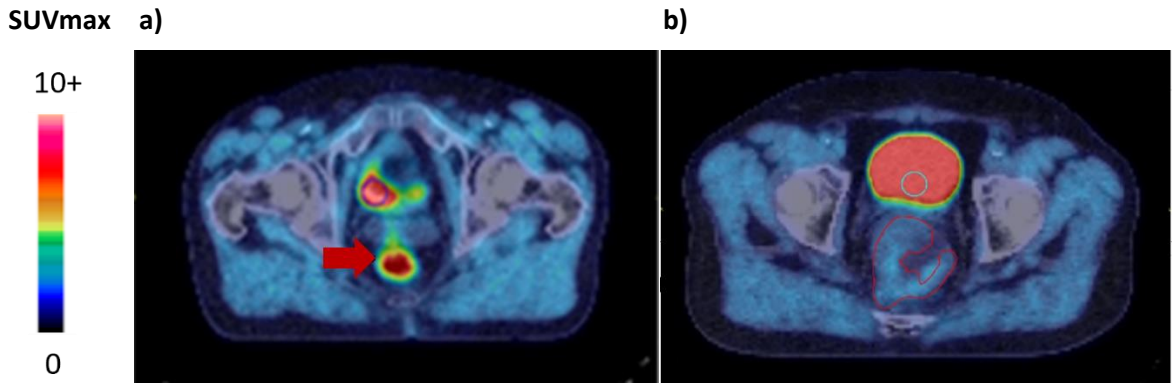
3.1.3 Bladder spillover

Emptying of the bladder before scanning was encouraged throughout the trial. However, high activity within the bladder leading to spillover into the tumour ROI (Figure 3.6b) also rendered 2 scans uninterpretable (one also had faecal excretion artefact).

3.1.4 Protocol alteration

As a result of the issues, the RHYTHM trial protocol was updated to include a micro-enema prior to the 4-hour scan and patients were verbally reminded to void their bladder shortly prior to each scan. These changes resulted in no further unanalysable scans.

Figure 3.6: Spill-over affecting interpretation of FMISO PET-CT images. a) Faecal excretion of tracer (red arrow)**; b) Bladder excretion of tracer** (tumour outlined in red, bladder maximum uptake in blue)



3.1.5 Bladder spill-in

This analysis was performed in collaboration with Dr T. Puri (Department of Oncology, University of Oxford).

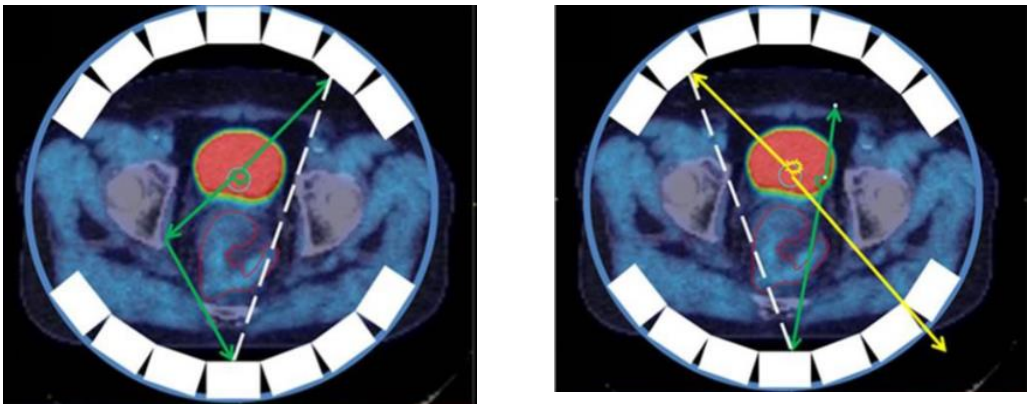
FMISO is reduced by hypoxia and binds covalently to cellular molecules at a rate inversely proportional to intracellular oxygen concentration. The nucleus of the radioisotope emits a positron which collides with an electron in the tissue, leading to an annihilation reaction producing two photons emitted at almost 180 degrees to each other. These are then detected by the scanner which identifies the coincident photons and coincidence lines are processed to determine the origin i.e., spatial location of the reaction. This is correlated with the anatomical CT scan[261].

Two mechanisms may affect the measured tumour SUV due to spill-in and are demonstrated in Figure 3.7. The first is due to scatter of photons e.g., by bone, leading to misplacement and therefore incorrect detection as to the position of the annihilation reaction. The second occurs when two annihilation events occur simultaneously with one of each photon pair either lost or

undetected by the scanner, again leading to incorrect attribution of the location of origin.

Figure 3.7: Mechanisms of bladder spill-in affecting FMISO PET 4-hour results: Scatter of photon leads to false detection of event in tumour; Two annihilation events occur with one of each photon pair lost/undetected (Adapted from Puri et al EJNMMI Research 2017[262]*)

a) **b)**



*Under Open Access terms of the Creative Commons Attribution 4.0 International Licence

Correcting for this is challenging owing to the non-linear random/scatter characteristics of the activity. The values will be affected by urinary excretion rate, activity concentration within and volume of the bladder, proximity to area of interest and the accuracy of attenuation correction among others. Bladder catheterisation may represent one solution, but it is invasive for patients and not desirable for radiotherapy planning purposes, where the bladder is usually filled to limit small bowel radiation dose.

3.1.6 Image co-registration

Rectal tumour ROIs were outlined on anatomical T2 weighted axial MRI given the difficulties visualising these cancers on CT. The MRI and CT component of the PET underwent rigid co-registration with transfer of the ROI outline and modification to take account of, for example, peristalsis, gas and rotation. Whilst these scans were undertaken on the same day, there were several hours between each and therefore potential variability in ROI outlines. If available, PET-MRI could be a potential alternative to overcome some of the issues of the limited spatial resolution of

PET, particularly in pelvic tumours.

3.1.7 Logistic challenges

Tracer was unavailable, often at short notice, on multiple occasions due to cyclotron breakdown at the remote facility. Scans were rebooked where possible but were constrained by chemoradiotherapy start dates and scanner availability. Supply and logistical issues would restrict routine use of FMISO currently.

2.4 Discussion of FMISO PET in rectal cancer

Radiotherapy appears to modify the hypoxic volume but this alone does not seem to alter response outcome. The link between hypoxia and radioresistance has been established from *in vitro, in vivo* and clinical outcome data[58, 263, 264]. However, in this small study there appears to be limited predictive benefit in imaging with FMISO in rectal cancer.

In terms of clinical practicality, SUVmax is a less analytically demanding marker to determine and in other tumour types, several studies have found FMISO tumour SUVmax to be predictive of response to treatment or a poor prognostic indicator, for example, NSCLC[114, 131, 265], head and neck squamous cell carcinoma[121, 266, 267] and glioblastoma multiforme[268, 269]. However, tumour SUVmax did not appear to predict response to radiotherapy in this study. Heterogeneity within tumours may mean single voxel markers do not always provide sufficient information for response prediction. SUVpeak (mean SUV within a 1 cc sphere centred around the maximum) has been suggested as an alternative to SUVmax. This is potentially more robust across different scanners and less sensitive to image noise. It would not however overcome issues of bladder spillover or faecal excretion seen in this study.

There did appear to be some indication that hypoxic volume at baseline as defined by T:M >1.3 may be associated with response. This would be consistent with the association of hypoxia and

radioresistance. However, the hypoxic volume in all those with poor response did also reduce with chemoradiotherapy. It may be that the remaining hypoxic cells in these patients are particularly radioresistant. FMISO reduces in oxygen levels <10 mm Hg but there is evidence of a precipitous fall in radiosensitivity with values of pO_2 <3 mm Hg[270].

Another factor which may impact the results include the limits for defining tumour hypoxia using T:M and T:B ratios. Various figures have been provided in the literature mainly between 1.2 and 1.4, in the setting of a variety of tumour types including sarcoma[120], glioblastoma[268] and head and neck squamous cell carcinoma[121] but there is no consensus on which value to use.

The spatial distribution of hypoxia may also be a relevant factor when irradiating tumours, which is not indicated when defining hypoxic volume using specified ratios as above. Radiotherapy boost to severely hypoxic areas would require the reliable identification of a hypoxic volume of a size that could be targeted using modern techniques. Furthermore, it would need to be established that this remains relatively consistent throughout radiotherapy. There is also the risk of misregistration of PET-CT as well as limited anatomical detail, mandating the additional use of MRI when planning treatment.

In this trial, there were significant issues with both faecal excretion of tracer and overspill from luminal and bladder contents leading to difficulties with interpretation. Other issues included the low tumour to background signal ratio and lack of evidence for reproducibility. These factors suggest the usefulness of FMISO-PET imaging at 4 hours in rectal cancer may be limited and is reflected in other trials[140, 142]. Other tracers such as FAZA[139] or [^{60}Cu]ATSM[141] have been assessed as alternatives and were also found to have limitations similar to those of FMISO PET[271].

3. Oxygen-enhanced MRI

Inhaled oxygen may be used as a weakly paramagnetic contrast agent for MR imaging. Increased

inspired oxygen leads to increased molecular oxygen dissolved in arterial plasma which in turn reduces T1 (longitudinal relaxation time). ShMOLLI is a rapid T1 mapping technique originally developed at the University of Oxford[163, 272] in the cardiac setting. It is a useful feature in multiparametric MRI to limit total scan time for patient comfort and in order to reduce the potential for peristalsis to affect quality of rectal imaging.

The analysis of the ShMOLLI scans was carried out with Professor D. Bulte (Institute of Biomedical Engineering, University of Oxford).

3.1 Methods

Oxygen-enhanced MRI was undertaken within RIT and RHYTHM studies following protocol amendments towards the end of recruitment. Within the RIT 2 study, 3 patients were imaged as were 5 patients within RHYTHM (2 in RHYTHM A and 3 in RHYTHM B). In RHYTHM A, imaging was done at baseline. For those undergoing radiotherapy, it was undertaken at baseline, after 10 (+/-2) fractions of radiotherapy and 6 weeks post treatment with standard imaging for response assessment.

3.1.1 Sequence acquisition

Sequences were acquired on 1.5T GE HDX twinspeed MRI scanner with 8 channel TORSO. Parameters and full list of sequences are found in Appendix 1. The region of interest was identified by the researcher (JF, MA, the author) and anatomical sequences obtained initially. Two T1 mapping MRI sequences were performed with patients breathing room air during the first sequence and then breathing supplemental 100% oxygen (15 litres) via a non rebreathe mask in the second sequence. Monitoring of expired oxygen levels was undertaken using Powerlab/Labchart system (ADInstruments, Oxford, UK). Expired oxygen and carbon dioxide levels were monitored using the Powerlab/Labchart system (ADInstruments, Oxford, UK). Scanning on oxygen was commenced once expired oxygen levels had stabilised and were consistently

approaching 100%, which usually took a few minutes. A single slice ShMOLLI image was obtained through the ROI, chosen by the investigator and replicated visually on repeat imaging.

3.1.2 Image processing

MATLAB (R2017b, The MathWorks, Inc., Natick, Massachusetts, United States) was used for image processing and a T1 and R1 map created for analysis. The tumour ROI from the T2 axial MRI was registered to the T1 map using ITK-SNAP (Version 3.6.0; University of Pennsylvania, PA 19104-6274, United States)[273] and the T1 (ms) and R1 (s^{-1})results extracted. Muscle ROI in the gluteal muscles was directly outlined in ITK-SNAP and data extracted. ΔR1 is the change in R1 with supplemental oxygen, where R1 is the longitudinal relaxation rate (/s) (Box 3.1). ΔR1 is proportional to oxygen concentration change (mM) at given timepoint t[274].

Box 3.1

$$\Delta R1 = 1/T1(t_{O2}) - 1/T1(t_{air})$$

ΔR1 – change in longitudinal relaxation rate (/s)

T1 – longitudinal relaxation time (s)

t – time point specified

$$\Delta[O_2]\ R1 \propto \Delta R1$$

$[O_2]$- oxygen concentration

ΔR1 – change in longitudinal relaxation rate (/s)

To assess the ShMOLLI data during post-processing, a goodness of fit image was created during post-processing (MATLAB R2017b, The MathWorks, Inc., Natick, Massachusetts, United States). If multiple data points were visually absent, the related ShMOLLI image was deemed unanalysable.

3.2 Results

An example of ShMOLLI images at baseline on air and inhaled oxygen is shown in Figure 3.8. T1 (longitudinal relaxation time in ms) was acquired on air and with inspired 100% oxygen.

3.2.1 ShMOLLI slice and total tumour volume

Total tumour volume was compared with that obtained on the single ShMOLLI slice. The ShMOLLI tumour volume presented in Table 3.6 reflects the area of the ROI outlined with a slice thickness of 3mm. In terms of analysable scans, the median tumour ShMOLLI slice volume at baseline for all patients (n=8) was 5.90 cm^3 (IQR 5.30), which represented a median 26.9% (IQR 7.9) of the total tumour volume on the contemporaneous T2 axial sFOV sequence. During chemoradiotherapy tumour slice median volume was 2.40 cm^3 (IQR 2.40) or 28.0% (IQR 21.1) of tumour volume (n=4). At 6 weeks post treatment median tumour slice volume was 3.60 cm^3 (IQR 3.04), a median of 31.5% (IQR 3.0) total tumour volume (n=5). These data suggest that the slice volume chosen usually involved a reasonable proportion of the total tumour volume. However, RHB10 had little tumour on the chosen slice at 0.9 cm^3. The wide IQR for the on-treatment scan is largely due to the significant tumour shrinkage of patient RHB11 who had a relatively small disease volume at baseline.

Figure 3.8: Baseline oxygen-enhanced ShMOLLI MRI T1 maps in a good responder (red outline – artery, white arrow – bladder, blue outline – gluteal muscle, pink outline – rectum)

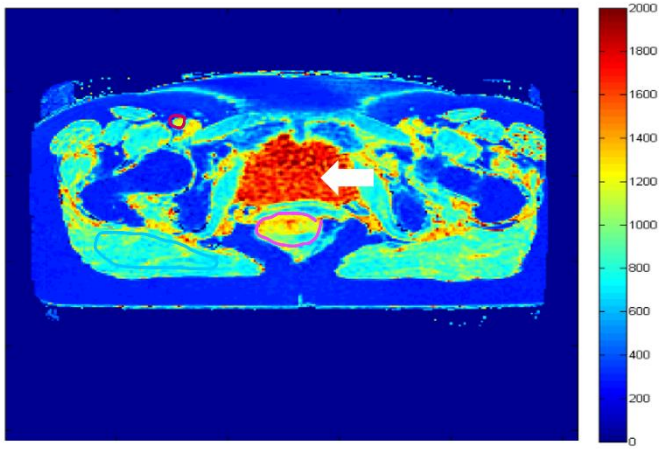
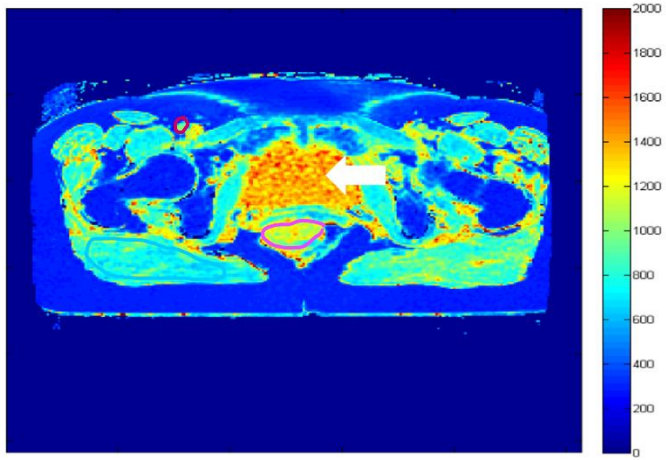
ShMOLLI T1 on air (ms)	**ShMOLLI T1 on O_2 (ms)**
	
Tumour mean T1 (S.D.) = 1221.5 (113.9)	Tumour mean T1 (S.D.) = 1200.4 (113.5)

Table 3.6: ShMOLLI MRI tumour single slice volume (SSV) as a proportion of T2 axial MRI total tumour volume (TTV) in RHYTHM A/B and RIT studies

Study #	Baseline			During RT			6 weeks post RT		
	SSV (cm^3)	TTV (cm^3)	% SSV/TTV	SSV (cm^3)	TTV (cm^3)	% SSV/TTV	SSV (cm^3)	TTV (cm^3)	% SSV/TTV
CRT patients (RHYTHM B, RIT)									
RHB09	5	16.4	30.4	4.9	15.0	32.7	3.6	4.7	77.1
RHB10	0.6	39.6	1.5	2.4	36.7	6.5	5.9	33.5	17.6
RHB11	2.4	10.1	23.8	1.3	5.6	23.3	0.9	2.9	30.6
RIT59	7	23.3	30.0	-	-	-	2.86	8.5	33.6
RIT60	20.2	66.1	30.5	1.6	**	*	12.02	38.2	31.5
RIT61	11.3	48.1	23.5	4	6.4	62.9	**	1.6	**

Straight to surgery patients (RHYTHM A)

RHA02	6.8	34.4	19.8	-	-	-	-	-	-
RHA03	2.9	7.8	37.2	-	-	-	-	-	-
Median (IQR)	5.9 (5.3)	28.8 (26.9)	26.9 (7.9)	2.4 (2.4)	10.7 (14.3)	28.0 (21.1)	3.6 (3.0)	6.6 (23.9)	31.5 (3.0)

* Incomplete data; ** Artefact – unable to analyse; - Scan not undertaken

3.2.2 ShMOLLI MRI on air and inspired oxygen in RHYTHM A

Only one of the two RHYTHM A patients had analysable ShMOLLI scans on air and oxygen (Table 3.7). For RHA03, the mean T1 fell with inspired 100% oxygen from 959.24 ms to 887.17 ms giving ΔR1 of 0.085 s^{-1}. All 3 mean T1 values obtained for the straight to surgery patients were less than all the mean T1 values for those going for downstaging chemoradiotherapy, both on air and oxygen (Table 3.8) at < 1000 ms. The ΔR1 of RHA03 was also higher than all those for patients having neoadjuvant CRT.

Table 3.7: ShMOLLI MRI tumour T1 & ΔR1* with and without supplemental inspired oxygen in RHYTHM A (1.5T scanner)

Study #	Air Mean T1 [ms] (S.D.)	Oxygen Mean T1 [ms] (S.D.)	ΔR1 [/s] (S.D.)
RHA02	811.12 (237.89)	**	**
RHA03	959.24 (126.99)	887.17 (95.51)	0.085

* ΔR1 is the change in R1 with supplemental oxygen where R1 is the longitudinal relaxation rate (R1 (/ms) ≡ 1/T1 (ms)); **Artefact

3.2.3 Changes in ShMOLLI MRI on air & oxygen with chemoradiotherapy

T1 on air and oxygen

Six patients within the RIT and RHYTHM studies had baseline ShMOLLI imaging prior to neoadjuvant chemoradiotherapy. Mean T1 (ms) was calculated within the regions of interest (Table 3.9). The median of these values on air was 1098.5 ms (IQR 121.1), falling to 1076.2 ms (IQR 66.6) on 100% inspired oxygen. Similarly, T1 on treatment fell with inspired oxygen from 1078.2 ms (IQR 103.5) to 1163.1 ms (IQR 64.3). At 6 weeks post chemoradiotherapy imaging, the median was 1114.1 ms (IQR 37.0) on air and 1121.1 ms (44.7) on oxygen.

In the majority of instances, the mean tumour T1 fell when inspired oxygen was applied. There was a minimal increase in T1 from air to oxygen in two patients' tumours at baseline (RHB09 and RIT60, both poor responders) and in a different patient at 6 weeks post CRT imaging (RHB111, good responder) (Figures 3.9 and 3.10).

Figure 3.11 demonstrates that native (on air) mean T1 values for poor responders showed a trend towards being higher than those for good responders both on and post treatment but not at baseline. There did not appear to be any association between mean T1 on oxygen and response at any timepoint. Binary logistic regression analysis confirms there was no significant association between T1 on air or oxygen at baseline ($\chi2(1) = 0.58$, $p = 0.47$, and $\chi2(1) = 0.00$, $p = 0.97$). This was also the case during CRT (on air $\chi2(1) = 5.55$, $p = 0.11$ and on oxygen $\chi2(1) = 0.01$, $p = 0.93$) and 6 weeks after (on air $\chi2(1) = 6.73$, $p = 0.07$ and on oxygen $\chi2(1) = 0.61$, $p = 0.50$).

ΔR1

ΔR1 (s^{-1}) was calculated for each time point. The median at baseline was 0.003 (IQR 0.015). During CRT it was 0.056 (IQR 0.056) and post CRT was 0.024 (IQR 0.047). Table 3.8 shows increasing ΔR1 during treatment from the lowest baseline levels for RHB09 and RIT60 (both poor responders). There was a subsequent fall at the scan 6 weeks post radiotherapy but not back to baseline levels for these patients. The tumour of RHB10 (good responder) demonstrated a stable ΔR1 during treatment which than increased 6 weeks post therapy. The two participants without on-treatment ShMOLLI imaging demonstrated a fall in ΔR1 post CRT to below baseline levels (RHB11, RIT 59 both good responders). Figure 3.11 demonstrates the relationship between ΔR1 and response. There was a significant relationship between the two at baseline ($\chi2(1) = 6.73$, $p = 0.04$, Cox & Snell $R^2 = 0.74$) at baseline. It is difficult to draw firm conclusions due to small numbers multiple missing data points and this finding would need further validation. There was no statistically significant relationship on RT $\chi2(1) = 3.82$, $p = 0.18$ or following therapy $\chi2(1) = 0.27$, $p = 0.61$.

Table 3.8: ShMOLLI MRI tumour mean T1 & ΔR1* with and without supplemental inspired oxygen (O_2) in RIT and RHYTHM B studies (1.5T scanner) before, during and after chemoradiotherapy

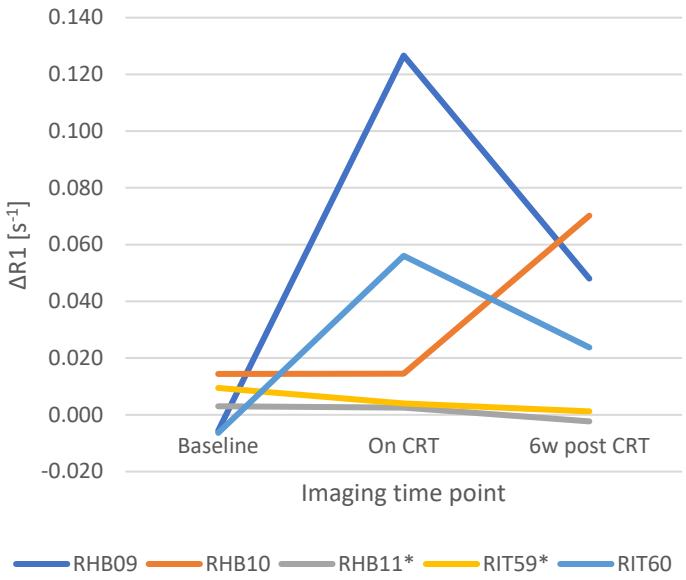
Study #	Outcome	Baseline			During RT			6 weeks post RT		
		Air T1 [ms] (S.D.)	O_2T1 [ms] (S.D.)	ΔR1 [s^{-1}]	Air T1 [ms] (S.D.)	O_2T1 [ms] (S.D.)	ΔR1 [s^{-1}]	Air T1 [ms] (S.D.)	O_2T1 [ms] (S.D.)	ΔR1 [s^{-1}]
RHB09	Poor	1069.8 (133.6)	1076.2 (145.6)	-0.006	1178.5 (114.8)	1025.4 (131.9)	0.127	1160.6 (153.0)	1099.4 (179.9)	0.048
RHB10	Good	1221.5 (113.9)	1200.4 (113.5)	0.014	1147.8 (112.5)	1129.0 (140.6)	0.015	1089.2 (177.2)	1011.8 (243.7)	0.070
RHB11	Good	1071.0 (171.5)	1067.5 (125.5)	0.003	1113.1 (106.0)	**	**	1141.1 (70.2)	1144.2 (116.3)	-0.002
RIT59	Good	1063.0 (229.1)	1052.4 (238.4)	0.009	N/A	N/A	-	1123.7 (290.8)	1122.1 (278.7)	0.001
RIT60	Poor	1126.0 (193.1)	1134.1 (237.3)	-0.006	1278.0 (184.6)	1192.6 (179.5)	0.056	1187.9 (194.9)	1154.3 (219.1)	0.024

RIT61	Good	1212.9 (333.7)	**	**	**	1078.2 (328.9)	**	**	**	**
Median (IQR)		1098.5 (121.1)	1076.2 (66.6)	0.003 (0.015)	1163.1 (64.3)	1078.2 (103.5)	0.056 (0.056)	1141.1 (37.0)	1122.1 (44.7)	0.024 (0.047)

N/A = not applicable; * ΔR1 is the change in R1 with supplemental oxygen where R1 is the longitudinal relaxation rate (R1 (s^{-1}) ≡ 1/T1 (s));

**Scan unanalysable

Figure 3.9: ShMOLLI MRI ΔR1 changes with chemoradiotherapy (baseline, after 8-10 fractions and 6 weeks post treatment)



*On-CRT values not available

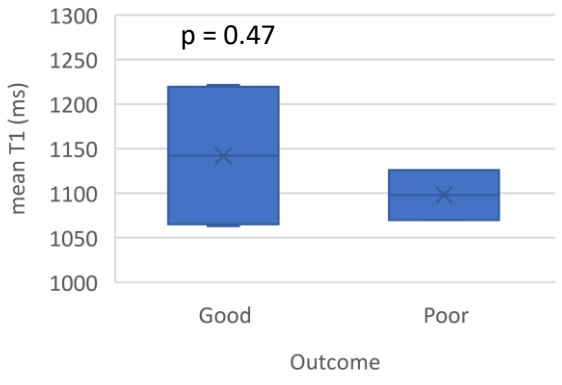
Figure 3.10: Changes in ShMOLLI MRI mean T1 (ms) with inspired oxygen at a) baseline, b) during radiotherapy and c) 6 weeks post treatment



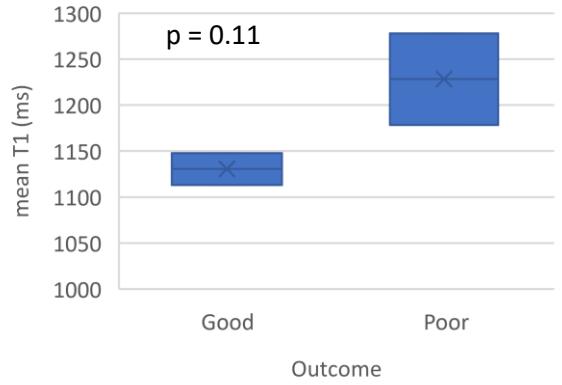
Figure 3.11: ShMOLLI results by response at baseline (BL), during RT, 6 weeks post RT for mean T1 (ms) on air (a-c) and 100% oxygen (d-f), ΔR1 (s^{-1}) (g-i)

Mean T1 on air (ms)

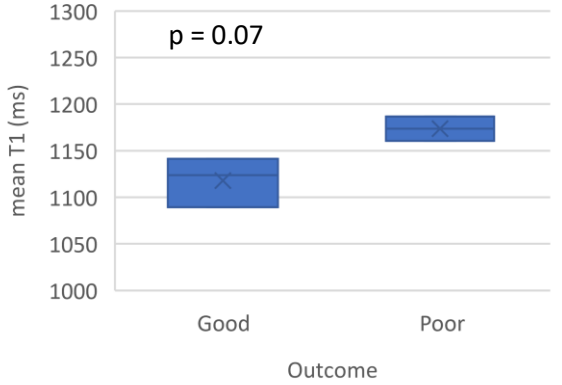
a) Baseline



b) During RT

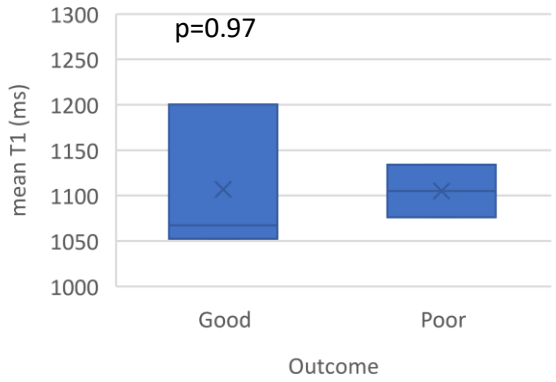


c) Post RT

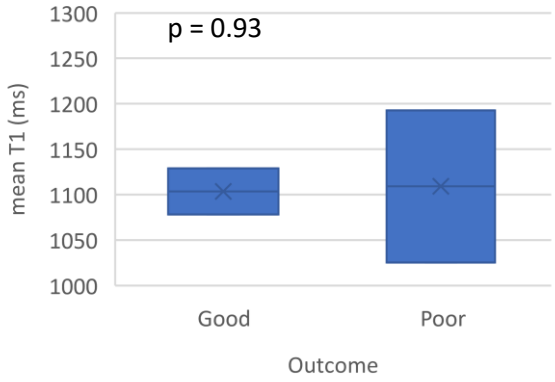


Mean T1 on oxygen (ms)

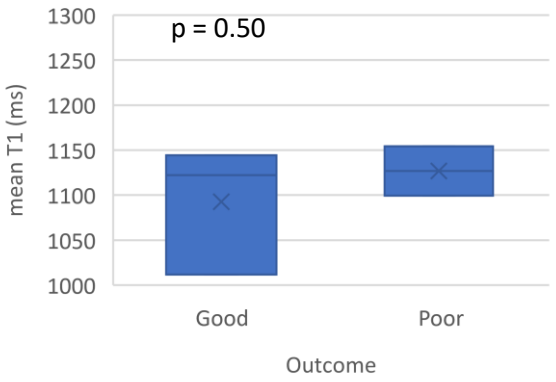
d) Baseline



e) During RT

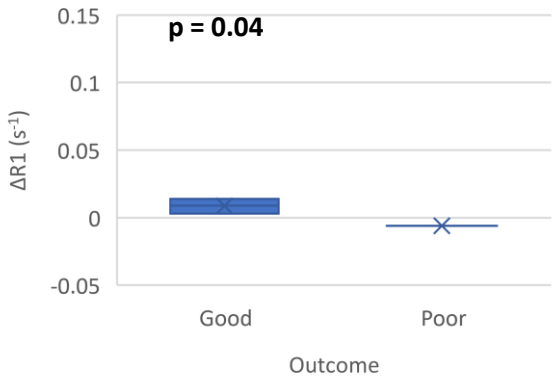


f) Post RT

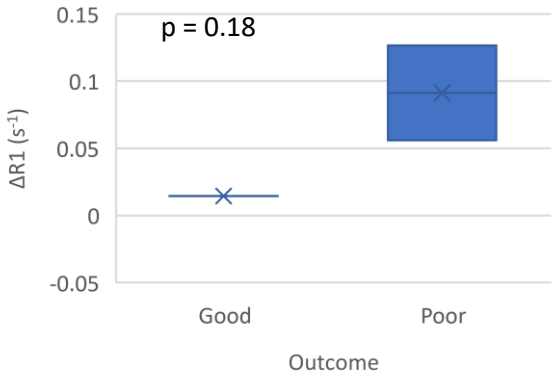


ΔR1 (s^{-1})

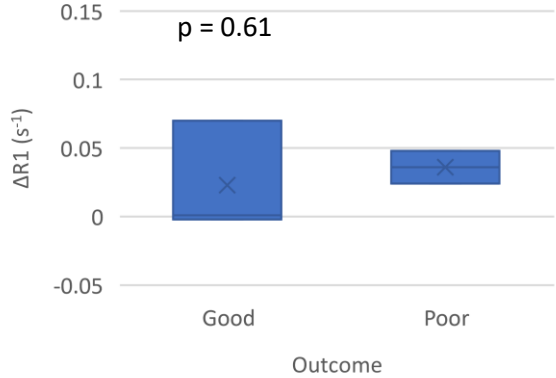
g) Baseline



h) During RT



i) Post RT



Normal tissue

T1 values for gluteal muscle on air and oxygen at the three imaging timepoints are shown in Table 3.9. The median T1 values for muscle were all lower than the equivalent median T1 in tumour at each time point. At baseline, T1 did not appear to change substantially from air to oxygen breathing. On RT, there were 3 paired scans. One showed a fall in T1 with oxygen but the others again showed little difference. Post treatment, 5 paired scans were available. Of these, two showed an appreciable fall in T1 with oxygen. Native T1 changes over the course of CRT were noted. For the majority of patients (3/5), values remained stable throughout treatment. For one patient T1 rose at each scan and another had stable T1 on treatment which fell subsequently. Potential reasons for changes in muscle readings during radiotherapy are discussed in Chapter 4 section 2.3.

There was a consistently visualisable difference in the T1 map on air and 100% oxygen in the bladder though this was not formally planned for assessment (Figure 3.8).

Table 3.9: Mean ShMOLLI T1 in muscle on air and oxygen at baseline, during and post RT

	Mean T1 [ms] (S.D)					
Study #	**Baseline**		**On RT**		**Post RT**	
	Air	**Oxygen**	**Air**	**Oxygen**	**Air**	**Oxygen**
RHB09	750.9 (127.1)	771.2 (131.1)	1008.8 (128.6)	799.0 (136.4)	1136.5 (165.6)	1089.3 (137.8)
RHB10	1105.9 (233.4)	1107.0 (229.8)	1039.7 (167.3)	1107.1 (223.8)	920.1 (125.5)	910.9 (140.3)
RHB11	855.7 (128.0)	859.7 (139.9)	*	*	871.2 (97.0)	860.6 (89.2)
RIT59	1132.6 (176.4)	1108.6 (166.0)	N/A	N/A	1148.1 (868.7)	1146l6 (156.7)
RIT60	873.32 (87.5)	856.36 (85.7)	849.0 (84.3)	817.5 (93.6)	868.68 (97.3)	773.8 (84.1)
RIT61	1285.0 (168.1)	*	*	1205.1 (243.8)	*	*
Median (IQR) (IQR)	989.6 (265.8)	859.7 (250.6)	1008.76 (110.8)	959.9 (322.4)	920.1 (265.3)	910.94 (228.7)

*Poor fit, N/A = non applicable, scan not undertaken

3.2.4 Goodness of fit

Of the 34 ShMOLLI slice sequences undertaken, 5 were deemed unanalysable due to poor model fit.

3.3 Discussion of ShMOLLI T1 mapping with oxygen

The analysis of ShMOLLI slice volume versus total tumour volume demonstrates limitations in the potential to use a representative slice sequentially for assessment of treatment response. It would require further investigation with whole tumour volume ShMOLLI sequences to confirm the slice chosen is likely to be representative and the time taken per slice would likely be prohibitive.

The majority of paired scans at all timepoints showed a reduction in tumour T1 from air to 100% oxygen breathing. A fall in tissue T1 with inspired oxygen would be expected physiologically as by increasing dissolved oxygen in blood plasma and tissue fluid, the longitudinal relaxation time reduces with corresponding increase in the rate (R1)[275]. In the three instances where the T1 rose with inspired oxygen, this change was minimal and may be due to non-physiological factors such as ROI shift between scans. Alternatively, a minimal change in mean T1 could suggest tumours are hypoxic and/or have poor perfusion or reflect a heterogeneous tumour.

The fact that all mean T1 values for the 2 RHYTHM A patients going straight to surgery were lower, and accordingly the ΔR1 higher, than those of the 6 patients requiring neoadjuvant therapy should be investigated further to see if T1 could be a useful biomarker pre-treatment. This has been demonstrated in renal cell carcinomas where native T1 values were found to be significant lower in lower grade tumours than high. T1 values were also significantly associated with histological collagen fraction[276].

It was noted that native mean T1 values for poor responders to CRT appeared higher than that for good responders both on and post treatment but not at baseline. Biopsy studies in the cardiac and

hepatic settings suggest that a longer T1 is associated with increased fibrosis[166, 167] [165]. Given that rectal tumour regression grading is based upon levels of fibrosis, the findings here in rectal cancer would not be expected. Imaging on and post radiotherapy is likely to reflect a range of processes including changes in oedema levels and the microvasculature[277]. It has been noted in cardiac imaging that oedema can alter T1[164]. Therefore T1 values may be reflecting a more complex process modifying the extracellular space than fibrosis alone.

There was no clear correlation at any timepoint between outcome and mean T1 for patients who received neoadjuvant chemoradiotherapy. However ΔR1 did show a significant association with outcome at baseline. This finding would need validation given the small numbers involved but is consistent with findings of O'Connor et al.[153] who noted a significant increase in R1 with oxygen, independent of tumour size and R1. During treatment the ΔR1 rose considerably on CRT in two tumours - this finding is in keeping with FMISO imaging showing a reduction in hypoxic volume on CRT. This could suggest tumour oxygen uptake was increased following 8-10 fractions of radiotherapy and may represent a reoxygenation effect. This is an important factor particularly in fractionated radiotherapy as radioresistant hypoxic tumour cells become reoxygenated. Changes in microvascular permeability secondary to inflammation may also be a factor in tumour oxygenation on treatment[277]. As the ΔR1 did not fall back to baseline, this could reflect a remaining hypoxic fraction 6 weeks post treatment, albeit reduced. Given these two patients had a poor response, CRT may have had a limited effect on the most hypoxic, radioresistant cells.

One good responder had stable ΔR1 during CRT with a rise following treatment. This may be because the initial reoxygenating effect with radiotherapy did not take place, however this could have happened later during treatment or even in the weeks following radiotherapy. For the two patients whose tumour ΔR1 fell from baseline, unfortunately the on-treatment value was unavailable. The fact that ΔR1 was low initially suggests that the addition of 100% inspired oxygen did not significantly change tumour oxygenation. This remained the case following treatment in

these two good responders. This could be because of hypoxia or possibly that the tumour was already very well perfused. A measure of the perfusion of these tumours may give some indication as to which scenario is correct. Perfusion imaging is discussed in Chapter 4. Numbers are small here and so test-retest information and larger datasets would be needed to validate whether these are true findings that reflect the underlying physiology as discussed.

In addition to small sample size, a clear limitation of these studies is lack of repetition to confirm reproducibility. This was largely due to time constraints given patients were due to start radical cancer therapy. Poor model fit was an issue in several ShMOLLI scans. Further modification of the imaging technique to improve noise to signal ratio and reduce motion may improve this.

Other issues may include lack of sensitivity using mean values in heterogeneous tumours, inability to detect change on a less powerful 1.5T clinical MRI or because the tumours are significantly hypoxic and hypoperfused so ΔR1 is not altered with increasing oxygen inspiration levels. Patient physiology may also impact on tumour oxygenation for example lung function, vessel patency and haemoglobin levels. However, the fact that bladder T1 was consistently altered would suggest that oxygen uptake was occurring to some extent – this effect has been described by Wang et al[278].

ShMOLLI with inspired oxygen as a contrast agent requires technique refinement to further assess its practicality. Mean tumour T1 and ΔR1 require further assessment as to their reflection of tumour oxygenation in rectal cancer. Spatial variation should also be considered to account for heterogeneity.

4. Comparing imaging with histopathological markers of hypoxia

Whilst functional imaging allows visualisation of tumour pathophysiologic activity, IHC can provide a snapshot of tissue function. Comparison of the two can lead to deeper understanding of the underlying processes and improvement of both approaches.

4.1 Methods

Resection specimen processing

The 3 patients in RHYTHM-A took oral pimonidazole 500mg/m^2 between 16 to 24 hours prior to surgical excision. Following resection, tumours were mounted and fixed in formalin. An *ex vivo* MRI was performed and the specimens sectioned in axial plane guided by the imaging as interpreted by JF or MA (Department of Radiology, Oxford University Hospitals NHS Foundation Trust). Sectioning was undertaken by LMW (Department of Pathology, Oxford University Hospitals NHS Foundation Trust).

IHC

Staining was undertaken on one slice per section for haematoxylin and eosin (H&E) in addition to pimonidazole, CAIX and CD31. This work was undertaken at the Oxford Cancer Centre Good Clinical Practice Laboratory by Dr L. Campo. Once optimised, all protocols were automated on the Leica Bond-Max (Leica Biosystems, Milton Keynes, UK).

The antibodies used were:

- CAIX: Rabbit polyclonal anti-CAIX (Abcam, Cambridge, UK), diluted to 1:2000 in dilution buffer
- Pimonidazole: Hydroxyprobe-1 Mab1 anti-pimonidazole mouse IgG1 monoclonal antibody (NPI, Burlington, MA, USA), 1:1000 dilution
- CD31: monoclonal mouse anti-CD31 JC70A (DAKO, Ely, UK), 1:800 dilution

The primary antibody was added for 30 minutes followed by the post-primary antibody (Novocastra Bond Polymer Refine Detection Kit, Leica Biosystems) for 8 minutes, diaminobenzidine (DAB) for 10 minutes and haematoxylin for 5 minutes.

Image processing

All slides were imaged using an Aperio Scanscope slide scanner (Leica Biosystems, Milton Keynes, UK) at 20x magnification. Computational imaging analysis of the whole tumour area on each slide was undertaken by histopathologst Dr V. Koelzer (VK) using a machine learning algorithm (HALO® Image Analysis Platform, Indica Labs, Albuquerque, New Mexico, USA). VK manually outlined the tumour area. For CAIX and pimonidazole, a three point scale was graded for staining intensity. The boundaries were derived from this dataset based on internal control. The values were divided into thirds along the optical density of the stain. They were standardised across all slides using the established markers.

CD31 based capillary counting was undertaken using a machine learning algorithm which was trained to differentiate CD31 positive vessels from CD31 positive inflammatory cells based on based on ground truth pathologist assessment of linear stained structures and lumen, and a minimum size criteria. Vessel quantification within the annotated tumour region was combined with a machine learning step (random forest classifier) to exclude non-specifically stained tumour areas. A vessel density visualisation was then produced. This digital imaging analysis technique has previously described by Koelzer et al[279] who compared the automated process of PDL1 staining in melanoma patient samples with blinded findings of two pathologists, showing good correlation. Di Tacchio et al[280] went on to develop the technique to identify immune cells and vessels in mouse model and patient glioblastoma samples. Ideally we would compare this with a well-established method such as Chalkley counting[281] but there was insufficient availability of pathology expertise to carry out this time-consuming technique[282].

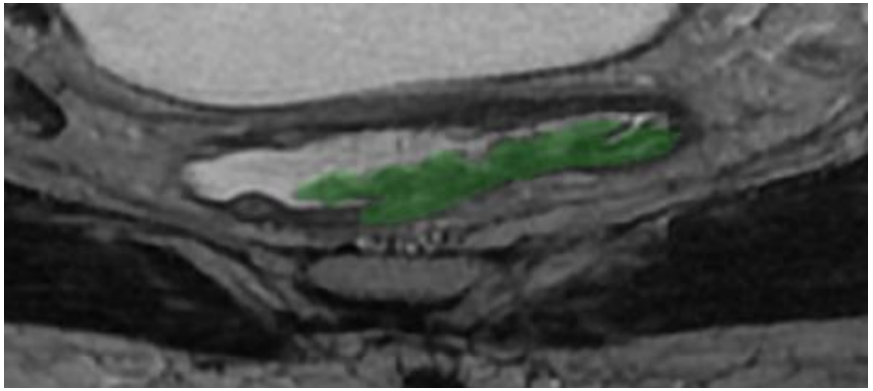
4.2 Results

An example of multimodality imaging and pimonidazole staining across a single tumour slice is shown in Figure 3.12. It proved challenging to directly correlate the sectioned slices to specific

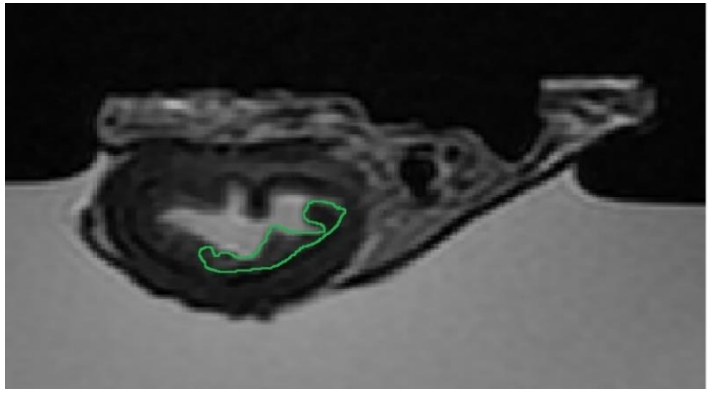
imaging slices reliably despite the *ex vivo* MRI. Therefore total values and percentages across all slides in each tumour were obtained for comparison rather than a direct slide to imaging slice tumour ROI spatial comparison as intended. The full dataset can be found in Appendix 2. Figure 3.13 demonstrates the different stains used for analysis and Figure 3.14 shows the cell level analysis and heatmapping provided by the machine leaning algorithm for pimonidazole and CAIX. The former uses nuclear segmentation to identify singe cells. The latter indicates tumour stain intensity in the tumour and stromal tissue. Figure 3.15 demonstrates the identification of blood vessels on a CD31 stained slide.

Figure 3.12: Example of Rhythm A tumour imaging a) in vivo MRI, b) ex vivo MRI, c) FMISO PET-CT at 4 hours & d) slide stained for pimonidazole (tumour ROI in green)

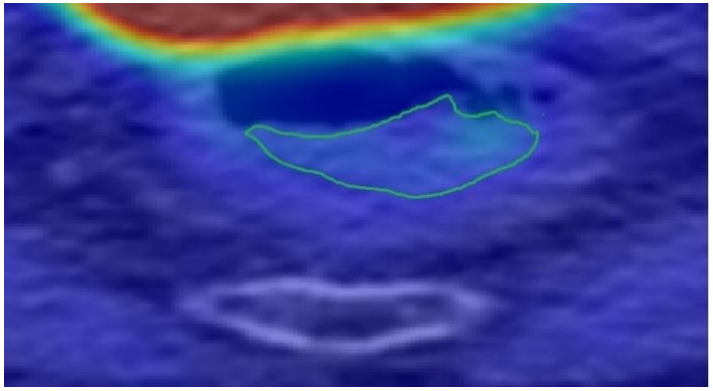
a) ***In vivo*** **T2w axial MRI**



b) ***Ex vivo*** **T2w axial MRI**



c) Static FMISO PET/CT at 4 hours



d) Pimonidazole stained slides

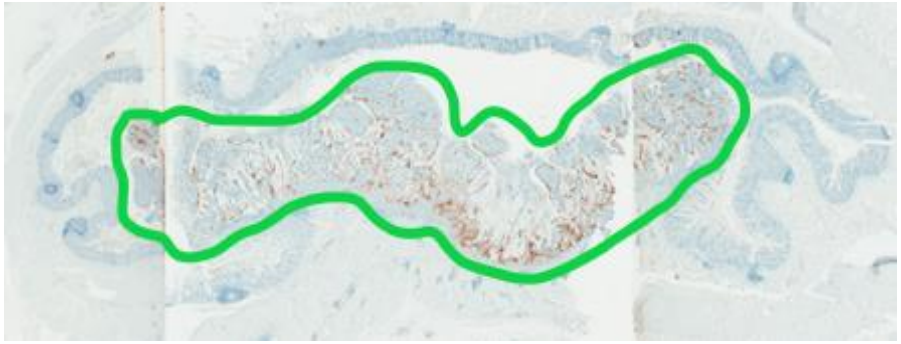
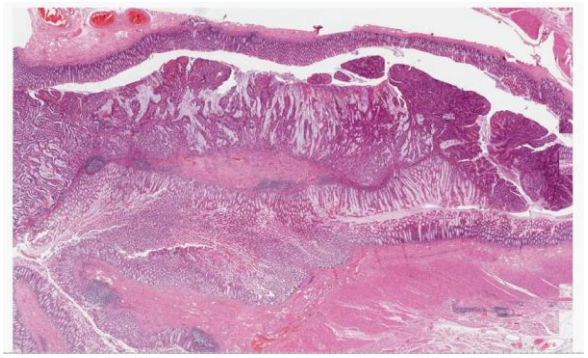


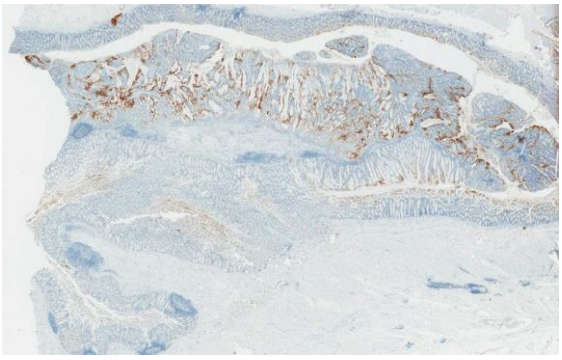
Figure 3.13: Example slice of consecutive stained histopathology slices for RHYTHM A patient

a) H&E, b) pimonidazole, c) CAIX, d) CD31

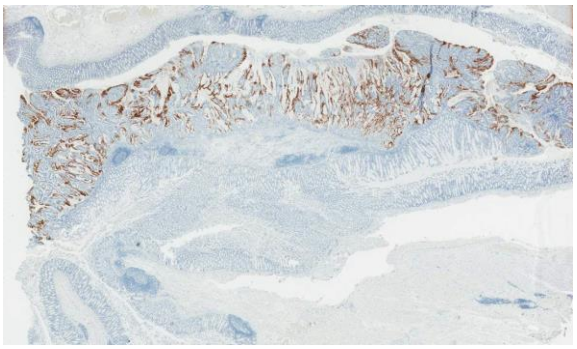
a)



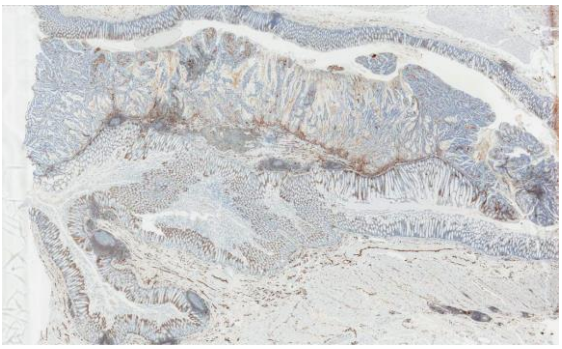
b)



c)

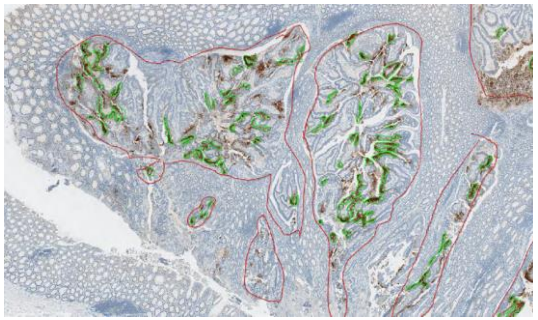
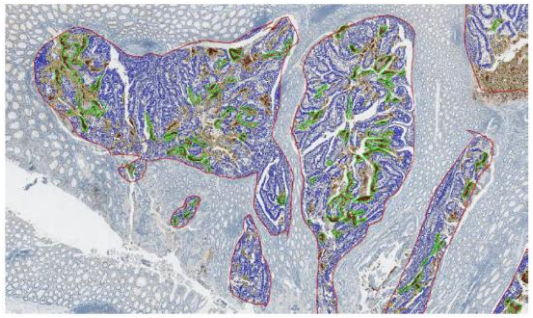
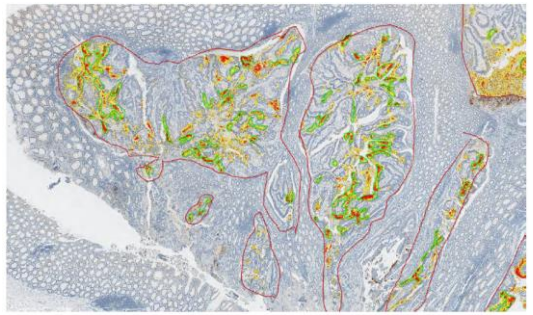
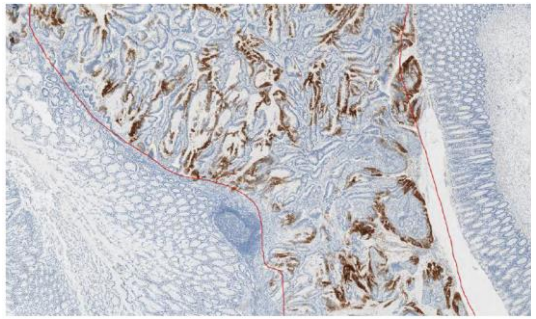
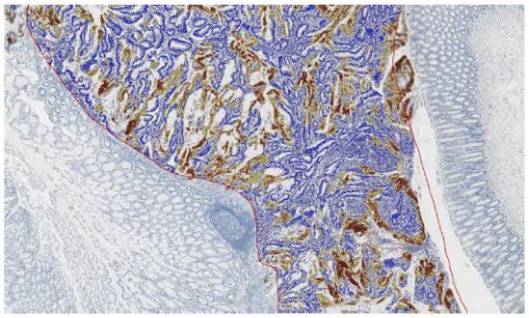
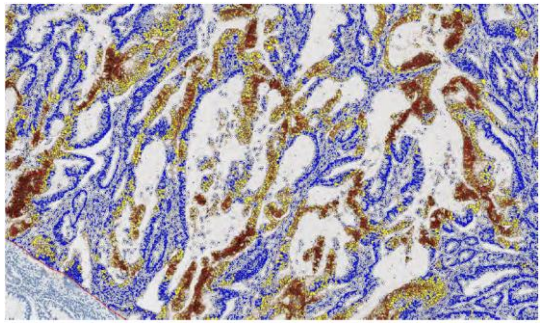


d)



H&E: haematoxylin & eosin

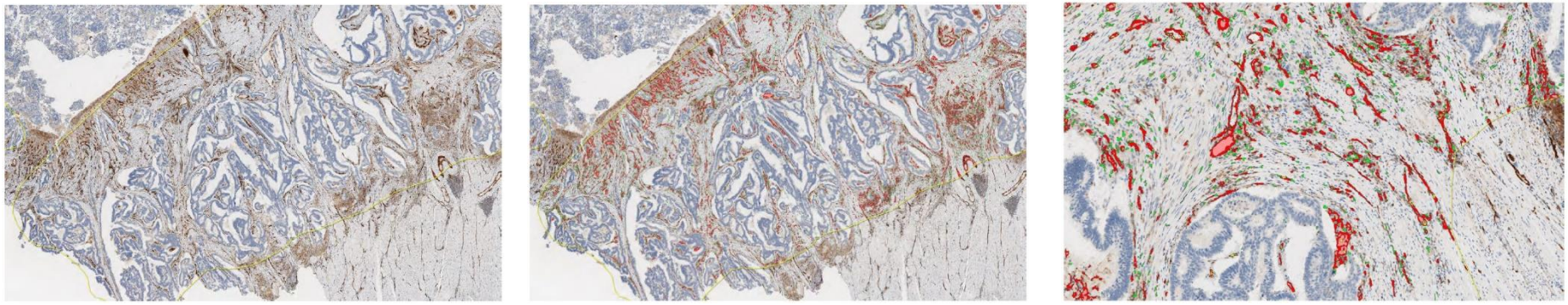
Figure 3.14: RHYTHM A example of slice cell level analysis and heatmapping for tumour stain intensity for pimonidazole and CAIX

	Stained slide	Cell level analysis	Heatmapping
Pimonidazole			
CAIX			

Red line annotation: total tumour area, Green line annotations: necrotic tumour tissue (both outlined by VK); Negative (blue), Weak positive (yellow), moderate positive (orange), strong positive (red) in vital tumour tissue

Figure 3.15: RHYTHM A CD31 vessel density quantifation a) stained slide, b) vessel density visualisation, c) detailed higher magnification vessel density visualisation

a) **b)** **c)**



Yellow line annotation: total tumour area (outlined by VK)

Pimonidazole

Table 3.10 describes the pimonidazole staining characteristics in RHYTHM A. It can be seen from Figure 3.12 that there was diffuse staining of varying intensity and this pattern was seen in all 3 RHYTHM A patients. The number of slides reflects the different volumes of the tumours ranging from 7.1 cm^3 in RHA03 to 28.8cm^3 in RHA02 on T2 axial MRI. The proportion of pimonidazole staining is 14% in both RHA01 and RHA03, being lower at 5.6% in RHA02. The breakdown of staining intensity is comparable between patients.

Table 3.10: Pimonidazole staining characteristics in RHYTHM A

Study #	No. of slides	Tot tis A (cm^2)	Tot pimo A (cm^2)	% pimo +	% pimo weak	% pimo moderate	% pimo strong
RHA01	20	14.26	2.06	14.4	67.5	19.5	13.1
RHA02	32*	21.29	1.19	5.6	61.2	19.5	19.4
RHA103	13	3.92	0.57	14.5	60.8	23.0	16.3

Tot tis A = total tissue area; Tot pimo A = total pimonidazole area; % pimo + = percent of ROI staining for pimonidazole; *One slide removed due to overstaining

CAIX

CAIX staining characteristics are presented in Table 3.11. In all patients the proportion of tumour area staining positive with CAIX was less than that with pimonidazole. In the case of RHA02 the figure was 10 times lower. In terms of staining intensity, like pimonidazole, the proportion of weak intensity was the highest followed by moderate and then strong. However the tumour with the greatest proportion of strong intensity staining was RHA03 for CAIX with RHA02 having the least.

Using pimonidazole, RHA02 had the greatest proportion of strong staining and RHA01 the least.

Table 3.11: CAIX staining characteristics in RHYTHM A

Study #	No. of slides	Tot tis A (cm^2)	Tot CAIX A (cm^2)	% CAIX +	% CAIX weak	% CAIX moderate	% CAIX strong
RHA01	12	6.69	0.90	13.4	62.5	21.9	15.6
RHA02	29	23.91	0.12	0.49	72.1	18.0	9.9
RHA103	15	5.40	0.52	9.66	55.2	24.3	20.6

Tot tis A = total tissue area; Tot CAIX A = total CAIX area; % CAIX + = percent of ROI staining for CAIX

CD31

Table 3.12 summarises the tissue, tumour and vessel area analysed in each RHYTHM A patient's tumour. The total tissue area ranged from 5.96 cm^2 in RHA03 to 21.25 cm^2 in RHA02. In the former, the tumour area comprised 55.7% of the total tissue area, whereas for the latter it was 44.6%. RHA01 contained the lowest proportion of tumour at 39.0%. The remainder was comprised of vessels, inflammation, stroma and white space areas as designated by machine learning algorithm. The lowest proportion of tissue area occupied by vessels was 6.0% in RHA03, being highest at 11.2% in RHA02. Mean vessel density similarly was lowest in RHA03 at 56.33 mm^{-2} (S.D. 18.09) and highest in RHA02 at 18.93 $^{-2}$ (S.D. 14.33), being 71.90 $^{-2}$ (S.D.28.11) in RHA01.

Table 3.13 summarises the IHC and hypoxia imaging results for RHYTHM A, which are discussed below.

Table 3.12: Tumour area and microvessel density defined by CD31 in RHYTHM A

Study #	No. of slides	Tot tis A* [cm^2]	Tot ROI A [cm^2] (%)	Tot vessels A [cm^2] (%)	Tot CD31 cap count**	MVD [mm^2] (S.D.)
RHA01	16	9.44	3.68 (39.0)	0.70 (7.4)	69,273	71.90 (28.11)
RHA02	32	21.25	9.48 (44.6)	2.19 (11.2)	174,557	80.93 (14.33)
RHA03	13	5.96	3.20 (53.7)	0.35 (6.0)	34,164	56.33 (18.09)

No. = number; Tot tis A = total tissue area; Tot ROI A = total region of interest (tumour) area; Tot vessels A = total vessels area; Tot CD31 cap count = total CD31 capillary count; MVD = mean vessel density; S.D. = standard deviation; *Includes tumour, vessels, inflammation, stroma and white space areas; **Corrected by non-specific reaction for CD31 in inflammatory cells and tumour cells (excluded by machine learning)

Table 3.13: Summary of hypoxia IHC and imaging results

Study #	IHC: pimonidazole, CAIX and CD31			Imaging: FMISO PET-CT and ShMOLLI MRI		
	% pimo +	**% CAIX +**	**MVD CD31 [mm^{-2}] (S.D.)**	**T:M hVOL [cm^3] (% tot)**	**T:B hVOL (cm^3) (% total)**	**ShMOLLI ΔR1 (s^{-1})**
RHA01	14.4	13.4	71.90 (28.11)	*	*	N/A
RHA02	5.6	0.49	80.93 (14.33)	0.12 (0.4)	0.15 (0.5)	*
RHA03	14.5	9.66	56.33 (18.09)	0.10 (1.6)	0.19 (2.7)	0.085

% pimo + = percent of ROI staining for pimonidazole; % CAIX + = percent of ROI staining for CAIX; MVD = mean vessel density; T:M hVOL = FMISO tumour:muscle hypoxic volume; T:B hvol = FMISO tumour:blood hypoxic volume *Scan could not be analysed/artefact present; N/A – not applicable, scan not undertaken

4.3 Discussion

Pimonidazole and CAIX staining exhibited broadly similar proportions in terms of percentage area positive with comparable proportions of stain intensity. Both hypoxia markers showed RHA02 to be less hypoxic than the other 2 tumours despite its larger size. However there were some notable discrepancies, for example RHA02 had the largest proportion of strong intensity pimonidazole but the least of CAIX. This may well reflect the different underlying pathways reflected with CAIX induced by HIF and pimonidazole being an exogenous agent which diffuses intraceullarly and is reduced at low partial oxygen pressures. These findings are in keeping with other colorectal cancer studies which found similar but not identical distributions[241, 283].

CD31 based capillary counting was undertaken using a machine learning algorithm which requires

validation in an independent cohort. There may be limitations to this process, for example if involving a small area. It is also possible using this algorithm that some vessels could be counted more than once. It does allow for additional detailed analysis of vessel count and morphology, better for large vessels than capillaries, although not discussed here.

MVD analysis showed that this rose in line with the total areas of tissue, tumour and vessels examined. In this case, the largest tumour, RHA02 had the highest MVD. This did equate, as might be expected, with it having the lowest proportion of hypoxia as defined by pimonidazole and CAIX staining. However, it did exhibit the highest proportion of strong intensity pimonidazole staining, which may be particularly important if considering neoadjuvant therapy and hypoxia related resistance. It would be interesting to assess this tumour for levels of angiogenesis factors such as vascular endothelial growth factor compared to the others in the cohort.

When compared to imaging findings, the FMISO-defined hypoxic volumes were lower in RHA02 than RHA03, in keeping with the IHC. The percentage of pimonidazole area staining positive was higher than the percentage of tumour volume identified as hypoxic on FMISO PET-CT though both are nitroimidazoles. This may be related to the comparison of area versus volume, method of administration (oral versus intravenous) or true differences in uptake. Troost et al found a weak but significant correlation between FMISO imaging and pimonidazole hypoxic fraction in HNSCC xenografts[284]. A murine breast cancer model also showed a positive linear correlation between FMISO PET SUV and percent pimonidazole staining following systemic therapy[285].

4.4 Conclusion of IHC and imaging

Comparison of imaging with immunohistochemistry provides one mechanism of validating semi- and quantitative parameters. However this does involve challenges such as spatial matching, differences in scale and sampling, accounting for tumour shrinkage and anatomical distortion and variation in range of oxygenation levels measured. In this study, it was challenging to draw spatial

distribution comparisons with histology and imaging. Whole mount histology would potentially provide an appropriate comparator to imaging but again may be limited by the significant processing required and requirement for multiple stains. There are limitations of the stains themselves, for example CD31 may stain cells other than endothelial such as macrophages[286]. Even using consecutive slides of tissue, there were differences in tissue area that may confound attempts to compare stains. Dual or triple staining a single slide may overcome this but analysis becomes more complex, would require differential tagging and automation. Machine based learning and artificial intelligence may have a significant role in future histopathological analysis but require appropriate testing and validation with standard techniques. In the RHYTHM study, immunohistochemistry demonstrated diffuse patterns of hypoxia, concurring with imaging findings.

5. Conclusion

Measuring tumour oxygenation by means of imaging in rectal cancer is challenging for a variety of reasons including tumour factors such as heterogeneity, anatomical factors such as bowel peristalsis and faecal tracer uptake as well as limitations in imaging resolution. FMISO-PET use in rectal cancer provided significant issues, consistent with previous studies[140, 142]. Alternative hypoxia tracers with higher tumour uptake such as 18F-FAZA[139] may be considered but many of the aforementioned challenges remain.

Novel imaging techniques such as oxygen-enhanced MRI require further investigation but demonstrated considerable limitations such as time required to image a single slice and SNR. Dynamic perfusion imaging biomarkers that may provide an alternative indicator of tumour hypoxia will be discussed in the next chapter.

Chapter 4: Perfusion and dynamic imaging with perfusion CT, dynamic contrast enhanced MRI and dynamic FMISO PET-CT

1. Introduction

Dynamic imaging is investigated in this chapter with results from the RIT and RHYTHM studies. Three different imaging modalities are assessed for change in perfusion parameters with radiotherapy and association with response to treatment.

The aims are to assess the use of dynamic imaging in rectal cancer by:

- Assessment of dynamic FMISO PET imaging parameters in tumour response to radiotherapy
- Identification of changes in blood volume and flow with radiotherapy using perfusion CT
- Investigation of DCE MRI parameter Ktrans in patients being treated with radiotherapy

2. Dynamic FMISO PET-CT

Tumour hypoxia[58] influences radiotherapy response and has been suggested to be inversely related to perfusion[93]. Dynamic FMISO PET-CT may provide useful information about both these pathophysiological features, which could allow targeting through radiotherapy boost and/or systemic therapy.

2.1 Methods

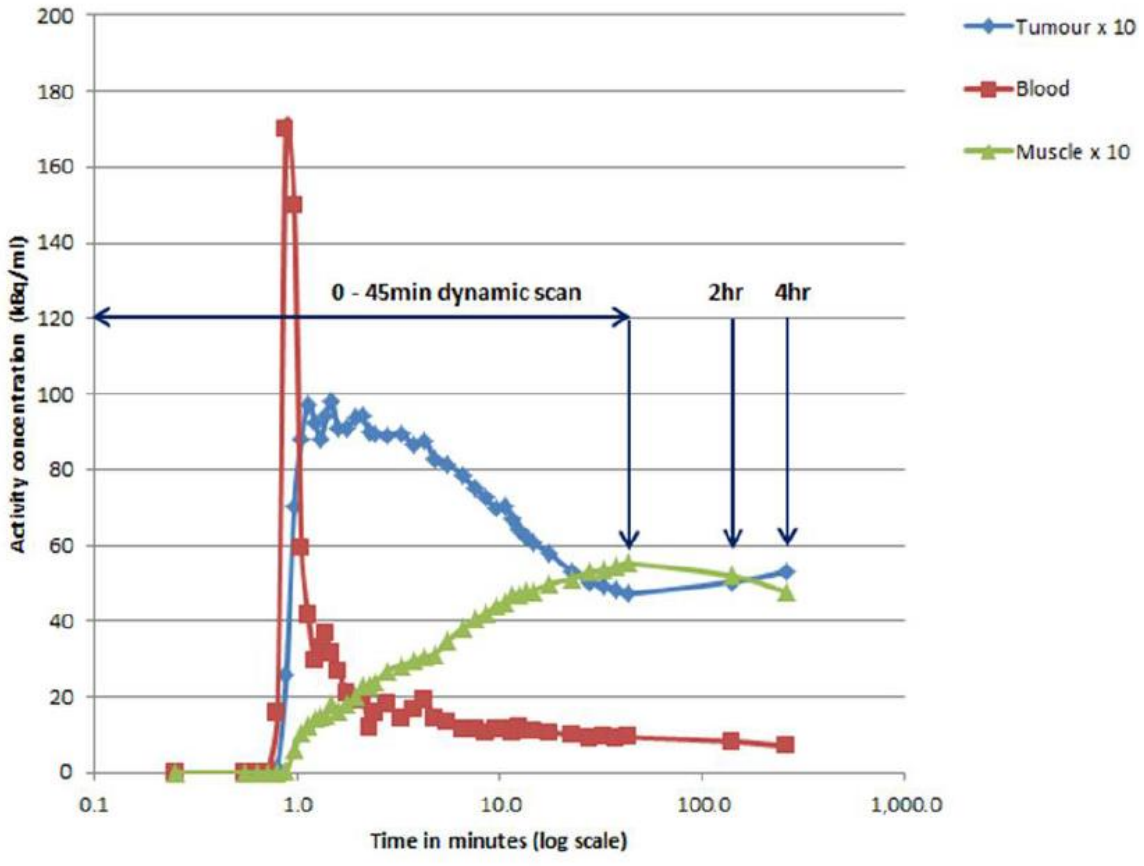
Dynamic FMISO PET imaging in the RHYTHM B study was planned at baseline and 8-10 fractions of radiotherapy. A 0 to 45 minute scan was done followed by repeat scanning at 2 and 4 hours post-

injection for 10 minutes each. ROI outlining was as per Chapter 3, section 2.1.3.

Dynamic FMISO PET analysis was done in collaboration with Dr T. Puri (Department of Oncology, University of Oxford), who processed the dynamic FMISO PET-CT scans and the time-activity curves. Time activity curves (TAC) were established for tumour, muscle, and blood. The former used the image-defined ROIs and the latter combined bilateral pelvic arterial counts to determine an image-derived arterial input function, which were then calibrated to plasma concentrations (Figure 4.1).

Figure 4.1: Example FMISO time activity curve in tumour, blood and muscle

(Adapted from Puri et al EJNMMI Research 2017[262]*)



*Under Open Access terms of the Creative Commons Attribution 4.0 International Licence

Various models were used to interrogate the data. Within PMOD image processing software

(PMOD Technologies (v3.6) Ltd, Zurich, Switzerland), standard 1, 2 and 3-tissue compartmental models with 3, 5 and 7 parameters respectively were analysed. The Casciari model[147] (8 parameters), developed specifically for [^{18}F]FMISO, was analysed within MATLAB (R2013b, The MathWorks, Inc., Natick, Massachusetts, United States). Akaike information criteria (AIC) were used to assess the data fit for the different pharmacokinetic models in SPSS (IBM Corp. Released 2017. IBM SPSS Statistics for Windows, Version 25.0. Armonk, NY) by Dr Puri.

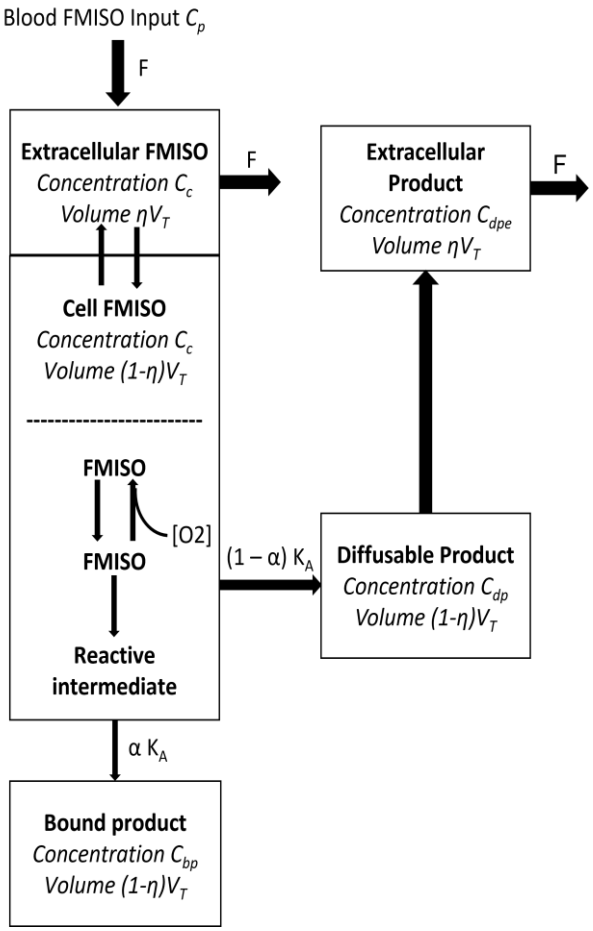
Casciari Model

The Casciari compartmental model is shown in Box 4.1 and accounts for bound and diffusible product in terms of the parent drug concentration[147]. For physiological relevance, the lower-limit of fitting parameters was set at 0, the upper-limit for η and α was set to unity as these were fractional values and the upper-bound of other parameters was set at 5 to obtain results in per second units.

Statistical analysis

The PET parameters in this small sample size were reviewed on histogram and noted to be non-normally distributed so a non-parametric analysis was undertaken.

Box 4.1: Casciari compartmental model (adapted from Casciari et al[147])



$$\frac{dCc}{dt} = \frac{F}{Vt} \text{ x } (Cp - Cc) - (1-\eta) \text{ x } Ka \text{ x } Cc$$

$$\frac{dCbp}{dt} = \alpha \text{ x Ka x Cc}$$

$$\frac{Cdp}{dt} = (1-\alpha) \text{ x } Ka \text{ x } Cc - Kb \text{ x } Cdp$$

$$\frac{dCdpe}{dt} = \left(\frac{1-\eta}{\eta}\right) \text{x Kb x Cc} - \left(\frac{\text{F}}{\eta \text{ x Vt}}\right) \text{ x } Cdpe$$

$$A(t) = \beta 1\ x\ Cp + \beta 2 \text{ x Vt x } \{\text{Cc} + (1 + \eta) \text{ x } (\text{Cbp} + \text{Cdp}) + \eta\ x\ Cdpe\}$$

C_x: Concentration (counts per minute/mL or % injected dose/mL)

F: blood perfusion (microvascular flow rate in mL/g/min)

K_A: cellular FMISO reaction rate related to fraction of cells in a region that are hypoxic (min^{-1}) [inversely related to O_2 concentration]

V_T: tissue specific volume (mL/g)

η: the fraction of V_T occupied by extracellular space (no units)

α: the fraction of hydroxylamine reactive intermediate that is converted to bound products

Not shown in diagram:

A(t): total activity of FMISO in tissue

β_1: partial volume correction factor

β_2: spill-in correction factor

K_b: rate constant for transport of diffusible products out of the cell (min^{-1})

2.2 Results

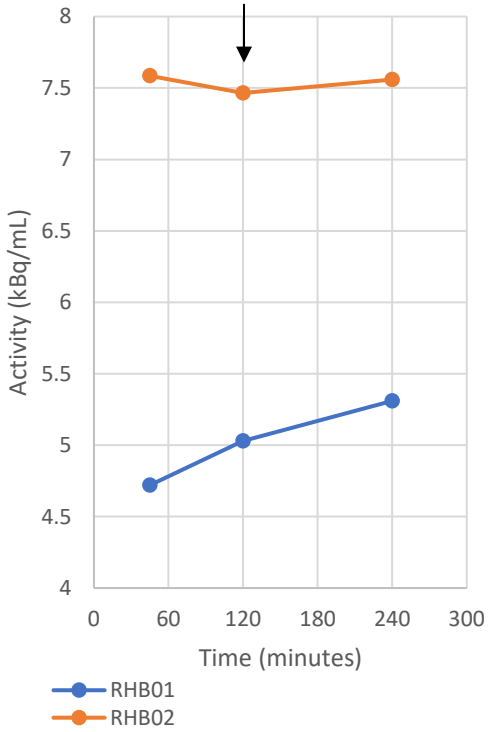
Dynamic FMISO PET imaging data were available for 10 of the 11 RHYTHM B patients at baseline and 9 patients whilst on radiotherapy.

2.2.1 Selection of 0 – 45 minute data

As discussed in Chapter 3, spill-in from bladder and faecal excretion of tracer contributed to difficulties in analysing the 4-hour PET scans. The protocol change mandating an enema prior to the 4-hour scan mitigated some of these issues but they were also present at the 2-hour images. Bladder emptying may also affect the activity recorded in the tumour. This is demonstrated by the Time-Activity Curve (TAC) examples in Figure 4.2 with imaging in Figure 4.3. Patient RHB02 voided their bladder shortly before the 2-hour PET scan, causing a drop in activity in the tumour. This then reaccumulated before the final scan at 4 hours in contrast to the steady increase noted in RHB01. In view of these potential effects, the 0 – 45 minute dynamic scans were analysed as all the available datasets could be included

Figure 4.2: Examples of change in activity (KBq/mL) between baseline FMISO PET scans over time in a) tumour and b) bladder in RHYTHM B study (↓ indicates bladder voided in RHB02)

a)



b)

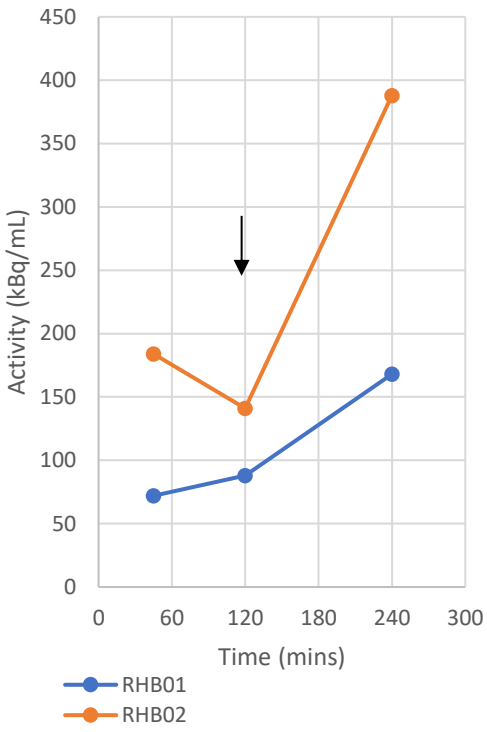
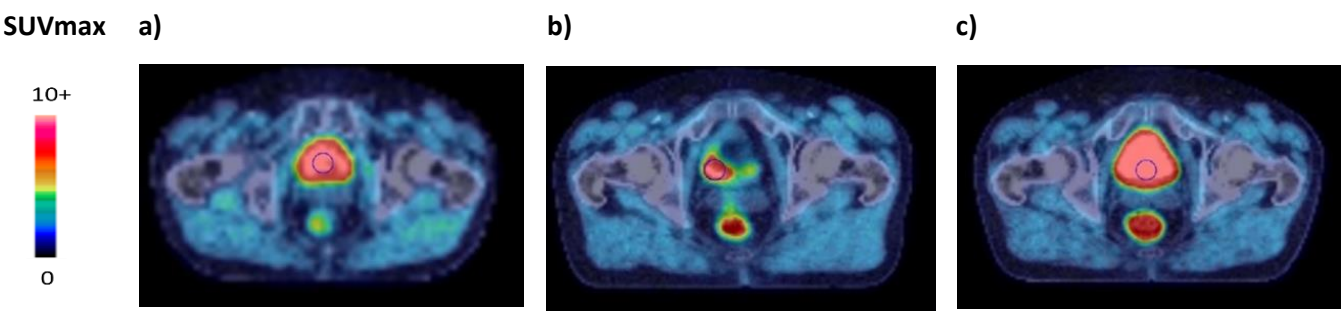


Figure 4.3: RHYTHM B study RHB02 FMISO imaging at a) 45 mins b) 2 hours (post bladder void) and c) 4 hours (bladder refilled)



Blue circular ROI 10mm radius within bladder. Tumour not shown on these slices. Uptake in rectum at 2 and 4 hours is due to faecal excretion.

2.2.2 Pharmacokinetic model fitting

Table 4.1 shows the tumour AIC values for the dynamic PET data from 0 to 45 minutes at baseline and after 8 to 10 fractions of radiotherapy. The lowest AIC value determines the best fit and for 17 of 19 data points, this was the Casciari model. It was also found to be the best fit for muscle data in 18 of 19 scans (Table 4.2).

Table 4.1: Tumour AIC values for 0 – 45 minute dynamic FMISO PET data fitting to pharmacokinetic models - 1, 2 and 3 tissue compartmental (TCM) and Casciari

Study #	Baseline				On radiotherapy			
	1 TCM	**2 TCM**	**3 TCM**	**Casciari**	**1 TCM**	**2 TCM**	**3 TCM**	**Casciari**
RHB01	26	-20	-19	-71	6	-34	-29	-39
RHB02	86	44	47	-21	70	61	66	0
RHB03	50	73	17	-38	50	27	31	-52
RHB04	36	-23	18	-70	40	39	44	5
RHB05	63	42	39	-19	58	56	61	-17
RHB06	50	5	9	17	N/A	N/A	N/A	N/A
RHB07	84	65	72	-36	126	118	124	74
RHB08	27	8	6	-8	26	3	9	-5
RHB09	8	-10	-6	1	8	1	7	-4
RHB10	N/A	N/A	N/A	N/A	N/A	N/A	N/A	N/A
RHB11	65	30	30	-53	82	Failed	Failed	80

TCM = Tissue compartmental mode

Table 4.2: Muscle AIC values for 0 – 45 minute dynamic FMISO PET data fitting to pharmacokinetic models - 1, 2 and 3 tissue compartmental (TCM) and Casciari

Study #	Baseline				On radiotherapy			
	1 TCM	2 TCM	3 TCM	Casciari	1 TCM	2 TCM	3 TCM	Casciari
RHB01	27	31	37	-137	-20	-41	-36	-106
RHB02	-27	-69	-65	-157	-53	-46	-38	-132
RHB03	-5	1	8	-195	19	-9	-5	-159
RHB04	28	-46	-43	-152	14	-17	-12	-78
RHB05	38	42	49	-117	10	15	21	-17
RHB06	31	35	41	-73	N/A	N/A	N/A	N/A
RHB07	-23	-17	-12	-101	23	28	36	-64
RHB08	-30	-24	-7	-71	34	41	47	-125
RHB09	12	15	27	-122	0	-31	-16	-69
RHB10	N/A	N/A	N/A	N/A	N/A	N/A	N/A	N/A
RHB11	-2	-1	4	-114	-5	-40	-39	-18

TCM = Tissue compartmental mode

2.2.3 Tumour hypoxia (K_A) and perfusion (F) using the Casciari model

Tumour hypoxia (K_A) and perfusion (F) parameter data are provided in Table 4.3. The median F was 4.10 mL/g/min (IQR 1.71) at baseline, falling to 2.48 (IQR 3.62) on RT, a median fall of 29.0% (IQR 68.1). For K_A the median at baseline was 0.92 min^{-1} (IQR 0.14), falling to 0.70 min^{-1} (IQR 0.10) on treatment, a median difference of 23.7% (IQR 41.6).

These data show that most (6/9 evaluable patients) had a reduction in tumour perfusion (F) during radiotherapy. In contrast, three patients showed an increase in perfusion (F). Similarly most patients (8/9 evaluable) showed a reduction in hypoxia (KA) in the second week of radiotherapy with only one patient (RHB04) showing a modest increase in hypoxia. There was no apparent relationship between the measured changes in perfusion and hypoxia with the onset of radiotherapy in this dataset.

2.2.4 Muscle hypoxia (K_A) and perfusion (F) using the Casciari model

Table 4.4 shows muscle hypoxia (K_A) and perfusion (F) parameter data. Median F was 0.12 mL/g/min (IQR 0.04) at baseline, which increased by 388% to 0.60 mL/g/min (IQR 0.12) on CRT. Median K_A was 0.02 min^{-1} (IQR 0.03), increasing to 0.86 min^{-1} (IQR 0.76) on CRT, which represented a 3314% (IQR 2933.5) change.

Table 4.3: Casciari model tumour parameters perfusion (*F,* mL/g/min) and hypoxia (K_A min^{-1}) for 0 – 45 minute dynamic FMISO PET data at baseline and during RT

Study #	Response	Baseline		On RT		% Change	
		F	K_A	F	K_A	F	K_A
RHB01	Good	0.59	1.38	0.29	1.19	-50.0	-14.0
RHB02	Good	1.43	1.58	2.47	0.70	73.1	-55.5
RHB03	Poor	3.20	0.91	2.48	0.70	-22.3	-23.7
RHB04	Poor	4.41	0.63	3.31	0.70	-29.0	11.4
RHB05	Good	6.71	0.92	4.38	0.72	-34.6	-22.1
RHB06	Poor	6.71	0.93	N/A	N/A	N/A	N/A
RHB07	Good	3.94	0.92	4.66	0.62	18.1	-33.1
RHB08	Good	4.37	0.87	0.75	0.31	-82.8	-64.1
RHB09	Poor	4.25	0.71	0.76	0.10	-82.2	-86.6
RHB10	Good	N/A	N/A	N/A	N/A	N/A	N/A
RHB11	Good	2.53	0.76	6.19	0.72	145.1	-5.5
Median	-	4.10	0.92	2.48	0.70	-29.0	-23.7
IQR	-	1.71	0.14	3.62	0.10	68.1	41.6

N/A = non-applicable, scan not done

Table 4.4: Casciari model muscle parameters perfusion (*F,* mL/g/min) and hypoxia (K_A min^{-1}) for 0 – 45 minute dynamic FMISO PET data at baseline and after 8 – 10 fractions radiotherapy

Study #	Response	Baseline		On RT		% Change	
		F	K_A	F	K_A	F	K_A
RHB01	Good	0.14	0.02	0.57	0.86	296.0	4700.0
RHB02	Good	0.10	0.04	0.67	1.43	559.0	3314.0
RHB03	Poor	0.12	0.02	0.60	0.36	400.0	1900.0
RHB04	Poor	0.13	0.02	0.60	0.36	376.0	1400.0
RHB05	Good	0.14	0.01	0.60	0.36	335.0	5900.0
RHB06	Poor	0.60	0.44	N/A	N/A	N/A	N/A
RHB07	Good	0.17	0.00	0.05	1.12	−69	n.d.
RHB08	Good	0.08	4.81	0.35	2.06	346.0	−57
RHB09	Poor	0.08	0.04	0.48	1.06	471.0	2833.0
RHB10	Good	N/A	N/A	N/A	N/A	N/A	N/A
RHB11	Good	0.11	0.01	0.60	0.37	426.0	6000.0
Median	-	0.12	0.02	0.60	0.86	388.0	3314.0
IQR	-	0.04	0.03	0.12	0.76	94.0	2933.5

N/A = non-applicable, scan not done; n.d. = not defined

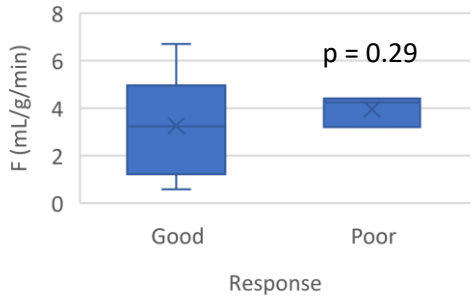
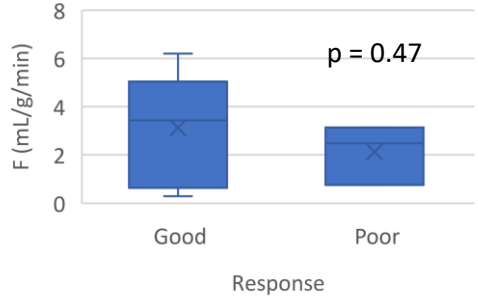
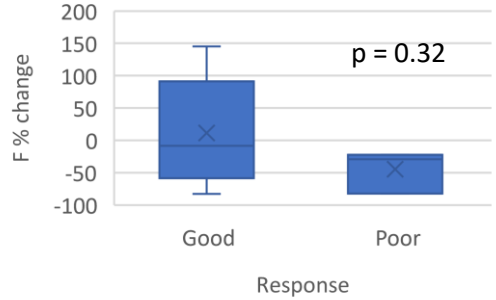
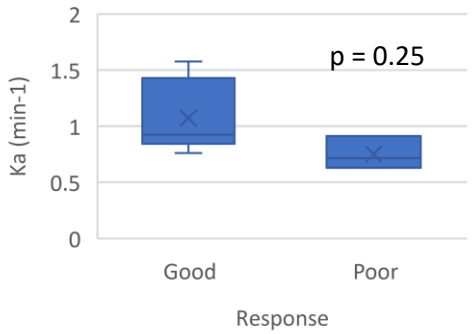
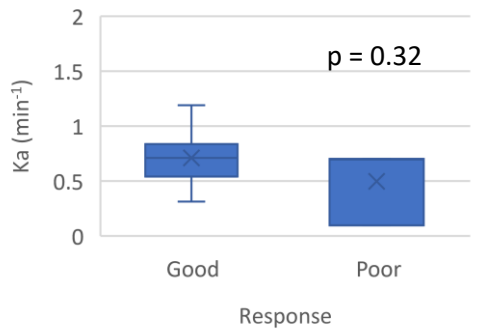
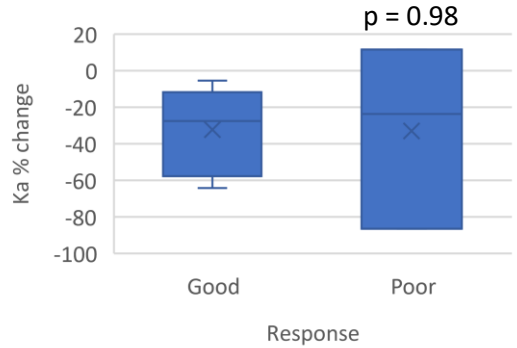
2.2.5 Casciari model tumour hypoxia (K_A) and perfusion (F) by response

Figure 4.4 summarises the hypoxia (K_A) and perfusion (F) data by response to radiotherapy at baseline and after 8 – 10 fractions of radiotherapy. At baseline the median F for good responders was 3.23 mL/g/min (IQR 3.73) versus 4.25 mL/g/min (IQR 1.00) for poor. Binary logistic regression shows no evidence of association with outcome ($\chi2(1) = 1.35$, $p = 0.29$). Median F fell for all 3 poor responders with paired scans and 3 of the 6 good responders. Thus all three patients who had an increase in perfusion in week 2 of radiotherapy had a good response to treatment. Median F on treatment was 3.43 mL/g/min (IQR 4.40) for good responders and 2.48 mL/g/min (IQR 1.19) for poor, again showing no significant correlation ($\chi2(1) = 0.58$, $p = 0.47$). The percent change in median F was also non-significant ($\chi2(1) = 1.54$, $p = 0.32$).

In terms of hypoxia (K_A), median at baseline was 0.92 min^{-1} (IQR 0.59) for good responders compared to 0.71 min^{-1} (IQR 0.22) in poor ($\chi2(1) = 3.34$, $p = 0.25$). The good response group median K_A reduced to 0.71 min^{-1} (IQR 0.30) but showed minimum change in poor responders on treatment being 0.70 min^{-1} (IQR 0.30) ($\chi2(1) = 1.18$, $p = 0.32$) with percent change in K_A showing no relationship with outcome ($\chi2(1) = 0.00$, $p = 0.98$). All but one patient, RHB04 (a poor responder), showed a reduction in K_A with RT. In Chapter 3, hypoxia levels determined by Tumour SUVmax or T:B and T:M SUVmax hypoxic volumes on the 4-hour PET scan also fell in all patients but one (RHB11 and RHB01 respectively).

The on-treatment histogram for K_A (Figure 4.4) shows two outliers, RHB01 at the upper end and RHB08 at the lower. Both showed reasonable model fitting according to AIC values and were good responders.

Figure 4.4: Casciari model perfusion (*F*) [a – c] and hypoxia (K_A) [d – f] for 0 – 45 minute dynamic FMISO PET at baseline, during RT and percent change by response

	Baseline	On RT	% change
Perfusion (*F*)	**a)** 	**b)** 	**c)** 
Hypoxia (K_A)	**d)** 	**e)** 	**f)** 

2.2.6 Casciari model muscle hypoxia (K_A) and perfusion (F) by response

In good responders the median baseline F was 0.13 mL/g/min (IQR 0.05) compared with 0.12 mL/g/min (IQR -) in poor. Binary logistic regression shows no evidence of association with outcome ($\chi2(1) = 1.42$, $p = 0.39$) Baseline median K_A was 0.02 min^{-1} (IQR 1.22) and 0.02 (IQR -) respectively ($\chi2(1) = 0.69$, $p = 0.55$). On CRT, median F for good responders was 0.59 mL/g/min (IQR 0.34) and for poor it was 0.60 mL/g/min (IQR -), ($\chi2(1) = 0.52$, $p = 0.53$). In terms of K_A the on-treatment values were 0.99 min^{-1} (IQR 1.22) and 0.36 min^{-1} (IQR -) for good and poor responders respectively ($\chi2(1) = 1.42$, $p = 0.31$). There was no evidence of difference between good and poor responders.

2.3 Discussion of dynamic FMISO PET

Dynamic FMISO PET provides many similar challenges to static FMISO PET as discussed in Chapter 3. For example, FMISO was seen to accumulate in the bladder from ten minutes post injection so even the choice to limit the analysis to the 0 – 45 minute dataset may be affected by the spill-in issues considered previously.

Mathematical models are sensitive to the AIF used. In this study, AIF was not corrected for the presence of metabolites as over 90% of FMISO in plasma is intact by 90 minutes post injection[146]. An imaging derived AIF was used rather than arterial blood sampling due to the inherent logistical challenges and risks of the latter, which may have led to bias in the TACs and derived parameters. However, the fact that muscle data also fitted best to the Casciari model rather than the three TCMs supports this more complex and specific model.

The Casciari model requires parameter initialisation and the recommended values were used to improve precision of the model parameters. However, parameter fixing often failed or gave different results. In the absence of a ground truth, Casciari et al found fixing may bias model estimates[147]. In the RHYTHM study, different initial values were trialled to obtain better fit but

it was noted that multiple solutions may exist. A better fit may not translate into improved physiological correlation[287]. Certainly, *in vivo* and human studies have found the 2-[288] and 3-[289] compartmental models adequate respectively.

Baseline median K_A in tumour was 46 times higher than in muscle, which suggests tumour is likely to contain hypoxic cells whereas resting muscle is well oxygenated. Baseline median *F* in tumour was 34 times higher than that in muscle, suggesting some difference in tumour and muscle vasculature. Within muscle, *F* and K_A values obtained here were higher than those obtained by Shwartz et al[143], possibly due to differences in model or muscle region used. There was a several fold increase in *F* and K_A between baseline and on CRT, with values rising in all patients but one for each parameter. This could be explained by differing signal-to-noise ratios and test-retest data could help to clarify this, as originally intended in RHYTHM A. However, this finding could possibly be due to the RT. Gluteal muscle will receive a dose bath of radiation although they are not usually defined as an 'organ at risk' for dose constraint purposes. Primary human myoblast cell culture evidence suggests an acute stress response is induced by radiation[290], which may explain this change in parameters seen in normal skeletal muscle.

In this small dataset we have found that the expected improvement in perfusion levels and reduced hypoxia with radiotherapy only occurred in a subset of patients. Four patients demonstrated an inverse relationship between hypoxia and perfusion within the tumour on treatment, with K_A falling as *F* increased, as might be expected[287]. However, both overall median K_A and *F* fell on treatment, reflecting the 5 of 9 paired scans which showed this pattern. These findings suggest a more complex relationship between hypoxia and perfusion than a simple inverse. A fall in perfusion may reflect a range from partial to total and this will impact differently upon levels of hypoxia[291].

There was no clear relationship between the Casciari-defined perfusion and hypoxia parameters and treatment outcome. The only finding of note was the three patients who showed an increase in perfusion at 2 weeks RT all had a good response to radiotherapy. However the other three good

response patients showed a reduction in perfusion, suggesting this is of little value as a predictive imaging biomarker. Further methods of assessing perfusion through pCT and DCE MRI are discussed below.

3. Perfusion CT

Perfusion CT (pCT) has been evaluated as both a predictive and prognostic biomarker and for monitoring treatment effects[292]. Blood flow and blood volume alteration with radiotherapy may provide some indication as to tumour pathophysiology and response.

3.1 Methods

Perfusion CT imaging was undertaken in the RHYTHM A and B study.

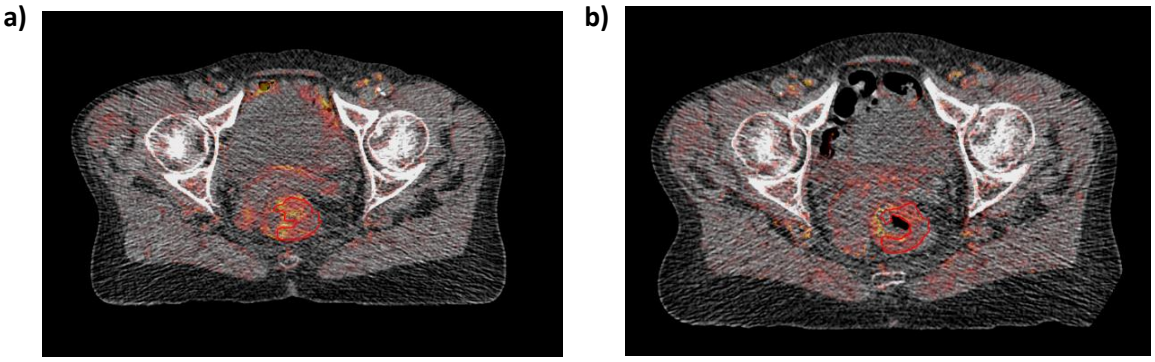
Perfusion CT acquisition

Patients were scanned immediately following the FMISO-PET scan, in the same scanner and radiotherapy position (Chapter 3, section 2.1.2). Noncontrast pelvic images were acquired and a 4cm area in the cranio-caudal direction was chosen by the clinical research fellow (JW or the author) or a radiologist (JF). Where the whole tumour could not be included, a central point of the tumour was placed in mid of field. A 50 mL bolus of IV contrast (Omnipaque 300) was injected at 5 mL/s followed by 25 - 50 mL saline flush. Contrast-enhanced 5mm axial slices were acquired 10 seconds after the start of the injection, to account for the time-lag before contrast reaches the pelvic vessels. Arterial phase and a wash-out phase were obtained. 240 images as 30 sets were acquired every second followed by 40 images total as 5 sets acquired every 14.5 secs. Scan parameters are shown in Appendix 1.

Perfusion CT processing

Images were anonymised and imported into GE Perfusion 4.0 software (GE Healthcare, Chalfont St Giles, UK) on an Advantage 4.4 Workstation (GE Healthcare Technologies, Waukesha, WI, USA). This software uses a modified distributed parameter analysis[182]. A processing threshold of between 0 and 120 Hounsfield units (HU) was utilised. A large pelvic artery with contrast enhancement and minimal movement artefact was manually outlined. The perfusion maps obtained were transferred to Mirada XD3 software (Mirada Medical UK, Oxford). ROIs outlined on contemporaneous T2W MRI as per FMISO PET-CT above were registered and transposed to the relevant perfusion map for analysis. Blood volume (BV in mL/100g tissue) and blood flow (BF in mL/min/100g tissue) were extracted. An example of BV perfusion maps in a patient undergoing CRT is shown in Figure 4.5.

Figure 4.5: Example of Blood Volume (BV) maps in a RHYTHM B patient (good responder) at a) baseline and b) after 2 weeks of radiotherapy (Tumour ROI outlined in red)



mean BV = 3.5 (S.D. 3.2)

mean BV = 3.0 (S.D 3.0)

3.2 Results

3.2.1 RHYTHM A pCT

In RHYTHM A (straight to surgery), all 3 patients underwent pCT imaging with RHA101 having 2

scans 14 days apart. The results are summarised in Table 4.5 alongside the tumour volume (T vol) captured on pCT and as a percentage of the total tumour volume defined by MRI.

Table 4.5: RHYTHM A pCT and MRI tumour volume

Study # (scan number)	**pCT Tvol * [cm^3] (% MRI Tvol)**	**MRI total Tvol ** [cm^3]**
RHA01 (1)	6.5 (42%)	15.4
RHA01 (2)	15.9 (103%)	15.4
RHA02	32.6 (95%)	34.4
RHA03	1.9 (24%)	7.8
Median	11.2	15.4
IQR	28.4	-

Tvol = Tumour volume; *Tumour volume – volume within 4 cm sup-inf pCT scan; **Total tumour volume from sFOV T2W MRI

It can be seen that the pCT tumour volume of the RHA01 retest scan was different from the baseline scan being 15.9 cm^3 and 6.5cm^3 respectively. It was consistent at 15.4 cm^3 on MRI. The validation pCT scan appeared to capture all the tumour (103%), the 3% discrepancy likely due to the transposition of volumes and adaptation carried out in post processing. The values for mean BF and mean BV were also different between the two RHB01 pCT scans. Time constraints prevented second scans for RHA02 and 03. A small proportion of the total tumour volume was captured for RHA03 whereas the whole volume appeared to be included for RHA02. For all tumours, the median BV was 7.3 mL/100g tissue (IQR 1.2) and median BF was 57.1 mL/min/100g tissue (IQR 28.0) (Table

4.6).

Table 4.6: RHYTHM A mean blood volume (BV) and mean blood flow (BF)

Study # (scan #)	Mean BV [mL/100g] (S.D.)	Mean BF [mL/min/100g] (S.D.)
RHA01 (1)	6.3 (3.9)	61.2 (54.6)
RHA01 (2)	7.7 (5.4)	52.9 (46.4)
RHA02	6.9 (3.4)	67.0 (34.4)
RHA03	7.6 (3.2)	32.4 (21.1)
Median	7.3	57.1
IQR	1.2	28.0

3.2.2 RHYTHM B pCT

All 11 RHYTHM B patients underwent pCT at baseline and at week 2 CRT. The results are shown in Table 4.7.

pCT volume versus total tumour volume by MRI

Total tumour volume was defined by the region of interest outlined on small FOV T2 axial MRI and compared with the volume included on the pCT. It can be seen that for the majority of patients (9 of 11) over 50% of the tumour volume was captured on the pCT and the volume was higher for the baseline scan than on treatment in all cases. This may reflect the changes due to radiotherapy but also in some cases, difficulty seeing and replicating the original region captured.

The tumour volumes (cm^3) outlined on pCT and MRI were correlated both at baseline and on

treatment (Spearman's rank r(11)=0.89, p=0.00 for scan 1 and r(11)=0.96, p=0.00 for scan 2). However, the percentage of total tumour volume included on pCT did not appear to correlate with the total tumour volume defined by MRI at either scan timepoint (Spearman's rank r(11)=-0.09, p=0.79 at baseline and r(11)=0.53, p=0.10 on treatment). This suggests that the proportion of the tumour represented on the pCT was not defined by the size of the total tumour volume defined by MRI, which may be related to tumour morphology, particularly tumour length and the 4cm craniocaudal pCT limit.

Table 4.7: RHYTHM B pCT and MRI tumour volume

Study #	Response to CRT	Baseline		On CRT	
		pCT Tvol* [cm^3] (% total**)	MRI total Tvol [cm^3]	pCT Tvol* [cm^3] (% total**)	MRI total Tvol [cm^3]
RHB01	Good	43.3 (72%)	60.4	40.2 (59%)	68.2
RHB02	Good	2.1 (12%)	18.2	0.7 (14%)	5.1
RHB03	Poor	37.6 (53%)	71.4	19.3 (79%)	24.6
RHB04	Poor	11.8 (58%)	20.3	9.3 (86%)	10.8
RHB05	Good	4.1 (27%)	15.1	3.0 (36%)	8.4
RHB06	Poor	18.5 (95%)	19.4	14.0 (95%)	14.7
RHB07	Good	4.8 (92%)	5.2	0.2 (26%)	0.8
RHB08	Good	32.3 (88%)	36.7	30.6 (86%)	35.6
RHB09	Poor	16.5 (100%)	16.4	13.6 (91%)	15.0
RHB10	Good	39.2 (99%)	39.6	29.1 (79%)	36.7
RHB111	Good	8.2 (81%)	10.1	3.1 (56%)	5.6
Median	-	11.8 (81%)	19.4	9.3 (79%)	14.7
IQR		27.6	24.5	18.4	30.0

Tvol = Tumour volume; *Tumour volume within 4cm sup-inf pCT scan; **Total tumour volume from sFOV T2W MRI

Blood volume and blood flow at baseline and on CRT

The median blood volume in all patients RHYTHM B was 3.3 mL/100g tissue (S.D. 1.6) at baseline (Table 4.8). The median blood flow was 30.1 mL/min/100g tissue (S.D. 17.2). When compared to RHYTHM A values of BV 7.3 mL/100g tissue (IQR 1.2) and BF 57.1 mL/min/100g tissue (IQR 28.0), there is a suggestion that those tumours suitable for a straight to surgery approach may have different perfusion characteristics to those requiring downstaging, being higher for both parameters. Numbers are small and this would need confirmation in a larger sample.

For RHYTHM B patients the median BV on RT was lower than baseline 3.0 mL/100g tissue (S.D. 2.0) for all patients. Median BF also fell to 26.9 mL/min/100g tissue (S.D. 21.6).

There did not appear to be a clear relationship between changes in BF and BV. Three patients, all good responders, showed an inverse relationship between the two parameters. For all others the change was in the same direction but not along lines of response.

Blood volume and blood flow by response outcome

Figure 4.6 shows the mean BV and BF at baseline and on treatment by response. In good responders the median BV at baseline was 3.3 (IQR 1.6) mL/100g compared with 3.5 (IQR 2.1) mL/100g for poor responders (using binary logistic regression $\chi2(1) = 0.09$, $p = 0.76$). On treatment, median BV was 3.0 (IQR 2.8) and 3.7 (IQR 3.6) mL/100g respectively ($\chi2(1) = 0.23$, $p = 0.63$). In terms of BF, median for good responders at baseline was 30.1 (IQR 24.1) mL/min/100g and for poor responders it was 27.7 (IQR 15.0) mL/min/100g ($\chi2(1) = 0.35$, $p = 0.56$). On CRT the values were 26.9 (IQR 12.6) mL/min/100g and 34.6 (IQR 83.6) mL/min/100g respectively, $\chi2(1) = 1.87$, $p = 0.33$. From these findings, there was no evidence of any difference in blood volume or blood flow

between good and poor responders at baseline or on CRT.

Poor responders had a wider range of values for mean blood volume and flow for the on-treatment scan when compared with good responders. Whilst participant numbers are small, this could suggest perfusion is only one contributory factor to the poor response outcome.

RHB05 is an upper range outlier in both BV and BF at baseline, and BV on treatment. In this case, the tumour volume on pCT was low at 27% of total volume so may not be representative. However, this was the only tumour to have a complete radiological response following CRT, consistent with being better perfused.

RHB02 is an upper range outlier for mean BF on treatment, which rose to 50.1 mL/min/100g from 39.9. Again there was limited coverage of the total tumour on pCT being less than 15% at each scan. The tumour volume for this good responder reduced considerably between baseline and week 2 chemoradiotherapy, which could also explain the improved flow value.

Blood volume and flow changes with chemoradiotherapy

Figure 4.7 demonstrates the absolute and percent change in mean blood volume and blood flow from baseline by response. In good responders the median BV absolute change was 0.1 mL/100g (IQR 1.9) with median percent change +6% (IQR 50). For poor responders BV change was 0.8 (IQR 2.48) mL/100g with median percent change +24% (IQR 60.5). Binary logistic regression demonstrated no significant relationship between change in BV on CRT and overall response ($\chi2(1) = 0.30$, $p = 0.59$). In terms of BF, the median absolute change was -2.9 mL/min/100g (IQR 13.2) in good responders versus 12.3 mL/min/100g (IQR 81.2) for poor ($\chi2(1) = 2.91$, $p = 0.32$). This equated to -8.0% (IQR 68) and +57.5% (IQR 251) respectively. Whilst no clear difference can be inferred between good and poor responders from these data, for blood flow in particular, once again there appears greater variability in the poor responders than good.

RHB05 was an outlier for BF change showing an absolute reduction of -29.3 mL/min/100g. As discussed above this patient was a good responder and had a comparatively high initial flow and volume. The apparent fall in flow could be due to the small tumour size sampled at pCT leading to an erroneous difference and/or compounded by the tumour volume reduction with RT of just under 50%.

Four of eleven patients showed a fall in BV with treatment, 1 of whom, RHB09 was a poor responder. BF fell in 5 of 11 patients, once again RHB09 being the only poor responder in this group. This mixed picture is in keeping with the dynamic FMISO PET-CT above.

Table 4.8: RHYTHM B pCT mean blood volume (BV) and mean blood flow (BF) at baseline and during CRT

Study #	Response to CRT	Baseline		On CRT		Percent Change	
		Mean BV (S.D.) [mL/100g tissue]	Mean BF (S.D.) [mL/min/100g tissue]	Mean BV (S.D.) [mL/100g tissue]	Mean BF (S.D.) [mL/min/100g tissue]	BV [%]	BF [%]
RHB01	Good	2.5 (1.5)	25.7 (27.8)	2.8 (1.9)	21.3 (31.7)	12.0	-17.1
RHB02	Good	3.3 (2.2)	39.9 (33.4)	4.7 (3.6)	50.1 (40.4)	42.4	25.6
RHB03	Poor	3.0 (3.0)	22.2 (30.50	4.4 (2.5)	43.2 (35.2)	46.7	94.6
RHB04	Poor	5.0 (3.2)	33.1 (25.6)	7.0 (3.8)	127.3 (78.9)	40.0	284.6
RHB05	Good	5.8 (3.5)	63.2 (45.1)	7.9 (3.1)	33.9 (22.7)	36.2	-46.4
RHB06	Poor	2.5 (1.4)	18.0 (11.4)	2.7 (1.6)	21.6 (13.5)	8.0	20.0
RHB07	Good	2.8 (3.3)	15.8 (19.3)	1.9 (3.6)	23.9 (46.2)	-32.1	51.3
RHB08	Good	4.1 (3.4)	35.2 (31.3)	3.8 (3.1)	32.3 (29.6)	-7.3	-8.2

Study #	Response to CRT	Baseline		On CRT		Percent Change	
		Mean BV (S.D.) [mL/100g tissue]	Mean BF (S.D.) [mL/min/100g tissue]	Mean BV (S.D.) [mL/100g tissue]	Mean BF (S.D.) [mL/min/100g tissue]	BV [%]	BF [%]
RHB09	Poor	3.9 (2.5)	34.3 (2.6.)	3.0 (2.5)	26.0 (25.1)	-23.1	-24.2
RHB10	Good	1.7 (2.6)	12.2 (22.5)	1.8 (3.0)	21.0 (38.3)	5.9	72.1
RHB111	Good	3.5 (3.2)	30.1 (36.1)	3.0 (3.0)	26.9 (29.2)	-14.3	-10.6
Median	-	3.3	30.1	3.0	26.9	8.0	20.0
IQR	-	1.6	17.2	2.0	21.6	54.3	89.2

Figure 4.6: RHYTHM B pCT mean blood volume (BV - mL/100g tissue) a) at baseline and b) during week 2 CRT and mean blood flow (BF - mL/min/100g tissue) c) at baseline and d) during week 2 CRT

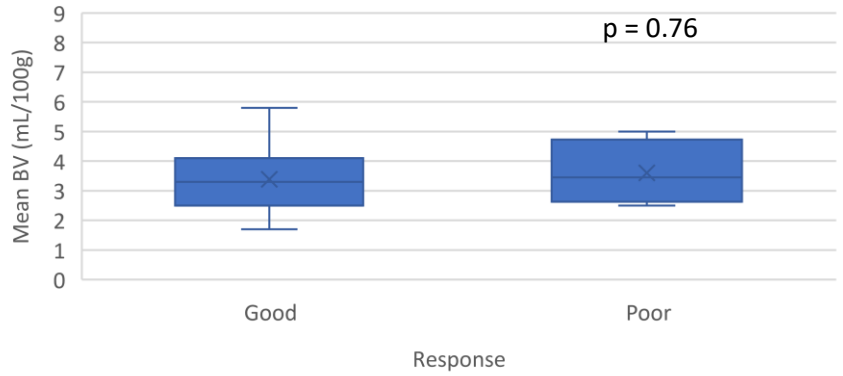
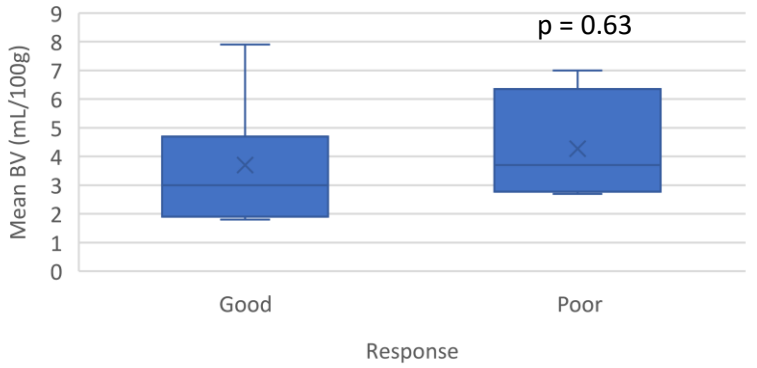
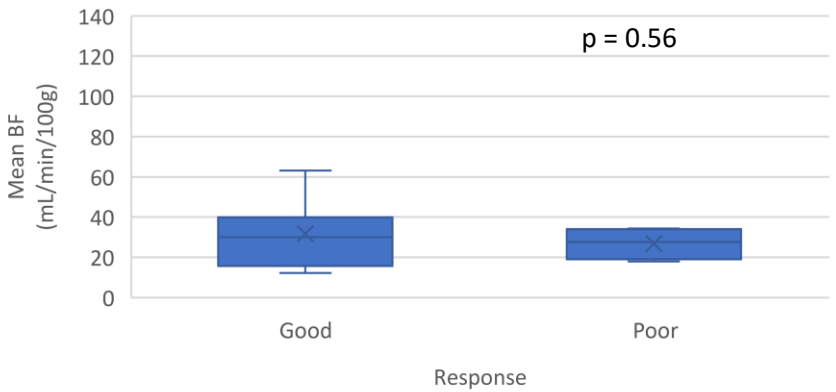
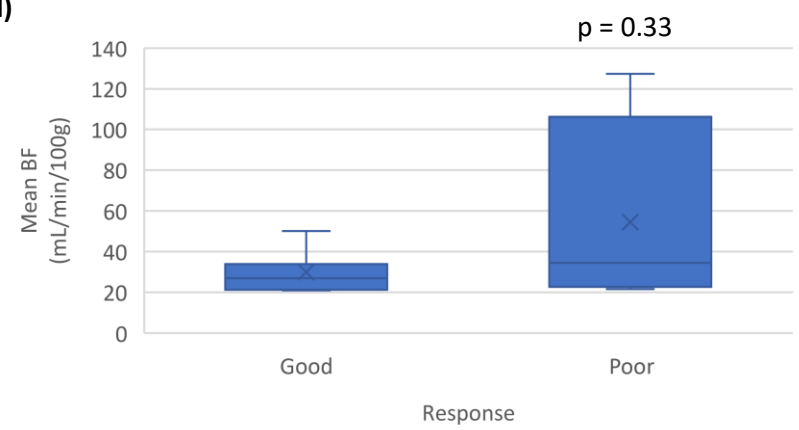
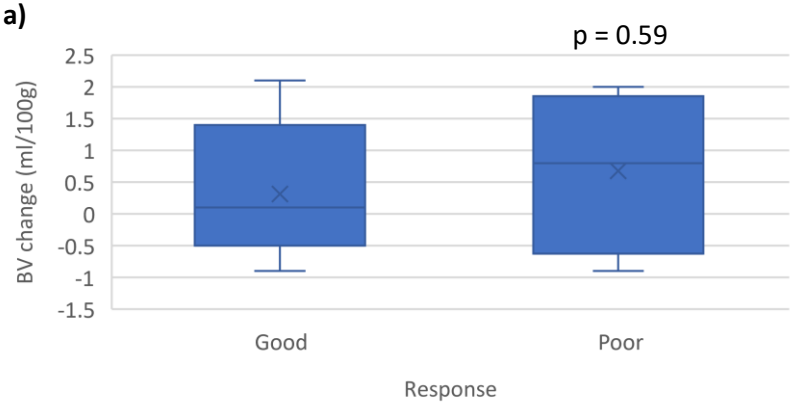
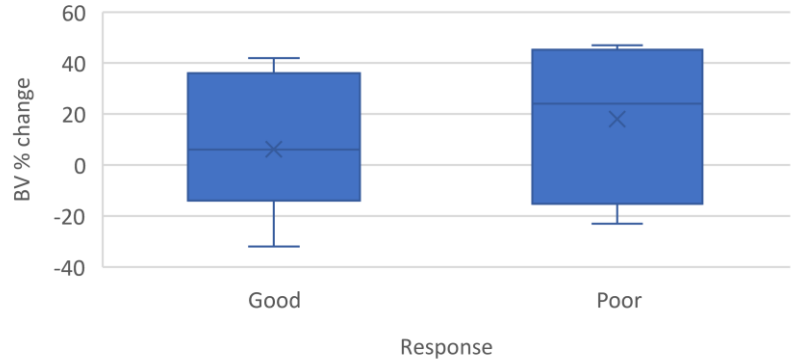
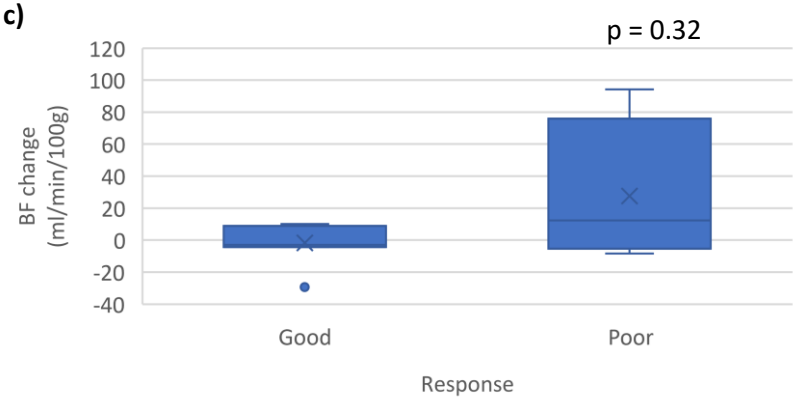
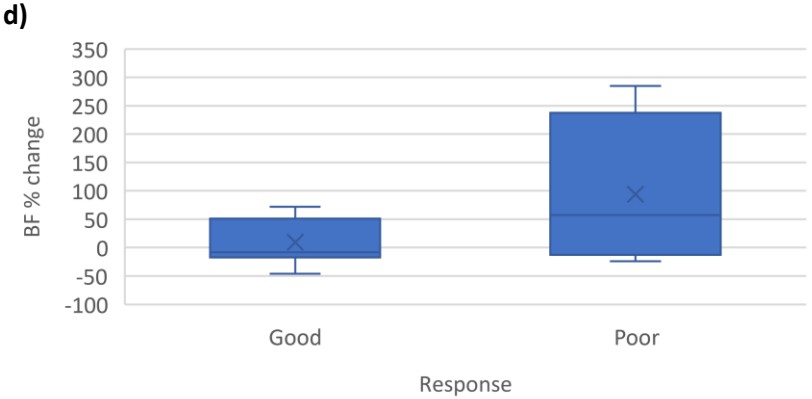
	Baseline	On CRT
BV	**a)** 	**b)** 
BF	**c)** 	**d)** 

Figure 4.7: Change with RT from baseline in blood volume (BV - mL/100g tissue) by response as a) absolute and b) percent, and blood flow (BF - mL/min/100g tissue) as c) absolute and d) percent

	Absolute change	Percentage change
BV	**a)** 	b) 
BF	**c)** 	**d)** 

3.3 Discussion of pCT

BV and BF at baseline or change with therapy did not appear to discriminate those likely to go on to have a good response to CRT. However there was a suggestion that those with tumours suitable for primary surgery in the RHYTHM A arm had higher blood volume and flow values compared with RHYTHM B baseline imaging. This would be consistent with a better perfused, less aggressive tumour but would require confirmation on a larger sample size. Additionally, poor responders appeared to show greater variability in perfusion parameters, perhaps reflecting increased heterogeneity in more aggressive malignancies.

Challenges in using pCT

Radiotherapy may affect tumour perfusion acutely, where an increase in blood flow and volume might be expected, and long term, where these parameters subsequently decrease[293]. In this study, imaging was carried out in the on treatment setting but an increase in pCT parameters from baseline was not consistently seen. This could be due to a variety of issues discussed below.

Firstly, the selection of which tumour region to include for imaging. The pCT scan here was limited to 4 cm in the superior-inferior direction, limiting the volume captured for larger tumours. Including a different part of a tumour each time may give different results and obscure any variation due to radiotherapy.

In this study, only one validation scan was performed but the volume of tumour included was different suggesting replication may be problematic. This could be compounded with imaging those on treatment given the changes and potential shrinkage induced by radiation. Fixed anatomy such as bony structures may be used to match pCT fields but rectal tumours are moveable, for example with gaseous distension or peristalsis. This is also an issue when registering and fusing CT and MRI for ROI outlining.

Whilst all processing was done using the same software version in this study, pCT parameter extraction has been shown to rely on the software platform used. Goh et al[294] showed that even within the same platform, different software versions may give different values depending on the inputs and models used by the developer. This suggests limited utility in using pCT parameter values as a biomarker across sites.

Perfusion CT has clear limitations in its use as a clinical tool for assessing rectal tumours, requiring a trained operator to identify a suitable field through the tumour for each scan. MRI may allow for improved anatomical definition of rectal tumours with larger fields captured than CT and is discussed in the next section.

4. DCE-MRI

Dynamic contrast-enhanced MRI provides the capability to image the whole tumour in an imaging modality preferred for pelvic tumours alongside providing pathophysiological information that may indicate disease response to treatment. Ktrans has been more consistently associated with outcome than the other parameters Kep, Ve and Vp[61, 196].

4.1 Methods

Dynamic contrast enhanced MRI was undertaken in the RIT and RHYTHM studies. RIT1 patients underwent baseline imaging. Patients in RHYTHM B and RIT2 were scanned at baseline, during week 2-3 radiotherapy and 6 weeks post treatment when standard response assessment is undertaken.

MRI rectum set up

Patients were scanned supine, feet first. For RHYTHM a hard top couch and radiotherapy knee stocks were used for positioning. For RIT a soft top couch and radiotherapy knee stocks were used. Patients were given an intravenous injection of hyoscine butylbromide 20 mg prior to scanning as per standard

MR procedure.

MRI rectum acquisition

Sequences were acquired on 1.5T GE HDX twinspeed MRI scanner with 8 channel TORSO coil (except for RIT3, see below). Appendix 1 contains the MRI parameters and sequences. The region of interest was identified by the researcher (JF, MA, the author) and anatomical sequences obtained initially. Three flip angles (3, 9, 15) were acquired for post-processing T1 correction to account for inhomogeneity. For the dynamic contrast enhanced images a pre and post contrast 3D LAVA sequence was used. Gadolinium-based contrast was injected at a rate of 3 mL/s followed by a saline flush of 20 mL at the same rate. Axial LAVA Asset sequences pre and post gadolinium injection were acquired.

MRI rectum image processing

Tumour was outlined by JF (7 years' experience) on T2 weighted axial images and registered to the mid-volume of the DCE-MRI to correct for minor abdominal motion between scans by Dr B. Irving (Institute of Biomedical Engineering, University of Oxford)[295]. The transformation was then applied to the delineations, which were then further corrected by the radiologist. The variable flip angle sequence was coregistered to the baseline DCE-MRI image in order to derive baseline T1 values. For each voxel in the DCE-MRI image, the signal was converted to contrast concentration. In-house PKView software (Version 0.31) developed by Dr Irving was used for analysis[296]. The Tofts-Kety two-compartmental model[195] was used with a population model for arterial input function (AIF)[191] and fitted to the contrast enhancement curve at each voxel to produce the pharmacokinetic parameter map and extract Ktrans (min^{-1}), a volume transfer constant between blood plasma and extracellular space, which indicates capillary permeability.

Statistical analysis

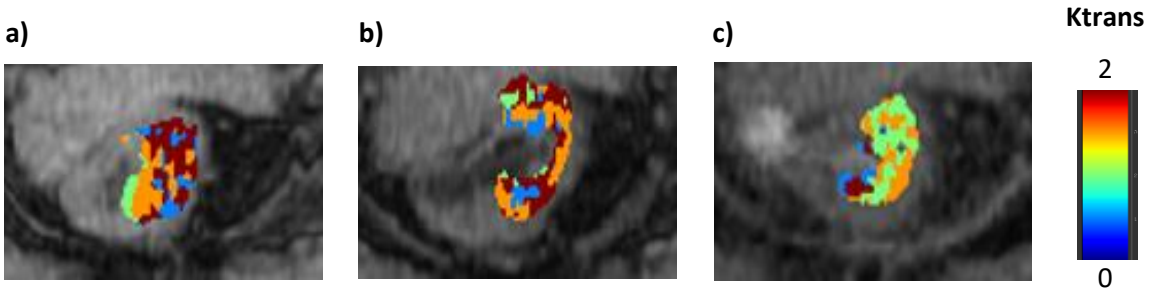
Results were normally distributed (Shapiro-Wilk test) and analysed within SPSS (IBM Corp. Released

2017. IBM SPSS Statistics for Windows, Version 25.0. Armonk, NY).

4.2 Results

An example of DCE-MRI Ktrans changes in a tumour slice at each time point is found in Figure 4.8, showing an increase on treatment then subsequent decrease.

Figure 4.8: DCE MRI Ktrans (min^{-1}) in tumour slice of a good responder in RIT at a) baseline, b) after 2 weeks RT and c) 6 weeks post RT



4.2.1 Tumour volume changes with RT in RIT study

RHYTHM volume and outcome data were presented in Chapter 3. RIT1 and RIT2 cohort tumour volumes alongside treatment outcomes are shown in Table 4.9. For RIT29 (both scans) and RIT06 (scan 2), the MRI anatomical imaging was not available for volume analysis. RIT27 did not tolerate the MRI scanner. Data are not available for 2 patients who were withdrawn and 1 patient who declined scans.

Table 4.9: RIT1 and RIT2 tumour volumes at baseline and 6 weeks post chemoradiotherapy on T2 axial sFOV MRI

Study #	Response	Pre-RT vol (cm^3)	Post-RT vol (cm^3)	Δ vol (cm^3)	% Δ vol
RIT01	Poor	35.9	8.2	-27.7	-77.2
RIT02	Poor	44.7	21.1	-23.7	-52.9
RIT03	Poor	45.4	37.3	-8.1	-17.9
RIT04	Poor	22.1	1.1	-21.0	-94.8
RIT05	Poor	93.5	25.9	-67.6	-72.3
RIT06	Poor	28.7	*	-	-
RIT07	Poor	34.4	4.8	-29.6	-86.1
RIT08	Poor	35.7	5.8	-29.9	-83.8
RIT09	Good	40.7	32.0	-8.7	-21.4
RIT10	Poor	13.0	3.5	-9.5	-73.2
RIT11	Poor	50.3	26.3	-23.9	-47.6
RIT12	Good	37.6	10.4	-27.1	-72.2
RIT13	Poor	21.5	4.9	-16.6	-77.2
RIT14	W/d	N/A	N/A	-	-

Study #	Response	Pre-RT vol (cm^3)	Post-RT vol (cm^3)	Δ vol (cm^3)	% Δ vol
RIT15	Poor	41.7	13.2	-28.4	-68.2
RIT16	Good	10.0	10.4	0.4	3.8
RIT17	Good	53.2	5.6	-47.6	-89.5
RIT18	Good	79.6	18.5	-61.1	-76.8
RIT19	Poor	17.7	2.2	-15.5	-87.5
RIT20	Good	17.7	11.0	-6.7	-37.8
RIT21	Good	42.6	6.1	-36.5	-85.6
RIT22	Good	N/A	N/A	-	-
RIT23	Poor	13.0	1.4	-11.6	-89.0
RIT24	Good	44.8	20.2	-24.6	-54.9
RIT25	Good	12.0	11.4	-0.6	-5.0
RIT26	Poor	48.9	*	-	-
RIT27	Poor	N/A	N/A	-	-
RIT28	Good	40.1	26.7	-13.4	-33.4
RIT29	Good	*	*	-	-
RIT30	Poor	107.2	66.4	-40.8	-38.1

Study #	Response	Pre-RT vol (cm^3)	Post-RT vol (cm^3)	Δ vol (cm^3)	% Δ vol
RIT31	Good	30.8	4.1	-26.7	-86.8
RIT32	W/d	N/A	N/A	-	-
RIT33	Poor	31.6	14.4	-17.2	-54.5
RIT34	Good	19.8	6.4	-13.3	-67.4
RIT35	Poor	42.3	20.0	-22.3	-52.6
RIT36	Poor	21.9	2.7	-19.2	-87.9
RIT37	Good	2.6	1.4	-1.2	-47.3
RIT38	Good	70.9	16.2	-54.6	-77.1
RIT39	Good	20.1	2.9	-17.1	-85.4
RIT40	Poor	76.5	22.0	-54.5	-71.3
RIT41	Poor	61.1	25.4	-35.7	-58.5
RIT42	Poor	42.2	8.4	-33.8	-80.2
RIT43	Poor	23.3	8.5	-14.8	-63.5
RIT44	Good	66.1	38.2	-27.9	-42.2
RIT45	Good	48.1	1.6	-46.4	-96.6

Mean (S.D.)	-	41.4 (6.30	12.6 (3.1)	-25.4 (2.7)	-63.4 (4.1)

Vol = volume; Δ = change; W/d = withdrawn; N/A = not applicable; *images unavailable

4.2.2 Tumour volumes at baseline and post treatment by response outcome in RIT

At baseline the mean tumour volume was 35.7 cm^3 (S.D. 21.5) for good responders and 42.4 cm^3 (S.D. 24.2) for poor responders. A two-tailed independent t-test was performed and there was no significant difference between the two groups (t(38)=0.9, p=0.37). There were two outliers in the poor response group – both of these had large tumours involving EMVI and adjacent tumour deposits, which were included in the ROI. Post treatment mean volume was 11.6 cm^3 (S.D. 9.0) in the good response group versus 16.4 cm^3 (S.D. 16.0) in the poor response group. An independent t-test showed no significant difference (t(36)=1.1, p=0.28).

4.2.3 Change in tumour volume with treatment in RIT

All but one patient showed a decrease in tumour size from baseline to post treatment with RT. In good responders the mean change in volume from baseline was -24.1 cm^3 (S.D. 20.0), mean percent change -58.3% (S.D. 31.6). For poor responders this was -26.3 cm^3 (S.D. 14.2) and -67.1% (S.D 19.6). The only patient who demonstrated an increase in tumour size from baseline was RIT16, a good responder, with a minimal change of 0.4 cm^3 (3.8%). The MR TRG in this patient was 3 i.e. poor response but superseded by the pathological AJCC TRG of 1 following surgery almost 5 weeks post imaging.

4.2.4 DCE MRI mean Ktrans in RIT and RHYTHM-B studies

In RIT1, 23 patients had baseline DCE-MRI images available for analysis. Of these, 1 was removed due to poor model fit. Three patients did not have scans undertaken and four scans could not be located for analysis. Ten patients in RHYTHM-B and fourteen in RIT2 had DCE-MRI at all three time points. One

patient in RHYTHM B had baseline data corrupted on the scanner. Ktrans results for both studies are shown in Table 4.10.

Table 4.10: RHYTHM and RIT mean Ktrans (min^{-1}) at baseline, on radiotherapy and 6 weeks post treatment

Study #	BL (min^{-1})	On RT (min^{-1})	Post-RT (min^{-1})	% Δ BL to on RT	% Δ BL to post-RT	% Δ On RT to post-RT
RIT						
RIT01	**	N/A	N/A	-	-	-
RIT02	0.36	N/A	N/A	-	-	-
RIT03	0.35	N/A	N/A	-	-	-
RIT04	0.18	N/A	N/A	-	-	-
RIT05	0.57	N/A	N/A	-	-	-
RIT06	0.28	N/A	N/A	-	-	-
RIT07	0.16	N/A	N/A	-	-	-
RIT08	0.13	N/A	N/A	-	-	-
RIT09	0.24	N/A	N/A	-	-	-
RIT10	0.53	N/A	N/A	-	-	-
RIT11	***	N/A	N/A	-	-	-
RIT12	0.42	N/A	N/A	-	-	-
RIT13	0.20	N/A	N/A	-	-	-

Study #	BL (min^{-1})	On RT (min^{-1})	Post-RT (min^{-1})	% Δ BL to on RT	% Δ BL to post-RT	% Δ On RT to post-RT
RIT14	N/A	N/A	N/A	-	-	-
RIT15	0.16	N/A	N/A	-	-	-
RIT16	0.41	N/A	N/A	-	-	-
RIT17	0.33	N/A	N/A	-	-	-
RIT18	0.27	N/A	N/A	-	-	-
RIT19	0.60	N/A	N/A	-	-	-
RIT20	0.52	N/A	N/A	-	-	-
RIT21	**	N/A	N/A	-	-	-
RIT22	N/A	N/A	N/A	-	-	-
RIT23	0.28	N/A	N/A	-	-	-
RIT24	0.30	N/A	N/A	-	-	-
RIT25	0.25	N/A	N/A	-	-	-
RIT26	**	N/A	N/A	-	-	-
RIT27	N/A	N/A	N/A	-	-	-
RIT28	0.45	N/A	N/A	-	-	-

Study #	BL (min^{-1})	On RT (min^{-1})	Post-RT (min^{-1})	% Δ BL to on RT	% Δ BL to post-RT	% Δ On RT to post-RT
RIT29	**	N/A	N/A	-	-	-
RIT30	0.19	N/A	N/A	-	-	-
RIT31	0.37	0.22	0.13	-40.5	-64.9	-40.9
RIT32	N/A	N/A	N/A	-	-	-
RIT33	0.39	0.60	0.23	53.8	-41.0	-61.7
RIT34	0.36	0.12	0.18	-66.7	-50.0	50.0
RIT35	0.33	0.45	0.44	36.4	33.3	-2.2
RIT36	0.15	0.52	0.50	246.7	233.3	-3.8
RIT37	0.53	0.55	0.17	27.9	-60.5	-69.1
RIT38	0.63	0.60	0.54	-4.8	-14.3	-10.0
RIT39	0.31	0.57	0.53	83.9	71.0	-7.0
RIT40	0.16	0.29	0.40	81.3	150.0	37.9
RIT41	0.42	0.52	0.35	23.8	-16.7	-32.7
RIT42	0.30	0.43	0.42	43.3	40.0	-2.3
RIT43	0.20	0.31	0.11	55.0	-45.0	-64.5

Study #	BL (min^{-1})	On RT (min^{-1})	Post-RT (min^{-1})	% Δ BL to on RT	% Δ BL to post-RT	% Δ On RT to post-RT
RIT44	0.22	0.24	0.18	9.1	-18.2	-25.0
RIT45	0.36	0.54	0.31	50.0	-13.9	-42.6
RHYTHM						
RHB01	*	0.31	N/A	-	-	-
RHB02	0.36	0.26	0.12	-27.8	-66.7	-53.8
RHB03	0.26	0.41	0.18	57.7	-30.8	-56.1
RHB04	0.37	0.50	0.33	35.1	-10.8	-34.0
RHB05	0.31	0.56	0.18	80.6	-41.9	-67.9
RHB06	0.23	0.29	0.30	26.1	30.4	3.4
RHB07	0.27	0.16	0.21	-40.7	-22.2	31.3
RHB08	0.30	0.58	0.34	93.3	13.3	-41.4
RHB09	0.35	0.18	0.18	-48.6	-48.6	0.0
RHB10	0.24	0.48	0.29	100.0	20.8	-39.6
RHB11	0.28	0.36	0.25	28.6	-10.7	-30.6
Mean (S.D.)	0.32 (0.12)	0.41(0.16)	0.29 (0.13)	37.6 (64.5)	1.5 (69.6)	-23.4 (33.5)

BL = baseline; *data corrupted on scanner, unable to analyse; ** images not available for analysis; ***poor fit to model, excluded from analysis; N/A – not applicable, scan not done

4.2.5 Baseline mean Ktrans

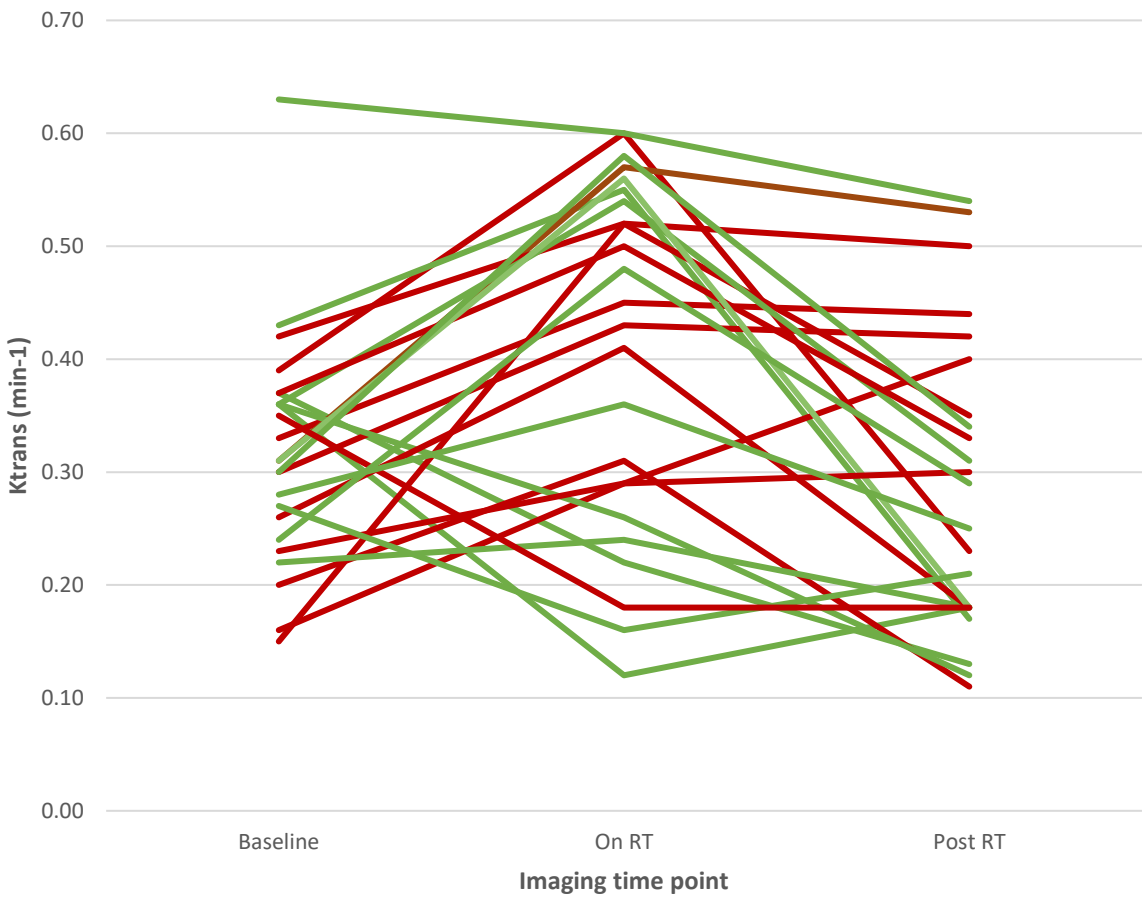
Mean Ktrans at baseline for all 46 patients with data were 0.32 min^{-1} (S.D. 0.12) at baseline. A one-way ANOVA test was performed using SPSS to compare the effect of study group (RIT1, RIT2 or RHYTHM) on mean Ktrans. This revealed no significant difference between the study cohorts (F=0.26, p=0.78).

There were 22 good and 24 poor responders. Mean Ktrans was 0.35 min^{-1} (S.D. 0.10) in the good and 0.30 min^{-1} (S.D. 0.13) in poor response group. RIT38, a good responder, is an upper limit outlier with a relatively large tumour at 70.9 cm, around double the mean for good responders in RIT. There was no significant difference between the response groups means with an independent t-test on SPSS (t(44)=-1.39, p=0.17).

4.2.6 Change in mean Ktrans with radiotherapy

In 18 of the 24 participants within RIT2 and RHYTHM-B who had three sequential imaging timepoints, tumour Ktrans increased on treatment. The baseline mean of 0.32 min^{-1} (S.D. 0.10) rose to 0.41 min^{-1} (S.D. 0.16) on RT. At least six weeks post treatment, this value fell to 0.29 (S.D. 0.13), reflecting the 20 of 24 tumours where Ktrans decreased from on-treatment levels. Of these, 13 had final Ktrans values lower than that at baseline and seven were good responders (Figure 4.9).

Figure 4.9: Mean Ktrans (min^{-1}) in RHYTHM-B and RIT2 at baseline, on treatment and 6-8 weeks post radiotherapy (Red = poor responders, Green = good responders)



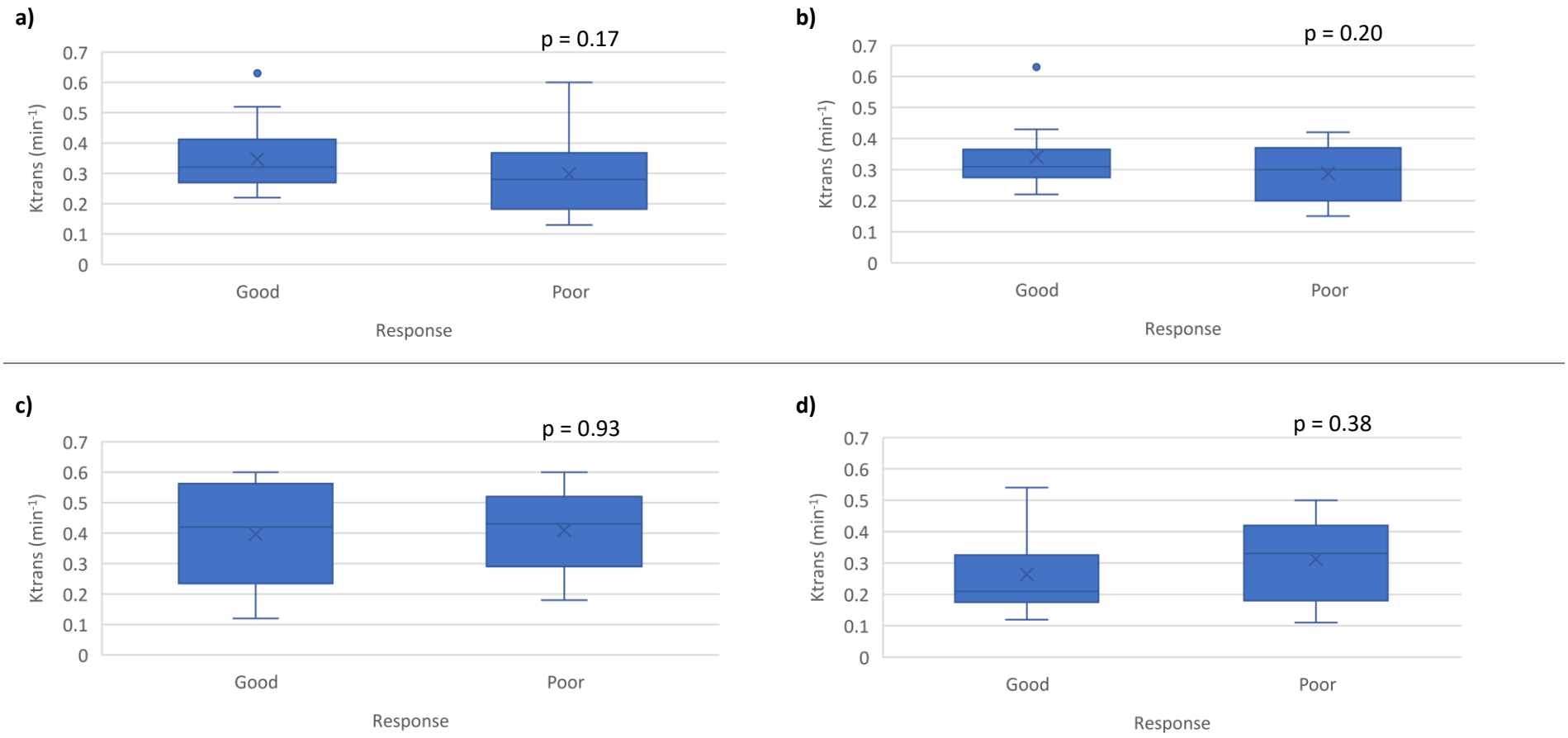
4.2.7 Mean Ktrans changes with RT by response outcome in RIT2 and RHYTHM-B

In the 24 patients with DCE-MRI imaging at all 3 timepoints, mean Ktrans at baseline for good responders was 0.34 min^{-1} (S.D. 0.10), being 0.29 min^{-1} (S.D. 0.09) for poor responders (Figure 4.11). There was no significant difference between the two response groups seen using an independent t-test ($t(22)=-1.33$, $p=0.20$). RIT38 is once again the upper limit outlier.

On treatment mean Ktrans showed little difference between good and poor responders being 0.40 min^{-1} (S.D. 0.18) and 0.41 min^{-1} (S.D. 0.13) respectively. An independent samples t-test showed no significant difference ($t(22)=0.09$, $p=0.93$)

Following radiotherapy, mean values fell for both groups, to 0.26 min^{-1} (S.D. 01.4) for good and 0.31 min^{-1} (S.D. 0.12) for poor responders. Again there was no significant difference on an independent t-test in SPSS (t(22)=00.91, p=0.38). RIT 38 and 39 are upper limit outliers. They are at opposite ends of the size spectrum being 70.9cm^3 and 20.1cm^3 respectively at baseline, both showing a good response to treatment with shrinkage of over 75%.

Figure 4.11: Mean Ktrans by response in RIT1, RIT2 and RHYTHM-B studies for all patients at a) baseline (n = 46) and patients with 3 imaging timepoints (n = 24) at b) baseline c) on RT and d) 6 weeks post RT



4.3 Discussion of DCE-MRI

Mean Ktrans did not appear to be associated with response to radiotherapy in these studies of rectal cancer. There was a pattern of rising values on treatment, falling again a few weeks following completion. This would be consistent with radiation causing increased vascular permeability acutely as part of the early inflammatory response, which resolves post treatment[293]. Extracellular matrix changes and fibrosis formation may explain the fall below baseline levels[297]. Mean Ktrans may not adequately reflect the pathology within heterogeneous tumours although unlike here, others have found it a predictor of response at baseline[61, 298] and useful to determine good response[197-199] to RT. Segmentation based upon DCE-MRI parameters may be one way to provide useful spatial information as well as indicating variability within tumours[296]. A population AIF was used for analysis due to the invasive nature of blood sampling and difficulties with obtaining an image-based individualised AIF. However, this can introduce errors due to ignoring potential differences in AIF between subjects. Irving et al[299] have suggested a method which automatically estimates the AIF from the tumour tissue in order to personalise the estimation.

5. Comparison of dynamic imaging findings

5.1 Change in perfusion parameters with radiotherapy

Table 4.11 shows the percent change in Blood flow (BF - pCT), Ktrans (DCE-MRI) and perfusion (*F* – FMISO-PET) from baseline to on treatment. In only one patient do all the parameters fall. Less than half of the 10 patients with paired scans showed a similar direction of change between p-CT blood flow and Ktrans. Only 2 of 8 patients did the same for Ktrans and FMISO-PET perfusion. However there was concordance in 7 of 9 patients with paired p-CT and FMISO parameters. There did not appear to be any pattern of change differentiating good and poor responders.

Table 4.11: Comparison of dynamic imaging parameter changes – pCT (blood flow - BF), DCE MRI (Ktrans) and dynamic FMISO PET-CT (Perfusion - *F*) - from baseline to on CRT

Study #	Response	BF Δ%	Ktrans Δ%	*F* Δ%	Direction of change		
					BF	Ktrans	F
RHB01	Good	-17.1	N/A	-50.0	↓	N/A	↓
RHB02	Good	25.6	-27.8	73.1	↑	↓	↑
RHB03	Poor	94.6	57.7	-22.3	↑	↑	↓
RHB04	Poor	284.6	35.1	-29.0	↑	↑	↓
RHB05	Good	-46.4	80.6	-34.6	↓	↑	↓
RHB06	Poor	20.0	26.1	N/A	↑	↑	N/A
RHB07	Good	51.3	-40.7	18.1	↑	↓	↑
RHB08	Good	-8.2	93.3	-82.8	↓	↑	↓
RHB09	Poor	-24.2	-48.6	-82.2	↓	↓	↓
RHB10	Good	72.1	100.0	N/A	↑	↑	N/A
RHB11	Good	-10.6	28.6	145.1	↓	↑	↑
Median (IQR)	-	20.0 (89.2)	31.9 (115)	-29.0 (68.1)	↑	↑	↓

Δ% = percentage change

5.2 Discussion of dynamic imaging methods

Variations between the different parameters with radiotherapy may be due to a multitude of factors. Different imaging modalities are used with differing analysis techniques and models for parameter derivation. Whilst the scans were contemporaneous, the contribution of acute versus chronic changes in perfusion may be an issue. The use of a mean or median parameter value is unlikely to reflect the heteregenous nature of tumours.

A relative concordance between pCT blood flow and Casciari model perfusion in FMISO PET was noted. Both these techniques used an image derived arterial input function rather than a population based value as in the DCE-MRI analysis.

6. Conclusion

Dynamic imaging measures of tumour perfusion varied both at baseline and in response to radiotherapy treatment but not in a similar pattern. The differing models used and assumptions therein may be one reason and could limit generalised clinical use. No clear association with response to radiotherapy was seen for any of the parameters investigated. Small numbers of participants in the clinical trials likely limited the ability to discriminate. Spatial correlation and techniques such as using supervoxels to describe the heterogeneity of tumours could provide a more accurate assessment than using tumour mean or median values.

Establishing alterations in perfusion with non-invasive imaging remains challenging in heterogeneous tumours with multiple complex physiological systems. Clearly, there are potentially multiple contributing factors affecting treatment response and another of these will be further investigated in the next chapter looking at glucose metabolic imaging.

Chapter 5: Glucose metabolism imaging

1. Introduction

The use of FDG-PET to assess locally advanced rectal cancer in the RIT study and the potential to image glucose using MRI (GlucoCEST) is investigated in this chapter. The BIOPIC study, using GlucoCEST in assessment of head and neck squamous cell carcinoma (HNSCC) patients undergoing radical radiotherapy, is also discussed.

The aims in this chapter are to:

- Assess the utility of FDG-PET parameters for CRT response prediction in LARC
- Establish the use of glucoCEST using phantoms and volunteers
- Evaluate glucoCEST MRI use in LARC and HNSCC patients undergoing radiotherapy

2. ^{18}F-Fluorodeoxyglucose (FDG) PET-CT

2.1 Methods

FDG PET scanning was undertaken in the RIT2 and RIT3 study. Patients with rectal adenocarcinoma for long course downstaging RT had FDG-PET scans at baseline.

Image acquisition

FDG PET imaging was done on a Discovery 690 PET-CT scanner with acquisition parameters found in Appendix 1. Patients were given standard clinical advice to have clear fluids only within the 6 hours before the scan. Capillary blood glucose level was tested on arrival and could not exceed 10 mM to proceed. Those recruited within RIT1 and early RIT2 were scanned in standard position

(supine, head supported by pillow, soft top couch). Following a protocol amendment, patients were positioned supine on the flat-top couch, head to scanner. The radiotherapy Combifix was used to support knees and feet in the same position to the RT planning scan. Pelvic radiotherapy tattoos were aligned using laser guidance.

18F-Fluorodeoxyglucose (FDG) was injected at a dose of 4 MBq/kg body weight at 1 mL per 5 seconds. Static PET images were acquired at 60 minutes post injection followed by a CT chest, abdomen and pelvis.

Image processing

Rectal tumour was outlined by one radiologist (JF, 7 years' experience) on T2 weighted axial sFOV MRI. These were transferred to the CT component of the PET-CT using rigid registration within Eclipse radiation treatment planning software (version 10, Varian Medical Systems, Inc., Palo Alto, CA) and modified for air and to ensure contiguity of tumour. ROIs were transferred to Mirada XD3 software (Mirada Medical UK, Oxford) for analysis. Tumour SUVmax, Peak SUV and total lesion glycolysis (TLG) were obtained.

2.2 FDG PET-CT results

FDG PET scanning was undertaken at baseline in 14 of 17 patients in RIT 2 and RIT 3. The tumour SUVmax, SUV peak and TLG results are shown in Table 5.1. Three patients did not undergo FDG-PET scanning; one (RIT32) was withdrawn as their FDG PET showed liver metastases and they had neoadjuvant chemotherapy rather than RT first line. Two others (RIT33, RIT43) did not have time to have scans rearranged following cancellation due to failure of FDG delivery. Another patient (RIT39) was found to have liver metastases on scan review but had already commenced radiotherapy and continued in the study.

A Shapiro Wilk test for normality revealed that two of the parameters did not have a normal

distribution - SUVpeak (W(14)=0.781, p=0.003) and TLG (W(14)=0.723, p=0.001). Median and IQR is therefore provided for all datasets for comparison purposes and non-parametric statistical analysis was undertaken using SPSS (IBM Corp. Released 2017. IBM SPSS Statistics for Windows, Version 25.0. Armonk, NY).

Table 5.1: FDG PET-CT parameters volume, SUVmax, SUVpeak and TLG at baseline within the RIT study

Study #	Response	Vol (cm^3)	SUVmax (g/mL)	SUVpeak (g/mL)	TLG (g cm^3/mL)
RIT31	Good	31.1	21.2	17.1	237.6
RIT32	W/d	N/A	N/A	N/A	N/A
RIT33	Poor	N/A	N/A	N/A	N/A
RIT34	Good	32.3	28.2	18.7	246.1
RIT35	Poor	31.0	23.6	18.2	248.2
RIT36	Poor	22.6	20.2	15.7	213.3
RIT37	Good	12.1	30.0	19.4	98.8
RIT38	Good	2.3	10.9	9.5	13.8
RIT39	Good	20.0	26.4	21.8	222.2
RIT40	Poor	77.1	27.4	20.1	540.5
RIT41	Poor	45.2	37.2	26.6	535.4
RIT42	Poor	43.1	17.7	15.6	291.2
RIT43	Poor	N/A	N/A	N/A	N/A
RIT44	Poor	66.6	30.7	21.9	650.5

Study #	Response	Vol (cm^3)	SUVmax (g/mL)	SUVpeak (g/mL)	TLG (g cm^3/mL)
RIT45	Good	48.5	48.8	44.3	1604.7
RIT46	Good	5.3	20.6	13.6	13.6
RIT47	Good	40.7	19.7	17.3	321.2
Median (IQR)	-	31.7 (27.9)	25.1 (10.1)	18.5 (8.1)	247.1 (27.9)

N/A = non-applicable (see text); TLG = Total lesion glycolysis; Vol = volume; W/d = withdrawn

2.2.1 Tumour volume

Tumour volumes for the RIT cohort are provided in Chapter 4. The median volume in this FDG PET-CT subgroup was 31.7 cm^3 (IQR 27.9). For all patients with volume data in the RIT study, the median was 38.9 cm^3 (IQR 27.1).

In this cohort, the median volume at baseline for good responders was 25.5 cm^3 (IQR 31.6) whereas for poor responders it was 44.1 cm^3 (IQR 40.4) shown in Figure 5.1. Binary logistic regression showed no significant difference between the response groups ($\chi 2(1) = 5.1$, $p = 0.08$). This trend towards larger baseline volumes for poor responders is not replicated in the larger cohort discussed in Chapter 4 and underscores the limitations of a smaller sample set.

2.2.2 SUVmax

Median tumour SUVmax at baseline was 25.1 g/mL (IQR 10.1). Little difference was seen between median for good responders of 23.8 g/mL (IQR 9.6) and for poor of 25.5 g/mL (IQR 12.7) (Figure 5.1). Again there was no significant difference between the response groups ($\chi 2(1) = 0.01$, $p = 0.93$). RIT45 was the upper outlier in the good responders. On review of the imaging, this is unlikely to

represent an artefact due to spill-in as the tumour is not adjacent to the bladder and there is minimal bowel uptake in this area.

2.2.3 SUVpeak

SUVpeak median at baseline for all scans was 18.5 g/mL (IQR 6.12). The median values were 19.2 g/mL (IQR 7.4) versus 18.0 g/mL (IQR 6.7) respectively for good and poor responders. As with SUVmax, the difference was not statistically significant ($\chi2(1) = 0.02$, $p = 0.90$) and RIT45 was the upper outlier in good responders (Figure 5.1).

2.2.4 TLG

Median TLG at baseline was 247.1 g cm^3/mL (IQR 352.0). For the good response group the median was 229.9 g cm^3/mL (IQR 267.4) and for poor it was 413.3 (IQR 328.5) (Figure 5.1). There appears to be a trend towards lower TLG in the good responders but this is not confirmed statistically ($\chi2(1) = 0.12$, $p = 0.75$), with RIT45 once again being the upper outlier in this group.

2.2.5 FDG PET parameters compared with tumour volume at baseline

Figure 5.2 shows scatter plots comparing tumour volume with SUVmax and SUVpeak at baseline. Pearson correlation was non-significant for SUVmax ($r(14) = 0.45$, $p = 0.11$) and SUVpeak ($r(14) = 0.44$, $p = 0.11$).

Figure 5.1: FDG PET-CT parameters by response a) volume (cm^3), b) SUVmax (g/mL), c) SUVpeak (g/mL), d) TLG (g cm^3/mL)

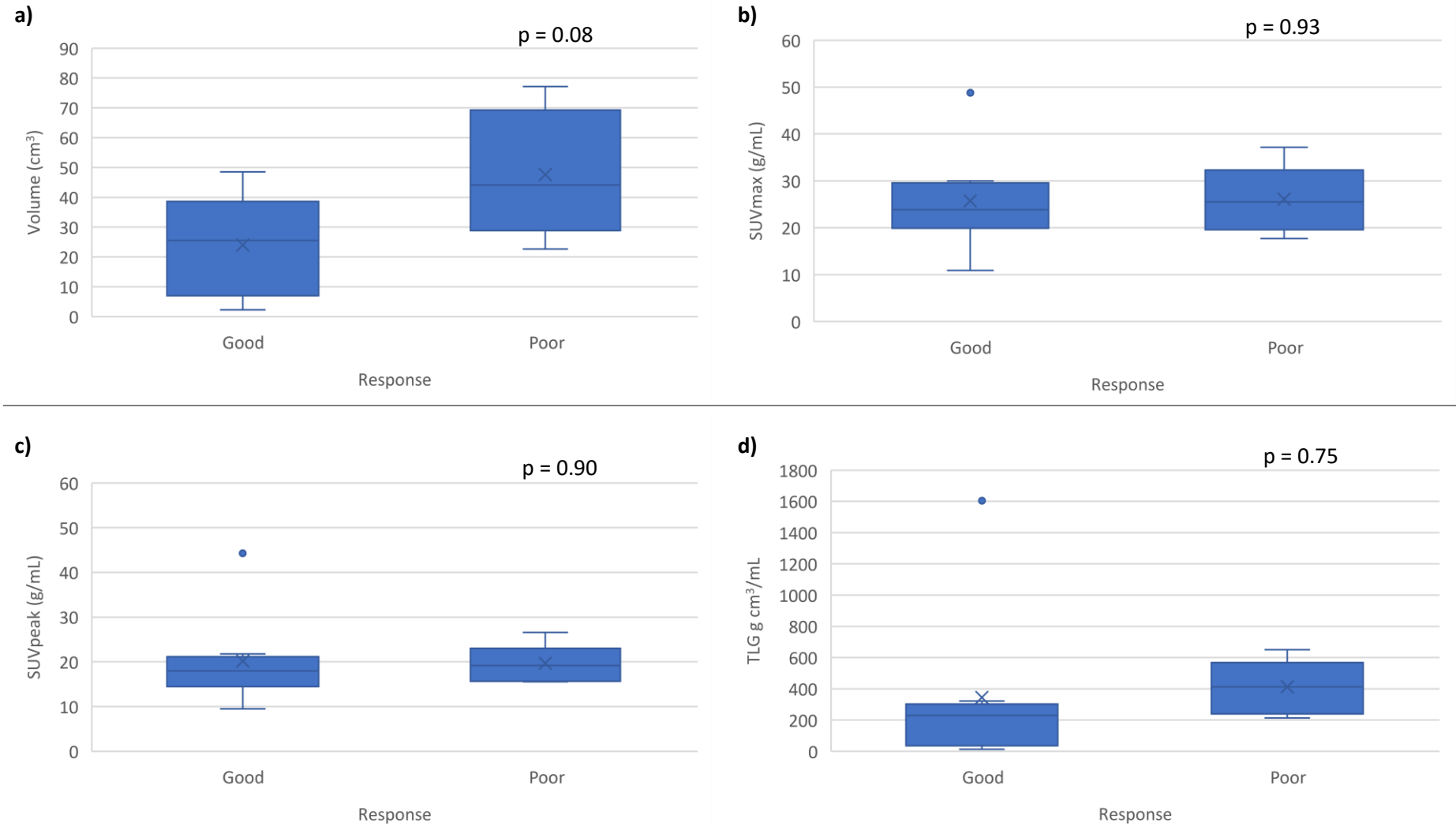
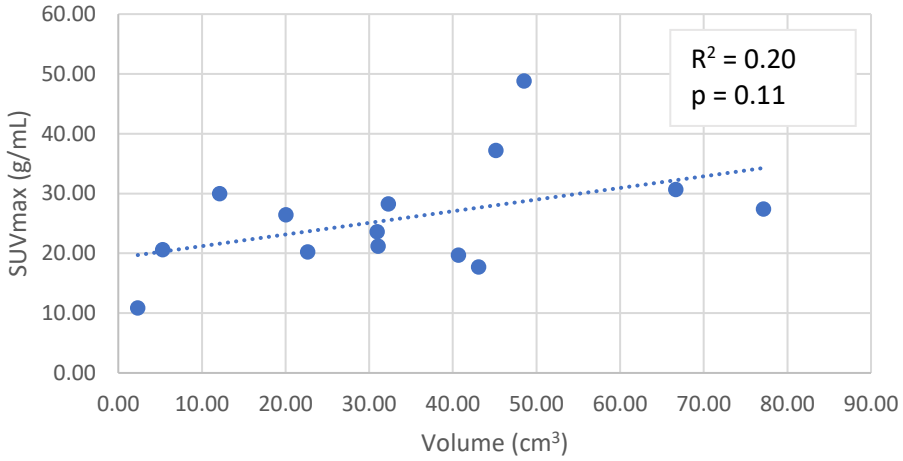
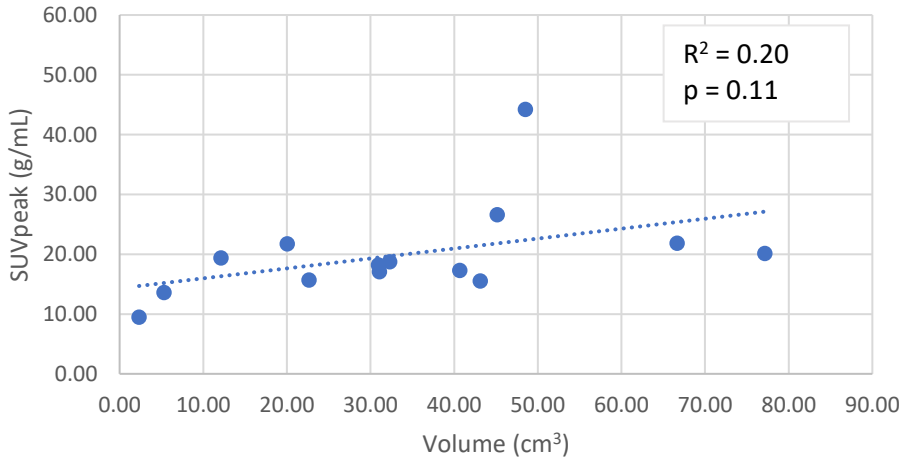


Figure 5.2: FDG PET parameters versus volume (cm^3) - a) Tumour SUVmax (g/mL); b) Tumour SUVpeak (g/mL)

a)



b)



2.3 Discussion of FDG PET-CT in rectal cancer

2.3.1 Tumour volume and SUV

Whilst there was a non-significant positive association between tumour volume and SUVmax or SUVpeak, in both instances there was a trend towards this, albeit weak. This would be consistent with findings of Li et al[300] in preoperative colon cancer who noted a significant correlation between SUVmax and tumour length on preoperative FDG PET-CT. Similarly in advanced NSCLC,

Chen et al[301] saw higher prevelance of larger tumours in patients with a pre-treatment SUVmax of at least 8.0. Tumour size itself has been shown in some series to be predictive of pCR[302, 303] post RT in rectal cancer.

2.3.2 SUVmax

Within this small study of rectal adenocarcinoma patients undergoing CRT, baseline FDG SUVmax was not correlated with response. There are clear limitations to using this parameter: as it is defined by the most active pixel it does not reflect tumour heterogeneity, whilst potentially being adversely affected by noise[115, 116].

The difference in SUVmax over time with therapy may provide a more useful metric as noted by Caruso et al[304] who found a change from baseline to post RT was associated with TRG response in rectal cancer. However this does not provide the opportunity to adapt therapy. Gu et al[305] found that SUVmax after 2 weeks RT differentiated response by pathological TRG in rectal cancer. Whilst scanning during radiotherapy could indicate less responsive regions to target, re-planning takes time and gaps or prolongation in treatment should be minimised as they may compromise efficacy[306].

FDG PET-CT post treatment may indicate response to radiotherapy but in rectal cancer treated with neoadjuvant CRT, resection remains the recommended standard of care. Given MRI and endoscopy have limited ability to determine complete response, FDG-PET is unlikely to be further discriminating in this scenario, as confirmed by Guillem et al[307] who found that FDG-PET post RT could not identify patients with pCR.

2.3.3 SUVpeak

SUVpeak, is purported to be more robust the SUVmax given that a small region of interest centred on a high uptake part of the tumour is used rather than a single pixel[208]. Studies in other tumour

types have shown a correlation with for example survival in NSCLC patients receiving CRT[308], metastasis free survival in nasopharyngeal carcinoma treated with RT[309] and pathologic response to neoadjuvant therapy in pancreatic cancer[310]. However, inaccuracies such as inclusion of areas outside of the tumour are possible because pixels at the edge of the region of interest may include external areas in the surrounding sphere[311]. Whilst the 1 cm^3 volume as used in this study has been suggested as standard[208], there is also no fixed definition of the volume and derivation of SUVpeak with various sizes and shapes used, making comparisons across studies problematic[312].

2.3.4 TLG

In this small series, TLG appeared to show a trend towards lower levels in good responders. This is consistent with a smaller metabolically active tumour volume being more likely to respond to radiotherapy, as seen in oesophageal cancer patients undergoing CRT[313] and lung cancer patients undergoing SABR[314]. In colorectal adenocarcinoma, a preoperative FDG PET-CT revealed TLG was a strong independent predictor for disease free survival[315]. It is unclear as to the extent volume rather than FDG activity provides the association with response and outcome. If considering dose painting or radiotherapy boost to highly active regions, TLG would not provide a volume to target.

2.3.5 Future directions

Determining the most useful way to define the MTV could be useful for RT target volume.. This can be done in multiple ways including by absolute or relative thresholding, algorithm-based segmentation and statistical modelling, with the most appropriate varying according to tumour and application[209]. However FDG PET may not include viable tumour cells in hypoxic areas. As demonstrated by Roels et al[140], regions in rectal cancer as defined by FDG PET activity do not directly correlate with hypoxic regions on FMISO PET. This may be particularly problematic given

the relative aggressiveness and radioresistance of hypoxic areas.

FDG PET in rectal cancer is not suggested by The National Institute for Health and Care Excellence NICE[13] for routine use unless there is evidence of extra-hepatic metastases potentially amenable to radical therapy. However in the RIT study several patients were found to have liver metastases on FDG PET that were not visible on CT. Further investigation may indicate the usefulness of FDG PET-CT to determine the extent of metastatic disease in high risk patients. Future research may also focus on the use of FDG PET in rectal tumour delineation, where it has been shown to reduce interobserver variability[316].

3. GlucoCEST MRI

GlucoCEST MRI may be used to detect endogenous or exogenous glucose via a process of chemical exchange saturation transfer. This work was undertaken in phantoms, volunteers and two patient imaging studies, RIT in LARC and BIOPIC in HNSCC.

3.1 Methods

GlucoCEST MRI analysis was undertaken in collaboration with Dr B. Burns (Department of Oncology, University of Oxford) and Dr A. Smith (Wellcome Centre for Integrative Neuroimaging, FMRIB, University of Oxford). Images were obtained on a 3T 750 GE MRI scanner at the Churchill Hospital, Oxford. Imaging parameters are found in Appendix 1.

Magnetisation Transfer Ratio (MTR) asymmetry analysis was performed using MATLAB (MATLAB R2017b, The MathWorks, Inc., Natick, Massachusetts, United States).

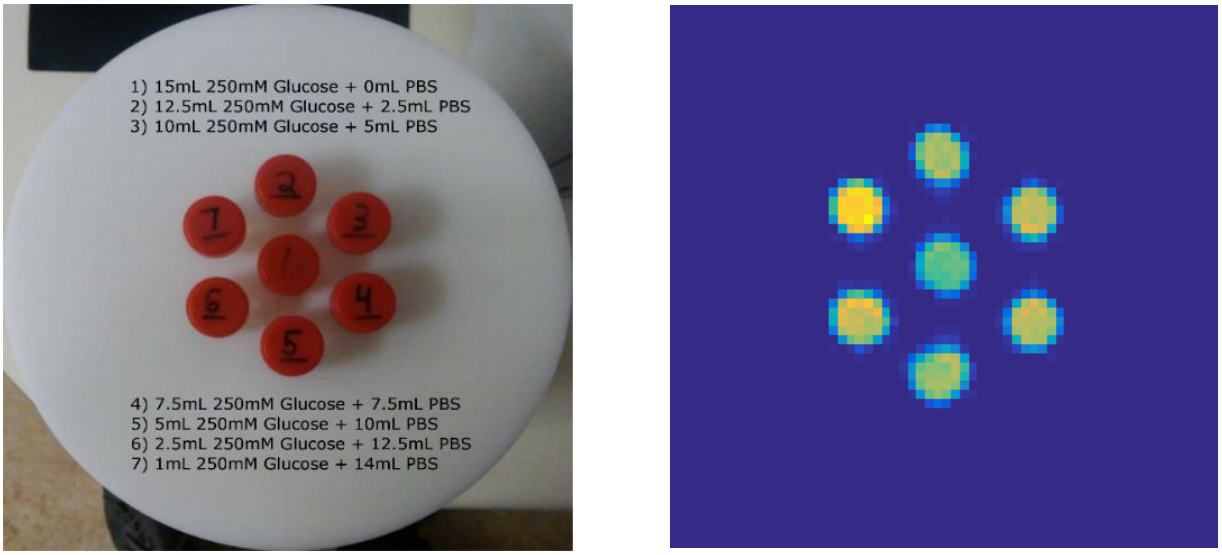
3.2 Phantom studies

3.2.1 Methods

Phantom studies were undertaken using glucose solutions at varying concentrations within a phosphate buffer solution (PBS) with 4% Bovine Serum Albumin (BSA) to more closely replicate physiological conditions. Figure 5.3 shows the phantom set up within a purpose-made 3D-printed delrin container and the derived glucoCEST image.

Figure 5.3: GlucoCEST phantom imaging: a) Phantom with solutions of glucose and PBS with BSA at different concentrations; b) GlucoCEST image of phantom

a) **b)**



PBS = phosphate buffer solution; BSA = bovine serum albumin

3.2.2 Results of phantom studies

Table 5.2 and Figure 5.4 summarise the MTR asymmetry findings at different glucose concentrations and radiofrequency saturation power (B1). As expected, increasing CEST effects are seen with increasing glucose concentration and B1. PBS with BSA alone demonstrated negligible

CEST effect. Signal-to-noise ratio was 250-300. Figure 5.5 shows examples of the Z-spectra (the CEST effect defined as S_{sat}/S_0 or M_s/M_0) obtained at the lowest and highest glucose concentrations with varying B1 input. The maximum MTR% signal obtained at 1.2 ppm using 2µT B1 for 200mM Glucose + BSA was 15%. As can be seen, the Z-spectra were broadly symmetrical around water at 0 ppm and the parabola was consistent across applied B1 except on a few occasions. Repeated experiments did not show these discrepancies appearing for the same B1 or glucose concentration, suggesting they were likely artefactual.

Table 5.2: Percentage MTR asymmetry at different applied RF pulse B1 and glucose concentration levels

	Glucose concentration (mM)				
B1 (µT)	**12.5**	**25**	**50**	**100**	**200**
0.4	0.3	0.3	0.4	0.8	1.6
0.8	0.4	0.5	1.3	2.8	6.0
1.2	0.9	1.5	2.4	5.6	11.1
1.6	1.5	2.2	3.9	8.7	16.3
2.0	2.3	3.4	5.4	11.3	18.1

Figure 5.4: Phantom percent MTR asymmetry at 1.2 ppm versus glucose concentration levels at various B1 inputs

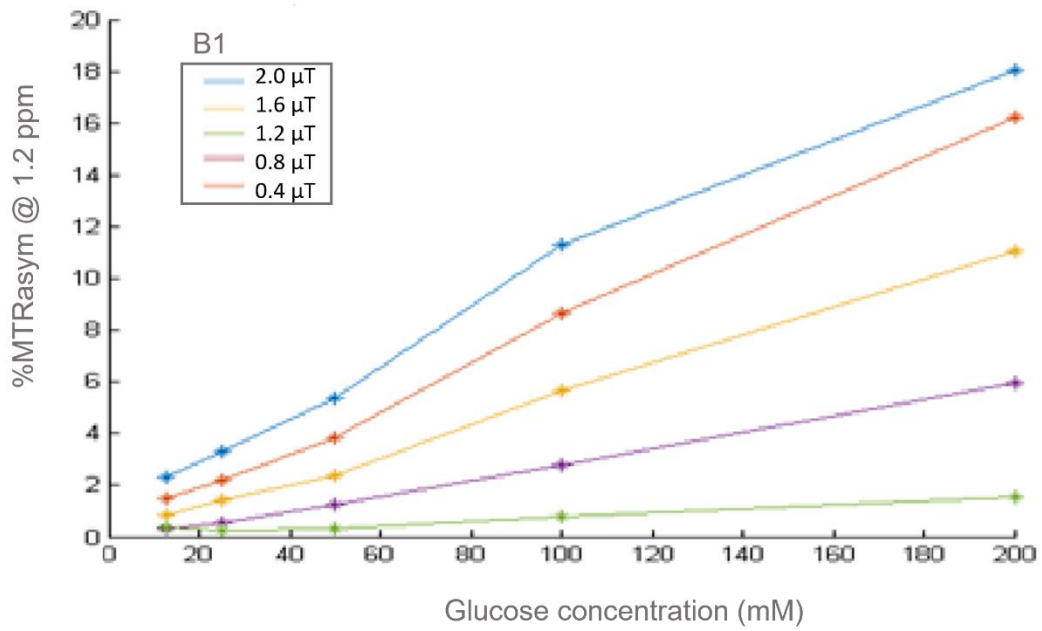
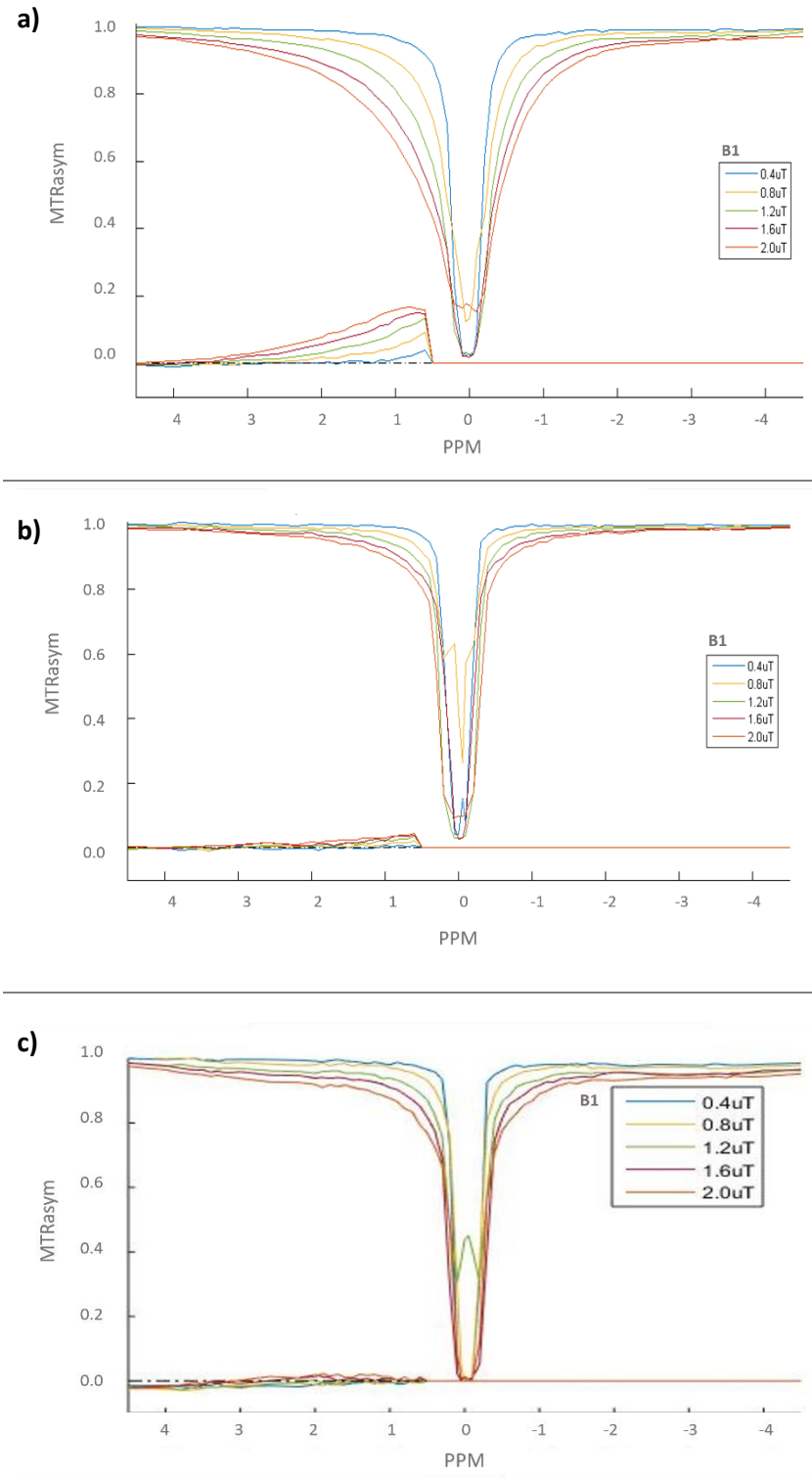


Figure 5.5: Examples of phantom study MTR asymmetry Z-spectra at various B1 inputs in glucose concentration a) 200 mM, b) 12.5 mM, c) 0 mM



MTRasym = MTR asymmetry; PPM = parts per million

3.3 Volunteer studies

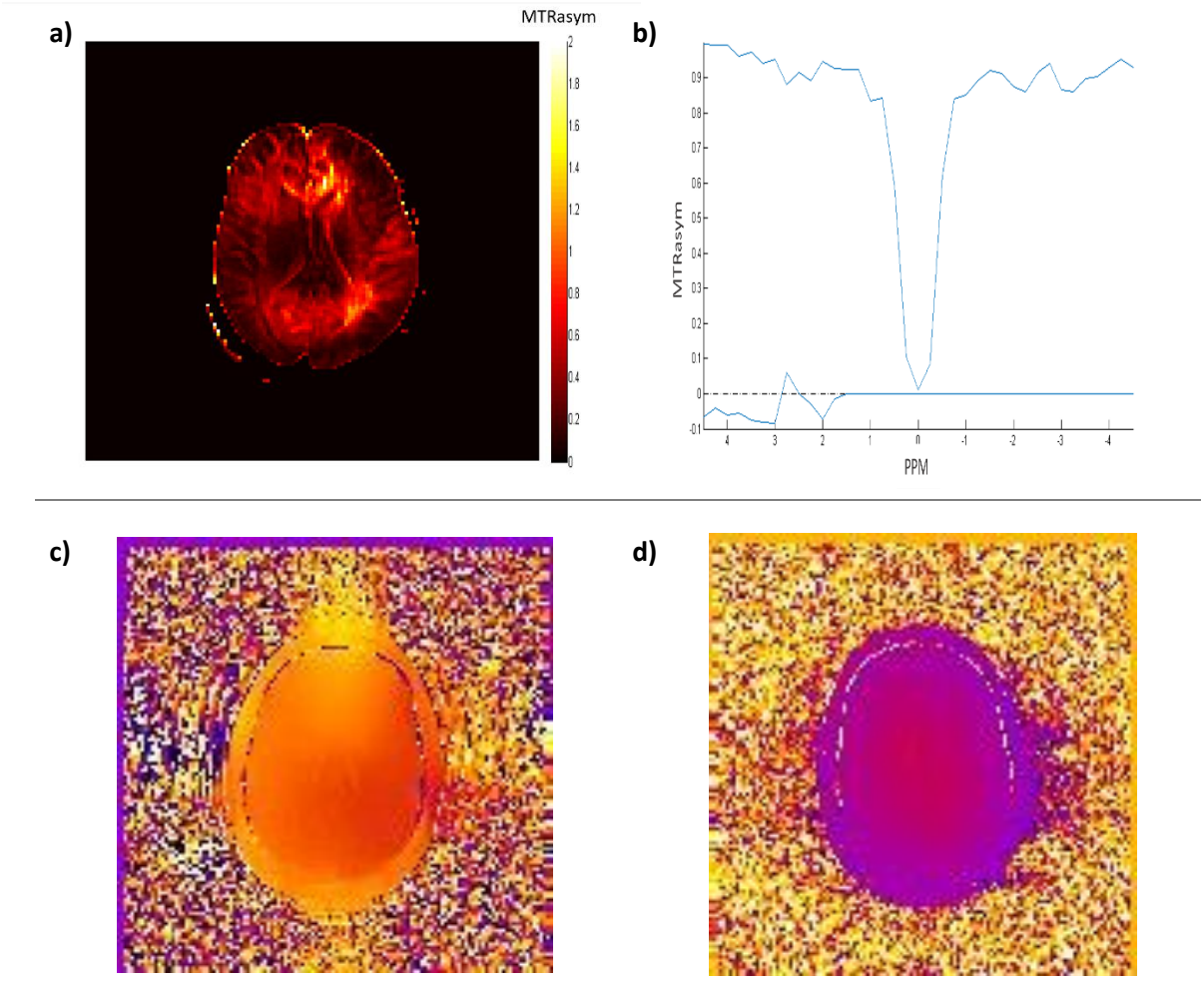
3.3.1 Methods

Five healthy volunteers' brains were scanned using the MRI head coil. B0 (main magnetic field) and B1 (applied field, perpendicular to main) maps were obtained to correct for inhomogeneity in the main and applied magnetic field respectively. One volunteer (the author) took a 75g glucose load (in form of 1 L of Lucozade™) shortly prior to glucoCEST MRI on 2 occasions and following 6 hours of fasting except for clear fluids. This amount of glucose is based upon the protocol for the oral glucose tolerance test[317].

3.3.2 Results

An unenhanced CEST image of a volunteer brain with equivalent z-spectrum, B0 and B1 maps is shown in Figure 5.6. In the volunteer who took the glucose load, no change was seen in the brain signal between the baseline glucoCEST scan and images taken over 30 minutes post glucose load. This is probably because the brain is the priority organ for glucose and protected from physiological alterations in serum glucose. Studies have suggested that peak plasma glucose levels occur at around 30 - 60 minutes post glucose load ingestion and gradually fall[318],[319]. In comparison, intravenous glucose tolerance tests have shown a sharp rise in plasma glucose[320] and to higher levels than with oral loads[321], with the ability to maintain levels with a short infusion[322, 323]. Given this and results from pre-clinical[230, 324] and clinical studies[325, 326] which used glucose infusions for glucoCEST imaging, the decision was made to give dextrose (glucose solution) intravenously in subsequent clinical studies.

Figure 5.6: CEST imaging in healthy volunteer brain at 1uT RF saturation B1 from 4 to 1 ppm showing a) MTR asymmetry image; b) *In vivo* spectrum; c) B0 map; d) B1 map



RF = radiofrequency; MTRasym = MTR asymmetry; PPM = parts per million

3.4 Patient studies

3.4.1 Methods

The RIT study was amended to include glucoCEST MRI at baseline and during CRT. This necessitated altering the scanner used from 1.5T to 3T and this cohort is RIT 3. Given the MTR% obtained on phantom and volunteer studies on the 3T scanner was at most 15%, it was felt that the 1.5T scanner would provide negligible signal and would not warrant the time and cost of developing a glucoCEST

sequence. Whilst there is a 7T scanner available at the research facility at the FMRIB centre at Oxford John Radcliffe Hospital, the Oncology patients have all their scans and treatments at the Churchill Hospital, Oxford. For practical purposes, it was decided to use the 3T scanner for this study and the BIOPIC study, introduced below.

GlucoCEST MRI was carried out within the RIT and BIOPIC studies, imaging rectal adenocarcinoma and head and neck squamous cell carcinoma (HNSCC) respectively. A single slice for glucoCEST imaging was chosen in order to include the bulk of tumour in a reproducible position with respect to bony landmarks. The slice was placed manually at each scan and modified as required to replicate the previous scan(s). It was then copied to all other single slice sequences within that scan session.

GlucoCEST imaging was first undertaken without exogenous glucose. Intravenous dextrose was then administered via a bolus of 25g in 50 mL (50%) over 1 minutes followed by a dextrose infusion of 20% (20g in 100 mL at 0.08 mL/sec until the sequence was complete, to a maximum of 20g). The aim was to maintain raised serum glucose levels during the glucoCEST scan given the long duty cycle of just over 4 minutes per slice. Patients with type I or uncontrolled type II diabetes mellitus were excluded from receiving intravenous dextrose in both imaging studies.

GlucoCEST imaging both with and without i.v. dextrose was undertaken on air and inspired 100% oxygen. We hypothesised that oxygen breathing would result in an improved SNR for CEST imaging. As an increase in the amount of dissolved oxygen in the blood leads to a decrease in T1 and an increase in T2[327], the SNR is increased as the signal recovers faster from the shortened T1 and secondarily from the longer T2 because of slower signal dephasing. In addition, a longer T2 leads to narrowing of the z-spectrum, simplifying resolution of the CEST signal from exchanging labile proton pools[328].

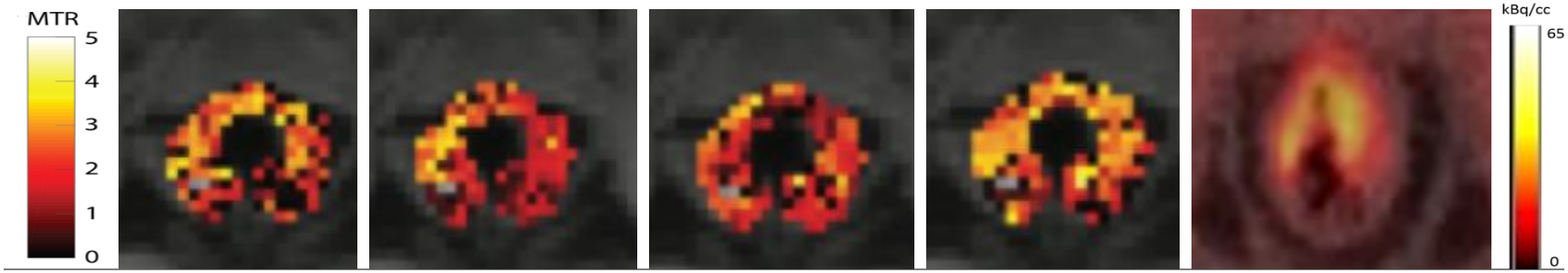
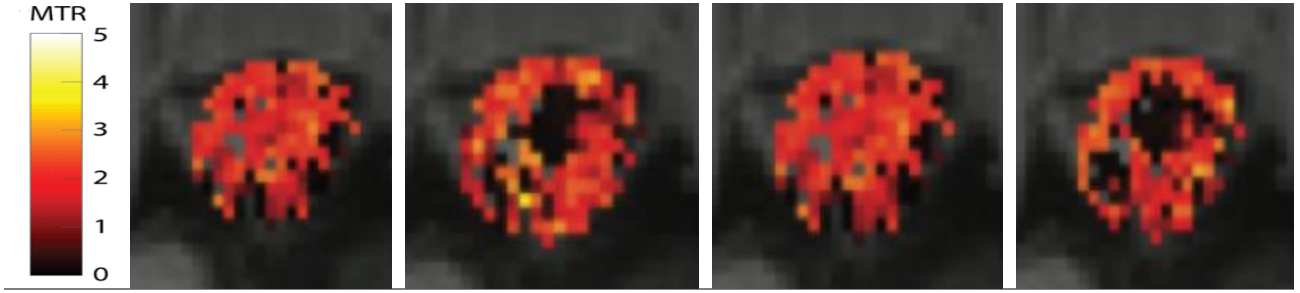
Additional sequences at each timepoint included standard anatomical views, B0 and B1 maps to

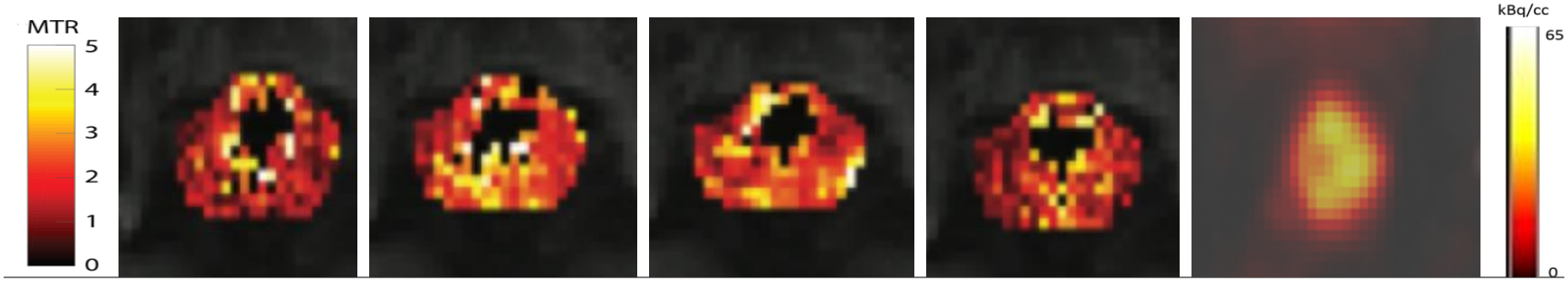
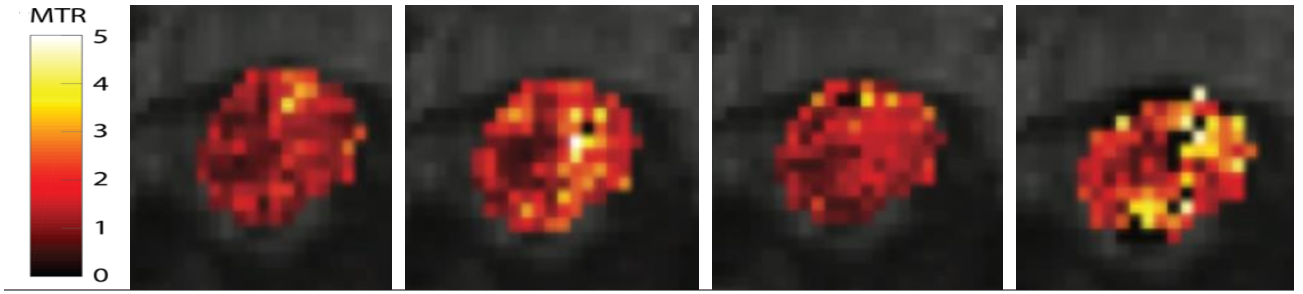
correct for inhomogeneity and single slice MOLLI sequence for T1 mapping.

3.4.2 RIT study

Two patients (P1 and P2) with LARC underwent glucoCEST imaging on air and oxygen at baseline and after 8 – 10 fractions of radiotherapy. The results are shown in Figure 5.7 with the baseline FDG PET for comparison. Both patients had T3 N0 disease. One was found to have liver metastases on baseline FDG PET imaging but had already commenced CRT at time of confirmation. Both were good responders. When compared visually, the glucoCEST MRI images appeared similar to FDG PET-CT scans at baseline.

Figure 5.7: Rectal cancer Magnetisation Transfer Ratio (MTR) at baseline (BL) and on RT +/- 100% inspired oxygen +/- intravenous dextrose

Scan	GlucoCEST MRI				FDG PET-CT
	Air, no dextrose	Air, i.v. dextrose	Oxygen, no dextrose	Oxygen, i.v. dextrose	
P1 BL					
(S.D.)	1.01 (0.56)	0.85 (0.45)	0.92 (0.43)	1.14 (0.54)	SUVmax: 20.63
P1 On RT					N/A
(S.D.)	0.89 (0.37)	0.80 (0.40)	0.76 (0.4)	0.79 (0.49)	

	GlucoCEST MRI				FDG PET-CT
Scan	**Air, no dextrose**	**Air, i.v. dextrose**	**Oxygen, no dextrose**	**Oxygen, i.v. dextrose**	
P2 BL					
(S.D.)	1.71 (1.25)	2.30 (1.58)	1.99 (0.96)	1.54 (0.93)	SUVmax: 19.86
P2 On RT					N/A
(S.D.)	1.05 (0.48)	1.46 (0.78)	1.16 (0.61)	2.54 (2.00)	

i.v. = intravenous; N/A = non-applicable

MTR with and without dextrose

It was expected that MTR would increase with dextrose infusion due to rise in tumour uptake. However in P1, MTR on air fell with the addition of iv dextrose both at baseline and on treatment. In P2 this pattern was replicated on oxygen at baseline. This could be due to a multitude of factors including blood glucose levels, change in anatomical position or differential glucose uptake within the tumour. For P2 at baseline, the connection with the dextrose bolus was accidentally disconnected. This led to blood glucose levels measured by pinprick capillary testing falling from baseline of 6.2 mM to 4.1 mM at the start of glucoCEST imaging. However this rose to 7.5 mM by the end of the infusion. During this patient's on-treatment scan, blood glucose levels levels rose from 5.4 mM at baseline to 10.3 mM by the end of scanning. Figures for P1 were unfortunately unavailable.

MTR on air versus inspired oxygen

The addition of 100% inspired oxygen would be expected to increase the T1 signal and hence the MTR but this only happened on half of the paired scans. Various factors may impact on the delivery of oxygen to the tumour including patient respiratory function and tumour perfusion. Furthermore, movement between scans may affect the results. The use of a single slice is particularly susceptible to this and is also limited by the small area captured, which may not reflect the heterogeneity of tumour oxygenation.

MTR changes with treatment

All MTR values fell on treatment from baseline, except for P2 scan on oxygen and dextrose which rose by 64%. In these two good responders, it would be anticipated that MTR would fall with response to treatment as a marker of reduce metabolic activity.

3.4.3 BIOPIC study design

The BIOPIC study was conceived by the author in collaboration with chief investigator Professor F. Gleeson (Department of Radiology, University of Oxford) and co-investigators Dr B. Burns (Department of Oncology, University of Oxford) and Professor D. Bulte (Institute of Biomedical Engineering, University of Oxford).

BIOPIC is an imaging study with the aim of assessing novel MRI techniques including glucoCEST in HPV positive, oropharyngeal squamous cell carcinoma patients undergoing radical CRT. This group was chosen as FDG PET-CT imaging is already in routine use to assess the extent of disease and response to CRT as per the NICE guideline[329]. Furthermore, HPV positive disease is associated with increased radiosensitivity[330] and would be more likely to show changes with therapy. It was postulated that the anatomical detail of MRI coupled with the functional data of CEST would be particularly useful in this group and that FDG PET imaging findings could be used as a comparator.

Study aims

The primary objective was to assess the changes in T1 with oxygen inspiration during and post RT. Secondary objectives included assessment of changes in CEST signal on treatment and comparison of glucoCEST with FDG PET-CT findings.

Patient selection

Patients with HPV positive oropharyngeal squamous cell carcinoma planned for radical radiotherapy +/- concurrent systemic therapy were eligible. Tumour staging was at least T2 or nodal disease had to be at least 2 cm minimum diameter on anatomical MRI.

Exclusion criteria

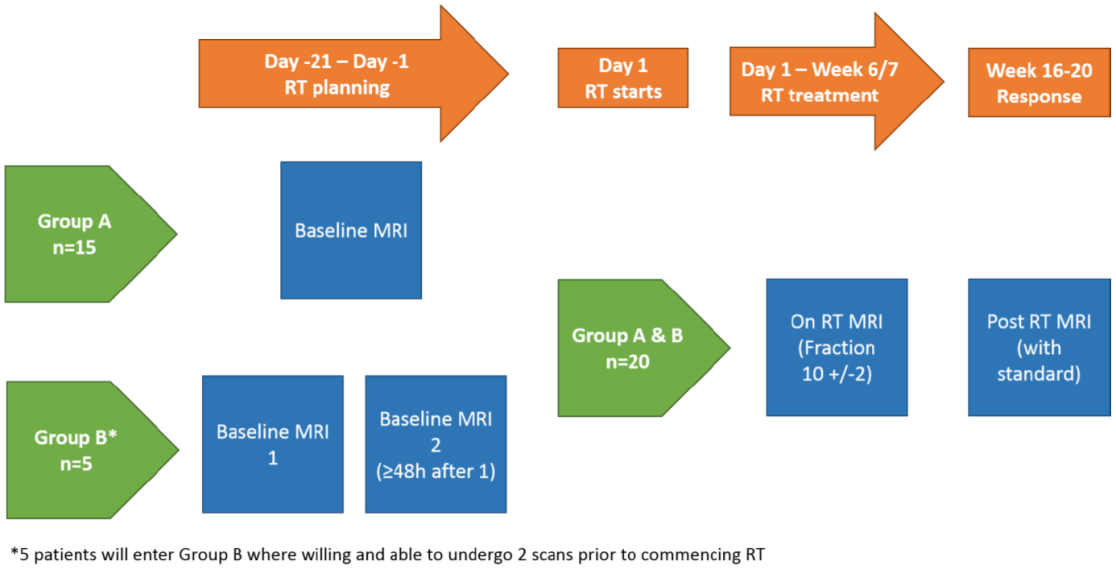
Patients were excluded if they had any contraindications to study interventions. This included those with type 1 diabetes mellitus or poorly controlled type 2 and lung disease rendering the patient

unsuitable for 100% oxygen breathing.

Study timeline

Figure 5.8 shows the timeline of events for the BIOPIC study.

Figure 5.8: BIOPIC study timeline



Trial interventions

Group A

Group A patients undergo a functional MRI at baseline, on RT (fraction 10 +/-2) and 10 – 14 weeks post RT with routine CT CAP and MRI head and neck. The MRI includes anatomical sequences, DWI, T1 and T2* on air and oxygen, CEST on air and oxygen, with and without intravenous dextrose and DCE MRI.

Group B

Group B patients follow the same schedule as Group A but have two baseline scans, at least 48 hours apart, prior to commencing RT.

Recruitment

The first 5 patients, all in Group A, were recruited by the author from 24/04/17. The remaining 11 patients were recruited by Dr Andrew Murchison (AM) and Dr Ketan Shah (KS) (Oxford University Hospitals NHS Foundation Trust) into Group A. One patient could not have any imaging due to scanner breakdown and was replaced. Two withdrew after their pre-treatment scan. One withdrew after their on treatment scan. It proved difficult to recruit to arm B due to limited time prior to commencing treatment and the additional burden the scans placed on patients undergoing cancer therapy. The study was closed on 6/09/18.

Methods

Patients were imaged at baseline and after 8 – 10 fractions of CRT. Images were acquired as per section 3.4.1. The tumour and any involved nodal GTV was outlined by Dr N. Taylor (Consultant Radiologist, Department of Radiology, Churchill Hospital, Oxford University Hospital Trust, Oxford) who has 15 years' experience. Images were outlined on the contemporaneous T2 anatomical MRI on ITK-SNAP (Version 3.6.0; University of Pennsylvania, PA 19104-6274, United States)[273] and transferred to Matlab (MATLAB R2017b, The MathWorks, Inc., Natick, Massachusetts, United States) for analysis.

3.4.4 Biopic study results

The first patient, BIO1, withdrew before having images taken because of machine breakdown and rescheduling limitations prior to commencing CRT. The remaining four patients had scans at baseline and during RT. Further results will be reported on by AM and KS. Table 5.3 records demographic and tumour information. All patients had tonsillar primary although this was not visible on imaging for BIO5, where it was confirmed on incision biopsy. P16 positivity and HPV high-risk serotypes on in situ hybridisation were reported on standard NHS biopsies for every patient.

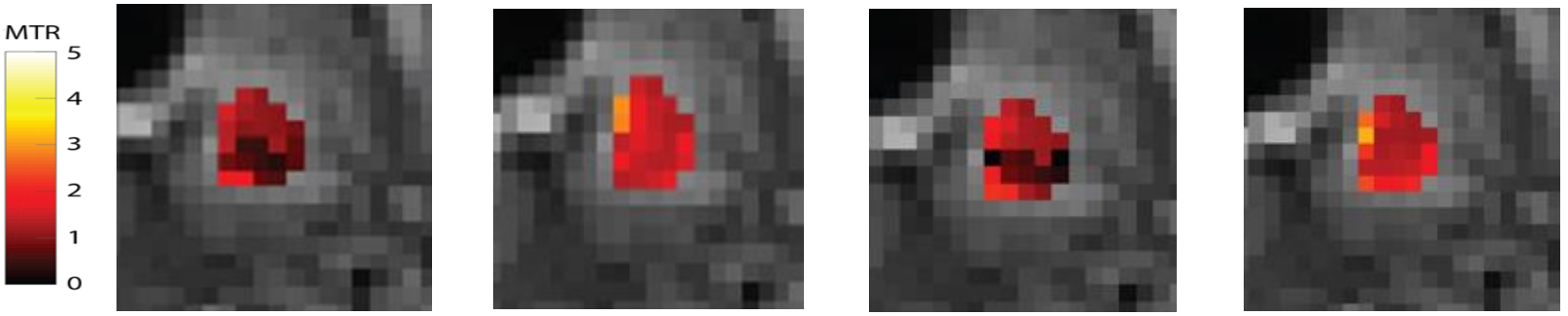
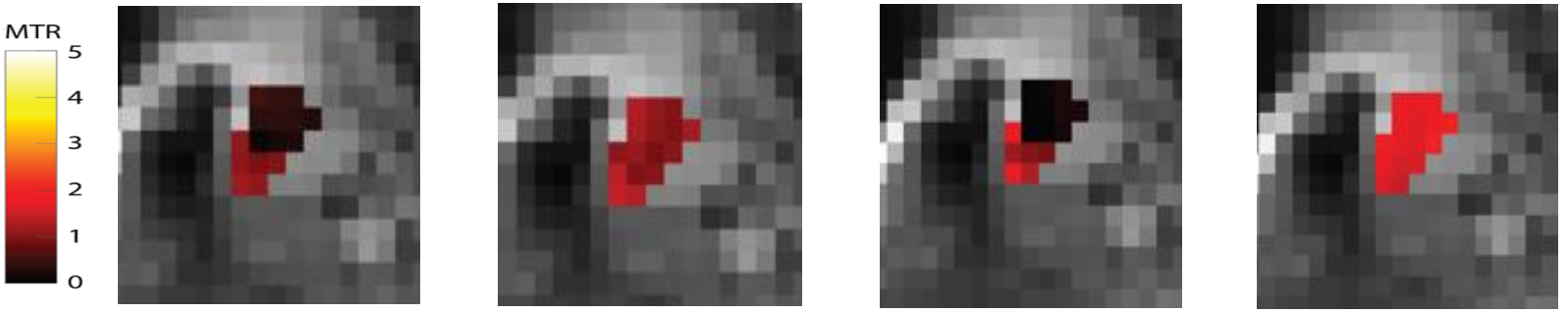
All patients were planned for 65Gy in 30 fractions radiotherapy, with BIO2 and BIO3 receiving bilateral neck treatment. All patients except BIO4 had concurrent cisplatin 100 mg/m^2 weekly. BIO4 had weekly cetuximab 400 mg m^2 loading followed by 250 mg/m^2 weekly as platinum-based therapy was contraindicated. An example of glucoCEST imaging in patient BIO4 is shown in Figure 5.9.

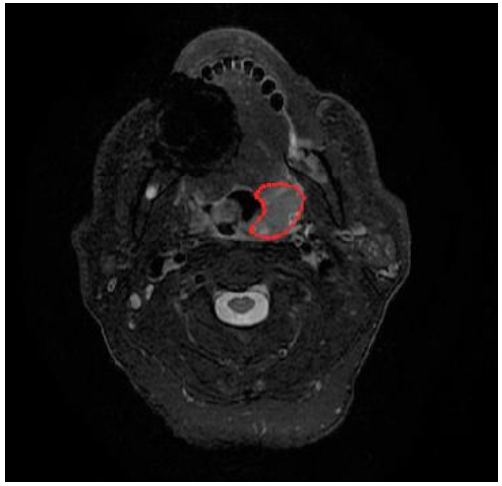
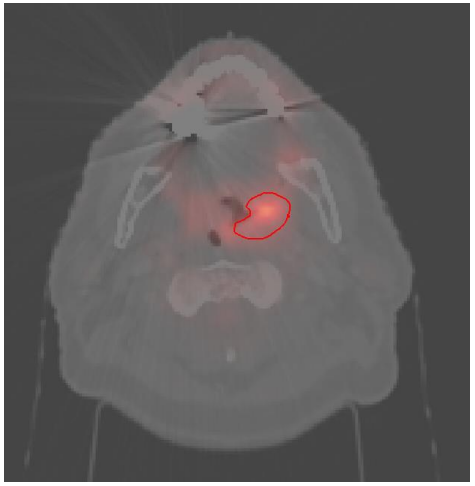
Table 5.3: BIOPIC study demographics and tumour staging

Study #	Age at RT start	T stage	N stage
BIO1	*	*	*
BIO2	56	2	2c
BIO3	43	3	2b
BIO4	69	3	1
BIO5	53	1	3

*Withdrawn

Figure 5.9: BIO4 a) GlucoCEST imaging at baseline (BL) and on CRT +/- i.v. dextrose +/- inspired oxygen; b) standard imaging (MRI, FDG PET-CT)

a)	Air		Oxygen	
	No dextrose	Dextrose	No dextrose	Dextrose
BL				
(S.D.)	1.18 (0.47)	2.16 (0.57)	1.20 (0.43)	2.02 (1.00)
CRT				
(S.D)	0.94 (0.18)	0.77 (0.19)	1.18 (0.31)	1.10 (0.21)

b)	T2 axial MRI	FDG PET-CT
BL standard imaging		 SUVmax = 16.4

The artefact at the right jaw is due to a dental implant; region of interest outlined in red for standard imaging**;** i.v. = intravenous

MTR at baseline

The MTR results of the primary tumour and involved nodes at baseline are shown in Table 5.4 and 5.5 respectively.

MTR on air

Two paired glucoCEST images on air +/- intravenous dextrose were available for the primary tumour and for the nodes at baseline. One scan for BIO2 was corrupted. As expected, the MTR rose in BIO3 and BIO4 tumours with intravenous dextrose by 41.3 and 83.1% respectively. However, the same pattern was not seen for the nodes in BIO3 and BIO5 where MTR fell 32.5% and 16.7% respectively. Movement between sequences may be a factor or differential uptake within the node due to heterogeneity, for example between an active 'rim' and more necrotic core. There may also be some differences between the way tumour primary and nodal metastases are perfused. Both tumour and nodal lesions were noted to have uptake on baseline FDG PET.

Table 5.4: Baseline tumour MTR with and without intravenous dextrose and on air versus 100% inspired oxygen in oropharyngeal SCC

	Air mean MTR (S.D.)			Oxygen mean MTR (S.D.)			FDG PET SUV max	
Study #	**no dex**	**i.v. dex**	**% Δ**	**no dex**	**i.v. dex**	**% Δ**	**Whole T**	**SS***
BIO2	**	1.83 (2.81)	N/A	2.03 (2.52)	2.04 (2.25)	0.5	24.6	21.4
BIO3	1.21 (1.26)	1.71 (1.34)	41.3	1.35 (0.86)	3.04 (3.38)	204.0	34.1	23
BIO4	1.18 (0.47)	2.16 (0.57)	83.1	1.20 (0.43)	2.02 (1.00)	68.3	16.4	10.2
BIO5	***	***	N/A	***	***	N/A	N/A	N/A

MTR=Magnetisation Transfer Ratio; SCC = squamous cell carcinoma; SUV = standardised uptake variable; i.v. = intravenous; dex = dexamethasone; Δ = change; T = tumour; SS = single slice; N/A = non applicable; * single slice equivalent to glucoCEST slice; ** scan corrupted; *** no identifiable primary on imaging

MTR on oxygen

Three paired scans were available for MTR on oxygen with and without i.v. dextrose in the primary tumour. When compared to the equivalent values on air, all except BIO2 with dextrose were higher, as would be expected due to the oxygen increasing T1 signal intensity. The difference between MTR on oxygen with and without dextrose was highly variable ranging from 0.5% in BIO2 to 204% in BIO3 tumours. Once again the findings in the nodal disease were not as consistent. Both the non-

dextrose scans with oxygen had lower MTR than on air. The MTR fell with i.v. dextrose for BIO3 node by 10.0% but rose for BIO5 node by 17.8%. Given the oxygenation levels were over 95% for both patients, the potential reasons for these unexpected findings are as those in the previous section.

Table 5.5: Baseline nodal MTR with and without i.v. dextrose and on air versus 100% inspired oxygen in oropharyngeal SCC

	Air mean MTR (S.D.)			**Oxygen mean MTR (S.D.)**			**FDG PET**
Study #	**no dex**	**i.v. dex**	**% Δ**	**no dex**	**i.v. dex**	**% Δ**	**SUVmax**
BIO2	*	*	N/A	*	*	N/A	N/A
BIO3	1.26 (1.50)	0.85 (0.23)	-32.5	1.11 (0.25)	0.90 (0.25)	-10.0	34.4
BIO4	*	*	N/A	*	*	N/A	N/A
BIO5	0.90 (0.88)	0.75 (0.66)	-16.7	0.61 (0.43)	1.26 (1.36)	106.6	27.1

MTR=Magnetisation Transfer Ratio; SCC = squamous cell carcinoma; SUV = standardised uptake variable; i.v. = intravenous; dex = dexamethasone; Δ = change; T = tumour; SS = single slice; N/A = non applicable; *no nodes visible on glucoCEST slice

Glucose levels

Capillary blood glucose levels at baseline and on CRT are indicated in Table 5.6. BIO3 had the highest blood glucose level recorded following the dextrose bolus of 10.6 mM. However, the tumour MTR on air was the lowest of the three patients. At 11.6 mM, this patient's blood glucose level remained the highest for the oxygen-inspiration glucoCEST scan with dextrose. At this point, the highest MTR of all baseline values was obtained at 3.04 (S.D. 3.38), representing a rise of 204.0% from the

oxygen-enhanced, non dextrose sequence. Interestingly, this patient did also exhibit the highest SUVmax at baseline, being 34.1.

Table 5.6: Changes in capillary blood glucose levels (mM) with intravenous dextrose bolus and infusion during baseline and on CRT scans

Study #	BL	Post bolus	On infusion	End of CEST
BIO2	5.7	7.9	6.8	10.9
BIO3	4.6	10.6	11.6	11.2
BIO4 BL	6	8*	U	11.2
BIO4 CRT	5.7	U	9.7	10.4
BIO5 BL	5.3	8.1	8.2	8.3
BIO5 CRT	6.4	9.2	9.8	10.4

BL – baseline; CRT – chemoradiotherapy; *difficult to obtain sample, possibly not representative result; U=unable to obtain sample

All patients except BIO5 had blood glucose levels over 10 mM on completion of the dextrose infusion. This patient did record the lowest MTR value at 0.61 (S.D. 0.43) in the nodes on oxygen, without dextrose. These findings suggest there may be a contribution of blood glucose levels to the MTR results obtained but it is unlikely to explain all the variation seen. Differences in patient and tumour physiology also likely impact, for example, in terms of perfusion and tumour cell glucose uptake.

Effects of oxygen-enhanced MRI

MOLLI-derived mean T1 results are shown in Table 5.7. Mean T1 fell with inspired oxygen in the two patients where paired scans were available, as would be expected. For the remaining patients, there was a poor fit to the model in one scan each. The T1 for BIO5 nodal disease on air was lower than that for the three tumour T1 values recorded.

Overall, the T1 range obtained was 750 to 950 ms whether on air or oxygen, which is comparable to the figures obtained for the two straight-to-surgery rectal adenocarcinoma patients discussed in Chapter 3. The rectal cancer patients who required neoadjuvant CRT had mean T1 values between 1000 to 1300 ms on air or oxygen and at baseline, during CRT and post therapy. This suggests some difference between HNSCC and LARC requiring neoadjuvant treatment, which may be due to tumour perfusion, oxygenation or potentially extracellular composition reflected by native T1 values.

Table 5.7: Baseline MOLLI mean T1 for tumour and nodes of oropharyngeal SCC on air and oxygen

Tumour		
Study #	**Air**	**Oxygen**
BIO2	781.9 (549.7)	757.8 (363.1)
BIO3	922.3 (252.7)	866.6 (416.7)
BIO4	948.7 (277.6)	*
Nodes		
Study #	**Air**	**Oxygen**
BIO5	753.8 (161.3)	*

*poor fit

GlucoCEST changes with CRT

GlucoCEST results on treatment were available for BIO4 (tumour) and BIO5 nodes at time of writing and are shown in Table 5.8. A mixed pattern is seen with BIO4 MTR falling with the addition of glucose both on air and oxygen. In contrast to the baseline findings, BIO5 node MTR levels rose with dextrose by 17.8% and 39.7% on air and oxygen respectively. Absolute levels on oxygen were comparable to those on air.

When compared to the baseline values, MTR for BIO4 on air was higher at baseline with no dextrose (1.18 (S.D. 0.47) or on dextrose 2.16 (S.D. 0.57)) than when on CRT with no dextrose (0.94 (S.D. 0.18) or on dextrose 0.77 (0.19)). With oxygen breathing, MTR values were similar at 1.20 (S.D.

0.43) at baseline versus 1.18 (S.D. 031) on CRT. With the addition of dextrose, baseline MTR was 2.02 (1.00), reducing to 1.10 (0.21) on treatment. This reduction in MTR with treatment would be expected with response to therapy, which was confirmed on the contemporaneous anatomical MRI.

Table 5.8: On CRT MTR with and without intravenous dextrose and on air versus 100% inspired oxygen in oropharyngeal SCC

	Air mean MTR (S.D.)			**Oxygen mean MTR (S.D.)**		
Study #	**no dex**	**i.v. dex**	**% Δ**	**no dex**	**i.v. dex**	**% Δ**
BIO4 (T)	0.94 (0.18)	0.77 (0.19)	-18.1	1.18 (0.31)	1.10 (0.21)	-6.8
BIO5 (N)	0.90 (0.71)	1.06 (0.80)	17.8	0.78 (0.59)	1.09 (1.04)	39.7

MTR=Magnetisation Transfer Ratio; SCC = squamous cell carcinoma; (T) = tumour; (N) = node; dex = dexamethasone; i.v. = intravenous; Δ = change

In contrast, there was minimal size response reported in BIO5 nodes following 10 fractions of radiotherapy. Accordingly, there was little change in MTR non dextrose values. Baseline MTR values on air were the same at 0.90 (S.D. 0.88 at baseline, 0.71 on CRT). This changed with dextrose to 0.75 (S.D. 0.66) and 0.77 (S.D. 0.19) respectively. On oxygen at baseline MTR was 0.61 (S.D. 0.43) compared with 0.78 (S.D. 0.59) on treatment. With dextrose, values were 1.26 (S.D. 1.36) at baseline and 1.09 (S.D. 1.04) on treatment.

Effects of oxygen-enhanced MRI on CRT

MOLLI T1 values on CRT are shown in Table 5.9. Mean T1 for BIO5 fell from a value of 802.1 ms (S.D. 244.6) on air to 606.7 ms (S.D. 143.0) on oxygen. This is consistent with expected findings as discussed in Chapter 3 as oxygen acts as a paramagnetic agent. The air mean MOLLI was higher on

CRT (802.1 ms [S.D. 244.6]) than that at baseline (753.8 ms [S.D. 277.6]), which could be related to fibrotic or oedematous response reaction to radiotherapy. Further comparisons are unavailable due to poor model fit.

Table 5.9: On CRT MOLLI mean T1 for tumour and nodes of oropharyngeal SCC on air and oxygen

Study #	**T1 on air (S.D.) [ms]**	**T1 on O_2 (S.D.) [ms]**
BIO4 (T)	*	648.0 (377.9)
BIO5 (N)	802.1 (244.6)	606.7 (143.0)

(T) = tumour; (N) = node, *poor fit; O_2 = Oxygen

3.5 Discussion of glucoCEST

GlucoCEST MRI has been undertaken in a small number of patients to date. The expected rise in MTR with intravenous dextrose or inspired oxygen was not always seen, which could reflect true physiological differences between malignancies in perfusion, oxygenation and glucose uptake. There are various other factors that may impact on the findings related to patient physiology, image acquisition and post-processing including model fitting.

In terms of patient factors, various parameters may affect the proton transfer exchange rate including temperature and pH. The signal obtained depends on the concentration of the compound, usually limited to mM levels for proton exchange CEST. In this study, signal may be impacted by both endogenous and exogenous glucose and vary with differing patient and tumour glucose metabolism. In addition, time taken to reach steady state may be an issue particularly in the clinical setting. With a long RF pulse time (over 3 seconds on 3T scanner), the specific absorption rate limits must be considered. A single slice scan over several minutes is also susceptible to

motion-related errors. On the scanner, inhomogeneity in B0 and B1 may distort results. MTR may also vary as a function of the RF pulse bandwidth and frequency offset.

As discussed above, assumptions are required for the asymmetry analysis calculation such that the MTC is symmetrical about water compared with the CEST effect and that there are independent contributions of solute and water protons. Another method to eliminate the effects of asymmetric MTC, not undertaken here, is to compare the CEST effects between target and control tissue such as muscle, as the asymmetric MTC effects may still be comparable. The nuclear Overhauser enhancement (NOE) effect, thought to be a type of cross-relaxation that occurs within −1.0~−4.0 ppm of water, was not accounted for in these results but these tend to be more problematic at higher Tesla[331].

The addition of inspired oxygen as a paramagnetic agent to enhance signal adds complexity to the glucoCEST MRI data obtained and itself has limitations, as discussed in Chapter 3. Model fitting was a particular issue with the MOLLI sequence used for T1 mapping, with 3 of the 12 slices obtained demonstrating poor fit.

Further analysis of these data and other sequences including DCE-MRI is ongoing to interrogate and minimise these potential issues.

4. Conclusion

FDG PET-CT is regularly used in oncological clinical practice to provide an indication of metabolically active tumour but it is not recommended routinely in non-metastatic rectal adenocarcinoma. Whilst the assessed FDG PET-CT parameters did not prove predictive of response to CRT, this modality may have some utility in excluding metastases, particularly to the liver, in patients with locally advanced disease who have no evidence of distant disease on CT imaging. It may also prove to have a role in radiotherapy planning tumour volume outlining.

GlucoCEST MRI provides the ability to assess glucose uptake activity with the benefit of the anatomical definition of this modality. However, there are many limitations to this technique. It may be possible to overcome some of these but inherent issues such as varying patient metabolism, lengthy scans due to the time taken to reach saturation and assumptions at processing regarding the symmetry of non-CEST effects will remain. Further investigation of CEST MRI may focus on a number of different compounds of interest in addition to glucose, such as amides, or specific exogenous contrast agents[228, 229].

Chapter 6: Conclusions & future directions

The era of personalised medicine heralds the opportunity to tailor cancer therapy to the individual patient and tumour, taking into account clinical, pathophysiologic and genetic information. The ability to identify which patients are likely to benefit from a specific therapy increases the therapeutic index. In the field of radiotherapy, many advances have been made with modern technology. Adaptive RT with simultaneous integrated boost is now realistic and requires reliable, reproducible and accurate imaging to plan and administer. Functional imaging to visualise suitable areas for dose boost, such as radioresistant hypoxic regions, has the potential to revolutionise treatment and increase tumour control, whilst potentially reducing toxicity to organs at risk. In LARC, the ability to maximise response can lead to complete response in a subset of patients who, if reliably identified, could avoid the major surgical resection usually recommended in this context.

The two rectal imaging trials in this study focus upon functional imaging. The response outcome used, based upon tumour regression grade, is reflective of response to radiotherapy and is not always comparable between imaging and pathological moieties. However, local recurrence or survival outcomes are more relevant clinically and would be preferable if time allowed. Sample size also remained a significant limitation.

Static imaging with FMISO can identify tumour regions likely to be radioresistant due to hypoxia. Within rectal cancer, FMISO SUVmax did not appear to identify those likely to respond to therapy. There was a suggestion at baseline that good responders had a lower hypoxic value when defined by T:M ratio but the findings would need to be confirmed in order to suggest a predictive value here.

We postulated that dynamic FMISO PET would provide information about tumour hypoxia and perfusion. The Casciari model[147] provided the best model fit and showed most patients had a reduction in hypoxia during week 2 CRT, which did not allow discrimination for prognostic

purposes. This complex model requires an arterial input function which ideally would be derived from arterial blood sampling. In addition, parameter initialisation is necessary and multiple solutions could potentially exist. Its use beyond a research tool is therefore problematic.

The logistical challenges associated with acquiring and administering FMISO although surmountable would severely limit clinical usage. Issues with image processing and analysis were significant. In particular, faecal and urinary excretion of tracer lead to issues of spillover and spill-in, which is difficult to correct due to the non-linear random characteristics of the activity. The findings of the RHYTHM study were that the use of FMISO in rectal cancer cannot be recommended.

The combination of a novel rapid T1 mapping technique ShMOLLI with oxygen enhancement was limited by the single slice obtained each time. Further research should look to include a significant portion or whole of the tumour for comparison purposes. The expected fall in T1 with inspired oxygen due to its paramagnetic properties was generally seen. T1 values were noted to be higher in the LARC patients when compared with those going straight to surgery. Native T1 values did also appear to be higher in poor responders both on and after RT. Whilst T1 has been associated with fibrosis[165-167], this finding would not be in keeping with reduced levels of fibrotic regression in these patients when compared to good responders. Other changes within the extracellular, extravascular space may be impacting and further investigation correlating tumour histopathology at baseline and resection specimens with and without neoadjuvant RT may be helpful to determine the underlying processes. Time required to image and signal-to-noise ratio are being further optimised as this technique is being investigated further in the BIOPIC study.

The comparison of functional imaging findings of hypoxia with immunohistochemistry in order to establish a likely ground truth is important for the establishment of imaging biomarkers. There was significant challenges in spatially correlating imaging with IHC. Ideally, digital direct comparison of functional imaging with whole mount serial sections would be made to account for tumour heterogeneity and better validate the imaging findings. Multiple tissue stains on the same

histopathology slice can be analysed by modern pathology software, allowing colocalisation to be assessed between for example hypoxia and vascular markers. RIT and RHYTHM samples were included within the larger Stratification in Colorectal Cancer consortium (S:CORT), looking into biopsy-based hypoxia metagene analysis[332], which could complement imaging and IHC findings.

DCE MRI and perfusion CT are established within the research setting including in rectal cancer. In DCE MRI, only Ktrans was assessed here based on previous studies suggesting this was associated with response outcomes, although other parameters such as K_{ep} and V_e could provide additional information and are being collated in RIT and RHYTHM. The potential to personalise the arterial input function using tumour imaging-based data could provide a more accurate input without compromising on scan time and resolution[299]. The use of mean Ktrans to describe heterogeneous tumours did not provide any useful indication as to response. The next step would be analysis of these data using segmentation based upon DCE-MRI parameters. This may be one way to provide useful spatial information as well as indicating variability within tumours[296]. Perfusion CT, as with DCE MRI, was analysed using mean values to describe a tumour, and therefore suffered with the same limitations. Furthermore findings were reliant on proprietary software for analysis and even within the same platform, different software versions have been shown to provide different values[294]. This inherently limits clinical use of this modality.

FDG PET-CT is a modality in common clinical use although in LARC this is primarily for assessment of metastatic disease. In the RIT study, FDG PET SUVmax, SUVpeak and TLG at baseline were not discriminatory. Assessment of various methods of defining MTV in order to determine the most relevant for delineation of radiotherapy boost volumes could be considered. Within the RIT study, patients also underwent a dynamic FDG PET at baseline, following 2 weeks CRT and post treatment with routine imaging. Assessment of FDG tracer kinetics may help to differentiate pathological from physiological uptake change[333, 334], potentially useful at baseline when outlining the tumour target volume for radiotherapy treatment. The ability of dynamic FDG PET to assess and

differentiate a tumour in an environment being treated by radiation or other therapy is yet to be determined.

The glucoCEST MRI sequence and technique showed promise in two RIT study patients, where it appeared comparable to FDG-PET. The BIOPIC study of HNSCC patients continues to investigate the potential of glucoCEST MRI to assess response to RT. This was the clinical first study to our knowledge that used oxygen-enhancement with the aim of increasing the MTR signal. Improvements in image processing and analysis are ongoing to improve the accuracy of the MTR values acquired. Extending the glucoCEST sequence beyond one slice in order to cover more of the tumour would allow clearer comparison with other imaging, such as FDG PET-CT, and IHC markers of glucose metabolism for validation.

Imaging is vital element of multiple facets of oncological management. Ideally, imaging evaluation would be embedded in the majority of oncological research studies alongside genetic, histopathological and circulating biomarkers to allow for collection of robust prospective data. This may help to overcome the limitations associated with small sample size, found in many imaging studies such as those presented here. Like imaging, radiotherapy has benefitted from significant technological advances over the last few years. The advent of MRI-linac provides the opportunity for combining anatomical definition with precision therapy. Defining tumour pathophysiology including its heterogeneity provides the opportunity to target tumours with radiation boost alongside the administration of complementary biological and chemotherapy. Personalised, adaptive radiotherapy is possible, with the right imaging.

Appendix

Appendix 1: Imaging acquisition parameters and sequences

1.1 FMISO PET-CT scanning parameters		
	Dynamic SCAN	STATIC SCAN
SLICE THICKNESS	helical 3.75 mm slices (CTAC) CT 2.5 mm slices	helical 3.75 mm slices (CTAC) CT 2.5 mm slices
KV	120	120
TILT	0	0
TUBE CURRENT	smart mA (max 250)	Smart mA (max 250)
PITCH	0.984:1	0.984:1
ROTATION TIME	0.5	0.5
PET DURATION	45 minutes	10 minutes (approximately)
PET BED	single bed covering pelvis for scan duration	single bed covering pelvis for scan duration

1.2 FDG PET-CT scanning parameters	
PROTOCOL	static
SLICE THICKNESS	helical 3.75 mm slices (CTAC) CT 2.5 mm slices
Kv	120
TILT	0
TUBE CURRENT	Smart mA (max 250)
PITCH	0.984:1
ROTATION TIME	0.5
PET DURATION	10 minutes (approximately)
PET BED	single bed covering pelvis for scan duration
TRACER	FDG

1.3: Perfusion CT scan acquisition parameters		
	PRE-CONTRAST IMAGES	DYNAMIC IMAGES ARTERIAL PHASE & WASH OUT
SLICE THICKNESS	0.625 mm as a 2.5 mm contiguous helical block taken in free breathing	5 mm axial in free breathing
Kv	100	100
TILT	0	0
TUBE CURRENT	130 mA fixed	130 mA fixed (if BMI < 30 use 170 mA)
PITCH	1.375:1	1.375:1
ROTATION TIME	0.5 seconds	0.5 seconds
ROTATION INTERVAL	-	1 second
Images per rotation	-	8 (240 images total as 30 sets of images acquired every second then 40 images total as 5 sets acquired every 14.5 secs)
Field of view	Field of view 36cm; may be increased for patients with large body habitus.	Field of view 36cm; may be increased for patients with large body habitus.

ACQUISITION START	-	10 seconds after injection
NOISE INDEX	32.00	7.81
BMI = body mass index		

Box 1.1 MRI sequences in RHYTHM and RIT studies

- 3-plane localiser & axial calibration
- Anatomical: Sagittal T2, Coronal T2, Small field of view T2 Axial
- VFA: 15’ alone, 9’ alone, 3’ alone
- ShMolli** (Flip angle 35, TE Min Full, No. echoes 1)
  (VFA/ShMOLLI sequences repeated with patient breathing supplemental oxygen)
- T2* Pre
- DCE: axial LAVA Asset Pre Gad & axial LAVA Asset Post Gad
- Coronal T2* Post Gad
  **ShMOLLI and oxygen breathing added in RIT2, RIT3 and RHYTHM following protocol amendments

Box 1.2 RHYTHM *ex vivo* MRI sequences

- 3 Plane localiser
- Axial FRFSE T2 hr
- Sagittal CUBE T2
- Axial T1 FSE

Box 1.3 MRI sequences in the BIOPIC study

- 3 Plane localiser & axial calibration
- Anatomical: Sagittal T2, Coronal T2, Axial IDEAL T2
- Fast SPGR with variable flip angles 15', 10', 5', 2'
- Axial MOLLI T1 mapping
- T2* pre
- GlucoCEST without i.v. dextrose

On 100% inhaled oxygen:

- Variable flip angles: 15' alone, 9' alone, 3' alone
- MOLLI T1 mapping
- GlucoCEST without/with i.v. dextrose

Oxygen stopped, room air supplied

- GlucoCEST with i.v. dextrose
- B0 map & B1 map
- Axial T1 LAVA Asset Pre & post Gad
- Coronal T2* Post Gad

BOX 1.4: GlucoCEST MRI imaging sequences & parameters

- 2D single-shot EPI sequence
- 20mm FOV with 64x64 matrix
- 10mm slice thickness
- TR per image/offset freq = 4s; TE = 21.4ms
- ASSET acceleration factor = 2

Appendix 2: IHC

2.1: Pimonidazole (Pimo) IHC in RHYTHM A					
Slide	**Tissue area (µm²)**	**Pimo area (µm²)**	**Pimo weak area (µm²)**	**Pimo moderate area (µm²)**	**Pimo strong area (µm²)**
RHA01-01	9.79E+07	1.31E+07	9.75E+06	2.19E+06	1.20E+06
RHA01-02	1.06E+08	1.35E+07	1.00E+07	2.22E+06	1.22E+06
RHA01-03	3.89E+07	4.30E+06	3.16E+06	7.17E+05	4.27E+05
RHA01-04	1.50E+08	2.99E+07	1.87E+07	6.31E+06	4.91E+06
RHA01-05	1.23E+08	1.88E+07	1.22E+07	3.94E+06	2.60E+06
RHA01-06	8.20E+07	7.35E+06	5.28E+06	1.29E+06	7.79E+05
RHA01-07	1.29E+08	2.65E+07	1.72E+07	5.67E+06	3.69E+06
RHA01-08	9.03E+07	1.27E+07	9.26E+06	2.16E+06	1.25E+06
RHA01-09	9.41E+07	1.22E+07	8.89E+06	2.11E+06	1.26E+06
RHA01-10	9.31E+07	1.17E+07	8.47E+06	2.05E+06	1.17E+06
RHA01-11	2.11E+07	1.78E+06	1.23E+06	3.33E+05	2.21E+05

RHA01-12	4.17E+06	6.56E+05	4.80E+05	1.22E+05	5.44E+04
RHA01-13	1.01E+08	1.67E+07	1.07E+07	3.60E+06	2.41E+06
RHA01-14	1.74E+07	1.38E+06	9.83E+05	2.48E+05	1.44E+05
RHA01-15	6.21E+07	1.14E+07	6.98E+06	2.41E+06	2.05E+06
RHA01-16	7.51E+07	1.68E+05	1.45E+05	1.78E+04	5.50E+03
RHA01-17	2.69E+07	3.29E+06	2.56E+06	5.18E+05	2.15E+05
RHA01-18	1.01E+08	1.97E+07	1.23E+07	4.03E+06	3.38E+06
RHA01-19	3.63E+06	3.81E+05	2.90E+05	5.87E+04	3.21E+04
RHA01-20	9.00E+06	2.58E+05	2.06E+05	3.53E+04	1.62E+04
RHA02-01	3.46E+07	1.97E+06	1.21E+06	3.76E+05	3.83E+05
RHA02-02	1.95E+07	6.59E+05	3.87E+05	1.28E+05	1.43E+05
RHA02-03	5.42E+06	7.97E+05	4.75E+05	1.58E+05	1.64E+05
RHA02-04	1.81E+08	1.17E+07	7.10E+06	2.40E+06	2.20E+06
RHA02-05	3.74E+07	1.29E+06	8.29E+05	2.30E+05	2.33E+05

RHA02-06	3.92E+07	1.27E+06	8.22E+05	2.26E+05	2.25E+05
RHA02-07	8.90E+07	6.61E+06	3.90E+06	1.29E+06	1.42E+06
RHA02-08	9.18E+07	7.08E+06	4.23E+06	1.39E+06	1.46E+06
RHA02-09	1.08E+08	6.17E+06	3.64E+06	1.30E+06	1.24E+06
RHA02-10	4.02E+07	2.75E+06	1.52E+06	5.55E+05	6.71E+05
RHA02-11	6.77E+07	5.58E+06	3.25E+06	1.10E+06	1.23E+06
RHA02-12	7.22E+07	3.09E+06	1.89E+06	6.16E+05	5.83E+05
RHA02-13	1.03E+08	5.34E+06	3.37E+06	1.11E+06	8.47E+05
RHA02-14	7.96E+07	4.92E+06	2.89E+06	9.69E+05	1.06E+06
RHA02-15	2.60E+07	5.76E+05	3.61E+05	9.81E+04	1.17E+05
RHA02-16	5.53E+07	3.32E+06	1.99E+06	6.79E+05	6.47E+05
RHA02-17	2.59E+07	9.72E+05	5.70E+05	1.62E+05	2.41E+05
RHA02-18	1.14E+07	6.57E+05	3.85E+05	1.20E+05	1.53E+05
RHA02-19	3.57E+07	2.89E+06	1.67E+06	5.51E+05	6.70E+05

RHA02-20	8.14E+06	4.01E+05	3.30E+05	4.24E+04	2.93E+04
RHA02-21	1.67E+07	2.22E+06	1.52E+06	4.00E+05	3.00E+05
RHA02-22	8.19E+07	3.87E+06	2.36E+06	7.64E+05	7.49E+05
RHA02-23	8.79E+07	5.06E+06	3.22E+06	1.01E+06	8.35E+05
RHA02-24	1.43E+08	4.99E+06	2.92E+06	1.04E+06	1.02E+06
RHA02-25	2.58E+07	1.39E+06	8.03E+05	2.61E+05	3.27E+05
RHA02-26	1.20E+08	5.43E+06	3.36E+06	9.78E+05	1.10E+06
RHA02-27	1.10E+08	4.90E+06	2.72E+06	1.07E+06	1.11E+06
RHA02-28	1.96E+07	1.24E+06	6.62E+05	2.51E+05	3.31E+05
RHA02-29	5.18E+07	1.79E+06	1.13E+06	3.16E+05	3.41E+05
RHA02-30	1.43E+08	1.04E+07	6.72E+06	1.83E+06	1.87E+06
RHA02-31	7.97E+07	5.10E+06	3.59E+06	8.85E+05	6.21E+05
RHA02-32	1.19E+08	4.75E+06	3.09E+06	8.82E+05	7.80E+05
RHA03-01	4.46E+07	5.48E+06	3.52E+06	1.20E+06	7.56E+05

RHA03-02	4.32E+07	7.18E+06	4.68E+06	1.60E+06	8.99E+05
RHA03-03	1.76E+06	3.82E+05	2.01E+05	8.91E+04	9.14E+04
RHA03-04	1.06E+07	6.68E+05	4.63E+05	1.35E+05	6.96E+04
RHA03-05	5.82E+07	5.02E+06	3.20E+06	1.11E+06	7.23E+05
RHA03-06	6.75E+06	5.51E+05	3.41E+05	1.19E+05	9.10E+04
RHA03-07	6.07E+06	7.45E+05	4.70E+05	1.79E+05	9.59E+04
RHA03-08	2.13E+07	3.96E+06	2.30E+06	9.41E+05	7.15E+05
RHA03-09	7.04E+06	1.25E+06	7.95E+05	2.72E+05	1.87E+05
RHA03-10	9.51E+07	1.73E+07	9.98E+06	4.19E+06	3.16E+06
RHA03-11	3.77E+06	8.20E+05	3.89E+05	2.05E+05	2.26E+05
RHA03-12	1.49E+07	1.89E+06	1.18E+06	4.37E+05	2.77E+05
RHA03-13	7.88E+07	1.18E+07	7.18E+06	2.65E+06	1.98E+06
Pimo = pimonidazole					

2.2: CAIX IHC in RHYTHM A					
Slide	**Tissue area (µm²)**	**CAIX area (µm²)**	**CAIX weak area (µm²)**	**CAIX moderate area (µm²)**	**CAIX strong area (µm²)**
RHA01-01	3.20E+07	9.66E+06	4.69E+06	2.32E+06	2.65E+06
RHA01-02	6.38E+07	7.28E+06	4.68E+06	1.60E+06	9.98E+05
RHA01-03	1.68E+08	1.79E+07	1.19E+07	3.73E+06	2.25E+06
RHA01-04	5.13E+06	7.25E+04	5.94E+04	1.00E+04	3.00E+03
RHA01-05	1.11E+07	2.02E+06	1.27E+06	4.55E+05	2.90E+05
RHA01-06	1.24E+08	1.98E+07	1.25E+07	4.31E+06	3.06E+06
RHA01-07	1.42E+07	1.68E+06	1.13E+06	3.27E+05	2.25E+05
RHA01-08	9.04E+07	1.14E+07	7.20E+06	2.51E+06	1.70E+06
RHA01-09	2.57E+07	1.72E+06	1.22E+06	3.33E+05	1.68E+05
RHA01-10	2.51E+07	6.41E+06	3.83E+06	1.49E+06	1.09E+06
RHA01-11	6.15E+06	5.78E+05	4.90E+05	7.03E+04	1.77E+04
RHA01-12	1.03E+08	1.12E+07	7.13E+06	2.51E+06	1.54E+06

RHA02-01	7.39E+07	1.39E+05	1.26E+05	9.91E+03	3.04E+03
RHA02-02	1.28E+08	2.18E+05	1.88E+05	2.38E+04	6.66E+03
RHA02-03	3.18E+07	9.46E+04	6.50E+04	1.90E+04	1.06E+04
RHA02-04	4.17E+07	5.87E+04	5.25E+04	5.18E+03	1.03E+03
RHA02-05	9.68E+07	1.14E+05	9.71E+04	1.28E+04	4.22E+03
RHA02-06	6.38E+07	7.28E+06	4.68E+06	1.60E+06	9.98E+05
RHA02-07	6.33E+07	2.98E+05	2.59E+05	3.02E+04	8.90E+03
RHA02-08	1.38E+08	1.39E+05	1.20E+05	1.38E+04	5.64E+03
RHA02-09	4.20E+07	6.20E+04	5.52E+04	5.33E+03	1.49E+03
RHA02-10	7.64E+07	1.49E+05	1.28E+05	1.72E+04	3.77E+03
RHA02-11	1.06E+08	1.72E+05	1.54E+05	1.64E+04	2.48E+03
RHA02-12	2.90E+07	7.66E+04	6.78E+04	7.00E+03	1.80E+03
RHA02-13	1.60E+07	2.14E+04	1.92E+04	1.63E+03	6.43E+02
RHA02-14	4.44E+06	2.67E+04	2.41E+04	2.06E+03	4.91E+02

RHA02-15	7.52E+07	7.92E+04	7.14E+04	6.37E+03	1.40E+03
RHA02-16	5.06E+07	5.60E+04	4.56E+04	8.38E+03	2.06E+03
RHA02-17	6.33E+07	2.98E+05	2.59E+05	3.02E+04	8.90E+03
RHA02-18	1.38E+08	1.39E+05	1.20E+05	1.38E+04	5.64E+03
RHA02-19	4.20E+07	6.20E+04	5.52E+04	5.33E+03	1.49E+03
RHA02-20	7.64E+07	1.49E+05	1.28E+05	1.72E+04	3.77E+03
RHA02-21	1.06E+08	1.72E+05	1.54E+05	1.64E+04	2.48E+03
RHA02-22	2.90E+07	7.66E+04	6.78E+04	7.00E+03	1.80E+03
RHA02-23	1.60E+07	2.14E+04	1.92E+04	1.63E+03	6.43E+02
RHA02-24	4.44E+06	2.67E+04	2.41E+04	2.06E+03	4.91E+02
RHA02-25	7.52E+07	7.92E+04	7.14E+04	6.37E+03	1.40E+03
RHA02-26	5.06E+07	5.60E+04	4.56E+04	8.38E+03	2.06E+03
RHA02-27	2.43E+07	2.31E+04	2.14E+04	1.54E+03	1.78E+02
RHA02-28	6.17E+07	2.43E+05	1.64E+05	5.02E+04	2.89E+04

RHA02-29	1.19E+08	5.34E+05	4.24E+05	8.42E+04	2.57E+04
RHA02-30	8.85E+07	6.89E+04	6.25E+04	5.71E+03	7.12E+02
RHA02-31	7.55E+07	8.35E+04	7.53E+04	6.75E+03	1.40E+03
RHA02-32	6.10E+07	1.12E+05	8.49E+04	1.81E+04	8.81E+03
RHA02-33	8.45E+07	1.16E+05	1.04E+05	1.00E+04	1.92E+03
RHA02-34	7.42E+07	2.21E+05	1.80E+05	3.04E+04	1.05E+04
RHA02-35	2.84E+07	6.85E+04	6.40E+04	3.36E+03	1.14E+03
RHA02-36	5.06E+07	4.08E+04	3.66E+04	3.66E+03	4.77E+02
RHA02-37	3.51E+07	8.00E+04	7.47E+04	4.67E+03	6.09E+02
RHA02-38	4.10E+07	9.37E+04	8.38E+04	8.19E+03	1.78E+03
RHA02-39	1.01E+07	1.35E+04	1.24E+04	8.67E+02	2.79E+02
RHA03-01	5.74E+07	8.25E+06	4.34E+06	2.10E+06	1.81E+06
RHA03-02	5.76E+07	6.79E+04	5.82E+04	7.19E+03	2.46E+03
RHA03-03	1.25E+08	3.53E+06	2.37E+06	6.44E+05	5.21E+05

RHA03-04	4.33E+07	7.13E+06	3.55E+06	1.75E+06	1.83E+06
RHA03-05	1.55E+06	4.67E+05	1.90E+05	1.14E+05	1.64E+05
RHA03-06	7.13E+06	1.18E+06	6.32E+05	3.16E+05	2.32E+05
RHA03-07	4.33E+07	4.65E+06	2.82E+06	1.12E+06	7.07E+05
RHA03-08	8.54E+06	3.36E+05	2.47E+05	6.57E+04	2.33E+04
RHA03-09	9.74E+06	1.47E+06	7.34E+05	3.67E+05	3.71E+05
RHA03-10	1.39E+07	2.10E+06	1.03E+06	5.40E+05	5.30E+05
RHA03-11	6.30E+07	7.14E+06	4.39E+06	1.76E+06	9.96E+05
RHA03-12	4.04E+06	9.83E+05	4.87E+05	2.55E+05	2.40E+05
RHA03-13	2.52E+07	4.94E+06	2.63E+06	1.25E+06	1.06E+06
RHA03-14	7.41E+07	9.12E+06	4.92E+06	2.20E+06	2.00E+06
RHA03-15	6.49E+06	8.30E+05	3.93E+05	1.94E+05	2.43E+05

2.2: CD31 IHC in RHYTHM A					
Slide	**Total tissue area (mm^2)**	**Tumour area (mm^2)**	**Vessels area (mm^2)**	**Total capillary count**	**Capillary count ($/mm^2$)**
RHA01-01	2.18E+01	1.70E+01	8.98E-01	1.69E+03	7.79E+01
RHA01-02	1.11E+02	5.04E+01	6.35E+00	8.28E+03	7.48E+01
RHA01-03	6.11E+01	2.09E+01	2.80E+00	3.17E+03	5.22E+01
RHA01-04	1.05E+01	9.87E+00	2.40E-04	2.00E+00	1.92E-01
RHA01-05	2.12E+01	1.57E+01	1.03E+00	2.02E+03	9.56E+01
RHA01-06	9.22E+01	3.51E+01	4.09E+00	5.86E+03	6.38E+01
RHA01-07	3.21E+01	9.60E+00	2.33E+00	2.76E+03	8.65E+01
RHA01-08	2.18E+01	1.57E+01	1.50E+00	2.19E+03	1.01E+02
RHA01-09	1.30E+02	5.51E+01	1.03E+01	8.62E+03	6.65E+01
RHA01-10	1.29E+01	3.10E+00	1.51E+00	1.05E+03	8.18E+01
RHA01-11	5.92E+01	8.24E+00	2.86E+00	3.38E+03	5.74E+01
RHA01-12	3.34E+01	2.83E+00	9.98E-01	1.43E+03	4.31E+01

RHA01-13	2.54E+01	5.08E+00	1.09E+00	1.25E+03	4.96E+01
RHA01-14	4.72E+01	1.84E+01	9.10E+00	5.80E+03	1.24E+02
RHA01-15	8.80E+01	3.10E+01	8.48E+00	9.12E+03	1.04E+02
RHA01-16	1.76E+02	6.99E+01	1.62E+01	1.26E+04	7.22E+01
RHA02-01	1.13E+02	7.16E+01	9.97E+00	7.37E+03	6.55E+01
RHA02-02	4.84E+01	2.38E+01	6.22E+00	4.60E+03	9.58E+01
RHA02-03	3.16E+01	1.31E+01	4.92E+00	2.93E+03	9.36E+01
RHA02-04	6.14E+01	3.01E+01	6.95E+00	5.17E+03	8.47E+01
RHA02-05	3.08E+01	1.39E+01	4.51E+00	2.71E+03	8.88E+01
RHA02-06	9.21E+01	4.11E+01	9.67E+00	7.72E+03	8.43E+01
RHA02-07	9.08E+01	4.96E+01	1.10E+01	7.33E+03	8.13E+01
RHA02-08	8.80E+01	2.62E+01	1.24E+01	8.74E+03	1.00E+02
RHA02-09	3.06E+00	1.05E+00	3.54E-01	2.34E+02	7.69E+01
RHA02-10	6.98E+01	4.59E+01	4.90E+00	5.67E+03	8.17E+01

RHA02-11	8.88E+01	4.62E+01	1.05E+01	7.15E+03	8.10E+01
RHA02-12	4.45E+01	2.29E+01	5.44E+00	4.30E+03	9.71E+01
RHA02-13	3.96E+01	3.32E-01	9.38E-01	1.15E+03	2.90E+01
RHA02-14	1.53E+02	8.37E+01	1.59E+01	1.21E+04	7.98E+01
RHA02-15	6.92E+01	3.20E+01	1.05E+01	6.07E+03	8.82E+01
RHA02-16	8.28E+01	3.42E+01	1.10E+01	7.02E+03	8.54E+01
RHA02-17	1.20E+01	6.39E+00	1.33E+00	1.08E+03	9.02E+01
RHA02-18	3.00E+01	1.40E+01	3.22E+00	2.13E+03	7.14E+01
RHA02-19	1.55E+02	5.97E+01	1.87E+01	1.34E+04	8.69E+01
RHA02-20	2.09E+01	6.63E+00	1.85E+00	1.58E+03	7.57E+01
RHA02-21	2.19E+01	6.71E+00	2.41E+00	1.98E+03	9.09E+01
RHA02-22	1.54E+02	6.64E+01	1.92E+01	1.38E+04	9.03E+01
RHA02-23	1.22E+02	5.46E+01	1.19E+01	8.68E+03	7.17E+01
RHA02-24	4.81E+00	2.62E+00	5.81E-01	2.93E+02	6.12E+01

RHA02-25	2.35E+01	1.24E+01	2.57E+00	1.92E+03	8.22E+01
RHA02-26	1.46E+02	5.00E+01	1.89E+01	1.35E+04	9.30E+01
RHA02-27	7.90E+01	3.64E+01	8.62E+00	6.20E+03	7.90E+01
RHA02-28	1.31E+02	4.87E+01	9.51E+00	9.01E+03	6.90E+01
RHA02-29	2.41E+01	1.35E+01	2.40E+00	1.71E+03	7.13E+01
RHA02-30	6.10E+01	1.64E+01	8.43E+00	6.37E+03	1.05E+02
RHA02-31	1.73E+00	3.96E-01	1.61E-01	9.80E+01	5.70E+01
RHA02-32	3.19E+01	1.77E+01	3.95E+00	2.59E+03	8.18E+01
RHA03-01	5.38E+01	3.92E+01	2.67E+00	3.17E+03	5.92E+01
RHA03-02	7.27E+01	3.03E+01	9.26E+00	6.19E+03	8.57E+01
RHA03-03	6.38E+00	4.49E+00	3.87E-01	3.11E+02	4.89E+01
RHA03-04	5.21E+00	3.93E+00	3.21E-01	3.88E+02	7.48E+01
RHA03-05	1.07E+02	4.89E+01	6.17E+00	7.31E+03	6.87E+01
RHA03-06	3.25E+00	2.96E+00	1.18E-01	1.54E+02	4.76E+01

RHA03-07	1.97E+01	1.48E+01	8.66E-01	1.15E+03	5.85E+01
RHA03-08	1.09E+01	8.23E+00	2.36E-01	5.26E+02	4.84E+01
RHA03-09	6.76E+01	3.84E+01	1.02E+00	1.48E+03	2.20E+01
RHA03-10	6.61E+01	3.75E+01	9.71E-01	1.39E+03	2.12E+01
RHA03-11	4.24E+01	2.09E+01	2.90E+00	2.68E+03	6.35E+01
RHA03-12	4.36E+01	2.03E+01	3.05E+00	2.86E+03	6.59E+01
RHA03-13	9.70E+01	4.99E+01	7.54E+00	6.54E+03	6.78E+01

References

1. Ahmad, A.S., N. Ormiston-Smith, and P.D. Sasieni, *Trends in the lifetime risk of developing cancer in Great Britain: comparison of risk for those born from 1930 to 1960.* British Journal of Cancer, 2015. **112**(5): p. 943-947.
2. Cancer Research UK. *Cancer mortality statistics*. 2016 [cited 2016 13/04/2017]; Available from: http://www.cancerresearchuk.org/health-professional/cancer-statistics/mortality#YRRIYji6uGaPFYho.99.
3. Cancer Research UK. *Bowel cancer incidence statistics*. 2016 [cited 2016 13/04/2017]; Available from: http://www.cancerresearchuk.org/health-professional/cancer-statistics/statistics-by-cancer-type/bowel-cancer/incidence#KektAH2MGAVhHiDJ.99.
4. National Cancer Registration and Analysis Service, *Stage Breakdown by CCG 2014*. 2016: London.
5. Mokhles, S., et al., *Meta-analysis of colorectal cancer follow-up after potentially curative resection.* British Journal of Surgery, 2016. **103**(10): p. 1259-1268.
6. Sauer, R., et al., *Preoperative versus postoperative chemoradiotherapy for locally advanced rectal cancer: results of the German CAO/ARO/AIO-94 randomized phase III trial after a median follow-up of 11 years.* J Clin Oncol, 2012. **30**(16): p. 1926-33.
7. National Cancer Intelligence Network, *Colorectal Cancer Survival by Stage*. 2009.
8. National Institute for Health and Care Excellence, *Colorectal cancer (NG151)*. 2020.
9. National Comprehensive Cancer Network. *NCCN Clinical Practice Guidelines in Oncology: Rectal Cancer Version 2.2016*. 2016 02/04/2018]; Available from: https://www.tri-kobe.org/nccn/guideline/colorectal/english/rectal.pdf.
10. Glynne-Jones, R., et al., *Rectal cancer: ESMO Clinical Practice Guidelines for diagnosis, treatment and follow-up.* Ann Oncol, 2017. **28**(suppl_4): p. iv22-iv40.
11. Amin, M.B., *AJCC cancer staging manual*. Eighth ed. Cancer staging manual. 2017, Chicago: American Joint Committee on Cancer/Springer.
12. Department of Health, *The NHS cancer plan: a plan for investment: a plan for reform*, D.o. Health, Editor. 2000, Department of Health.
13. National Institute for Health and Care Excellence, *Colorectal cancer: diagnosis and management (CG131)*. 2011 updated 2014.
14. Cedermark, B., et al., *Improved survival with preoperative radiotherapy in resectable rectal cancer.* N Engl J Med, 1997. **336**(14): p. 980-7.
15. Kapiteijn, E., et al., *Preoperative radiotherapy combined with total mesorectal excision for resectable rectal cancer.* N Engl J Med, 2001. **345**(9): p. 638-46.
16. Sauer, R., et al., *Preoperative versus postoperative chemoradiotherapy for rectal cancer.* N Engl J Med, 2004. **351**(17): p. 1731-40.
17. Roh, M.S., et al., *Preoperative Multimodality Therapy Improves Disease-Free Survival in Patients With Carcinoma of the Rectum: NSABP R-03.* Journal of Clinical Oncology, 2009. **27**(31): p. 5124-5130.
18. Braendengen, M., et al., *Randomized phase III study comparing preoperative radiotherapy with chemoradiotherapy in nonresectable rectal cancer.* J Clin Oncol, 2008. **26**(22): p. 3687-94.

19. Gerard, J.P., D. Azria, and S. Gourgou-Bourgade, *Accord 12 trial of neoadjuvant treatment in rectal cancer: Clinical results at 3 years. on behalf of prodige group.* Radiotherapy and Oncology, 2012. **103**: p. S180.

20. Bosset, J.F., et al., *Chemotherapy with preoperative radiotherapy in rectal cancer.* N Engl J Med, 2006. **355**(11): p. 1114-23.

21. Liu, S., et al., *Total Neoadjuvant Therapy (TNT) versus Standard Neoadjuvant Chemoradiotherapy for Locally Advanced Rectal Cancer: A Systematic Review and Meta-Analysis.* Oncologist, 2021. **26**(9): p. e1555-e1566.

22. Petrelli, F., et al., *Total Neoadjuvant Therapy in Rectal Cancer: A Systematic Review and Meta-analysis of Treatment Outcomes.* Ann Surg, 2020. **271**(3): p. 440-448.

23. Garcia-Aguilar, J., et al., *Organ Preservation in Patients With Rectal Adenocarcinoma Treated With Total Neoadjuvant Therapy.* Journal of Clinical Oncology, 2022. **40**(23): p. 2546-2556.

24. Heald, R.J., E.M. Husband, and R.D. Ryall, *The mesorectum in rectal cancer surgery--the clue to pelvic recurrence?* Br J Surg, 1982. **69**(10): p. 613-6.

25. MacFarlane, J.K., R.D. Ryall, and R.J. Heald, *Mesorectal excision for rectal cancer.* Lancet, 1993. **341**(8843): p. 457-60.

26. Vennix, S., et al., *Laparoscopic versus open total mesorectal excision for rectal cancer.* Cochrane Database of Systematic Reviews, 2014(4).

27. Simillis, C., et al., *A systematic review of transanal total mesorectal excision: is this the future of rectal cancer surgery?* Colorectal Disease, 2016. **18**(1): p. 19-36.

28. Jimenez-Rodriguez, R.M., et al., *Comparing outcomes of robotic versus open mesorectal excision for rectal cancer.* BJS Open, 2021. **5**(6): p. zrab135.

29. Minsky, B.D. and C. Rodel, *Identifying the Most Predictive Post-Chemoradiation TRG System for Rectal Cancer.* Journal of the National Cancer Institute, 2014. **106**(10).

30. Trakarnsanga, A., et al., *Comparison of tumor regression grade systems for locally advanced rectal cancer after multimodality treatment.* J Natl Cancer Inst, 2014. **106**(10).

31. Maas, M., et al., *Long-term outcome in patients with a pathological complete response after chemoradiation for rectal cancer: a pooled analysis of individual patient data.* The Lancet Oncology, 2010. **11**(9): p. 835-844.

32. Maggiori, L., et al., *Does pathologic response of rectal cancer influence postoperative morbidity after neoadjuvant radiochemotherapy and total mesorectal excision?* Surgery, 2014. **155**(3): p. 468-75.

33. Fernández-Aceñero, M.J., et al., *Prognostic influence of histopathological regression patterns in rectal adenocarcinoma receiving neoadjuvant therapy.* J Gastrointest Oncol, 2017. **8**(1): p. 49-54.

34. Zorcolo, L., et al., *Complete pathologic response after combined modality treatment for rectal cancer and long-term survival: a meta-analysis.* Ann Surg Oncol, 2012. **19**(9): p. 2822-32.

35. Martin, S.T., H.M. Heneghan, and D.C. Winter, *Systematic review and meta-analysis of outcomes following pathological complete response to neoadjuvant chemoradiotherapy for rectal cancer.* British Journal of Surgery, 2012. **99**(7): p. 918-928.

36. Mandard, A.M., et al., *Pathologic assessment of tumor regression after preoperative chemoradiotherapy of esophageal carcinoma. Clinicopathologic correlations.* Cancer, 1994. **73**(11): p. 2680-6.

37. Dworak, O., L. Keilholz, and A. Hoffmann, *Pathological features of rectal cancer after preoperative radiochemotherapy.* Int J Colorectal Dis, 1997. **12**(1): p. 19-23.

38. Ryan, R., et al., *Pathological response following long-course neoadjuvant chemoradiotherapy for locally advanced rectal cancer.* Histopathology, 2005. **47**(2): p. 141-146.

39. Van Cutsem, E., et al., *Imaging in Colorectal Cancer: Progress and Challenges for the Clinicians.* Cancers (Basel), 2016. **8**(9).

40. Agarwal, A., et al., *FDG PET/CT in the management of colorectal and anal cancers.* AJR Am J Roentgenol, 2014. **203**(5): p. 1109-19.

41. Roels, S., et al., *Biological image-guided radiotherapy in rectal cancer: challenges and pitfalls.* Int J Radiat Oncol Biol Phys, 2009. **75**(3): p. 782-90.

42. Johnson, L.M., et al., *Multiparametric MRI in prostate cancer management.* Nat Rev Clin Oncol, 2014. **11**(6): p. 346-353.

43. Brown, G., et al., *Preoperative assessment of prognostic factors in rectal cancer using high-resolution magnetic resonance imaging.* Br J Surg, 2003. **90**(3): p. 355-64.

44. Taylor, F.G., et al., *Preoperative magnetic resonance imaging assessment of circumferential resection margin predicts disease-free survival and local recurrence: 5-year follow-up results of the MERCURY study.* J Clin Oncol, 2014. **32**(1): p. 34-43.

45. Patel, U.B., et al., *Magnetic resonance imaging-detected tumor response for locally advanced rectal cancer predicts survival outcomes: MERCURY experience.* J Clin Oncol, 2011. **29**(28): p. 3753-60.

46. Brown, G., et al., *Techniques and trouble-shooting in high spatial resolution thin slice MRI for rectal cancer.* The British Journal of Radiology, 2005. **78**(927): p. 245-251.

47. Berger, A., *Magnetic resonance imaging.* BMJ : British Medical Journal, 2002. **324**(7328): p. 35-35.

48. Westbrook, C., C.K. Roth, and J. Talbot, *MRI in Practice*. 2011: Wiley.

49. Brant, W.E. and E.E. de Lange, *Essentials of Body MRI*. 2012: Oxford University Press.

50. van der Paardt, M.P., et al., *Patients who undergo preoperative chemoradiotherapy for locally advanced rectal cancer restaged by using diagnostic MR imaging: a systematic review and meta-analysis.* Radiology, 2013. **269**(1): p. 101-12.

51. Wu, L.M., et al., *Is there a benefit in using magnetic resonance imaging in the prediction of preoperative neoadjuvant therapy response in locally advanced rectal cancer?* Int J Colorectal Dis, 2013. **28**(9): p. 1225-38.

52. Lee, J.H., et al., *Prediction of pathologic staging with magnetic resonance imaging after preoperative chemoradiotherapy in rectal cancer: pooled analysis of KROG 10-01 and 11-02.* Radiotherapy & Oncology, 2014. **113**(1): p. 18-23.

53. Sclafani, F., et al., *Comparison between MRI and pathology in the assessment of tumour regression grade in rectal cancer.* British Journal of Cancer, 2017. **117**(10): p. 1478-1485.

54. Couwenberg, A.M., et al., *Effect of Neoadjuvant Therapy and Rectal Surgery on Health-related Quality of Life in Patients With Rectal Cancer During the First 2 Years After Diagnosis.* Clin Colorectal Cancer, 2018. **17**(3): p. e499-e512.

55. Read, T.E., et al., *Neoadjuvant therapy for adenocarcinoma of the rectum: tumor response and acute toxicity.* Dis Colon Rectum, 2001. **44**(4): p. 513-22.

56. Ashburn, J.H. and M.F. Kalady, *Radiation-Induced Problems in Colorectal Surgery.* Clin Colon Rectal Surg, 2016. **29**(2): p. 85-91.

57. Erlandsson, J., et al., *Optimal fractionation of preoperative radiotherapy and timing to surgery for rectal cancer (Stockholm III): a multicentre, randomised, non-blinded, phase 3, non-inferiority trial.* Lancet Oncol, 2017. **18**(3): p. 336-346.

58. Gray, L.H., et al., *The concentration of oxygen dissolved in tissues at the time of irradiation as a factor in radiotherapy.* Br J Radiol, 1953. **26**.

59. Horsman, M.R. and J. Overgaard, *The impact of hypoxia and its modification of the outcome of radiotherapy.* J Radiat Res, 2016. **57**.

60. Torigian, D.A., et al., *Functional Imaging of Cancer with Emphasis on Molecular Techniques.* CA: A Cancer Journal for Clinicians, 2007. **57**(4): p. 206-224.

61. Tong, T., et al., *Dynamic contrast-enhanced MRI: Use in predicting pathological complete response to neoadjuvant chemoradiation in locally advanced rectal cancer.* J Magn Reson Imaging, 2015.

62. Lollert, A., et al., *Rectal cancer: dynamic contrast-enhanced MRI correlates with lymph node status and epidermal growth factor receptor expression.* Journal of Magnetic Resonance Imaging, 2014. **39**(6): p. 1436-42.

63. Prezzi, D. and V. Goh, *Rectal Cancer Magnetic Resonance Imaging: Imaging Beyond Morphology.* Clin Oncol (R Coll Radiol), 2016. **28**(2): p. 83-92.

64. Verheij, M., C. Vens, and B. van Triest, *Novel therapeutics in combination with radiotherapy to improve cancer treatment: Rationale, mechanisms of action and clinical perspective.* Drug Resistance Updates, 2010. **13**(1–2): p. 29-43.

65. Glynne-Jones, R. and R. Hughes, *Critical appraisal of the 'wait and see' approach in rectal cancer for clinical complete responders after chemoradiation.* British Journal of Surgery, 2012. **99**(7): p. 897-909.

66. Overgaard, J., *Hypoxic modification of radiotherapy in squamous cell carcinoma of the head and neck--a systematic review and meta-analysis.* Radiother Oncol, 2011. **100**(1): p. 22-32.

67. Horsman, M.R., et al., *Imaging hypoxia to improve radiotherapy outcome.* Nature Reviews Clinical Oncology, 2012. **9**(12): p. 674-687.

68. Mohiuddin, M., et al., *Neoadjuvant chemoradiation for distal rectal cancer: 5-year updated results of a randomized phase 2 study of neoadjuvant combined modality chemoradiation for distal rectal cancer.* International Journal of Radiation Oncology, Biology, Physics, 2013. **86**(3): p. 523-8.

69. Sato, T., et al., *A PHASE II TRIAL OF NEOADJUVANT PREOPERATIVE CHEMORADIOTHERAPY WITH S-1 PLUS IRINOTECAN AND RADIATION IN PATIENTS WITH LOCALLY ADVANCED RECTAL CANCER: CLINICAL FEASIBILITY AND RESPONSE RATE.* International Journal of Radiation Oncology Biology Physics, 2011. **79**(3): p. 677-683.

70. Schmoll, H.-J., et al., *Preoperative chemoradiotherapy and postoperative chemotherapy with capecitabine +/- oxaliplatin in locally advanced rectal cancer: Final results of PETACC-6.* Journal of Clinical Oncology, 2018. **36**(15_suppl): p. 3500-3500.

71. Des Guetz, G., et al., *Is There a Benefit of Oxaliplatin in Combination with Neoadjuvant Chemoradiotherapy for Locally Advanced Rectal Cancer? An Updated Meta-Analysis.* Cancers, 2021. **13**(23): p. 6035.

72. Salazar, R., et al., *A randomized phase II study of capecitabine-based chemoradiation with or without bevacizumab in resectable locally advanced rectal cancer: clinical and biological features.* BMC Cancer, 2015. **15**: p. 60.

73. McCollum, A.D., et al., *Randomized phase II trial of preoperative chemoradiotherapy with or without cetuximab in locally advanced rectal adenocarcinoma.* Journal of Clinical Oncology, 2014. **32**(3): p. Abstract 537.

74. Buijsen, J., et al., *Phase I trial of the combination of the Akt inhibitor nelfinavir and chemoradiation for locally advanced rectal cancer.* Radiotherapy & Oncology, 2013. **107**(2): p. 184-8.

75. Greenhalgh, T.A., C. Dearman, and R.A. Sharma, *Combination of Novel Agents with Radiotherapy to Treat Rectal Cancer.* Clinical Oncology, 2016. **28**(2): p. 116-139.

76. Samuelian, J.M., et al., *Reduced acute bowel toxicity in patients treated with intensity-modulated radiotherapy for rectal cancer.* Int J Radiat Oncol Biol Phys, 2012. **82**(5): p. 1981-7.

77. Ng, S.Y., et al., *Acute toxicity with intensity modulated radiotherapy versus 3-dimensional conformal radiotherapy during preoperative chemoradiation for locally advanced rectal cancer.* Radiother Oncol, 2016. **121**(2): p. 252-257.

78. Parekh, A., et al., *Acute gastrointestinal toxicity and tumor response with preoperative intensity modulated radiation therapy for rectal cancer.* Gastrointest Cancer Res, 2013. **6**(5-6): p. 137-43.

79. Ghaly, M., et al., *Dose escalation using dose-painted IMRT in locally advanced rectal cancer.* Journal of Clinical Oncology, 2013. **31**(4_suppl): p. 582-582.

80. Madani, I., et al., *Positron emission tomography-guided, focal-dose escalation using intensity-modulated radiotherapy for head and neck cancer.* Int J Radiat Oncol Biol Phys, 2007. **68**(1): p. 126-35.

81. Gerard, J.P., et al., *Clinical complete response (cCR) after neoadjuvant chemoradiotherapy and conservative treatment in rectal cancer. Findings from the ACCORD 12/PRODIGE 2 randomized trial.* Radiother Oncol, 2015.

82. Heald, R.J., et al., *Rectal Cancer: The Basingstoke experience of total mesorectal excision, 1978-1997.* Archives of Surgery, 1998. **133**(8): p. 894-899.

83. Habr-Gama, A., et al., *Local Recurrence After Complete Clinical Response and Watch and Wait in Rectal Cancer After Neoadjuvant Chemoradiation: Impact of Salvage Therapy on Local Disease Control.* International Journal of Radiation Oncology Biology Physics, 2014. **88**(4): p. 822-828.

84. Habr-Gama, A., et al., *Watch and wait approach following extended neoadjuvant chemoradiation for distal rectal cancer-are we getting closer to anal cancer management?* Diseases of the Colon and Rectum, 2013. **56 (4)**: p. e113-e114.

85. Dossa, F., et al., *A watch-and-wait approach for locally advanced rectal cancer after a clinical complete response following neoadjuvant chemoradiation: a systematic review and meta-analysis.* The Lancet Gastroenterology & Hepatology, 2017. **2**(7): p. 501-513.

86. Van Der Valk, M., et al., *First results of the International Watch & Wait Database (IWWD) for Rectal Cancer.* European Journal of Surgical Oncology, 2016. **42 (9)**: p. S99-S100.

87. Renehan, A.G., et al., *Watch-and-wait approach versus surgical resection after chemoradiotherapy for patients with rectal cancer (the OnCoRe project): a propensity-score matched cohort analysis.* The Lancet Oncology, 2016. **17**(2): p. 174-183.

88. Bach, S.P., *Can we Save the rectum by watchful waiting or TransAnal surgery following (chemo)Radiotherapy versus Total mesorectal excision for early REctal Cancer (STAR-TREC)? Protocol for the international, multicentre, rolling phase II/III partially randomized patient preference trial evaluating long-course concurrent chemoradiotherapy versus short-course radiotherapy organ preservation approaches.* Colorectal Dis, 2022.

89. Battersby, N.J., et al., *A rectal cancer feasibility study with an embedded phase III trial design assessing magnetic resonance tumour regression grade (mrTRG) as a novel biomarker to stratify management by good and poor response to chemoradiotherapy (TRIGGER): study protocol for a randomised controlled trial.* Trials, 2017. **18**(1): p. 394.

90. Samuel, J. and C. Franklin, *Hypoxemia and Hypoxia*, in *Common Surgical Diseases: An Algorithmic Approach to Problem Solving*, J.A. Myers, K.W. Millikan, and T.J. Saclarides, Editors. 2008, Springer New York: New York, NY. p. 391-394.

91. Challapalli, A., L. Carroll, and E.O. Aboagye, *Molecular mechanisms of hypoxia in cancer.* Clinical & Translational Imaging, 2017. **5**(3): p. 225-253.

92. Höckel, M. and P. Vaupel, *Tumor Hypoxia: Definitions and Current Clinical, Biologic, and Molecular Aspects.* JNCI: Journal of the National Cancer Institute, 2001. **93**(4): p. 266-276.

93. Vaupel, P., F. Kallinowski, and P. Okunieff, *Blood Flow, Oxygen and Nutrient Supply, and Metabolic Microenvironment of Human Tumors: A Review.* Cancer Research, 1989. **49**(23): p. 6449-6465.

94. Vaupel, P., M. Hockel, and A. Mayer, *Detection and characterization of tumor hypoxia using pO2 histography.* Antioxid Redox Signal, 2007. **9**(8): p. 1221-35.

95. Hoff, C.M., *Importance of hemoglobin concentration and its modification for the outcome of head and neck cancer patients treated with radiotherapy.* Acta Oncologica, 2012. **51**(4): p. 419-432.

96. McKeown, S.R., *Defining normoxia, physoxia and hypoxia in tumours—implications for treatment response.* The British Journal of Radiology, 2014. **87**(1035): p. 20130676.

97. Joiner, M.C. and A. van der Kogel, *Basic Clinical Radiobiology Fourth Edition*. 2009, London, UNITED KINGDOM: CRC Press.

98. Zhong, H., et al., *Overexpression of hypoxia-inducible factor 1alpha in common human cancers and their metastases.* Cancer Res, 1999. **59**(22): p. 5830-5.

99. Harris, A.L., *Hypoxia — a key regulatory factor in tumour growth.* Nature Reviews Cancer, 2002. **2**: p. 38.

100. Chen, C., et al., *Regulation of glut1 mRNA by hypoxia-inducible factor-1. Interaction between H-ras and hypoxia.* J Biol Chem, 2001. **276**(12): p. 9519-25.

101. Wykoff, C.C., et al., *Hypoxia-inducible expression of tumor-associated carbonic anhydrases.* Cancer Res, 2000. **60**(24): p. 7075-83.

102. Carmeliet, P., *Mechanisms of angiogenesis and arteriogenesis.* Nature Medicine, 2000. **6**(4): p. 389-395.

103. Finger, E.C. and A.J. Giaccia, *Hypoxia, inflammation, and the tumor microenvironment in metastatic disease.* Cancer Metastasis Rev, 2010. **29**(2): p. 285-93.

104. Rasey, J.S., et al., *Determining hypoxic fraction in a rat glioma by uptake of radiolabeled fluoromisonidazole.* Radiation Research, 2000. **153**(1): p. 84-92.

105. Brizel, D.M., et al., *Oxygenation of head and neck cancer: changes during radiotherapy and impact on treatment outcome.* Radiother Oncol, 1999. **53**(2): p. 113-7.

106. Brizel, D.M., et al., *Tumor hypoxia adversely affects the prognosis of carcinoma of the head and neck.* Int J Radiat Oncol Biol Phys, 1997. **38**(2): p. 285-9.

107. Fleming, I.N., et al., *Imaging tumour hypoxia with positron emission tomography.* Br J Cancer, 2015. **112**(2): p. 238-250.

108. Wang, K., et al., *Modeling acute and chronic hypoxia using serial images of 18F-FMISO PET.* Medical Physics, 2009. **36**(10): p. 4400-4408.

109. Rajendran, J.G. and K.A. Krohn, *F-18 fluoromisonidazole for imaging tumor hypoxia: imaging the microenvironment for personalized cancer therapy.* Semin Nucl Med, 2015. **45**(2): p. 151-62.

110. Dubois, L., et al., *Evaluation of hypoxia in an experimental rat tumour model by [(18)F]fluoromisonidazole PET and immunohistochemistry.* Br J Cancer, 2004. **91**(11): p. 1947-54.

111. Troost, E.G.C., et al., *Imaging hypoxia after oxygenation-modification: Comparing [18F]FMISO autoradiography with pimonidazole immunohistochemistry in human xenograft tumors.* Radiotherapy and Oncology, 2006. **80**(2): p. 157-164.

112. Troost, E.G., et al., *Correlation of [18F]FMISO autoradiography and pimonidazole [corrected] immunohistochemistry in human head and neck carcinoma xenografts.[Erratum appears in Eur J Nucl Med Mol Imaging. 2009 Feb;36(2):331].* European Journal of Nuclear Medicine & Molecular Imaging, 2008. **35**(10): p. 1803-11.

113. Sato, J., et al., *18F-fluoromisonidazole PET uptake is correlated with hypoxia-inducible factor-1α expression in oral squamous cell carcinoma.* J Nucl Med, 2013. **54**(7): p. 1060-5.

114. Watanabe, S., et al., *Combination of FDG-PET and FMISO-PET as a treatment strategy for patients undergoing early-stage NSCLC stereotactic radiotherapy.* EJNMMI research, 2019. **9**(1): p. 104-104.

115. Boellaard, R., et al., *Effects of Noise, Image Resolution, and ROI Definition on the Accuracy of Standard Uptake Values: A Simulation Study.* Journal of Nuclear Medicine, 2004. **45**(9): p. 1519.

116. Nahmias, C. and L.M. Wahl, *Reproducibility of Standardized Uptake Value Measurements Determined by 18F-FDG PET in Malignant Tumors.* Journal of Nuclear Medicine, 2008. **49**(11): p. 1804.

117. Lee, S.T. and A.M. Scott, *Hypoxia Positron Emission Tomography Imaging With 18F-Fluoromisonidazole.* Seminars in Nuclear Medicine, 2007. **37**(6): p. 451-461.

118. Koh, W.J., et al., *Imaging of hypoxia in human tumors with [F-18]fluoromisonidazole.* International Journal of Radiation Oncology, Biology, Physics, 1992. **22**(1): p. 199-212.

119. Rasey, J.S., et al., *Quantifying regional hypoxia in human tumors with positron emission tomography of [18F]fluoromisonidazole: a pretherapy study of 37 patients.* Int J Radiat Oncol Biol Phys, 1996. **36**(2): p. 417-28.

120. Rajendran, J.G., et al., *[18F]FMISO and [18F]FDG PET imaging in soft tissue sarcomas: correlation of hypoxia, metabolism and VEGF expression.* European Journal of Nuclear Medicine and Molecular Imaging, 2003. **30**(5): p. 695-704.

121. Rajendran, J.G., et al., *Tumor hypoxia imaging with [F-18] fluoromisonidazole positron emission tomography in head and neck cancer.* Clinical Cancer Research, 2006. **12**(18): p. 5435-5441.

122. Muzi, M., et al., *[F-18]-Fluoromisonidazole Quantification of Hypoxia in Human Cancer Patients using Image-derived Blood Surrogate Tissue Reference Regions.* Journal of nuclear medicine : official publication, Society of Nuclear Medicine, 2015. **56**(8): p. 1223-1228.

123. Yeh, S.H., et al., *Fluorine-18 fluoromisonidazole tumour to muscle retention ratio for the detection of hypoxia in nasopharyngeal carcinoma.* Eur J Nucl Med, 1996. **23**(10): p. 1378-83.

124. Eschmann, S.M., et al., *Prognostic impact of hypoxia imaging with 18F-misonidazole PET in non-small cell lung cancer and head and neck cancer before radiotherapy.* J Nucl Med, 2005. **46**(2): p. 253-60.

125. Hicks, R.J., et al., *Utility of FMISO PET in advanced head and neck cancer treated with chemoradiation incorporating a hypoxia-targeting chemotherapy agent.* European Journal of Nuclear Medicine and Molecular Imaging, 2005. **32**(12): p. 1384-1391.

126. Zimny, M., et al., *FDG--a marker of tumour hypoxia? A comparison with [18F]fluoromisonidazole and pO2-polarography in metastatic head and neck cancer.* Eur J Nucl Med Mol Imaging, 2006. **33**(12): p. 1426-31.

127. Bittner, M.I., et al., *Analysis of relation between hypoxia PET imaging and tissue-based biomarkers during head and neck radiochemotherapy.* Acta Oncol, 2016. **55**(11): p. 1299-1304.

128. Gagel, B., et al., *pO polarography, contrast enhanced color duplex sonography (CDS), [18F] fluoromisonidazole and [18F] fluorodeoxyglucose positron emission tomography: validated methods for the evaluation of therapy-relevant tumor oxygenation or only bricks in the puzzle of tumor hypoxia?* BMC Cancer, 2007. **7**: p. 113.

129. Koh, W.J., et al., *Evaluation of oxygenation status during fractionated radiotherapy in human nonsmall cell lung cancers using [F-18]fluoromisonidazole positron emission tomography.* Int J Radiat Oncol Biol Phys, 1995. **33**(2): p. 391-8.

130. Lee, S.T., et al., *Evaluation of 18F-FMISO PET and 18F-FDG PET Scans in Assessing the Therapeutic Response of Patients With Metastatic Colorectal Cancer Treated With Anti-Angiogenic Therapy.* Frontiers in Oncology, 2021. **11**(451).

131. Vera, P., et al., *Phase II Study of a Radiotherapy Total Dose Increase in Hypoxic Lesions Identified by (18)F-Misonidazole PET/CT in Patients with Non-Small Cell Lung Carcinoma (RTEP5 Study).* J Nucl Med, 2017. **58**(7): p. 1045-1053.

132. Hendrickson, K., et al., *Hypoxia imaging with [F-18] FMISO-PET in head and neck cancer: Potential for guiding intensity modulated radiation therapy in overcoming hypoxia-induced treatment resistance.* Radiotherapy and Oncology, 2011. **101**(3): p. 369-375.

133. Henriques de Figueiredo, B., et al., *Hypoxia imaging with [18F]-FMISO-PET for guided dose escalation with intensity-modulated radiotherapy in head-and-neck cancers.* Strahlenther Onkol, 2015. **191**(3): p. 217-24.

134. Toma-Dasu, I. and A. Dasu, *Quantitative hypoxia imaging for treatment planning of radiotherapy.* Advances in Experimental Medicine & Biology, 2014. **812**: p. 143-8.

135. Nehmeh, S.A., et al., *Reproducibility of intratumor distribution of (18)F-fluoromisonidazole in head and neck cancer.* International Journal of Radiation Oncology, Biology, Physics, 2008. **70**(1): p. 235-42.

136. Warren, D.R. and M. Partridge, *The role of necrosis, acute hypoxia and chronic hypoxia in 18F-FMISO PET image contrast: a computational modelling study.* Physics in Medicine & Biology, 2016. **61**(24): p. 8596.

137. Choi, W., et al., *Planning study for available dose of hypoxic tumor volume using fluorine-18-labeled fluoromisonidazole positron emission tomography for treatment of the head and neck cancer.* Radiother Oncol, 2010. **97**(2): p. 176-82.

138. Roels, S., et al., *Definition and delineation of the clinical target volume for rectal cancer.* Int J Radiat Oncol Biol Phys, 2006. **65**(4): p. 1129-42.

139. Havelund, B.M., et al., *Tumour hypoxia imaging with 18F-fluoroazomycinarabinofuranoside PET/CT in patients with locally advanced rectal cancer.* Nuclear Medicine Communications, 2013. **34**(2): p. 155-61.

140. Roels, S., et al., *Biological image-guided radiotherapy in rectal cancer: is there a role for FMISO or FLT, next to FDG?* Acta Oncol, 2008. **47**(7): p. 1237-48.

141. Dietz, D.W., et al., *Tumor hypoxia detected by positron emission tomography with 60Cu-ATSM as a predictor of response and survival in patients undergoing Neoadjuvant chemoradiotherapy for rectal carcinoma: a pilot study.* Dis Colon Rectum, 2008. **51**(11): p. 1641-8.

142. Loi, S., et al., *Oxaliplatin combined with infusional 5-fluorouracil and concomitant radiotherapy in inoperable and metastatic rectal cancer: a phase I trial.* British Journal of Cancer, 2005. **92**(4): p. 655-61.

143. Schwartz, J., et al., *Pharmacokinetic Analysis of Dynamic (18)F-Fluoromisonidazole PET Data in Non-Small Cell Lung Cancer.* J Nucl Med, 2017. **58**(6): p. 911-919.

144. McGowan, D.R., et al., *(18) F-fluoromisonidazole uptake in advanced stage non-small cell lung cancer: A voxel-by-voxel PET kinetics study.* Med Phys, 2017. **44**(9): p. 4665-4676.

145. Thorwarth, D., et al., *Kinetic analysis of dynamic 18F-fluoromisonidazole PET correlates with radiation treatment outcome in head-and-neck cancer.* BMC Cancer, 2005. **5**(1): p. 152.

146. Bruehlmeier, M., et al., *Assessment of Hypoxia and Perfusion in Human Brain Tumors Using PET with 18F-Fluoromisonidazole and 15O-H2O.* Journal of Nuclear Medicine, 2004. **45**(11): p. 1851.

147. Casciari, J.J., M.M. Graham, and J.S. Rasey, *A modeling approach for quantifying tumor hypoxia with [F-18]fluoromisonidazole PET time-activity data.* Medical Physics, 1995. **22**(7): p. 1127-39.

148. Tadamura, E., et al., *Effect of oxygen inhalation on relaxation times in various tissues.* Journal of Magnetic Resonance Imaging, 1997. **7**(1): p. 220-225.

149. Ogawa, S., et al., *Brain magnetic resonance imaging with contrast dependent on blood oxygenation.* Proceedings of the National Academy of Sciences of the United States of America, 1990. **87**(24): p. 9868-9872.

150. O'Connor, J.P., et al., *Organ-specific effects of oxygen and carbogen gas inhalation on tissue longitudinal relaxation times.* Magn Reson Med, 2007. **58**(3): p. 490-6.

151. Molinari, F., et al., *Oxygen-enhanced magnetic resonance imaging: influence of different gas delivery methods on the T1-changes of the lungs.* Investigative Radiology, 2008. **43**(6): p. 427-32.

152. Jiang, L., et al., *Blood oxygenation level-dependent (BOLD) contrast magnetic resonance imaging (MRI) for prediction of breast cancer chemotherapy response: A pilot study.* Journal of Magnetic Resonance Imaging, 2013. **37**(5): p. 1083-1092.

153. O'Connor, J.P., et al., *Preliminary study of oxygen-enhanced longitudinal relaxation in MRI: a potential novel biomarker of oxygenation changes in solid tumors.* International Journal of Radiation Oncology, Biology, Physics, 2009. **75**(4): p. 1209-15.

154. de Meester de Ravenstein, C., et al., *Histological Validation of measurement of diffuse interstitial myocardial fibrosis by myocardial extravascular volume fraction from Modified Look-Locker imaging (MOLLI) T1 mapping at 3 T.* Journal of Cardiovascular Magnetic Resonance, 2015. **17**: p. 48.

155. Kammerlander, A., et al., *Extracellular matrix expansion by cardiac magnetic resonance T1 mapping-validation with myocardial biopsy.* Journal of Cardiovascular Magnetic Resonance, 2015. **17**.

156. Sibley, C.T., et al., *T1 Mapping in cardiomyopathy at cardiac MR: comparison with endomyocardial biopsy.* Radiology, 2012. **265**(3): p. 724-32.

157. Henninger, B., et al., *Evaluation of MR imaging with T1 and T2 mapping for the determination of hepatic iron overload.* European Radiology, 2012. **22**(11): p. 2478-86.

158. Jamin, Y., et al., *Evaluation of clinically translatable MR imaging biomarkers of therapeutic response in the TH-MYCN transgenic mouse model of neuroblastoma.* Radiology, 2013. **266**(1): p. 130-40.

159. McSheehy, P.M.J., et al., *Quantified tumor T1 is a generic early-response imaging biomarker for chemotherapy reflecting cell viability.* Clinical Cancer Research, 2010. **16**(1): p. 212-225.

160. de Vries, A., et al., *Monitoring of tumor microcirculation during fractionated radiation therapy in patients with rectal carcinoma: preliminary results and implications for therapy.* Radiology, 2000. **217**(2): p. 385-91.

161. Lescher, S., et al., *Quantitative T1 and T2 mapping in recurrent glioblastomas under bevacizumab: earlier detection of tumor progression compared to conventional MRI.* Neuroradiology, 2014. **57**(1): p. 11-20.

162. Müller, A., et al., *Quantitative T1-mapping detects cloudy-enhancing tumor compartments predicting outcome of patients with glioblastoma.* Cancer Medicine, 2017. **6**(1): p. 89-99.

163. Piechnik, S.K., et al., *Shortened Modified Look-Locker Inversion recovery (ShMOLLI) for clinical myocardial T1-mapping at 1.5 and 3 T within a 9 heartbeat breathhold*, in *J Cardiovasc Magn Reson*. 2010. p. 69.

164. Ferreira, V., et al., *T1-mapping accurately detects acute myocardial edema: A comparison to T2-weighted cardiovascular magnetic resonance imaging.* Journal of Cardiovascular Magnetic Resonance, 2012. **14**.

165. Banerjee, R., et al., *Multiparametric magnetic resonance for the non-invasive diagnosis of liver disease.* J Hepatol, 2014. **60**(1): p. 69-77.

166. Fontana, M., et al., *Comparison of T1 mapping techniques for ECV quantification. Histological validation and reproducibility of ShMOLLI versus multibreath-hold T1 quantification equilibrium contrast CMR.* Journal of Cardiovascular Magnetic Resonance, 2012. **14**(1): p. 88.

167. Bull, S., et al., *Human non-contrast T1 values and correlation with histology in diffuse fibrosis.* Heart, 2013. **99**(13): p. 932-7.

168. Chung, A.S., J. Lee, and N. Ferrara, *Targeting the tumour vasculature: insights from physiological angiogenesis.* Nat Rev Cancer, 2010. **10**(7): p. 505-514.

169. Minchinton, A.I. and I.F. Tannock, *Drug penetration in solid tumours.* Nat Rev Cancer, 2006. **6**(8): p. 583-592.

170. Vaupel, P., *Tumor microenvironmental physiology and its implications for radiation oncology.* Semin Radiat Oncol, 2004. **14**(3): p. 198-206.

171. Goh, V., et al., *Quantitative colorectal cancer perfusion measurement by multidetector-row CT: does greater tumour coverage improve measurement reproducibility?* British Journal of Radiology, 2006. **79**(943): p. 578-583.

172. Sun, H., et al., *Assessment of tumor grade and angiogenesis in colorectal cancer: whole-volume perfusion CT.* Academic Radiology, 2014. **21**(6): p. 750-7.

173. Fischer, M.A., et al., *Integrated 18F-FDG PET/perfusion CT for the monitoring of neoadjuvant chemoradiotherapy in rectal carcinoma: correlation with histopathology.* European Journal of Nuclear Medicine & Molecular Imaging, 2014. **41**(8): p. 1563-73.

174. Dighe, S., et al., *Perfusion CT vascular parameters do not correlate with immunohistochemically derived microvessel density count in colorectal tumors.* Radiology, 2013. **268**(2): p. 400-10.

175. Kim, J.W., et al., *Perfusion CT in colorectal cancer: comparison of perfusion parameters with tumor grade and microvessel density.[Erratum appears in Korean J Radiol. 2012 Jul-Aug;13(4):522].* Korean Journal of Radiology, 2012. **13 Suppl 1**: p. S89-97.

176. Goh, V., et al., *The flow-metabolic phenotype of primary colorectal cancer: assessment by integrated 18F-FDG PET/perfusion CT with histopathologic correlation.* J Nucl Med, 2012. **53**(5): p. 687-92.

177. Yao, W.W., et al., *Rectal cancer: 3D dynamic contrast-enhanced MRI; correlation with microvascular density and clinicopathological features.* Radiologia Medica, 2011. **116**(3): p. 366-74.

178. Kim, Y.E., et al., *Perfusion parameters of dynamic contrast-enhanced magnetic resonance imaging in patients with rectal cancer: Correlation with microvascular density and vascular endothelial growth factor expression.* Korean Journal of Radiology, 2013. **14**(6): p. 878-885.

179. Atkin, G., et al., *Dynamic contrast-enhanced magnetic resonance imaging is a poor measure of rectal cancer angiogenesis.* Br J Surg, 2006. **93**(8): p. 992-1000.

180. Hayano, K., et al., *Computed tomography perfusion imaging as a potential imaging biomarker of colorectal cancer.* World Journal of Gastroenterology : WJG, 2014. **20**(46): p. 17345-17351.

181. Johnson, J.A. and T.A. Wilson, *A model for capillary exchange.* Am J Physiol, 1966. **210**(6): p. 1299-303.

182. Khan, S., et al., *Perfusion CT assessment of the colon and rectum: Feasibility of quantification of bowel wall perfusion and vascularization.* European Journal of Radiology, 2012. **81**(5): p. 821-824.

183. Bellomi, M., et al., *CT perfusion for the monitoring of neoadjuvant chemotherapy and radiation therapy in rectal carcinoma: initial experience.* Radiology, 2007. **244**(2): p. 486-93.

184. Sahani, D.V., et al., *Assessing tumor perfusion and treatment response in rectal cancer with multisection CT: initial observations.* Radiology, 2005. **234**(3): p. 785-92.

185. Curvo-Semedo, L., et al., *Usefulness of perfusion CT to assess response to neoadjuvant combined chemoradiotherapy in patients with locally advanced rectal cancer.* Academic Radiology, 2012. **19**(2): p. 203-13.

186. Hayano, K., et al., *Quantitative measurement of blood flow using perfusion CT for assessing clinicopathologic features and prognosis in patients with rectal cancer.* Diseases of the Colon & Rectum, 2009. **52**(9): p. 1624-9.

187. Goh, V. and R. Glynne-Jones, *Perfusion CT imaging of colorectal cancer.* The British Journal of Radiology, 2014. **87**(1034): p. 20130811.

188. Yankeelov, T.E. and J.C. Gore, *Dynamic Contrast Enhanced Magnetic Resonance Imaging in Oncology: Theory, Data Acquisition, Analysis, and Examples.* Current Medical Imaging Reviews, 2009. **3**(2): p. 91-107.

189. Gordon, Y., et al., *Dynamic contrast-enhanced magnetic resonance imaging: fundamentals and application to the evaluation of the peripheral perfusion.* Cardiovascular Diagnosis and Therapy, 2014. **4**(2): p. 147-164.

190. Fritz-Hansen, T., et al., *Measurement of the arterial concentration of Gd-DTPA using MRI: a step toward quantitative perfusion imaging.* Magn Reson Med, 1996. **36**(2): p. 225-31.

191. Orton, M.R., et al., *Computationally efficient vascular input function models for quantitative kinetic modelling using DCE-MRI.* Phys Med Biol, 2008. **53**(5): p. 1225-39.

192. McGrath, D.M., et al., *Comparison of model-based arterial input functions for dynamic contrast-enhanced MRI in tumor bearing rats.* Magnetic Resonance in Medicine, 2009. **61**(5): p. 1173-1184.

193. Tofts, P.S., *Modeling tracer kinetics in dynamic Gd-DTPA MR imaging.* J Magn Reson Imaging, 1997. **7**(1): p. 91-101.

194. Gaddikeri, S., et al., *Dynamic Contrast-Enhanced MR Imaging in Head and Neck Cancer: Techniques and Clinical Applications.* American Journal of Neuroradiology, 2016. **37**(4): p. 588.

195. Tofts, P.S., et al., *Estimating kinetic parameters from dynamic contrast-enhanced T(1)-weighted MRI of a diffusable tracer: standardized quantities and symbols.* J Magn Reson Imaging, 1999. **10**(3): p. 223-32.

196. Lim, K.S. and C.H. Tan, *Diffusion-weighted MRI of adult male pelvic cancers.* Clinical Radiology, 2012. **67**(9): p. 899-908.

197. Gollub, M.J., et al., *Limited accuracy of DCE-MRI in identification of pathological complete responders after chemoradiotherapy treatment for rectal cancer.* Eur Radiol, 2016.

198. Intven, M., O. Reerink, and M.E. Philippens, *Dynamic contrast enhanced MR imaging for rectal cancer response assessment after neo-adjuvant chemoradiation.* J Magn Reson Imaging, 2015. **41**(6): p. 1646-53.

199. Kim, S.H., et al., *Dynamic Contrast-Enhanced MRI to Evaluate the Therapeutic Response to Neoadjuvant Chemoradiation Therapy in Locally Advanced Rectal Cancer.* Journal of Magnetic Resonance Imaging, 2014. **40**(3): p. 730-737.

200. Gollub, M.J., et al., *Dynamic contrast enhanced-MRI for the detection of pathological complete response to neoadjuvant chemotherapy for locally advanced rectal cancer.* European Radiology, 2012. **22**(4): p. 821-31.

201. Shabana, W., et al., *Pretreatment rectal tumors quantitative dynamic contrast-enhanced MRI characterization and predictability of outcome: Pilot study.* Journal of Clinical Oncology, 2014. **1)**.

202. Anderson, E.M., et al., *Prediction of subsequent metastatic disease by dynamic contrast MRI in locally advanced rectal cancer*, in *European Congress of Radiology*. 2013.

203. Houn, F., *Review of F-18 Fluoro-2-Deoxyglucose (F-18 FDG) Positron Emission Tomography in the Evaluation of Malignancy*, U.S.F.D. Administration, Editor. 1999.

204. Warburg, O., F. Wind, and E. Negelein, *THE METABOLISM OF TUMORS IN THE BODY.* J Gen Physiol, 1927. **8**(6): p. 519-30.

205. Fadaka, A., et al., *Biology of glucose metabolization in cancer cells.* Journal of Oncological Sciences, 2017. **3**(2): p. 45-51.

206. Kawada, K., M. Iwamoto, and Y. Sakai, *Mechanisms underlying (18)F-fluorodeoxyglucose accumulation in colorectal cancer.* World journal of radiology, 2016. **8**(11): p. 880-886.

207. Kinahan, P.E. and J.W. Fletcher, *Positron emission tomography-computed tomography standardized uptake values in clinical practice and assessing response to therapy.* Seminars in ultrasound, CT, and MR, 2010. **31**(6): p. 496-505.

208. Wahl, R.L., et al., *From RECIST to PERCIST: Evolving Considerations for PET Response Criteria in Solid Tumors.* Journal of Nuclear Medicine, 2009. **50**(Suppl 1): p. 122S.

209. Im, H.-J., et al., *Current Methods to Define Metabolic Tumor Volume in Positron Emission Tomography: Which One is Better?* Nuclear medicine and molecular imaging, 2018. **52**(1): p. 5-15.

210. Larson, S.M., et al., *Tumor Treatment Response Based on Visual and Quantitative Changes in Global Tumor Glycolysis Using PET-FDG Imaging: The Visual Response Score and the Change in Total Lesion Glycolysis.* Clinical Positron Imaging, 1999. **2**(3): p. 159-171.

211. Gwynne, S., et al., *Imaging for Target Volume Delineation in Rectal Cancer Radiotherapy — A Systematic Review.* Clinical Oncology, 2012. **24**(1): p. 52-63.

212. Zhang, C., et al., *18F-FDG-PET evaluation of treatment response to neo-adjuvant therapy in patients with locally advanced rectal cancer: A meta-analysis.* International Journal of Cancer, 2012. **131**(11): p. 2604-2611.

213. Rosenberg, R., et al., *The predictive value of metabolic response to preoperative radiochemotherapy in locally advanced rectal cancer measured by PET/CT.* International Journal of Colorectal Disease, 2009. **24**(2): p. 191-200.

214. Guerra, L., et al., *Change in glucose metabolism measured by 18F-FDG PET/CT as a predictor of histopathologic response to neoadjuvant treatment in rectal cancer.* Abdominal Imaging, 2011. **36**(1): p. 38-45.

215. Travaini, L.L., et al., *PET/CT with Fluorodeoxyglucose During Neoadjuvant Chemoradiotherapy in Locally Advanced Rectal Cancer.* Ecancermedicalscience, 2016. **10**: p. 629.

216. Murcia Duréndez, M.J., et al., *The value of 18F-FDG PET/CT for assessing the response to neoadjuvant therapy in locally advanced rectal cancer.* European Journal of Nuclear Medicine and Molecular Imaging, 2013. **40**(1): p. 91-97.

217. Perez, R.O., et al., *Accuracy of positron emission tomography/computed tomography and clinical assessment in the detection of complete rectal tumor regression after neoadjuvant chemoradiation.* Cancer, 2012. **118**(14): p. 3501-3511.

218. Calvo, F.A., et al., *18F-FDG positron emission tomography staging and restaging in rectal cancer treated with preoperative chemoradiation.* International Journal of Radiation Oncology*Biology*Physics, 2004. **58**(2): p. 528-535.

219. Rymer, B., et al., *FDG PET/CT Can Assess the Response of Locally Advanced Rectal Cancer to Neoadjuvant Chemoradiotherapy: Evidence From Meta-analysis and Systematic Review.* Clin Nucl Med, 2016. **41**(5): p. 371-5.

220. Van de Wiele, C., et al., *Predictive and prognostic value of metabolic tumour volume and total lesion glycolysis in solid tumours.* European Journal of Nuclear Medicine and Molecular Imaging, 2013. **40**(2): p. 290-301.

221. Lee, S.-W., et al., *Prognostic Impact of Total Lesion Glycolysis (TLG) from Preoperative 18F-FDG PET/CT in Stage II/III Colorectal Adenocarcinoma: Extending the Value of PET/CT for Resectable Disease.* Cancers, 2022. **14**(3): p. 582.

222. Ogawa, S., et al., *Prognostic Value of Total Lesion Glycolysis Measured by 18F-FDG-PET/CT in Patients with Colorectal Cancer.* Anticancer Research, 2015. **35**(6): p. 3495.

223. Guillem, J.G., et al., *Prospective assessment of primary rectal cancer response to preoperative radiation and chemotherapy using 18-fluorodeoxyglucose positron emission tomography.* Diseases of the Colon & Rectum, 2000. **43**(1): p. 18-24.

224. Bang, J.-I., et al., *Prediction of neoadjuvant radiation chemotherapy response and survival using pretreatment [18F]FDG PET/CT scans in locally advanced rectal cancer.* European Journal of Nuclear Medicine and Molecular Imaging, 2016. **43**(3): p. 422-431.

225. Alongi, F., et al., *Radiation dose intensification in pre-operative chemo-radiotherapy for locally advanced rectal cancer.* Clinical and Translational Oncology, 2017. **19**(2): p. 189-196.

226. Sert, F., et al., *Prognostic Value of FDG-PET/CT Parameters in Patients with Locally Advanced Rectal Cancer Treated with Neoadjuvant Approach.* TURKISH JOURNAL OF ONCOLOGY, 2020. **35**: p. 134-43.

227. Okuno, T., et al., *Value of FDG-PET/CT Volumetry After Chemoradiotherapy in Rectal Cancer.* Dis Colon Rectum, 2018. **61**(3): p. 320-327.

228. Wu, B., et al., *An overview of CEST MRI for non-MR physicists.* Ejnmmi Physics, 2016. **3**(1): p. 19.

229. van Zijl, P.C.M. and N.N. Yadav, *Chemical Exchange Saturation Transfer (CEST): what is in a name and what isn't?* Magnetic resonance in medicine : official journal of the Society of Magnetic Resonance in Medicine / Society of Magnetic Resonance in Medicine, 2011. **65**(4): p. 927-948.

230. Walker-Samuel, S., et al., *In vivo imaging of glucose uptake and metabolism in tumors.* Nature Medicine, 2013. **19**(8): p. 1067-72.

231. Capozza, M., et al., *GlucoCEST MRI for the Evaluation Response to Chemotherapeutic and Metabolic Treatments in a Murine Triple-Negative Breast Cancer: A Comparison with[(18)F]F-FDG-PET.* Mol Imaging Biol, 2022. **24**(1): p. 126-134.

232. Wang, J., et al., *CEST Imaging in Head and Neck Cancer Patients.* Medical Physics, 2015. **42**(6): p. 3317-3317.

233. Potter, C. and A.L. Harris, *Hypoxia inducible carbonic anhydrase IX, marker of tumour hypoxia, survival pathway and therapy target.* Cell Cycle, 2004. **3**(2): p. 164-7.

234. Saarnio, J., et al., *Immunohistochemical study of colorectal tumors for expression of a novel transmembrane carbonic anhydrase, MN/CA IX, with potential value as a marker of cell proliferation.* The American journal of pathology, 1998. **153**(1): p. 279-285.

235. Russell, J., et al., *Immunohistochemical detection of changes in tumor hypoxia.* International journal of radiation oncology, biology, physics, 2009. **73**(4): p. 1177-1186.

236. van Kuijk, S.J.A., et al., *Prognostic Significance of Carbonic Anhydrase IX Expression in Cancer Patients: A Meta-Analysis.* Frontiers in oncology, 2016. **6**: p. 69-69.

237. Bekku, S., et al., *Expression of carbonic anhydrase I or II and correlation to clinical aspects of colorectal cancer.* Hepato-gastroenterology, 2000. **47 34**: p. 998-1001.

238. Korkeila, E., et al., *Expression of carbonic anhydrase IX suggests poor outcome in rectal cancer.* British journal of cancer, 2009. **100**(6): p. 874-880.

239. Rafajová, M., et al., *Induction by hypoxia combined with low glucose or low bicarbonate and high posttranslational stability upon reoxygenation contribute to carbonic anhydrase IX expression in cancer cells.* Int J Oncol, 2004. **24**(4): p. 995-1004.

240. Carnell, D.M., et al., *An immunohistochemical assessment of hypoxia in prostate carcinoma using pimonidazole: Implications for radioresistance.* International Journal of Radiation Oncology Biology Physics, 2006. **65**(1): p. 91-99.

241. Shin, K.H., et al., *Detecting changes in tumor hypoxia with carbonic anhydrase IX and pimonidazole.* Cancer Biol Ther, 2007. **6**(1): p. 70-5.

242. van Laarhoven, H.W., et al., *Hypoxia in relation to vasculature and proliferation in liver metastases in patients with colorectal cancer.* Int J Radiat Oncol Biol Phys, 2006. **64**(2): p. 473-82.

243. Verstraete, M., et al., *Investigation of possible endogenous hypoxia markers in colorectal cancer.* Int J Radiat Biol, 2013. **89**(1): p. 9-15.

244. Kaanders, J.H., et al., *Pimonidazole binding and tumor vascularity predict for treatment outcome in head and neck cancer.* Cancer Research, 2002. **62**(23): p. 7066-74.

245. Yaromina, A., et al., *Exploratory Study of the Prognostic Value of Microenvironmental Parameters During Fractionated Irradiation in Human Squamous Cell Carcinoma Xenografts.* International Journal of Radiation Oncology*Biology*Physics, 2011. **80**(4): p. 1205-1213.

246. McKenney, J.K., S.W. Weiss, and A.L. Folpe, *CD31 Expression in Intratumoral Macrophages: A Potential Diagnostic Pitfall.* The American Journal of Surgical Pathology, 2001. **25**(9).

247. Deliu, I.C., et al., *Correlations between endothelial cell markers CD31, CD34 and CD105 in colorectal carcinoma.* Rom J Morphol Embryol, 2016. **57**(3): p. 1025-1030.

248. Mohamed, S.Y., et al., *Role of VEGF, CD105, and CD31 in the Prognosis of Colorectal Cancer Cases.* J Gastrointest Cancer, 2019. **50**(1): p. 23-34.

249. Des Guetz, G., et al., *Microvessel density and VEGF expression are prognostic factors in colorectal cancer. Meta-analysis of the literature.* British Journal of Cancer, 2006. **94**(12): p. 1823-1832.

250. Hlatky, L., P. Hahnfeldt, and J. Folkman, *Clinical Application of Antiangiogenic Therapy: Microvessel Density, What It Does and Doesn't Tell Us.* JNCI: Journal of the National Cancer Institute, 2002. **94**(12): p. 883-893.

251. Goethals, L., et al., *Hypoxia in human colorectal adenocarcinoma: comparison between extrinsic and potential intrinsic hypoxia markers.* Int J Radiat Oncol Biol Phys, 2006. **65**(1): p. 246-54.

252. Pangare, T.B., et al., *Effect of Formalin Fixation on Surgical Margins in Patients With Oral Squamous Cell Carcinoma.* J Oral Maxillofac Surg, 2017. **75**(6): p. 1293-1298.

253. Royal College of Radiologists, *Radiotherapy dose fractionation, second edition*. London.

254. Edge, S.B. and C.C. Compton, *The American Joint Committee on Cancer: the 7th edition of the AJCC cancer staging manual and the future of TNM.* Ann Surg Oncol, 2010. **17**(6): p. 1471-4.

255. Taylor, F.G.M., et al., *A Systematic Approach to the Interpretation of Preoperative Staging MRI for Rectal Cancer.* American Journal of Roentgenology, 2008. **191**(6): p. 1827-1835.

256. Sebag-Montefiore, D., *Aristotle trial protocol*. 2013, CRUK & UCL Cancer trials centre.

257. Craven, I., et al., *Preoperative radiotherapy combined with 5 days per week capecitabine chemotherapy in locally advanced rectal cancer.* British journal of cancer, 2007. **97**(10): p. 1333-1337.

258. Glynne-Jones, R. and R. Hughes, *Complete Response after Chemoradiotherapy in Rectal Cancer (Watch-and-Wait): Have we Cracked the Code?* Clinical Oncology, 2016. **28**(2): p. 152-160.

259. Alauddin, M.M., *Positron emission tomography (PET) imaging with (18)F-based radiotracers.* American journal of nuclear medicine and molecular imaging, 2012. **2**(1): p. 55-76.

260. Kim, T.H., et al., *PATHOLOGIC NODAL CLASSIFICATION IS THE MOST DISCRIMINATING PROGNOSTIC FACTOR FOR DISEASE-FREE SURVIVAL IN RECTAL CANCER PATIENTS TREATED WITH PREOPERATIVE CHEMORADIOTHERAPY AND CURATIVE RESECTION.* International Journal of Radiation Oncology Biology Physics, 2010. **77**(4): p. 1158-1165.

261. Kapoor, V., B.M. McCook, and F.S. Torok, *An Introduction to PET-CT Imaging.* RadioGraphics, 2004. **24**(2): p. 523-543.

262. Puri, T., et al., *[18F]Fluoromisonidazole PET in rectal cancer.* EJNMMI Research, 2017. **7**(1): p. 78.

263. Brown, J.M., *The Hypoxic Cell.* A Target for Selective Cancer Therapy—Eighteenth Bruce F. Cain Memorial Award Lecture, 1999. **59**(23): p. 5863-5870.

264. Rockwell, S., et al., *Hypoxia and radiation therapy: past history, ongoing research, and future promise.* Current molecular medicine, 2009. **9**(4): p. 442-458.

265. Gagel, B., et al., *[18F] fluoromisonidazole and [18F] fluorodeoxyglucose positron emission tomography in response evaluation after chemo-/radiotherapy of non-small-cell lung cancer: a feasibility study.* BMC Cancer, 2006. **6**(1): p. 51.

266. Lanning, R.M., et al., *Preliminary results of a prospective trial of IMRT dose de-escalation to gross nodal disease in human papillomavirus (HPV)-positive oropharyngeal carcinoma (OPC) based on assessment of tumor hypoxia using 18f-fmiso pet imaging.* International Journal of Radiation Oncology Biology Physics, 2014. **88 (2)**: p. 474.

267. Hosono, M., et al., *Heterogeneity of intratumoral hypoxia on FMISO PET/CT in association with local control in radiation therapy.* International Journal of Radiation Oncology Biology Physics, 2014. **1)**: p. S792.

268. Spence, A.M., et al., *Regional hypoxia in glioblastoma multiforme quantified with [18F] fluoromisonidazole positron emission tomography before radiotherapy: Correlation with time to progression and survival.* Clinical Cancer Research, 2008. **14**(9): p. 2623-2630.

269. Gerstner, E., et al., *ACRIN 6684: Assessment of tumor hypoxia in newly diagnosed GBM using 18F-FMISO PET and MRI.* Clinical Cancer Research, 2016. **16**: p. 16.

270. Hall, E.J. and A.J. Giaccia, *Radiobiology for the Radiologist*. 6 ed. 2006.

271. Gregoire, V. and A. Chiti, *PET in radiotherapy planning: Particularly exquisite test or pending and experimental tool?* Radiotherapy and Oncology, 2010. **96**(3): p. 275-276.

272. Piechnik, S., et al., *Validation of the shortened modified look locker inversion recovery (Sh-MOLLI) sequence for cardiac gated T1 mapping.* Journal of Cardiovascular Magnetic Resonance, 2010. **12**(Suppl 1): p. O70.

273. Yushkevich, P.A., et al., *User-guided 3D active contour segmentation of anatomical structures: Significantly improved efficiency and reliability.* NeuroImage, 2006. **31**(3): p. 1116-1128.

274. Young, I.R., et al., *Enhancement of relaxation rate with paramagnetic contrast agents in NMR imaging.* Journal of Computed Tomography, 1981. **5**(6): p. 543-547.

275. Edelman, R.R., et al., *Noninvasive assessment of regional ventilation in the human lung using oxygen–enhanced magnetic resonance imaging.* Nature Medicine, 1996. **2**(11): p. 1236-1239.

276. Adams, L.C., et al., *Assessment of the extracellular volume fraction for the grading of clear cell renal cell carcinoma: first results and histopathological findings.* Eur Radiol, 2019. **29**(11): p. 5832-5843.

277. Wijerathne, H., et al., *Mechanisms of radiation-induced endothelium damage: Emerging models and technologies.* Radiotherapy and Oncology, 2021. **158**: p. 21-32.

278. Wang, Z.J., et al., *Urinary Oxygen Tension Measurement in Humans Using Magnetic Resonance Imaging.* Academic Radiology, 2008. **15**(11): p. 1467-1473.

279. Koelzer, V.H., et al., *Digital image analysis improves precision of PD-L1 scoring in cutaneous melanoma.* Histopathology, 2018. **73**(3): p. 397-406.

280. Di Tacchio, M., et al., *Tumor Vessel Normalization, Immunostimulatory Reprogramming, and Improved Survival in Glioblastoma with Combined Inhibition of PD-1, Angiopoietin-2, and VEGF.* Cancer Immunology Research, 2019. **7**(12): p. 1910-1927.

281. Chalkley, H.W., *Method for the Quantitative Morphologic Analysis of Tissues.* JNCI: Journal of the National Cancer Institute, 1943. **4**(1): p. 47-53.

282. Karslıoğlu, Y., N. Yiğit, and Ö. Öngürü, *Chalkley method in the angiogenesis research and its automation via computer simulation.* Pathology - Research and Practice, 2014. **210**(3): p. 161-168.

283. van Laarhoven, H.W.M., et al., *Hypoxia in relation to vasculature and proliferation in liver metastases in patients with colorectal cancer.* International Journal of Radiation Oncology Biology Physics, 2006. **64**(2): p. 473-482.

284. Troost, E.G., et al., *Correlation of [18F]FMISO autoradiography and pimonidazole [corrected] immunohistochemistry in human head and neck carcinoma xenografts.* Eur J Nucl Med Mol Imaging, 2008. **35**(10): p. 1803-11.

285. Sorace, A.G., et al., *Quantitative [18F]FMISO PET Imaging Shows Reduction of Hypoxia Following Trastuzumab in a Murine Model of HER2+ Breast Cancer.* Molecular Imaging and Biology, 2017. **19**(1): p. 130-137.

286. Hattori, H., *Caution should be taken in using CD31 for distinguishing the vasculature of lymph nodes.* Journal of Clinical Pathology, 2003. **56**(8): p. 638.

287. Shi, K., et al., *Quantitative Analysis of [18F]FMISO PET for Tumor Hypoxia: Correlation of Modeling Results with Immunohistochemistry.* Molecular Imaging and Biology, 2017. **19**(1): p. 120-129.

288. Tong, X., et al., *Monitoring Tumor Hypoxia Using 18F-FMISO PET and Pharmacokinetics Modeling after Photodynamic Therapy.* Scientific Reports, 2016. **6**(1): p. 31551.

289. McGowan, D.R., et al., *Whole tumor kinetics analysis of 18F-fluoromisonidazole dynamic PET scans of non-small cell lung cancer patients, and correlations with perfusion CT blood flow.* EJNMMI Research, 2018. **8**(1): p. 73.

290. Jurdana, M., et al., *Effect of ionizing radiation on human skeletal muscle precursor cells.* Radiology and Oncology, 2013. **47**(4): p. 376-381.

291. Kimura, H., et al., *Fluctuations in Red Cell Flux in Tumor Microvessels Can Lead to Transient Hypoxia and Reoxygenation in Tumor Parenchyma1.* Cancer Research, 1996. **56**(23): p. 5522-5528.

292. García-Figueiras, R., et al., *CT Perfusion in Oncologic Imaging: A Useful Tool?* American Journal of Roentgenology, 2013. **200**(1): p. 8-19.

293. Prezzi, D., A. Khan, and V. Goh, *Perfusion CT imaging of treatment response in oncology.* Eur J Radiol, 2015.

294. Goh, V., et al., *Commercial software upgrades may significantly alter Perfusion CT parameter values in colorectal cancer.* Eur Radiol, 2011. **21**(4): p. 744-9.

295. Heinrich, M.P., et al., *MIND: modality independent neighbourhood descriptor for multi-modal deformable registration.* Med Image Anal, 2012. **16**(7): p. 1423-35.

296. Irving, B., et al., *Pieces-of-parts for supervoxel segmentation with global context: Application to DCE-MRI tumour delineation.* Medical Image Analysis, 2016. **32**: p. 69-83.

297. Yarnold, J. and M.-C. Vozenin Brotons, *Pathogenetic mechanisms in radiation fibrosis.* Radiotherapy and Oncology, 2010. **97**(1): p. 149-161.

298. Li, S.P. and A.R. Padhani, *Tumor response assessments with diffusion and perfusion MRI.* Journal of Magnetic Resonance Imaging, 2012. **35**(4): p. 745-63.

299. Irving, B., et al., *Personalised Estimation of the Arterial Input Function for Improved Pharmacokinetic Modelling of Colorectal Cancer Using dceMRI*, in *Abdominal Imaging. Computation and Clinical Applications: 5th International Workshop, Held in Conjunction with MICCAI 2013, Nagoya, Japan, September 22, 2013. Proceedings*, H. Yoshida, S. Warfield, and M.W. Vannier, Editors. 2013, Springer Berlin Heidelberg: Berlin, Heidelberg. p. 126-135.

300. Li, D., et al., *The Correlation between 18F-FDG PET/CT Imaging SUVmax of Preoperative Colon Cancer Primary Lesions and Clinicopathological Factors.* Journal of Oncology, 2021. **2021**: p. 4312296.

301. Chen, F., et al., *Ratio of maximum standardized uptake value to primary tumor size is a prognostic factor in patients with advanced non-small cell lung cancer.* Translational Lung Cancer Research, 2014. **4**(1): p. 18-26.

302. Yang, F., et al., *Tumor Volume Predicts for Pathologic Complete Response in Rectal Cancer Patients Treated With Neoadjuvant Chemoradiation.* Am J Clin Oncol, 2022. **45**(10): p. 405-409.

303. Shin, J.K., et al., *Clinical prediction model of pathological response following neoadjuvant chemoradiotherapy for rectal cancer.* Scientific Reports, 2022. **12**(1): p. 7145.

304. Caruso, R., et al., *Role of 18F-PET-CT to predict pathological response after neoadjuvant treatment of rectal cancer.* Discover. Oncology, 2021. **12**(1): p. 16-16.

305. Gu, J., et al., *Combined use of 18F-FDG PET/CT, DW-MRI, and DCE-MRI in treatment response for preoperative chemoradiation therapy in locally invasive rectal cancers.* Clin Nucl Med, 2013. **38**(5): p. e226-9.

306. Royal College of Radiologists, *The timely delivery of radical radiotherapy: guidelines for the management of unscheduled treatment interruptions*. 2019: London.

307. Guillem, J.G., et al., *Neither FDG-PET Nor CT can distinguish between a pathological complete response and an incomplete response after neoadjuvant chemoradiation in locally advanced rectal cancer: a prospective study.* Ann Surg, 2013. **258**(2): p. 289-95.

308. Machtay, M., et al., *Prediction of survival by [18F]fluorodeoxyglucose positron emission tomography in patients with locally advanced non-small-cell lung cancer undergoing definitive chemoradiation therapy: results of the ACRIN 6668/RTOG 0235 trial.* J Clin Oncol, 2013. **31**(30): p. 3823-30.

309. Jeong, Y., et al., *Lymph node standardized uptake values at pre-treatment (18)F-fluorodeoxyglucose positron emission tomography as a valuable prognostic factor for distant metastasis in nasopharyngeal carcinoma.* The British journal of radiology, 2017. **90**(1071): p. 20160239-20160239.

310. Glazer, E.S., et al., *Association of decreased peak SUV on PET after neoadjvuant therapy in patients with borderline resectable pancreatic carcinoma with pathologic response.* Journal of Clinical Oncology, 2016. **34**(4_suppl): p. 423-423.

311. Mirada, *XD 3.6.11 Help Guide*.

312. Vanderhoek, M., S.B. Perlman, and R. Jeraj, *Impact of the Definition of Peak Standardized Uptake Value on Quantification of Treatment Response.* Journal of Nuclear Medicine, 2012. **53**(1): p. 4.

313. Tandberg, D.J., et al., *Intratreatment Response Assessment With 18F-FDG PET: Correlation of Semiquantitative PET Features With Pathologic Response of Esophageal Cancer to Neoadjuvant Chemoradiotherapy.* International Journal of Radiation Oncology*Biology*Physics, 2018. **102**(4): p. 1002-1007.

314. Takahashi, N., et al., *Metabolic tumor volume on FDG-PET/CT is a possible prognostic factor for Stage I lung cancer patients treated with stereotactic body radiation therapy: a retrospective clinical study.* J Radiat Res, 2016. **57**(6): p. 655-661.

315. Lee, S.-W., et al., *Prognostic Impact of Total Lesion Glycolysis (TLG) from Preoperative (18)F-FDG PET/CT in Stage II/III Colorectal Adenocarcinoma: Extending the Value of PET/CT for Resectable Disease.* Cancers, 2022. **14**(3): p. 582.

316. Buijsen, J., et al., *FDG-PET-CT reduces the interobserver variability in rectal tumor delineation.* Radiother Oncol, 2012. **102**(3): p. 371-6.

317. Committee, J.F., *British National Formulary*. Vol. 73. 2017, London: BMJ Group and Pharmaceutical Press.

318. Jackson, R.A., et al., *Forearm Glucose Uptake During the Oral Glucose Tolerance Test in Normal Subjects.* Diabetes, 1973. **22**(6): p. 442-458.

319. Nadon, G.W., et al., *A Comparison of the Oral and Intravenous Glucose Tolerance Tests in Non-Diabetic, Possible Diabetic and Diabetic Subjects.* Canadian Medical Association Journal, 1964. **91**(26): p. 1350-1353.

320. Lozner, E.L., et al., *THE INTRAVENOUS GLUCOSE TOLERANCE TEST.* Journal of Clinical Investigation, 1941. **20**(5): p. 507-515.

321. Cobelli, C., et al., *Assessment of beta-cell function in humans, simultaneously with insulin sensitivity and hepatic extraction, from intravenous and oral glucose tests.* Am J Physiol Endocrinol Metab, 2007. **293**(1): p. E1-e15.

322. Bingley, P.J., et al., *Standardization of IVGTT to Predict IDDM.* Diabetes Care, 1992. **15**(10): p. 1313-1316.

323. Colman, P.G., et al., *Comparison of Two Commonly Used Standard IVGTTs.* Diabetes Care, 1992. **15**(8): p. 1053-1055.

324. Rivlin, M., et al., *Molecular imaging of tumors and metastases using chemical exchange saturation transfer (CEST) MRI.* Sci Rep, 2013. **3**: p. 3045.

325. Wang, J., et al., *Magnetic Resonance Imaging of Glucose Uptake and Metabolism in Patients with Head and Neck Cancer.* Scientific Reports, 2016. **6**: p. 30618.

326. Xu, X., et al., *Dynamic Glucose-Enhanced (DGE) MRI: Translation to Human Scanning and First Results in Glioma Patients.* Tomography, 2015. **1**(2): p. 105-114.

327. Uematsu, H., et al., *Changes in T1 and T2 Observed in Brain Magnetic Resonance Imaging With Delivery of High Concentrations of Oxygen.* Journal of Computer Assisted Tomography, 2007. **31**(5).

328. Sun, P.Z. and A.G. Sorensen, *Imaging pH using the chemical exchange saturation transfer (CEST) MRI: Correction of concomitant RF irradiation effects to quantify CEST MRI for chemical exchange rate and pH.* Magnetic Resonance in Medicine, 2008. **60**(2): p. 390-397.

329. (NICE), T.N.I.f.H.a.C.E., *Cancer of the upper aerodigestive tract: assessment and management in people aged 16 and over*. 2016.

330. Zhou, C. and J.L. Parsons, *The radiobiology of HPV-positive and HPV-negative head and neck squamous cell carcinoma.* Expert reviews in molecular medicine, 2020. **22**: p. e3-e3.

331. Vinogradov, E., A.D. Sherry, and R.E. Lenkinski, *CEST: from basic principles to applications, challenges and opportunities.* Journal of magnetic resonance (San Diego, Calif. : 1997), 2013. **229**: p. 155-172.

332. Domingo, E., et al., *Multi-omic profiling and radiotherapy response in rectal cancer biopsies of COPERNICUS trial: results from SCORT (Stratification in COloRecTal cancer)*, in *NCRI Cancer Conference*. 2017.

333. Dimitrakopoulou-Strauss, A., L. Pan, and L.G. Strauss, *Quantitative approaches of dynamic FDG-PET and PET/CT studies (dPET/CT) for the evaluation of oncological patients.* Cancer imaging : the official publication of the International Cancer Imaging Society, 2012. **12**(1): p. 283-289.

334. Kotani, T., et al., *Comparison between dynamic whole-body FDG-PET and early-delayed imaging for the assessment of motion in focal uptake in colorectal area.* Annals of Nuclear Medicine, 2021. **35**(12): p. 1305-1311.